Wissenschaftszentrum Weihenstephan
für Ernährung, Landnutzung und Umwelt
der Technischen Universität München

Forest Biomass Estimation from Polarimetric SAR Interferometry

Dissertation von Tobias Mette

zur Erlangung des akademischen Grades eines Doktors rer.nat.

durchgeführt am Institut für Hochfrequenztechnik und Radarsysteme
des Deutschen Zentrums für Luft- und Raumfahrt e.V.
vorgelegt am Lehrstuhl für Waldwachstumskunde der TU München

Lehrstuhl für Waldwachstumskunde

Forest Biomass Estimation from Polarimetric SAR Interferometry

Tobias Mette

Vollständiger Abdruck der von der Fakultät Wissenschaftszentrum Weihenstephan für Ernährung, Landnutzung und Umwelt der Technischen Universität München zur Erlangung des akademischen Grades des Doktors der Naturwissenschaften (Dr. rer.nat.) genehmigten Dissertation.

Vorsitzender:
Univ.-Prof. Dr. Th. Knoke
Prüfer der Dissertation:
1. Univ.-Prof. Dr. H. Pretzsch (schriftliche Beurteilung)
1. Univ.-Prof. Dr. R. Mosandl (mündliche Beurteilung)
2. Univ.-Prof. Dr. A. Moreira (Universität Karlsruhe TH)
3. Univ.-Prof. Dr. R. Matyssek

Die Dissertation wurde am 11. Juli 2006 bei der Technischen Universität München eingereicht und durch die Fakultät Wissenschaftszentrum Weihenstephan für Ernährung, Landnutzung und Umwelt am 08. März 2007 angenommen.

Abstract

[english] Polarimetric SAR interferometry (Pol-InSAR) is a radar remote sensing technique that allows to extract forest heights by means of model-based inversions. Forest biomass is closely related to forest height, and can be derived from it with allometric relations.

This work investigates the combination of the two methods to estimate forest biomass from Pol-InSAR. It develops a concept for the use of height-biomass allometry, and outlines the Pol-InSAR height inversion. The methodology is validated against a set of forest inventory data and Pol-InSAR data at L-band of the test site Traunstein. The results allow to draw conclusions on the potential of Pol-InSAR forest biomass missions.

[deutsch] Polarimetrische SAR Interferometrie (Pol-InSAR) ist eine Radar-Fernerkundungs-Technik, die es ermöglicht, Waldhöhe mittels modell-basierter Invertierung zu extrahieren. Waldbiomasse steht in engem Bezug zur Waldhöhe und lässt sich mittels allometrischer Gleichungen daraus ableiten.

Diese Arbeit untersucht die Verknüpfung beider Methoden, mit dem Ziel, Biomasse aus Pol-InSAR Daten zu schätzen. Ein Konzept zur Einbindung der Höhe-Biomasse Allometrie wird entwickelt und die Höhen-Invertierung aus Pol-InSAR Daten dargelegt. Die Methodologie wird anhand von Forst-Inventurdaten und L-Band ‚single baseline' Pol-InSAR Daten für eine Waldfläche in Traunstein (Süddeutschland) validiert. Die Ergebnisse ermöglichen eine Einschätzung des Potentials von Pol-InSAR Waldbiomasse-Bestimmungen.

Preface

I acknowledge and thank the following people who have contributed to this work:

Prof. Dr. Hans Pretzsch and Prof. Dr. Alberto Moreira for advice and encouragement, Dr. Irena Hajnsek for continuous promotion, and Dr. Konstantinos Papathanassiou for the entire supervision.

My colleagues in science for support, scientific interaction, corrections and proof reading, only to name a few: Martin Hellmann, Ralf Horn, Angelo Liseno, Fifame Koudogbo, Florian Kugler, Matteo Nannini, Maxim Neumann, Rolf Scheiber, Rafael Schneider, Steffen Thölert, Reiner Zimmermann.

My family and friends for backing me up.

Munich, July 2006

Summary

The title, "Forest Biomass Estimation from Polarimetric SAR Interferometry", assigns the presented work to the field of remote sensing based forest biomass estimations. Biomass is the most integrative structural forest parameter and along with species composition the key parameter in forestry and ecology. Lately, it has been intensively discussed in terms of the global carbon cycle since ~50% of the dry plant matter consists of carbon. However, current global estimates are still afflicted with great uncertainties.

The methodology proposed in this work is a two-step approach: First, forest height is inverted from polarimetric interferometric (Pol-InSAR) radar data by using a coherent forest scattering model. Then forest biomass is derived from the extracted forest heights by means of allometric height-biomass relations. Both steps, the height extraction and the height-biomass conversion, are based on physical and biological relationships, and do not need to be parameterized from empirical regressions.

The challenge of this work was to link the two methodologies, Pol-InSAR height extraction and forest height biomass allometry, and to investigate the potential of combining them in a forest biomass estimation from Pol-InSAR.

The first part of the work approaches the task from the forest side. The main concept of how to use height-biomass allometry with remote sensing height data was addressed – keeping in mind a possible global application. The idea was to establish an allometric height-biomass reference function in the form of the allometric equation. This reference function can be adjusted to different forest types by introducing an allometric level, which serves as height-related density measure. However, before deriving the reference allometry, it was necessary to agree on a rational definition of forest height, forest biomass and consider a sensible forest type for the derivation of the reference allometry. In this respect, upper canopy height and stem biomass were chosen as reference measures; standard forestry yield tables were used to obtain the reference function.

Being a widespread, and economically important tree species, Norway spruce as described by the yield tables of Assmann and Franz (1963, average yield level) was selected for the definition of the reference function. Compared against the yield tables of 11 different common species the reference allometry of Norway spruce lies, for a given height, at the upper biomass limit. Most other species reach allometric levels between 0.7 and 1.0 (70%-100%) with the exception of birch and poplar that are characterised by significantly lower allometric levels. A tendency of a decreasing allometric level from climax to pioneer character of the species was noted, but also regional differences seem to play a role. On the contrary, the effect of site conditions – reflected by the yield classes – was comparably low. For strong thinning intensities it was necessary to reduce the biomass estimation by 10%-20%.

In the second part, the required radar remote sensing elements are introduced, discussed and analyzed. Based on an interferometric system model the individual contributions of the interferometric coherence are addressed. The most important contribution is the volume decorrelation which depends on the vertical scatterer distribution and allows to investigate the vertical structure of forests by means of interferometry.

Interpreting the vertical forest dimension as a two-layer medium, in terms of the Random-Volume-over-Ground (RVoG) model, the volume decorrelation is obtained as a function of forest height, extinction, volume and ground scattering. Polarimetric SAR interferometry allows to resolve these parameters and invert forest heights. Key of the inversion is the polarimetric sensitivity to different scattering contributions – namely the one of the ground. Since the RVoG inversion is based purely on volume decorrelation, any system-related or temporal effects in the coherence must be compensated.

Finally, in the third and last part, the methodology is validated against available ground measurements for the test site Traunstein. The test site is dominated by spruce stands, which may reach heights up to 40 m and locally exceed biomass levels of 450 t ha^{-1}. 20 homogeneous stands between 1 ha and 23 ha were selected for the validation. The radar data were acquired with the E-SAR L-band sensor of DLR. The height inversion was implemented on a fully polarimetric data set with a single interferometric baseline.

The concept of reference allometry and allometric level is validated first. Even if the forest structure at the test site was not as homogeneous as in the yield tables, the power-function character of the height-biomass allometry was clearly observed. Despite the exceptionally well growing conditions of the site, it was necessary to adjust the allometric level to 0.87 (87 %) when regarding all inventory plots, and 0.92 (92 %) when considering only the inventory plots of the relatively homogeneous validation stands. The low allometric level could partly be explained from the increased thinning in the regeneration stadiums, and the presence of leftover emergents in the youth stadium. The high variance about the average allometric level on plot scale ($r^2 = 0.40$) proved to be due to local density variations and compensated in large area averages ($r^2 = 0.86$).

In a second step, the height inversion from the Pol-InSAR data was carried out, first for a simplified uniform scatterer distribution, and then for the full RVoG model. Already the first case indicated the necessity to compensate non-volume related decorrelation contributions on the obtained coherences. Using an average decorrelation factor of 0.90, lower stands matched the inventory heights well, but taller heights were still overestimated. The RVoG-inversion allowed to interprete this overestimation as the result of temporal decorrelation and residual ground contribution in the coherence. The accuracy of the height inversion reached a coefficient of determination of $r^2 = 0.84$.

Forest biomass is then obtained by using the Pol-InSAR forest height estimates in the height-biomass allometric equation. In doing so, the biomass estimation combines both the height and the allometric errors. Nevertheless, the obtained accuracy of the height-biomass allometry and the Pol-InSAR height inversion allowed to achieve (very) satisfying biomass estimates ($r^2 = 0.75$).

In summary, the obtained results proves an unsaturated sensitivity of polarimetric SAR interferometry at L-band to heights up to 40 m and corresponding biomass levels in the order of 450 t ha^{-1}. The possibility to implement this technique on space-borne platforms encourages the discussion of a satellite Pol-InSAR mission for a global forest biomass inventory. The height sensitivity of such a system depends on the acquisition configuration, while an unbiased allometric height-biomass conversion requires regional or local adjustment of the allometric level to account for density variations.

Index

Index of Figures

Index of tables

1 Introduction

The title 'Forest biomass estimation from polarimetric SAR interferometry' apparently relates the topic of the work primarily to the field of remote sensing. Actually however, the proposed biomass estimation is a two-step procedure that combines remote sensing and forest allometry (Fig. 1.1):

1. Polarimetric SAR interferometry (Pol-InSAR) is a radar remote sensing technique that is sensible to the height distribution of scattering processes. This is used for the inversion of forest heights with the 'Random Volume over Ground'-model (RVoG).
2. Forest allometry studies the rules between the size proportions of a forest. It provides the tools for the conversion of the extracted forest heights to forest biomass.

Polarimetric SAR interferometry is a comparably new and advanced radar technique, and has proven considerable potential for model based parameter extraction (Cloude and Papathanassiou 1998/ 2003, Papathanassiou and Cloude 2001). In the beginning of the work, in 2001, the forest height inversion had been in a very early stage demonstrated for forests up to 25 m height using L-band Pol-InSAR data (Papathanassiou and Cloude 2001).

The objective of this work was to combine Pol-InSAR and forest allometry in a joint concept, to implement the processing chain and to validate the individual steps with real data, with the aim to evaluate potential and limits of Pol-InSAR systems for forest biomass inventories.

This work essentially merges two fields of science: radar remote sensing and forestry. Both disciplines have their own 'limited' horizon and it is not always easy to bridge the gap between them. The following sections provide a comprehensive overview over the two topics.

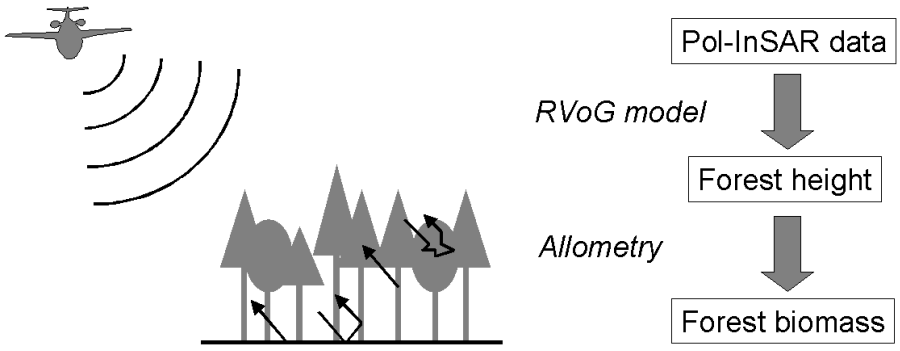

Fig. 1-1 Two-step procedure of the forest biomass estimation from Pol-InSAR data

1.1 Forest Biomass

Forests are tree-dominated plant formations that cover approximately 30% of the terrestrial surface or 40 Mio km^2. They play an important role as a natural resource, carbon storage and through their interactions with atmosphere and soil (FAO 2001a).

Forest volume or biomass is the most integrative structural forest parameter, and along with species composition the key parameter in forestry and ecology. Volume and biomass are in many senses equivalents; volume is rather the forestry standard (wood volume), biomass the ecological standard. Wood volume and biomass are related through the wood density which typically lies between 0.5-0.7 g/ cm^3. However, biomass standards may include also branch-, leaf-, and root-biomass, which are mostly extrapolated from stem diameter or biomass values (FAO 2001b, Brown 1997).

Besides the economic relevance in terms of timber extraction, forest biomass can be used to assess many important ecological functions of the forest, like the buffering of extreme temperature amplitudes, the alleviation of the impact of precipitation with respect to erosion and flooding, the filtering capacity of air and water, or the conservation of biodiversity (BMVEL 2001, WRI 2001). Furthermore, forest biomass is also a prime parameter for the assignment of growth stadiums, site quality assessments and forest classification (StMELF 1982, UNESCO 1973).

Lately, forest biomass has been discussed intensively with respect to the global carbon cycle, since ~50% of the dry plant matter is constituted of carbon. Although small, in comparison to lithosphere-, ocean- and also fossil carbon storages (> 75 Mio Gt, 38400 Gt, and 4130 Gt respectively), the vegetation carbon pool (2000 Gt) is of a special concern, because any changes directly affect the atmospheric carbon pool (700 Gt) (numbers from Falkowski et al. 2000). Above ground forest biomass accounts only for 15 % of the vegetation carbon (80% soil, 5% other vegetation, Dixon et al. 1994), but due to their short-term sequestration potential (IPCC 2001b), the impact of forest activities is explicitly considered in the Kyoto protocol (UNFCCC 1997).

Estimates for the carbon stocks in the global forest vegetation have tended to decrease over time, from 825 Gt (Whittaker and Likens 1973) to the current range of 352–536 Gt (e.g. Olson et al. 1983, Dixon et al. 1994, Houghton 1996, Brown 1998). “This range of estimates can be considered as the state-of-art of today, despite indication in Prentice et al. (2001) that the highest estimate 536 Gt (Saugier et al. 2001) is probably too high.” (Kauppi 2003). The latest estimate of the Forest Resource Assessment 2000 (FAO 2001b) further reduced the estimate to 210 Gt (257 Gt, when including belowground carbon, Kauppi 2003).

The compilation of national forest inventories for the mentioned estimates is very elaborate and has to contemplate with different methodologies and definitions, as well as the different availability of regional data (Houghton 2005). More certainty and regularity are central issues for an increased understanding of global carbon-flux, ecosystem changes, and long-sighted political decisions and actions. With respect to the large and often remote extension of forests – both forestry institutions and science community rely upon remote sensing data and techniques (e.g. Mooney and Hobbs 1990, FAO 2001b, Cihlar et al. 2001, WRI 2001).

1.2 Forest biomass inventories and remote sensing

Forest inventories are carried out to document the extent, structure and species composition of a forest in its development in time. Ground-based forest inventories typically consist of a grid of sample plots, and for each plot the required forest parameters are recorded. Ground inventories are very elaborate, but the information quality and the flexibility in terms of acquirable parameters are not feasible from any other source. Since the inventory only covers a sample tree population, the accuracy is a question of the sample plot size and the grid density (Zöhrer 1980, StMELF 1982).

In general, remote sensing system cannot achieve the parameter accuracy of a ground-based forest inventory. However, unlike the sampling grid of the ground inventory, remote sensing images provide complete area-coverage and make segmentation and classification possible. This becomes very important in large and remote areas of boreal and tropical forests. Here, remote sensing may be the only source of information. Another advantage of (satellite) remote sensing is the global conformity of the extracted parameter. This is still the major problem for inter-comparisons of national ground-based forest inventories (Kauppi 2003, FAO 2001a/b, Dixon et al. 1994). It is important, that the compatibility between forestry standards and remote sensing parameter is assured.

Traditionally, forest inventories have been supported by aerial photography. The high spatial resolution makes the precise delineation of emergent crowns possible and species can often be determined with some experience (except for tropical rain forest). Stereoscopic acquisitions make a relatively accurate tree height estimation possible if the stem foot is visible which is the case at stand borders, openings or for low stem densities. Stem volume or biomass estimates are feasible from tree heights, tree densities and crown dimensions, but very elaborate if not automated (Sayn-Wittgenstein 1961, U.S. Dep. Agr. 1978, Rhody 1982, Hildebrandt 1996, St-Onge and Cavayas 1995/ 1997, Bauer 2001).

Coarser resolutions like high-altitude aerial photography or most optical satellites loose the single tree resolution, but forest extension and canopy cover can still be extracted. Species determination becomes more difficult and is restricted to forests where single species dominate. Conifers and broadleaves are well distinguishable in the near infrared spectrum (Schade and Hildebrandt 1980, Hildebrandt 1996, Lillesand and Kiefer 1999). The extraction of stem volume or biomass is not based on structural parameters like tree height or crown dimension, but on vegetation indices like the NDVI often in combination with ecosystem models (Running et al. 1986, Sader et al. 1989, Running 1990, Baulis and Pons 1995, Foody 1996, Dong et al. 2003).

One major issue of optical satellite imagery has always been land cover classification. LandSAT and NOAA AVHRR data have the advantage of providing a continuous data availability since the 1970'ies. An important data source is the AVHRR Global Land Cover Characteristics data base (GLCCD 1998, Loveland et al. 2000). It was used for the global carbon estimate of the World Resource Institute (WRI 2001), and the global forest cover map of the United Nations Food and Agricultural Organisation (FAO 2001a/b, Zhu and Waller 2001). Another examples is the pan-tropical remote sensing survey based on LandSAT images (FAO 1996, FAO 2001a/b).

Radar has played a minor role in operational forestry applications. Two main reasons may be identified: (1) processing and interpretation of radar data appears complex to non-experts, and (2) optical data are more readily available due to a prevalence of optical systems. However, radar waves reveal object characteristics that differ from optical waves, and physical parameter extraction plays a much larger role than in optical image interpretation. Large scale forest classifications have been shown in the SIBERIA project and the Global Rain Forest and Boreal Forest Monitoring project (Santoro 2003, Wagner et al. 2000, Rosenqvist et al. 2000, Siqueira et al. 2000, De Grandi 2000).

A comparably new and promising remote sensing method is Lidar, 'Light detection and ranging'. Lidar is a hybrid between radar and optical systems in a sense that it uses an optical ranging system. The simplicity and accuracy in lidar data is unsurpassed, and although the space borne Vegetation Canopy Lidar mission was not realized, the ICE/SAT satellite carries a first laser altimeter with a 90 x 50m^2 footprint (Levsky et al. 1999a/b, Means et al. 1999, Drake et al. 2002, Dubayah et al. 1997, Ni-Meister et al. 2001, Harding and Carabajal 2005).

1.3 Forest biomass from radar-backscatter and -coherence

In contrast to optical waves, radar is sensible to the geometrical and dielectric properties of the 'scattering' object. This characteristic along with the unfamiliar radar geometry makes the image interpretation difficult in the beginning. Yet, land cover mapping from radar has evolved from unwanted 'clutter' to an important field of research with manifold applications (Elachi 1987, Curlander 1991, Ulaby 1986, Henderson, Lewis 1998).

Despite many technical advances, the original reasons to use radar for remote sensing are still valid: the capability to penetrate cloud cover, and the distinctive information in the radar spectrum of the object (Henderson, Lewis 1998, p. 4).

For radar remote sensing of forests, the most important feature is the capability of the radar wave to penetrate the canopy and 'see' the forests as a volume. Longer wavelengths like L- and P-band (~0.2-1 m) are mainly scattered from branches and trunks and, hence, to a certain extent sensitive to forest biomass. Authors generally agree upon a limit of 40-100 t ha^{-1} at L-band and 120-200 t ha^{-1} at P-band (Le Toan et al. 1992, Dobson et al. 1992, Imhoff 1995, Kellndorfer et al. 2003). Still longer wavelengths like the Swedish VHF sensor CARABAS do not appear to saturate with biomass (Fransson et al. 2000, Israelsson et al. 1997, Melon et al. 2001, Smith and Ulander 2000).

A new era of SAR began with the introduction of interferometry (Graham 1974, Zebker and Goldstein 1986). Conventional SAR interferometry refers to the acquisition of the a scene from two slightly different viewing angles. Like in photogrammetry these different angles enable the extraction of the 3rd (height) dimension, and the generation of Digital Elevation Models (DEMs) (Bamler and Hartl 1998, Rosen et al. 2000).

In forests, the height information depends on the penetration depth of the radar wave, which is a function of the wave extinction in the medium. This is exploited for example when calculating forest height as the difference between an X-band and a P-band DEM. But this approach leads to an underestimation, because the X-band DEM does not match the absolute crown top, and the P-band DEM not the absolute ground (Aulinger 2005a/b, Andersen et al. 2004, Mercer 2004, Santos et al. 2004, Moreira et al. 2001).

A second parameter from SAR interferometry is the interferometric coherence, i.e. the correlation between interferometric image pairs. The coherence decreases when the scatterer arrangement changes due to different look angles (baseline decorrelation), due to temporal changes between the image acquisitions (temporal decorrelation), or system noise and processing inaccuracies (system decorrelation) (Zebker and Villasenor 1992, Hagberg et al. 1995, Askne et al. 1997, Bamler and Hartl 1998)

Over boreal forests, interferometric C-band data from the ERS-1/2 tandem mission showed an almost linear decrease of the coherence with forest biomass (Koskinen et al. 2001, Santoro et al. 2002, Wagner et al. 2000). This has been interpreted with an interferometric water cloud model (Attema and Ulaby 1978, Hagberg et al. 1995, Askne et al. 1997, Santoro et al. 2002). In this model, the coherence is understood as the result of a ground and a forest contribution, and the ground-volume ratio is related to the stem volume. The coherence-biomass regression is scene specific and can be calibrated by using ground measurements. Good results were obtained for forests up to $200 m^3 ha^{-1}$ ($\sim 100 t\, ha^{-1}$) and under frozen winter conditions (Koskinen et al. 2001, Santoro et al. 2002, Wagner et al. 2000).

1.4 Forest biomass from Pol-InSAR and forest allometry

The Pol-InSAR biomass estimation is also based on the interferometric coherence. More specifically, it uses the height-dependent contribution, i.e. the volume decorrelation, of the baseline decorrelation. Forest height is then converted to forest biomass with allometric equations.

In contrast to the empirical coherence-biomass regressions discussed above, volume decorrelation is a deterministic function of the forest height and the baseline configuration (Hagberg et al. 1995, Askne et al. 1997, Bamler and Hartl 1998, Cloude and Papathanassiou 1998/ 2003, Papathanassiou and Cloude 2001, Treuhaft et al. 1996, Treuhaft und Siqueira 2000). This makes it principally possible, to invert forest heights directly without calibration from ground data, but it must be assured that in the coherence, volume decorrelation is separated from other decorrelation sources.

Under idealized assumptions, the coherence decreases with increasing volume height in the form of a sinc-function (sin(x)/x). But a realistic forest model should also account for extinction and ground contribution in the signal as is done by the Random-volume-over-ground model (RVoG, Attema and Ulaby 1978, Treuhaft and Siqueira 2000, Papathanassiou et al. 1999a/b, Papathanassiou and Cloude 2001). To match the increase in the number of variables (height, ground, extinction), the number of observables is increased by using the coherence at different polarizations. Height results from Pol-InSAR and the RVoG were shown for L-band data of DLR's E-SAR system in Papathanassiou and Cloude (2001), and Cloude and Papathanassiou (2003).

Forest height itself is also well suited as an indicator for many of the mentioned forest functions and classifications, but in comparison to biomass, it is more difficult to define a comprehensive and representative reference measure for all the different forest types. Therefore it makes sense to analyse the feasibility of converting forest heights – which are retrieved from Pol-InSAR measurements – to forest biomass.

The task was approached with allometric equations, of which the most common one is a power function of the form $y = a \cdot x^c$ (Huxley 1932). Actually, the allometric relation between forest height and biomass is not new, but has only not been used in combination with remote sensing data. Eichhorn (1902), Gehrhardt (1909), and Assmann and Franz (1963) have described important rules of the height-volume allometry based on managed forests in Middle Europe. The simple structure and species composition of these forest types impede a general validity, but can help to understand important principles behind height-biomass allometry. It is the basis for the conversion of Pol-InSAR forest heights to forest biomass, and was already applied in Mette (2004a/b/c).

1.5 Thesis objective and structure

The main objective of the presented work is the implementation and validation of the whole processing chain from the Pol-InSAR height extraction to the allometric biomass estimation. It essentially links the technical radar science and forestry life science, and must assure conformity between the used parameters. The development of a concept of height-biomass allometry for use with remote sensing height data is a new aspect although profound knowledge is at hand from forestry science. Also, some aspects of the Pol-InSAR height inversion have further evolved during the study.

The implementation of the methodology on real data of the test site Traunstein demands the transfer of theory into practise. The successful implementation allows to validate the approach with respect to biological constraints, system configuration and implementation alternatives. The synthesis of these aspects makes it possible to evaluate the potential and limitations of Pol-InSAR for forest biomass estimations.

The following paragraphs give a short structural overview of this work. The two steps of the ‘Forest biomass estimation from polarimetric SAR interferometry’ have a clear order: (1) the Pol-InSAR height inversion, (2) the conversion of the forest heights into forest biomass by means of allometry (Fig. 1-1). However, it was decided to treat the study object ‘forest’ first (Ch. 2), and then explain the Pol-InSAR perspective on forests (Ch. 3). An experimental validation of the methodology is carried out on a data set of the test site Traunstein (Ch. 4), which finally merges into the discussion of the potential of Pol-InSAR systems for forest biomass inventories (Ch. 5).

Ch. 2, Forest Allometry: is assigned to the development of a concept of how to estimate forest biomass from forest height. This requires the definition of a reference height and biomass, and an introduction to allometric principles. The height biomass relation was then investigated from standard yield tables for tree species in Middle Europe. They were used for the derivation a reference equation and a flexible factor, the allometric level, to account for differences due to species, yield class and thinning intensity.

Ch. 3, Polarimetric SAR Interferometry: describes the derivation and implementation of the Random-Volume-over-Ground model (RVoG) for polarimetric interferometric SAR data. The model interprets the interferometric coherence as volume decorrelation, which is a function of the height distribution of scattering processes. The effect of coherence degradation due to temporal or system decorrelation and the sensitivity to the baseline configuration is discussed.

Ch. 4, Validation and Discussion: presents the validation results over a test site near Traunstein in Southern Germany. The radar data were acquired in 2003, with the L-band of the airborne E-SAR system of the German Aerospace Center (DLR). The ground data were obtained from the 1998-forest inventory of the chair of forest yield science at the TU Munich. Each step – Pol-InSAR height inversion and forest allometry – are evaluated first individually and then combined in the resulting biomass estimation. Simplified scatterer distributions like the sinc-relation between coherence and height or the direct biomass estimation from coherence are compared to the RVoG-model.

Ch. 5, Conclusions and Outlook: reviews the results and critically reflects the height-biomass allometry and the Pol-InSAR height inversion. Considerations are made on the potential and limitations of future Pol-InSAR systems to measure global forest biomass.

2 Forest Allometry

Allometry is the science concerned with the size relations of living systems. Forest allometry refers to the size dimensions in a forest. In the methodological sequence of the biomass estimation from Pol-InSAR, forest allometry comes after the processing of the radar data. However, since forest is the object of investigation, it was decided to put this topic first.

The focus of this chapter lies on the relation between forest height and forest biomass, with the aim to provide a concept of how to estimate biomass from heights. In this work, the heights are retrieved from the Pol-InSAR data, but the concept may as well be applied to other remote sensing methods that extract forest heights (like stereoscopy, lidar, interferometric radar).

This concept of height-biomass allometry is developed on the basis of allometric principles. But it requires also the definition of reference units, i.e. forest height and biomass, as well as the selection of some sort of reference forest. This task was approached using the standard yield tables for Middle Europe as the database. The underlying forest structure is simple - even-aged, single species - and the discrimination of different species, yield classes and thinning practises allows to analysis the impact of these factors on height-biomass allometry. The validation of the height-biomass allometry is carried out in Ch. 4, where the concept is applied to forest inventory data of the test site Traunstein.

Ch. 2.1 serves as an introduction into the topic forest. Ch. 2.2 agrees on the definition of a reference height and biomass embedded in a dendrometric background. Ch. 2.3 explains the theory and principles of allometry. Ch. 2.4 develops and derives the concept of height-biomass allometry using the yield tables as the primary data source. In Ch. 2.5, the results are interpreted from an eco-physiological point of view, Ch. 2.6 finally reviews the concept of height-biomass allometry from the point of view its application with remote sensing (height) data.

2.1 Forests in a global perspective

This subchapter provides a brief introduction to important aspects about forests. Ch. 2.1.1 describes the classical criteria for the definition of forest, and its discrimination against other land cover types. Ch. 2.1.2 gives a rough overview over the zincification of the world's forests, their distribution and carbon pools. Ch. 2.1.3 addresses the role of forest in a socio-cultural, economic and global change perspective, and Ch. 2.1.4 focuses on forests and forestry in Germany.

2.1.1 Forest Definition

In the most general formulation, forests are defined as plant formations that are constituted mainly from trees and cover an extent sufficient for the development of a characteristic forest climate (Burschel and Huss 1997, p. 1). The first criterion 'tree' refers to woody, upright, perennial plants with branching at the top, reaching at maturity at least

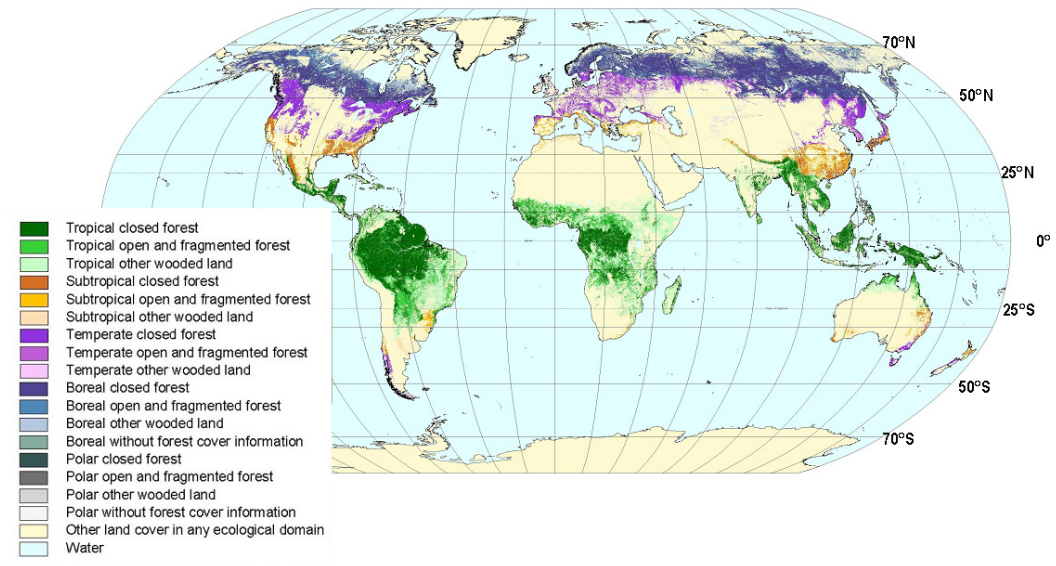

Fig. 2-1 Global distribution of forests and woodlands by major ecozones

Closed forests possess a canopy cover > 40%, open and fragmented forests 10-40%, other woodlands are woody vegetations that do not fulfil the forest criteria: > 5 m height at maturity, > 10% canopy cover, > 0.5 ha extension. Source: FAO 2001b

Tab. 2-1 Global carbon pools and carbon densities in vegetation and soil by major ecozones

Source: Dixon et al. 1994 forest statistics*, Atjay 1979 non-forest statistics

Zone	**Area**	**Carbon stock [Gt]**			**Carbon density [t ha^{-1}]**		
	[10^6 km^2]	Soil	Veg.	Total	Soil	Veg.	Total
Boreal high latitudes (55-70°)	1.372	471	88	559	343	64	407
Temperate mid latitudes (35-55°)	1.038	100	59	195	96	57	188
(Sub) tropical low latitudes (0-35°)	1.755	216	212	428	123	121	244
Total forest	4.165	787	359	1146	189	86	275
Trop. savannah, temp. grassland	3.500	559	75	634	160	21	181
Cultivated land	1.600	128	3	131	80	2	82
Wetlands	0.350	225	15	240	643	43	686
Other: tundra, alpine, (half-) desert	5.500	312	14	326	170	8	178
Global total	151.15	2011	466	2477	133	31	164

*The forest data are based on country inventories between 1987-1990. Where countries lie in more than one climate zone, they were assigned to a single zone (e.g. Australia to the temperate zone); subtropical forests were mostly included in temperate forests. The definition of forest includes both forest and woodland communities of the FAO definition (Ch. 2.1.1). The average carbon densities are therefore significantly lower than carbon densities of closed forest systems that may lie 200-500% higher, and it hides the fact that most of the carbon biomass is actually stored in forests of higher biomass densities. (c) vegetation carbon includes the total aboveground and belowground carbon of living tree and non-tree vegetation (Ch. 2.2.4).

5-7 m height. The second criterion 'characteristic forest climate' depends on height, density and extension of the forest.

The FAO (2001a/b, Annex 7.1) sets the limits of these parameters as follows:

- > 5m tree height at maturity (3m in cold or dry zones),
- > 10% canopy cover (open forest 10-40%, closed forest >40%),
- > 0.5 ha extension.

The criteria applied for the discrimination between forest and non-forest areas have important consequences. Statistics about forest cover, biomass etc. change with the definition of forest, and are often connected to legal questions concerning management, protection, subsidies, Kyoto etc., and (WBGU 1998, IPCC 2000).

2.1.2 Forest Distribution

The terrestrial ecosphere can be divided into five to nine biomes or life zones (FAO 2001a/b uses a synthesis of Köppen 1931 and Trewartha 1968 – Fig. 2-1; also common are Holdridge 1971, Bailey 1996, Walter and Breckle 1991). Biomes reflect climate zones, expressed by the annual course of temperature and precipitation. The dominant vegetation type of a biome is termed 'zonal' vegetation (Ellenberg 1996). The main zonification follows the latitudinal temperature gradient: polar – boreal – temperate – subtropical – tropical (Fig. 2-1, Tab. 2-1).

Forests are the characteristic plant formation of three biomes (latitudes roughly):

- boreal forest: continuous boreal belt between 55–70° North,
- temperate forest (often includes subtropical forest): humid temperate regions between 35–55° North and South,
- (sub) tropical forest: humid tropical regions between 0–35° North and South.

Transition zones between biomes are termed ecotones, mountainous terrain which exhibit special growth conditions are referred to as orobiomes (Walter and Breckle 1991). Local variations from the zonal vegetation due to special edaphic factors lead to the growth of azonal plant formations (Ellenberg 1996). Azonal vegetation types occur e.g. on riverbanks, at the coast, in swamps, bogs, moors, or on block fields.

As an ecological thumb rule, forests can grow where the length of the vegetation period exceeds 4 months, whereby vegetation period shall be defined as the season with a monthly average temperature higher than 5 °C and a precipitation higher than the evaporation (Schultz 1995, pp. 25). Several other factors such as soil conditions, climate history, herbivory, calamities, fires or extreme events have had and have an impact on forest distribution. The importance of these factors for the present forest distribution is controversially discussed. But today, certainly the human influence is the most decisive factor (BMVEL 2001, p. 25).

Tab. 2-1 summarizes the area and carbon (C-) storage of global forest ecosystems and non-forest land cover types (Dixon et al. 1994, Atjay et al. 1979). Since dry biomass consists to 50% of carbon (Ch. 2.2.3), carbon and biomass are often used in an equivalent sense. According to the statistics in Tab. 2-1:

- Vegetation accounts for 20% of the terrestrial carbon pool: 466 Gt of 2477 Gt. However, aboveground biomass is the only carbon pool that can actually be measured, estimates of soil biomass a largely modelled from land cover and climate data (Post et al. 1982, Dixon et al. 1994).
- Forests store 75% of the total vegetation carbon: 379 Gt of 466 Gt, and 40% of the total soil carbon: 787 Gt of 2011 Gt.
- Tropical forests represent 40% of the global forest area with 60% of the global forest carbon while the temperate and boreal forests account for 25% and 35% of the total forest cover and 15% and 25% of the forest carbon pool.

Since these numbers of Dixon et al. (1994) are still the most frequently cited carbon reference, it is important to be aware of the definitions behind them (Tab. 2-1 documentation). The Forest Resource Assessment 2000 (FAO 2001b) for instance, excludes woodlands and only regards aboveground living and dead woody biomass. The numbers are therefore significantly lower: global forest biomass 422 Gt ~ 210 Gt C, compared to 359 Gt C in Dixon et al. (1994). Houghton (2005) attributes most of the uncertainty to different assumptions of the average carbon densities in tropical countries (Brown 1997, DeFries et al. 2002, Houghton 2003, Archard et al. 2004), and to a lesser extent to an overestimation of temperate forest biomass in Russia and China by Dixon et al. (1994) compared to newer estimates by Goodale et al. (2002).

The uncertainties in the data in global forest biomass or carbon estimation can be summarized in three main problems: (1) different methodologies and definitions, (2) different availability of regional data, (3) forest area data are not enough for biomass or carbon estimates.

2.1.3 Forest importance

Due to their large area coverage and ubiquitous distribution, forests play an important role for the environmental conditions on earth, from local to global scale, and they are integrated in many ways as an economic and social good of human affairs.

In the frame of the biosphere flux of energy and matter, forests reduce atmospheric CO_2 using light energy, and thereby provide the constant replenishment of carbohydrates and oxygen for the heterotrophic levels. Forests have the capability to create favourable living conditions on the local and regional scale through manifold buffer functions. The absorption of radiation energy buffers temperature extremes in the tropics or enhances the thawing in spring in boreal regions. The reduction of the impact of precipitation and wind prevents or reduces soil erosion, the risk of landslides and excessive water runoff. The ability of forest to store large amounts of water smoothes regional runoff peaks, and buffers dry periods. The slow water percolation has also a filtering effect and improves the water quality. Of high importance is also the biodiversity, or genetic resource, of forests. Forests alone are estimated to give host to two thirds of the global biodiversity (WRI 2000, p. 99). 100000 vascular plant species or 40% of the global flora occurs alone in tropical rain forests (Archibold 1995, p. 20), of which 96% are phanerophytes, i.e. trees or shrubs (Strasburger 1983, p. 1019). Oldfield et al. (1998) estimate approximately 8700 tree species to be critically endangered worldwide.

Due to the importance of forests governments worldwide have agreed upon a catalogue of criteria to insure forest sustainability and effective functioning of forest ecosystems: ITTO – International Tropical Timber Organization in 1986, Helsinki Resolution in 1994, and Montreal Resolution in 1995 (see Grayson 1997).

Lately, most attention has been given to the possible role of forests in reducing the increase of greenhouse gases in the atmosphere, especially CO_2 (see FAO 2001a, Ch. 3). Remember, forests are the biggest aboveground vegetation C-pool (75% for 40% land cover), and contain also 40% of the soil carbon, especially the boreal forests. Most changes in the forest cover therefore affect directly the atmospheric CO_2 concentration. The growing concern about the global climate change has led to the formation of the UNFCCC (UN Framework Convention on Climate Change) in 1992 which holds the annual international Conference of Parties, short: COP.

In 1997, the COP3 passed the Kyoto Protocol (UNFCCC 1997):

- Article 3.1 legally binds the developed (Annex I) countries to reduce the emission of CO_2-equivalents[1] to at least 5% below the level of 1990 in the commitment period 2008-2012.
- Article 3.3 explicitly includes afforestation, reforestation and deforestation, abbreviated ARD-activities, in the calculation of the countries' carbon budgets.
- Article 3.4 leaves room for defining additional human-induced activities related to changes in greenhouse gas emissions and removals in the agricultural soil and land use change and forestry categories.

The issues of Article 3.3 and 3.4 are generally referred to as Land-use, Land-use-change and forestry activities, or LULUCF. The definition of the land use classes and activities, and the accounting and quantification of corresponding CO_2-equivalents is a delicate issue for the calculation of the countries' carbon budget (IPCC 2000, WBGU 1998). Yet, despite many insufficiencies in definitions and possible 'mal-interpretations', the Kyoto Protocol is generally viewed as a most important step to acknowledge an international cooperative responsibility for 'good global governance' (WBGU 1998, pp. 1). Opened for signature on March 16, 1998, and closed on March 15, 1999, the Kyoto agreement came into force on February 16, 2005 following ratification by Russia on November 18, 2004 (UNFCCC 2005).

According to Fig. 2-2, terrestrial ecosystems exchange annually 125 Gt C with the atmosphere. Despite the input from deforestation it is assumed that at the moment vegetation acts as a net sink for carbon of 1-2 Gt y^{-1} (Houghton 1999, Malhi et al. 1999, Schimel et al. 2001[2]). Still with the ocean- and vegetation C-sink of 5 Gt y^{-1} the anthro-

---

[1] Six Greenhouse Gases (GHG: CO_2, CH_4, N_2O, HFCs, PFCs, SF_6) are assigned a Global Warming Potential (GWP) in CO_2 equivalents. The GWP is the ratio of the radiative forcing that would result from the emissions of 1kg of that greenhouse gas to that from emission of 1kg CO_2 over a period of time (usually 100 years). (IPCC 2001a, p. 47, Tab. 3)

[2] The assumption of the terrestrial uptake results from the difference of [Emissions from fossil fuel combustion and cement production + LULUCF-activities] – [Storage in the atmosphere + Ocean uptake] = 1.8-2.3 +/- 1.0 Gt C(IPCC 2000, Ch.2).

pogenic emission of 8.5 Gt y^{-1} cannot be compensated and increases the atmospheric C-pool by 3.5 Gt y^{-1}. The role of forests in the global change scenario is complex. Carbon sequestration strategies like afforestation and reforestation yield a capacity for 38 Gt in the next 50 years (IPCC 2001b, Ch.3.2), carbon conservation strategies like the stop of deforestation, reduced impact logging or fire prevention another 10-20 Gt (IPCC 2001b, Ch. 3.2), and carbon substitution like an increased use of bio fuels already prevent the exhaustion of further 1.1 Gt (IPCC 2000, Ch. 5). The actual potential of these carbon management strategies is very uncertain given the projections of human population growth and energy consumption. But surely, forests will play a critical role for future environmental conditions and poverty alleviation (FAO 2001a, p. 26).

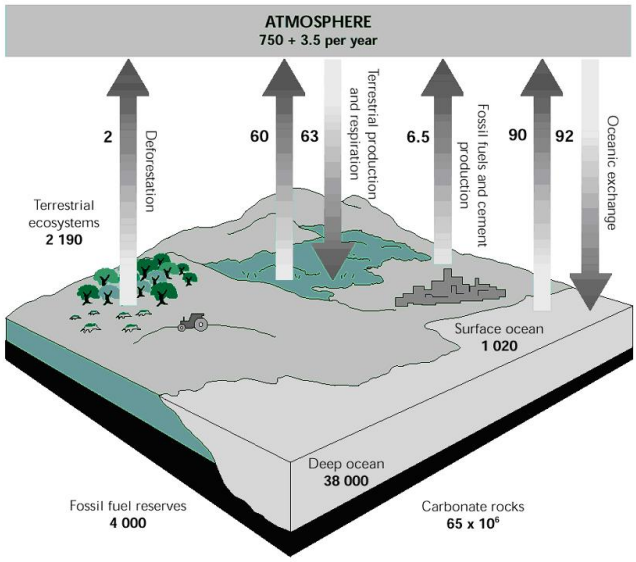

[1]All numbers are in gigatonnes (Gt) of carbon (1 Gt = 1 billion tonnes).

Note: The magnitude of the fluxes between the atmosphere and the oceans and terrestrial biosphere is still uncertain and is the subject of ongoing research.

Fig. 2-2 Global carbon cycle
Source: FAO 2001a

Further on, the forests themselves are subject to climate change. Falkowski et al. (2000, p. 293) comes to the conclusion that 'the negative feedback afforded by the terrestrial ecosystems in removing anthropogenic CO_2 from atmosphere will continue; however the sink strength will almost certainly weaken.' (see also: Burschel et al. 1992, Bazzaz 1990, Jarvis and Linder, 2000, Schimel et al. 2001).

2.1.4 Forests in Germany

Germany is part of the bio-geographical unit Middle Europe (in the sense of Ellenberg 1996) which represents the central part of the temperate forest biome of western Eurasia. Mild summers and winters (annual average ~10 °C) and perennial cyclonal rainfalls (typically 600-800 mm y^{-1}) favour the growth of cold-deciduous broadleaf forests as the zonal plant formation. Without anthropogenic interference, an estimated 80% of Germany would be covered by forest, in western and southern Germany mainly by European beech, *Fagus sylvatica* (Ellenberg 1996, pp. 117, Fig. 2-3). Today, 30% or 107000 km^2 are mostly commercially managed forests (BMVEL 2001). The highly competitive beech has often given way to fast growing Norway spruce (*Picea abies*, Fig. 2-3) or Scots pine (*Pinus silvestris*) forests, which would naturally be restricted to higher altitudes in the case of spruce or to unfavourable site conditions in the case of pine (Ellenberg 1996, p. 117). The present species spectrum is composed of 35% Norway spruce (incl. few other conifer species), 31% Scots pine (incl. European larch *Larix decidua*), 25% European beech (incl. few other broadleaf species), and 9% oak (*Quer-*

cus robur) (BMVEL 2001). The overall tree species diversity of Middle Europe is with 53 naturally occurring species (Ellenberg 1996, p. 31) small compared to the North American or East Asian humid temperate biome.

Norway spruce (*Picea abies*, L.)
Distribution: Nat. domination in upper montane, lower alpine region of Alps, SE-German mid-ranges, dominant Eurasian boreal species west of Ural, principal forestry species in Middle and North Europe
Growth: height and volume growth culmination after 40 a, heights up 50 m, to life span > 200 a
Ecology: evergreen conifer, medium light demand for regeneration, flat root system leads to storm-vulnerability, typical calamities: bar beetle, fungus

European beech (*Fagus sylvatica*, L.)
Distribution: Natural domination in most of South and West Germany, independent of substrate, marginal areal outside temperate Europe
Growth: height and volume growth culmination after 40 a and 75 a, respectively, heights up to 40 m (45 m), life span > 300 a
Ecology: cold-deciduous broadleaf, little light demand for regeneration, horizontal-vertical root system, typical calamity: browsing

Fig. 2-3 Ecological and forestry-related characteristics of Norway spruce and European beech

Source: Schütt et al. 2002, Burschel and Huss 1997, Aas and Riedlmiller 1987

In a global context, the forests of Germany represent 0.25% of the world's forest area, and 0.35% or 1.44 Gt of the world's aboveground woody biomass. The biomass density of 134 t ha^{-1} and volume density of 270 m^3 ha^{-1} are comparably high (numbers and definitions according to FAO 2001b, see also Ch. 2.2.4). According to Zanatta et al. (2000/ 2001) the annual volume growth amounts to 8 m^3 ha^{-1}, yet only 4.6 m^3 ha^{-1} are harvested each year including natural losses due to storms, fire, and insect calamities. The annual surplus of 3.4 m^3 ha^{-1} is higher than the 2.2 m^3 ha^{-1} BMVEL report (2000). The increase in volume or biomass density is a general trend in Europe and the northern hemisphere (Zanatta et al. 2000/ 2001) and accounts for much of the postulated terrestrial carbon sink (Schimel et al. 2000, Goodale et al. 2002). Environmental changes like the increased vegetation period, N-deposition and the increased atmospheric CO_2-concentration have altered growth conditions. From inventory data in Southern Germany, Pretzsch (1999) documented 12-43% growth increase for four main forestry species between 1970 and 1987, compared to the yield tables (from the first half of the 20th century). This finding seems to approve a general European trend (Kauppi et al. 1992, Spiecker et al. 2002).

As a highly industrialized and densely populated country (0.1 ha forest per capita), Germany has a long forest management history that pursues a sustainable high yield timber production (BMVEL 2001, BWaldG §§1 and 11). Timber production is still the most important financial source of forestry (90%, BMVEL 2001, p. 52), and the revenue from wood selling must also cover the costs for maintaining the recreational and protection functions of the forest. Against this background, an increased 'naturalness' of forests in form of promoting site-appropriate tree species and natural regeneration, is rather the consequence of stability and sustainability needs than expression of forest aesthetics or a trend towards natural forests (Burschel and Huss 1997, pp. 464). 10% of the total forest area in Germany is protected by national and federal forest and nature conservation laws (BMVEL 2001, p. 34).

2.2 Forest Parameters

This subchapter gives an overview over the definition, calculation and measurement of tree and forest parameters. The main importance lies in defining a reference height and biomass, that makes sense both from the forest and the remote sensing point of view. But also forest density needs to be addressed since it is indirectly included in the height-biomass allometry.

Ch. 2.2.1 and Ch. 2.2.2 describe the basic dendrometric parameters and relations on tree and forest level respectively. Ch. 2.2.3 treats the relation between volume, biomass and carbon in detail and leads to Ch. 2.2.4 where different volume and biomass standards are compared with the reference biomass used in this work. Ch. 2.2.5 shows how tree and forest parameters are acquired in a forest inventory. Such inventory data were used for the validation of the Pol-InSAR height extraction and the allometric biomass estimation in Ch. 4.

2.2.1 Tree parameters

A tree is a woody, upright, perennial plants with branching at the top, reaching at maturity at least 5-7 m height (Ch. 2.1.1). The main parameters that characterize a tree in a dendrometric sense are:

- Tree species: relates to wood density and tree shape
- Tree dbh [m]: diameter at breast height 1.3 m above ground
- Tree height [m]: vertical distance between ground and tree top
- Tree volume [m^3] or biomass [t]: most integrative structural tree parameter.

While volume is rather the forestry standard, biomass is the ecological standard. Biomass can be calculated from volume through multiplication with species-specific wood weight ρ [g cm^{-3}]:

$$Biomass = Volume \cdot \rho \qquad \textbf{Eq. 2-1}$$

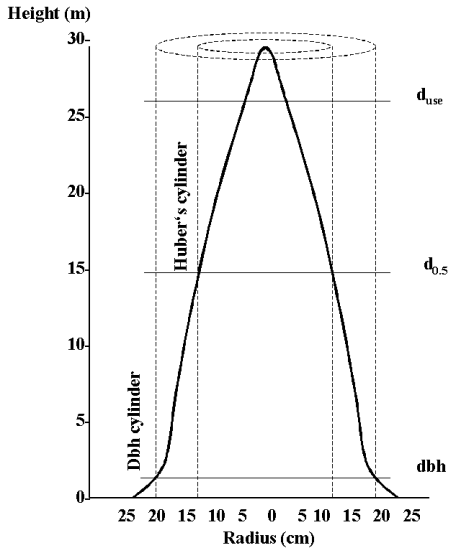

Fig. 2-4 Trunk of a Norway spruce tree

Diameters at different heights: dbh = diameter at breast height (1.3m above ground), $d_{0.5}$ = diameter at ½ the tree height, and d_{use} = diameter limit of usable wood volume (7cm).

Source: after Kramer and Akça 1995, p. 180, altered

Volume or biomass is typically defined as stem volume or biomass, usable wood volume or biomass, or total wood volume or biomass (Fig. 2-6). Biomass can also include non-woody parts of the tree. A closer treatment is given in Ch. 2.2.4.

The stem volume v_{stem} can be calculated from tree height h, diameter dbh (diameter at breast height, 1.3 m above ground) and the shape factor f_z; tree biomass b_{stem} is obtained after multiplication with the wood density ρ (Kramer and Akça 1995, pp. 68).

$$v_{stem} = h \cdot \pi\left(\tfrac{1}{2} dbh\right)^2 \cdot f_z$$
$$b_{stem} = h \cdot \pi\left(\tfrac{1}{2} dbh\right)^2 \cdot f_z \cdot \rho \qquad \textbf{Eq. 2-2}$$

The shape factor f_z accounts for the tree shape, for the height of the reference diameter (dbh at 1.3m), and for the definition of volume. It typically assumes values about 0.5. When measuring the diameter at the ½-height instead of the dbh, f_z equals 1 (Huber's cylinder in Fig. 2-4, Huber 1928).

2.2.2 Forest parameters

A forest comprises a population of trees with a certain extent and canopy cover (Ch. 2.1.1). The term 'stand' refers to a certain forest area, typically a management unit with similar species composition, structure, and management. In this sense, 'forest' parameters are mostly given as 'stand' parameters. In this work, the more general term 'forest' was preferred.

In a forest, tree height, diameter and volume or biomass are represented by frequency distributions and become forest height, basal area and forest volume or biomass. These dimensions have either a statistical nature, like average tree height, or an integrative nature, like basal area and volume or biomass. Forest parameters are typically given relative to the area unit hectare [ha]: 100m x 100m.

As long as remote sensing systems do not resolve single trees, the reference parameters must be forest parameters, not tree parameters. The considerations which measure to use as a reference depends on signal and model characteristics and forest structure.

Species composition: Forests dominated by a single-species are typically managed forests or plantations. In natural forests, the species diversity increases from boreal to temperate to tropical forest ecosystems (see Ch. 2.1.3).

Forest height: The height that was regarded the most characteristic height from a forestry-, ecology-, and also remote sensing perspective, was the 'upper canopy height'. The reasons for the decision are outlined in detail in the following (Mette et al. 2004a):

- Ecologically, the trees of the upper canopy are exposed to the sun light and concentrate a large part of the total forest biomass. Their height and density determines the microclimate and ecological processes within the forest.
- For mature forests, the upper canopy height is the main indicator of the site conditions (Assmann 1961, Barnes et al. 1998) and the forest type (UNESCO 1973), and can be used to estimate the growth and yield potential of a forest.
- In the field, the upper canopy height is simple to measure; few representative trees are sufficient for a good estimate. Sub-canopy trees can be disregarded.
- From the perspective of remote sensing and forest modelling, it makes sense to use a height measure that corresponds to the forest top and not some in-between-height.

An upper canopy height makes sense if the upper canopy is more or less closed. If the tallest tree layer consists of exceptional emergent trees or the canopy is open, the representativeness of any single height measure is questionable (see Fig. 2-5).

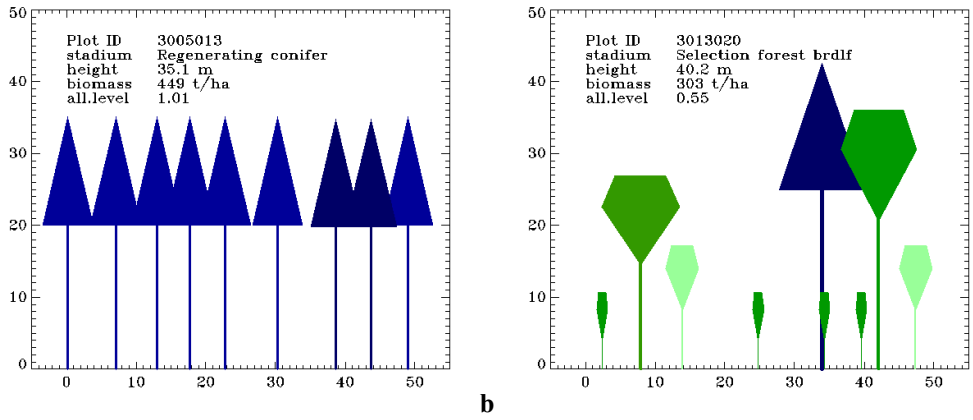

Fig. 2-5 Height definition in a dense even-aged forest and open uneven-aged forest

(a) even-aged dense spruce-fir forest; the height of 35m is representative, (b) uneven-aged open selection forest with 5 different layers. The upper canopy height of 40 m is not representative. Examples taken from the Traunstein forest inventory (Ch. 2.2.5, Ch. 4.1.2).

Related forestry definitions are the 'h_{100}', the Weise-height or the mid height of the highest tree layer (see below, Kramer and Akça 1995, p. 145):

- The top height h_{100} refers to the 100 trees per hectare of the highest diameter, other conventions use also 50 or 200 trees.
- The Weise-height h_w includes the highest 20% of all trees.
- The mid height h_{mid} includes all trees. It can serve as an upper canopy height when determined separately for the highest layer. It served as the reference height from the yield tables (Ch. 2.4.2), and from the forest inventory data where it was given separately for the upper canopy layers (Ch. 4.2.1, Eq. 4-1).

However, it is recommended to refrain from a too literal definition of the upper canopy height, to allow a wider applicability and include different national standards.

Forest Volume and Biomass: The choosing of an adequate volume or biomass definition was more complicated than the height definition. Several well established standards exist, each of which serves a certain demand (Ch. 2.2.4). After a closer inspection, the most sensible definition appeared to be the stem biomass, because it is a 1st order parameter from dbh- and height distributions, and is relatively accurate. The total tree biomass (including leaves, branches and roots) or ecosystem biomass are 2nd order parameters, mostly extrapolated from regressions (Ch. 2.2.4).

The forest stem biomass B_{forest} is calculated as sum of the individual stem biomasses $\Sigma\, b_{stem}$. If the tree dimensions are more or less similar – like in an even-aged forest – then the biomass of the basal-area weighted average tree, denoted with the suffix 'mid', is multiplied by the tree number per hectare N:

$$\begin{aligned} B_{forest} &= \sum b_{stem} \\ &= h_{mid} \cdot N \cdot \pi(\tfrac{1}{2} dbh_{mid})^2 \cdot f_z \cdot \rho_{mid} \\ &= h_{mid} \cdot G \cdot f_z \cdot \rho_{mid} \end{aligned} \qquad \textbf{Eq. 2-3}$$

In contrast to the stem biomass calculation for the single tree (Eq. 2-2), the shape factor f_z not only accounts for tree shape, dbh-height and biomass definition, but also for the

height and dbh frequency distributions. It can be roughly approximated with $f_z \sim 0.5$. The species-specific wood-density ρ relates volume to biomass (Eq. 2-1). For mixed-species forests, the average wood density ρ_{mid} must be derived from the species composition. Again, an approximation of $\rho = 0.5$ g cm^{-3} for conifers and $\rho = 0.6$-0.7 g cm^{-3} for broadleaves is possible. The product of $N \cdot \pi \cdot (½dbh)^2$ is termed basal area G (see below).

The forest stem biomass in Eq. 2-3 is closely related to the FAO standard VOB_{10} (volume over bark of all trees of > 10 cm diameter, FAO 2001a/b), and to the forestry standard 'usable' wood volume (stem + branches > 7 cm diameter, Fig. 2-6, Lohmann 2003, Kramer and Akça 1995, p. 63, Prodan 1965, pp. 7). Both forest inventory data and standard yield tables mostly refer to 'usable' wood volume[3] (Ch. 2.4.2, Ch. 2.4.5, Ch. 4.1.2). A strong disadvantage of the dbh-limits in the VOB_{10} and usable wood volume is, that trees and stands below ~10 m height have virtually no volume or biomass which leads to a poor representation of young re-growing trees and forests. This effect will be noted in the validation of the height-biomass allometry from the inventory data of the test site Traunstein (Ch. 4.1.4).

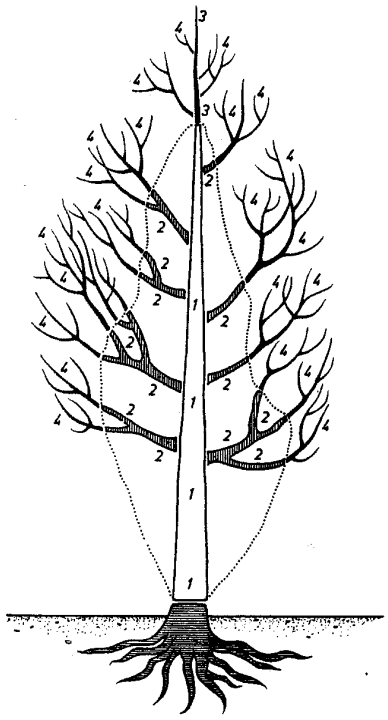

Fig. 2-6 Wood classification
Source: Prodan 1965, p. 11

Forest density: Forest density describes the horizontal forest dimension. It is not explicitly part of the height-biomass relation. But as Eq. 2-4 shows, the height-biomass relation is partly a self-correlation which is basically underlain by a height-basal area allometry (assuming a single-layered forest and a constant f_z in Eq. 2-3):

$$\begin{aligned} B_{forest} &\Leftrightarrow h_{mid} \\ h_{mid} \cdot G &\Leftrightarrow h_{mid} \\ G &\Leftrightarrow h_{mid} \end{aligned} \qquad \textbf{Eq. 2-4}$$

B_{forest} is the forest stem biomass, h_{mid} the mid height and G the basal area. The basal area therefore plays an important role in this work. It is defined as (Kramer and Akça 1995, pp. 147):

$$\begin{aligned} G &= \pi \cdot \sum (½\,dbh)^2 \\ &= N \cdot \pi \cdot (½\,dbh_{mid})^2 \end{aligned} \qquad \textbf{Eq. 2-5}$$

[3] In inventory data also bark subtraction (6-20%) and harvest loss (10%) (see Ch. 2.2.5).

Eq. 2-5 identifies the basal area as the cross-sectional area of all trees at their dbh-height. Another forest density measure that is used in this work is the stand density index SDI. In contrast to the basal area which is actually present, the SDI is allometrically projected to a mid dbh of 25.4 cm, i.e. 10 inches (Eq. 2-7). The stand density index is based on the self-thinning rule from Reineke (1933). He found that in even-aged Douglas fir stands, the relation between dbh-increase and tree number decrease followed an allometric function with a fixed allometric exponent of c = -1.605 (Eq. 2-6). The stand density index SDI is based on this relation (Eq. 2-7):

Reineke rule $$N \propto dbh_{mid}^{-1.605}$$ **Eq. 2-6**

Stand density index SDI $$SDI = N \cdot (25.4 / dbh_{mid})^{-1.605}$$ **Eq. 2-7**

While widely accepted and applied in US-forestry, in Germany the SDI was adopted to the metric system by Daniel et al. only in 1979 and verified for forests in Middle Europe by Sterba (1981). Lately, the universal validity of the Reineke exponent –1.605 was shown to vary between species (Pretzsch and Biber 2005, Pretzsch 2006). In an eco-physiological interpretation, the Reineke exponent stands for the self-tolerance of a tree species in the sequestration of crown space (Zeide 1985). For an exponent lower than –2 the crown expansion is so high that self-thinning exceeds dbh-growth, leading to a basal area reduction during growth. When the Reineke rule is applied to uneven-aged stands – here more generally termed size-density or size-frequency relation – the overall variation of the exponent has been regarded so low as to be called 'invariant' (Enquist and Niklas 2001). The relation between height-biomass allometry and the Reineke rule will be addressed in Ch. 2.4.4.

2.2.3 Wood chemistry, wood anatomy and wood density

For a better understanding of the relation between volume, biomass and carbon content of wood, a short background on wood anatomy is necessary. Wood is in first place the water conducting xylem tissue of the tree (Fig. 2-7). The xylem is composed mainly of elongated hollow dead cells with strong cell walls, termed tracheids in conifers, and vessels in broadleaves. These cell walls make up the most of the dry wood biomass. Chemically, they are composed of (Scheffer and Schachtschabel 1998, p. 247, Lohmann 2003, p. 1-212, Nultsch 1996, p. 120):

- 30-40% cellulose (C:H:O ~ 44:6:50)
- 30-40% hemicellulose (C:H:O ~ 44:6:50)
- ~25% Lignin (C:H:O ~ 63:7:30)
- 2% proteins, 1% lipids, and little Ca^{2+} and Mg^{2+}

The cambium, an actively dividing (meristematic) outer ring close beneath the bark, constantly adds new xylem tissue inwards to replace the old one. It also renews the assimilate conducting outer phloem; the bark has its own meristem. This continued inwards-adding of xylem tissue is the secondary growth, and leads to the diameter increase of the stem or branch. The cambium follows through radial cell division; phloem and bark are constantly replaced. Only the young outer xylem tissue actively conducts water (sap-wood), the older xylem tissue towards the centre of the stem or branch be-

comes inactive (heart-wood). The seasonal cyclical adding of xylem tissue causes the characteristic year rings in temperate and boreal trees.

The wood density is basically a mixture of pure wood, $\rho_{pure} = 1.5$ g cm^{-3}, and pore volumes, $\rho_{pores} = 0$ g cm^{-3} (Lohmann 2003, p. 1-199/ 2-272). While the pure wood density is species-independent, the average pore volume and hence the resulting density is highly species-specific. In boreal and temperate forests with distinct growing seasons, the wood density also shows an annual pattern: low density for early season tissue, high for late season tissue (Schweingruber 1983, p. 59, Fig. 2-8). The average density increases under favourable conditions in the late growing season, because then cell wall thickening is stronger (Schweingruber 1983, pp. 120). Intra-specific and inter-annual differences are due to the prevailing growth conditions: climate, soil, social position in the stand, hazards, calamities, etc. (Schweingruber 1983, pp. 115). For White fir, Trendelenburg and Mayer-Wegelin (1955) showed differences in average wood raw density between 0.33-0.60 g cm^{-3}, for Norway spruce, Pechmann (1974) documented 0.35-0.5 g cm^{-3}. Species of large ecological amplitudes and broadleaves in general probably respond stronger to growth conditions than evergreen conifers, because the width of broadleaf xylem vessels can be better adapted to water demand and availability than of the conifers' tracheids.

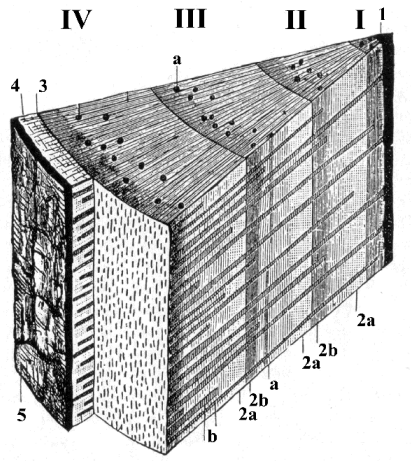

Fig. 2-7 Cut through a 4-year old pine stem

I-IV years, 1=mark, 2a=early season wood (xylem), 2b=late season wood (xylem), 3=cambium, 4=bast (phloem), 5=bark, a=resin channel, b=wood rays. Source: Strasburger 1985, p. 165

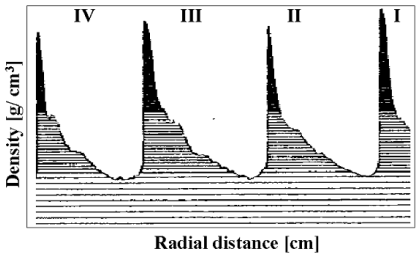

Fig. 2-8 Change of wood density between early and late season wood

Source: Schweingruber 1983, p. 77

The most common wood density unit which is also used in this work, is the raw density ρ_{raw} for 12% water content (Lohmann 2003, p 2-272). Wood raw densities vary species-specifically between 0.2 and 1.2, most densities range from 0.4 to 0.7 (Lohmann 2003, p 2-244/ 2-272). The terms soft- and hardwood refer to raw wood densities below and above 0.55 g cm^{-3} and – with few exceptions – divides conifer and broadleaf species.

An alternative density measure is the 'volume' density (german: 'Raumdichte') which relates the oven-dry wood mass (0% water) to the fresh volume (Lohmann 2003, p. 2-244). According to the chemical composition of the cell walls, the carbon content of wood is fairly constant 50% of the dry biomass (Lohmann 2003, p. 1-212).

2.2.4 Volume and Biomass standards

In this work, biomass was defined as stem biomass as a 1st order parameter from tree diameters, heights and wood density. Especially for carbon stock estimations, it is important to consider the biomass of all parts of the tree: stem, branches, leaves (flowers and roots). Direct measurements of all contributions are very elaborate and not practicable in large-scale inventories. Therefore most approaches are restricted to measuring dbh or stem biomass and deriving branch, leaf biomass and root biomass with regressions. Fig. 2-9 shows the biomass allocations of Norway spruce and European beech according to Nihlgard (1972), Ellenberg (1986), Pellinen (1986). It can be observed that: (1) stem biomass dominates once the tree exceeds 10m height, (2) the needles of Norway spruce represent a higher biomass fraction than the leaves of European beech, (3) branches play a higher role in beech during youth.

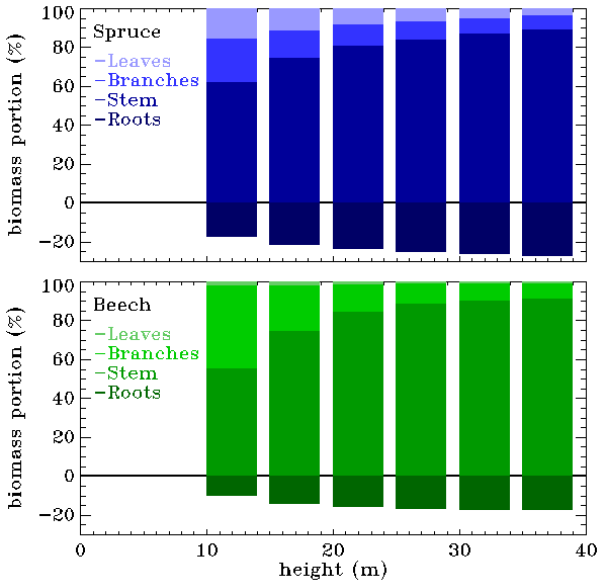

Fig. 2-9 Biomass partitioning between stem, branches, leaves and root for Norway spruce and European beech as a function of height

Values relative to above-ground biomass: 100% = stem + branch + leaves, height classes: 10, 15, 20, 25, 30, 35 m. Data source: Nihlgard 1972, Ellenberg 1986, Pellinen 1986

In general, the use of different volume and biomass standards makes the comparison between literature data almost impossible without tracing back the source data base. This problem became already apparent in Ch. 2.1.2 when trying to explain the global biomass differences between Dixon et al. (1994) and the FAO report (FRA 2001).

Most forest volume or biomass estimates are based on simple dbh-measurements and sometimes also height. Few studies have harvested the whole tree, even fewer also roots (Fig. 2-9), e.g. Cole and Rapp (1981) for boreal and temperate forest, Fittkau and Klinge (1973) for tropical forest. Almost none quantified the amount of non-tree or dead vegetation (e.g. Brown and Lugo 1982). Generalized regressions that extrapolate the tree dbh or volume measurements to the other biomass components are therefore often uncertain. In reference to Brown and Lugo (1992, see Brown 1997), these regression factors are termed biomass expansion factors (BEF). If the dbh limit was chosen very high, it might also be necessary to account for missing dbh classes with so-called volume expansion factors (VEF, Brown 1990, see Brown 1997). Fig. 2-10 tries to give an overview over the relation between the different volume or biomass standards.

The FAO uses two standards, the VOB_{10}, the volume over bark of all trees above 10 cm dbh, and aboveground biomass, which includes the woody part (stem, bark, branches, twigs) of trees, alive or dead, shrubs and bushes (FAO 2001b, p. 368, Annex 7.1). The VOB_{10} rather addresses the forestry community and represents what was actually meas-

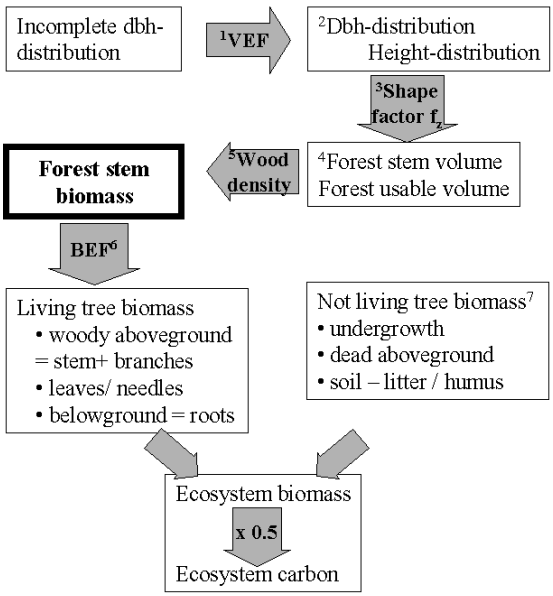

Fig. 2-10 Biomass allocations in a forest ecosystem

[1] VEF – Volume Expansion Factor compensates missing dbh-classes, [2] dbh distribution – easiest input measure to extrapolate on height, volume and biomass of stem, tree or ecosystem, 3 Shape factor fz – geometrical factor from dbh-height cylinder to volume, [4] Forestry standard - accurate determination from dbh and height measurement ('usable' in Germany), [5] wood density ~0.5 for softwood, ~0.6 for hardwood, [6] BEF – Biomass Expansion Factor, empirical regressions relatively accurate if some information on forest type, forest height, density, 7 only rough approximation through assumptions from ecosystem or forest type

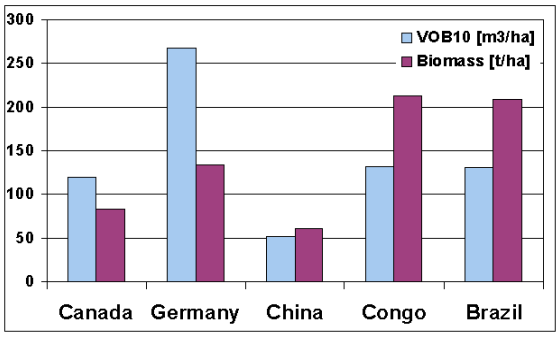

Fig. 2-11 Average stem volume and forest biomass for 5 sample countries

VOB_{10} = stem volume of trees above 10cm dbh, biomass = woody part (stem, bark, branches, twigs) of trees, alive or dead, shrubs and bushes

Data source: FAO 2001b

ured; aboveground biomass addresses more the ecology and global change community, and was derived from the dbh or volume data by using more or less generalizing regressions. Fig. 2-11 shows volume and biomass samples from the FAO forest resource assessment 2000 (FAO 2001b). While the biomass data seem to reflect a latitudinal gradient from boreal (Canada) to humid temperate (Germany) to ~ semiarid subtropical (China) to humid tropical (Congo, Brazil), the VOB_{10} is except for Canada and Germany lower than the biomass. Assuming an approximate wood weight of 0.6 (Reyes 1992, see Brown 1997), in China only 51%, in Brazil and Congo only 37% is concentrated in the stems of trees above 10cm. This contradicts many other literature sources (e.g. summaries by Schultz 1995, pp. 478/ 481), and can only be partly explained: (1) branch volume seems to be more important in tropical forest in general; Brown and Lugo (1992, see Brown 1997) propose biomass expansion factors of 3…1.75 for stem biomasses of 50…200t ha^{-1}, (2) the definition includes forest down to 10% canopy cover, where branches play a higher role, (3) in the search for the archetype of a the tropical forest, ecologists tend to choose unrepresentatively well developed sites (Brown 1997, Ch. 2, Dixon et al. 1994). However, it should not be forgotten that forming an average over forest from 10-100% canopy cover dilutes the fact that – assuming an even distribution in each canopy cover class, and biomass proportional to canopy cover – actually 70% of the total biomass is stored in forests with a biomass density higher than the average biomass density.

2.2.5 Forest inventory

The standard source for dendrometric data are forest inventories. Also in this work, the extracted heights from Pol-InSAR and the height-biomass allometry are validated from forest inventory data (Ch. 4).

Forest inventories are carried out to document the state of a forest in its spatial distribution and development in time (Zöhrer 1980, p. 13). Different inventory types focus on different parameters, e.g. forest area, (usable) wood volume, tree health, and biodiversity. Repeated inventories document changes in time, and are important to estimate growth rates, a-, re- and de-forestation (ARD), or responses to changing growth conditions. Until today, most inventory parameters can only be acquired from the ground. In contrast to air- or space borne images, which provide area-continuous information, ground inventories are essentially based on samples. Distribution and density of the samples as well as the sampling technique itself has to be adapted to the purpose of the inventory.

The standard forest inventory of Bavaria served as the most important quantitative forest information source in this work. It was developed in the mid 1970s and successively also adapted by other federal states (Biermayer 1999). The inventory is carried out district-wise and repeated every 10 years. A sampling grid of 100-225 m edge length (1-5 ha) is laid over the forest area, the sampling technique is based on single-tree measurements (StMELF 1982). In contrast to the national forest inventory (BMJ 2000), the federal inventory is only carried in federal forest.

One inventory plot represents a circular area of 400-500m^2 (0.04-0.05 ha), in which all trees are recorded in four concentric circles depending on their dbh. Fig. 2-12 shows an example for a spruce inventory plot in Traunstein.

Species, dbh are determined for every tree inside the corresponding circle, the height is measured for few representative individuals. These ‘raw’ data on the individual tree level are condensed to layers according to the following scheme:

- Layer assignment: (0) no stratification possible, (1) upper canopy: characteristic forest height, (2) understorey: second layer if distinguishable and upper canopy above 5 m, (3) regenerating, (4/5) emergents: solitary trees. The layers are species specific; the assignment of the sampled trees to layers is independent of the dbh limits used for the circles (see Fig. 2-12).
- Tree height measurements are very difficult and time-consuming especially if the forest is dense and tall. Therefore height is only measured for representative sampling trees of each species by averaging 2 triangulations. The height of the not-sampled trees is then calculated from a plot- and species-specific dbh-height regression according to Petterson (Kramer 1995, p. 134). The mid height is then derived as the height corresponding to the mid dbh in the plot- and species-specific dbh-height regression. Since trees in one layer do not deviate much in height, the mid height is a very representative height measure for each layer.
- Volume: is defined as harvestable usable wood volume without bark. This means that from the usable volume, i.e. stem + branches > 7 cm diameter, 10% harvest loss and 6-20% bark loss (species specific) are additionally subtracted. For our reference unit stem biomass, harvest and bark loss must be compensated, but the ‘usable’ cri-

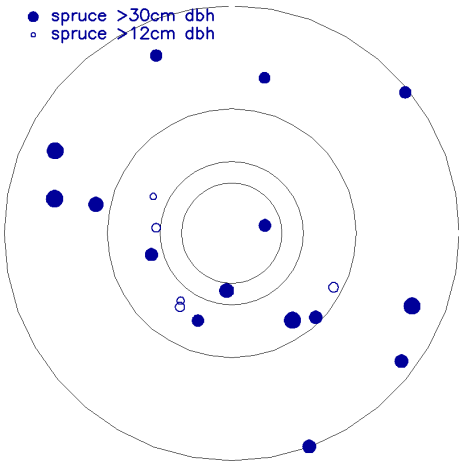

Fig. 2-12 Inventory plot example of the test site Traunstein

Circle parameters				Raw Inventory			Layer assignment			
No	Area (m^2)	Radius (m)	Dbh limits (cm)	Species	Samples	N (ha^{-1})	Layer	h_{mid} (m) dbh_{mid} (cm)	N (ha^{-1}) g (m^2 ha^{-1})	V_{use} (m^3 ha^{-1}) B_{use} (t ha^{-1})
1	500	12.62	> 30	spruce	15	300	Upper canopy	27.6 / 32.3	635 / 52.5	566 / 328
2	150	6.90	12-29.9	Spruce	5	335				
3	50	3.97	6-11.9	-	-	-		- / -	- / -	- / -
4	25	2.78	0-5.9	Spruce	15	6000	Regene-rating	0.2 / -	6000 / -	- / -
				Beech	2	800		0.2 / -	800 / -	- / -
				Sorbus	1	400		0.3 / -	400 / -	- / -

terion makes the volume data little representative for plots with a significant portion of regenerating and young trees.

Many forest inventories use a strictly rectangular sampling grid instead of stratified grids like a stand-wise sampling. This rectangular sampling assures objective and statistically representative information on the large scale (district), but the local representation area of the plot is confined by the (not rectangular) stand borders. This must be considered when using the inventory data for a spatial validation.

The accuracy of inventory parameters shall be discussed on three levels:

- On the tree level, the main uncertainty usually lies in the tree height measurement. Typical measurement errors in temperate forests can be assumed about 10%, increasing with density and height. An accuracy control of the Bavarian forest inventory showed dbh-accuracies better than 2 cm for more than 90% of all sampled trees, height accuracies with 1.4 m standard deviation and 6 m at maximum (Bauer, 2001, Ch. 3.7).
- On the plot level, the accuracy of these forest parameters is a statistical function of the number of sample trees so that the sampling area can be adapted to the tree number expected for given dbh-classes as done in the forest inventory. As already mentioned in Ch. 2.2.2, a few representative trees are sufficient for the upper canopy height estimation. However, any simple height value makes no sense heterogeneous canopies (Ch. 2.2.2, Fig. 2-5). The main problem of basal area is density variations

in the tree distributions which can only be accounted for with larger sample areas or a denser sampling grid. Volume or biomass as the product of height and basal area combines errors in height, dbh and tree number. Bauer (2001, Ch. 3.7) found volume accuracies of 30 m^3 standard deviation and 100 m^3 at maximum for the forest inventory in Bavaria.

- On the regional level, the accuracy of the forest parameters is a function of the density of inventory plots in comparison to the spatial heterogeneity of the forest. Yet, the main problem is not so much the statistical accuracy, but the representation area of the inventory plot. Often the spatial information - the 'where?' – is more important than a large statistical average. The spatial information can only be used where the sampling grid is smaller than the spatial heterogeneity of the forest. The big advantage of remote sensing is exactly this 'area-continuity', and its usefulness is a trade-off between possible parameter accuracy and needed spatial accuracy (e.g. Houghton 1999).

2.3 Theory of Allometry

This subchapter is concerned with the theory of allometry, which is the background for a concept of height-biomass allometry (Ch. 2.4.1). Ch. 2.3.1 introduces the general allometric equation of Huxley (1932), and the importance of reference function and allometric level. Ch. 2.3.2 reviews allometry in its original sense as growth allometry and distinguishes it from comparative allometry. Ch. 2.3.3 deals with theoretical aspects about plant allometry.

2.3.1 Allometric equation

Allometry [gr.: *allos metros* - indirect measure] is the science concerned with the description and causality of deterministic size relations in organisms. Today, size relations are understood as the result of phylo- and ontogenetic evolution, that have optimised and still optimise functional advantages and obligations: "Organic proportionalities often reflect consequences of natural selection operating on the relation between form and function" Niklas (1994, p. 1). In this sense, the study of allometry is motivated by the seeking to understand the adaptations of the living nature to its environment.

Besides the physiological and evolutionary implications, allometric relations are quite practical when estimating a size dimension from another that is much easier to measure. This is needed when forest biomass shall be estimated from forest height.

The allometric equation: Historically, Galileo Galilei's "Discorsi e dimostrazioni mathematiche" (1638) was the first record where – based on architectural principles – the shape of organisms is discussed on a functional (mechanical) background. Then, half a century after Darwin's theory of evolution, D'Arcy Thompson's "On growth and form" (1917), showed that form and shape of organisms have altered in the course of evolution towards a functional optimisation (transformation theory). Yet D'Arcy Thompson never acknowledged the work of his contemporary Huxley "Problems of relative growth" (1932) and Teissier (1934), who coined the word 'allometry' (also Huxley and Teissier 1936). They postulated that 'the relative growth of an organ keeps

a constant ratio to the relative growth of other organs or the whole organism' (Bertalanffy 1942, p. 275):

$$\frac{dy/y}{dx/x} = c \qquad \textbf{Eq. 2-8}$$

The mathematical solution of the relative growth equation (Eq. 2-8) is a power function, that is today so widely accepted that it is called 'allometric equation'. The allometric factor is denoted 'a', the allometric exponent 'c'. There is a linear and logarithmic representation):

$$\begin{aligned} y &= a \cdot x^c \\ \ln y &= \ln a + c \cdot \ln x \end{aligned} \qquad \textbf{Eq. 2-9}$$

In literature, the logarithmic representation is the most frequently applied one because the linearity is an easily visible indicator of an allometry in the sense of Huxley, and study objects may vary over several orders of magnitude. However, for limited size ranges with linear intervals the logarithmic representation overemphasizes low values.

Physiological relevance: The physiological relevance of the allometric equation becomes evident lies in the interpretation that any organ of the organism receives a part of the total growth energy that is proportional to the relative size. The allometric exponent 'c' is a measure for the organism's internal distribution strategy, which can be seen when writing Eq. 2-8 in the form of Eq. 2-10. For c = 1 (linear function) the resources are distributed equally (isometry); c < 1 is termed negative allometry, c > 1 positive allometry:

$$\frac{dy}{dx} = c \cdot \frac{y}{x} \qquad \textbf{Eq. 2-10}$$

Because of its physiological relevance, the allometric exponent 'c' has been strongly discussed ever since (Brown et al. 2000, pp. 4). Often it was proposed that volume or mass-related allometric functions scale with exponents of 3rds due to the 3-dimensional volume unit [m^3] (Bertalanffy 1942, Yoda et al. 1963). Yet, many empirical findings indicate al-

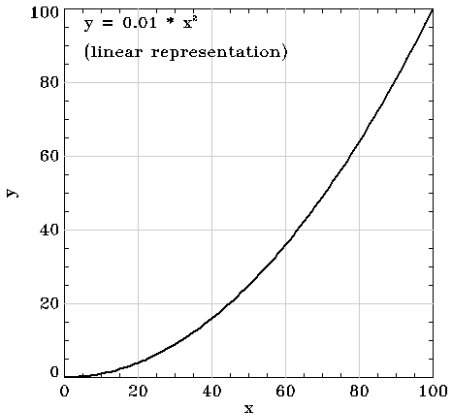

a

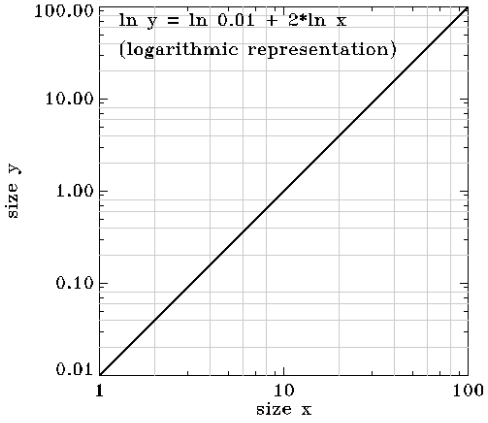

b

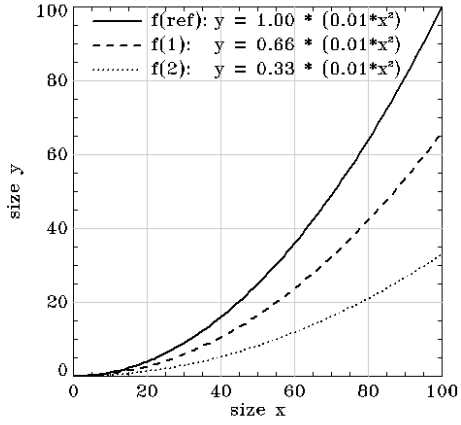

c

Fig. 2-13 The allometric equation

(a/b) Example for an allometric function in (a) linear and (b) logarithmic representation

(c) Allometric reference function f(ref) and two related functions with different allometric levels f(1) and f(2).

lometric exponents of 4th which was only recently interpreted in the WBE-theory which constitutes allometry on internal transport systems with fractal branching (WBE = West-Brown-Enquist, West et al. 1997/ 1999, Enquist et al. 1998).

Allometric reference functions and allometric level: For a set of allometric relations with a similar allometric exponent 'c', the ratio of the allometric factors 'a' directly scales the functions to each other. A well known example in forestry is the stand density index SDI which relates the mid dbh and the tree number N over an allometric exponent of –1.605, i.e. the Reineke exponent (Reineke 1933, Eq. 2-6 and Eq. 2-7):

$$\begin{aligned} SDI &= N \cdot (25.4 / dbh_{mid})^{-1.605} \\ N &= SDI \cdot (dbh_{mid} / 25.4)^{-1.605} \end{aligned} \qquad \textbf{Eq. 2-11}$$

Often, it makes sense to choose one equation as the 'allometric reference function' f_{ref} with a certain c_{ref} and a_{ref}. If for an allometric function f_1 the exponent c_{ref} is enforced, then the ratio of the allometric factors a_1/a_{ref} shall be defined as the 'allometric level l_a':

$$\begin{aligned} f_{ref} \quad y &= a_{ref} \cdot x^{c(ref)} \\ f_1 \quad y &= a_1 \cdot x^{c(ref)} \\ l_a \quad l_a &= a_1 / a_{ref} \end{aligned} \qquad \textbf{Eq. 2-12}$$

The allometric reference equation and the allometric level is fundamental for the concept of the height-biomass allometry in this work. Fig. 2-13.c displays the simple reference function $y = 0.01x^2$ and the functions f1 and f2 with an allometric level of l_a=0.66 and 0.33 respectively.

2.3.2 Growth allometry

Traditional allometry was concerned with the size relations of organs during growth, as Huxley's title: "Problems of relative growth" (1932) and the physiological interpretation in Eq. 2-10 indicate. The connection between growth and allometry can be studied from Bertalanffy (1942). His theory of 'dynamic morphology' means that "any organic system is essentially a hierarchy of processes in a dynamic balance" between assembly, or anabolism, and breakdown, or catabolism (Bertalanffy, 1942, p. 230). Defining growth as the increase in size over time, the antagonism between anabolic and catabolic processes can be described as:

$$dy / dt = a \cdot y^n - b \cdot y^m \qquad \textbf{Eq. 2-13}$$

The exponent m scales the growth-protagonism (anabolism), and n the growth-antagonism (catabolism). For n > m, the catabolic processes eventually compensate the assembling processes, leading asymptotically to the final size (Fig. 2-14.a). Bertalanffy solved Eq. 2-12 for volume growth, assuming the anabolism to scales to the surface (n = 2/3) and the catabolism to the volume (m = 1). Richards (1959) generalized the formula with for a variable exponent 'c':

Bertalanffy (1942) $$y(t) = A \cdot (1 - \exp(-k \cdot t))^3 \qquad \textbf{Eq. 2-14}$$

Richards (1959) $$y(t) = A \cdot (1 - \exp(-k \cdot t))^c \qquad \textbf{Eq. 2-15}$$

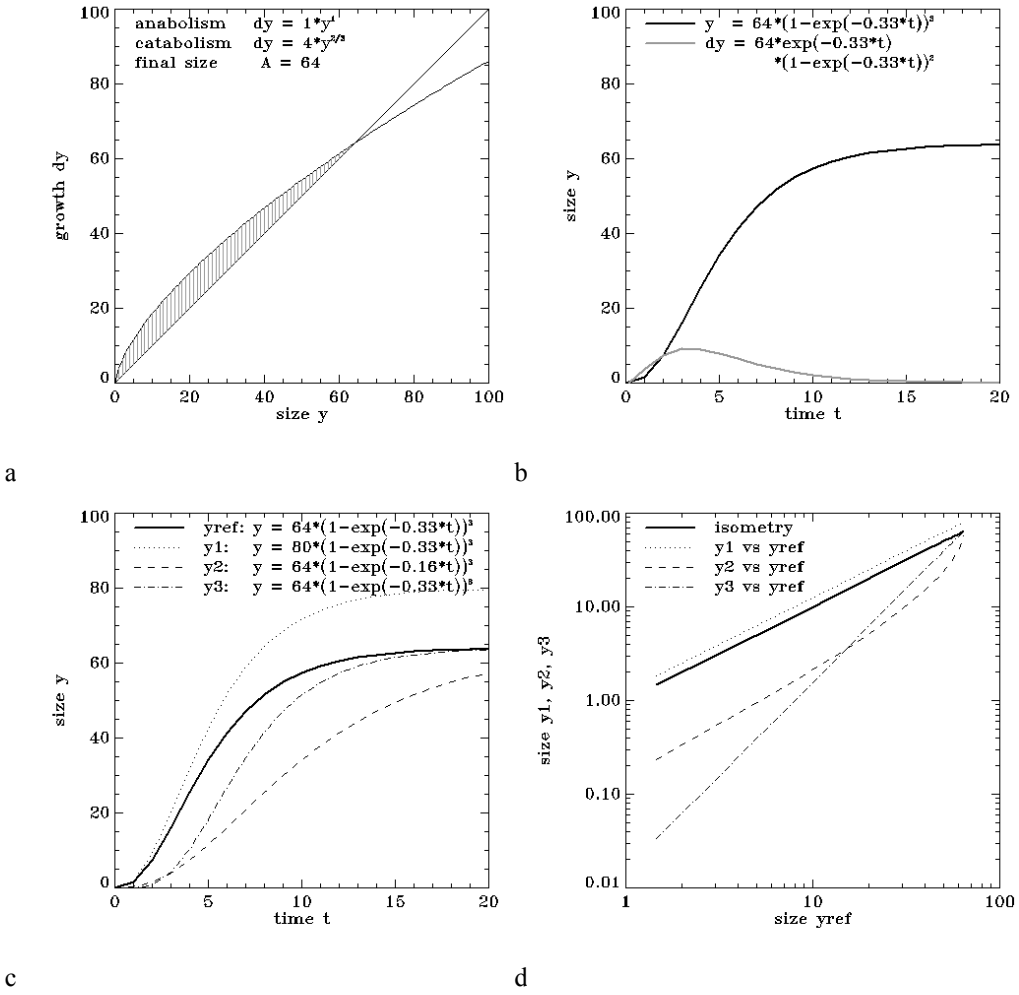

Fig. 2-14 Growth and growth allometry

(a) Growth vs. size; growth occurs as long as anabolism exceeds catabolism (dynamic morphology, Bertalanffy 1942), (b) growth function resulting from (a) (Bertalanffy 1942, Richards 1959). (c) Growth behaviour for different parameters of A, k and c in Richards' growth function (1959), (d) Allometry resulting from (c).

y represents the object size as a function of the time t, A the maximum size (asymptote), k the growth rate and c the sigmoidity; which is related to the exponents m in Eq. 2-13 (for n=1):

$$c = 1/(1-m) \qquad \textbf{Eq. 2-16}$$

As can be seen in Fig. 2-14.b/c, the growth function possesses a sigmoid (S-shaped) character. The curve can be interpreted as consisting of an exponential phase where anabolic processes dominate, and an asymptotic phase where catabolism approaches the level of the anabolism and leads to an asymptotic approaching of the final size. The exponent c in Richards' growth function is responsible for the strength of the 'sigmoidity' and describes the relation between the antagonistic processes (Eq. 2-16).

Comparing the formulas for growth from Eq. 2-15 and allometry from Eq. 2-9, it can be shown that two sizes can still be allometrically when possessing a different asymptote

A, or sigmoidity c, but not if the growth rate k differs (Mette et al. 2004a). This has been modelled in Fig. 2-14.c and Fig. 2-14.d using the growth equation from Fig. 2-14.b as the reference function. It can be seen, that the comparison of the growth rates k is a sensitive indicator for allometric growth.

Comparative allometry: Although allometry was originally developed as relative growth (Huxley 1932), the study of allometry is not essentially bound to growth (growth allometry). Comparing size relations between species or along environmental gradients or other factors is an important working field of allometry that can be termed 'comparative allometry'. Both fields complement each other in an understanding of the eco-physiological functionality behind the size relations. Growth allometry and comparative allometry seem not always to be well distinguished. Hence, a simple example shall highlight the difference: consider two 40-year old trees, one grown with competition, the other without. The first one has grown thin and tall (height : diameter ratio high), the second thick and less tall (height : diameter ratio low). This is an example of comparative allometry where the influence of the factor 'competition' on the height : diameter relation is analysed. Interpreted as growth allometry, this would mean that trees grow thinner as they increase in height, or become smaller as they increase in diameter.

Aut- and Syn-Allometry: A last consideration shall be made upon the level of organisation at which allometry is studied. On the organism scale, one could speak of aut-allometry, on the level of populations of syn-allometry. In terms of a forest, aut-allometry is concerned with the individual tree, syn-allometry with the 'system' forest. The mechanisms are essentially different, the key difference being the parameter population size. The competition for limited resources leads to a reduction of the populations size during growth. This way, a mature forest typically comprises merely 60% of the total produced biomass.

2.3.3 Considerations on the allometry of woody plants

Classical allometry was based on animals, but has been applied equally to plants and plant communities, especially trees and forests. Well known are tree dbh-height or dbh-biomass relations (Kramer and Akça 1995, p. 134, McMahon and Kronauer 1976, Niklas 1994, pp. 164, West et al. 1997/ 1999, Enquist et al. 1998, Zianis and Mencuccini 2004), size-frequency relations (Reineke 1933, Yoda 1963, Enquist and Niklas 2001, Pretzsch and Biber 2005, Pretzsch 2006), and also the sought-after forest height-biomass relations (Eichhorn 1902, Gehrhardt 1909, Assmann 1961, p. 158).

Bertalanffy himself questioned whether his dynamic theory of growth could be translated to plants (Bertalanffy 1942, p. 271). Some of the main differences between plant and animal growth behaviour are:

1. In general, the vegetative tissue of animals is determinate in growth, meaning organs and organisms reach a final size during maturity, i.e. closed ontogeny. Most plants in contrast can grow indeterminately, i.e. open ontogeny (Niklas 2000).
2. Unlike animals, woody plants consist to a great part of dead biomass, in essence the vascular xylem tissue. Only through the death of these cells can a transport system be built, that exceeds diffusion by several orders of magnitude. This transport system enables plants to grow in height in competition for light. The characteristic

strong cell walls are required both by the negative pressure through water conduction and the mechanical structural integrity. The living tissue therefore only consists of the photosynthetic apparatus, wood parenchyma, and a cell layers close to meristem tissues. In a big tree, this living biomass may only make up *3-5%*. It is logical that the evolution of animal has restricted dead biomass to a minimum (bones, cartilage) in order to minimize the energy necessary for locomotion. Trees on the other hand could never cover the energy need if the whole stem was living tissue. Attempts to reduce allometric relations of trees not to the living, but at least to the active xylem tissue have been undertaken e.g. by Pretzsch (2002/ 2005).

3. In animals, a serious alteration in the proportions of organs has lethal functional consequences. Plants on the contrary are highly flexible in shape. Niklas (1994, p. 9) terms this flexible growth modular: "[…] an indefinite increase in size by periodically and cyclically adding additional organs (e.g. leaves) or functional groups of organs (e.g. shoots), many of which are determinate in growth."

The strongest argument against allometry in the sense of Huxley's relative growth (Eq. 2-9) is Niklas' modular growth postulation. If the growth rates of organs are independent from each other, the proportions will vary as a function of the respective growth-stimulating factors. The first two arguments do not necessarily reject an allometric relation in the sense of Huxley, but require some care to the fitting and interpreting of growth and allometry. It is questionable whether the above-made considerations persists also on the forest-level (syn-allometry, Ch. 2.3.2), but they play an important role for the understanding of forest allometry.

2.4 Height-biomass allometry from the yield tables

This subchapter uses forestry yield tables for Middle-Europe to implement height-biomass allometry for the estimation of forest biomass from forest height data. In Ch. 2.4.1, a concept of height-biomass allometry to be used with remote sensing height data is developed; Ch. 2.4.2 introduces the yield tables that were used for the task. Ch. 2.4.3 applies the concept and establishes a reference function, and discusses the variation in dependence of species, site conditions and thinning practise. Ch. 2.4.4 takes a closer look at the mechanisms behind height-biomass allometry and examines related aspects like tree allometry or the relation between dbh-tree number allometry and height-biomass allometry.

2.4.1 Concept of height-biomass allometry

The first step in the development of a height-biomass allometry for use with remote sensing height data is the selection of an appropriate forest database. The following requirements were regarded important:

- simple forest structure to reduce the complexity of the height-biomass relation
- forestry standard to assure conformity with forestry applications
- large and differentiated data base to allow general conclusions

These demands are – in many aspects – fulfilled by standard forestry yield tables. They describe forests of a very simple structure – mostly for a single species, even-aged, and comparably dense. The mentioned requirements are met in the following way:

- single height layer avoids problems with complex height distributions, and due to the high stand density, the height-biomass relation in the yield tables can be expected to represent the upper biomass potential for a given height.
- standard tools in timber-oriented forestry in many countries
- discrimination of species, yield class and thinning allows to discriminate the influence of these factors on forest allometry,

In the second step, the complexity of relation between height and biomass with regard to species, site conditions, thinning practise and forest structure, must be condensed in a simple applicable approach. The way, that was chosen, was to define one yield table as the reference forest type, and then quantify the differences to the yield tables due to species, site conditions, and thinning. If the height-biomass relationship follows the allometric equation (Eq. 2-9), the reference forest will provide the allometric reference function, and it can be tried to quantify the differences to other yield tables by means of the allometric level (Ch. 2.3.1). This way the reference height-biomass relation can be flexibly adjusted to the actual forest situation.

It must be emphasized that the height-biomass relation from the yield tables is based purely on forest parameters. The relation between the heights extracted from remote sensing and the reference height for the allometry must be treated separately. It is therefore important to define a sensible reference height from forestry and remote sensing point of view – which was done with the choice of the upper canopy height in Ch. 2.2.2.

Last but not least, two problems connected with allometric relations from yield table shall be mentioned. On the one hand, the concept of a reference equation and an adjusting factor is flexible enough to be applied to more complex forest types. However, it meets limits when the upper canopy is highly heterogeneous as in the case of emergents or very open forests (see Fig. 2-5). On the other hand, the thinning actions interfere with the natural growth behaviour of the forest and constricts physiological conclusions from the yield tables. Both aspects are discussed in detail in Ch. 2.5 and Ch. 2.6, and will be encountered again in the validation of the height-biomass allometry from the forest inventory data in Ch. 4.

2.4.2 The yield tables

In a yield table, the most important structural forest parameters: tree number per hectare, forest height, basal area, shape factor and volume, are given as a function of age. They are based on empirical data from long-term forest research plots with defined thinning concepts, and were originally set up to predict the yield of a forest, and to serve as a guideline for a yield maximizing stand treatment (Assmann 1961). The German standard yield tables (Schober 1985) were set up for 16 species, 11 of which were considered in this work. Further more, the Norway spruce tables of Assmann and Franz (1963, BMELF 1979) were included which are the recommended reference for spruce forests in South Germany. For most of the described species, the tables are divided into

different yield classes according to their growth behaviour. Also, strong and moderate thinning intensity may be distinguished. Altogether, 21 yield tables were considered in this study (Tab. 2-2) whereby one yield table includes up to 6 yield classes.´

Tab. 2-2 The 21 yield tables used in this work (Assmann and Franz 1963, Schober 1985)

	Tree species common name (*scientific name*, wood density ρ [g cm^{-3}] according to Wagenführ 2000)	**Author/ Date**	**Yield classes**	**Thinning**
1	Norway spruce (*Picea abies*, 0.47)	Assmann and Franz 1963[1)]	OH40-20*	Average yield
2			OH40-28*	Upper yield
3			OH40-20*	Lower yield
4		Wiedemann 1936 (1942)	1-6	Moderate
5			1-3	Strong
6	Scots pine (*Pinus sylvestris*, 0.52)	Wiedemann 1943	1-6	Moderate
7			1-6	Strong
8	White fir (*Abies alba*, 0.45)	Hausser 1956	1-4	Mod. (Wuerttemberg)
9		Schmidt 1956	1-2	Mod. (NW-Germany)
10	Douglas fir (*Pseudotsuga menziesii*, 0.51)	Bergel 1985	1-3	Moderate
11			1-3	Strong
12	European larch (*Larix deciduas*, 0.59)	Schober 1946	1-3	Moderate
13			2	Strong
14	European beech (*Fagus silvatica*, 0.72)	Schober 1967	1-4	Moderate
15			1-4	Strong
16	Common oak (*Quercus robur*, 0.69)	Juettner 1955	1-4	Moderate
17			1-4	Strong
18	Ash (*Fraxinus excelsior*, 0.69)	Volquardts 1958	1-2	Moderate
19	Birch (*Betula pendula*, 0.65)	Schwappach 1903/29	1-2	
20	Black locust (*Rob. pseudoacacia*, 0.77)	Erteld 1951	1-3	
21	Poplar (*Populus canadensis* 'Robusta', 0.45)	Raetzel 1969	1-3	

* instead of yield classes numbers, Assmann and Franz (1963) refer to OH-classes: OH 40/36/32/28/24/20

The factors that are distinguished by the yield tables: species, yield class and thinning, can be analysed for their impact on height-biomass allometry. These three factors, as well as the structure and growth in the yield tables are detailed in the following:

(1) Species: 11 tree species were considered in this study, five conifers and six broad-leaves. The tables refer to growth under the temperate conditions of Middle Europe, although two species are originally from North-America (Douglas fir, Black locust), and others have also a boreal distribution (esp. spruce, pine and larch). The two fir tables were established for different regions in Germany (Annex 7.2).

Most yield tables were set up for single species forests and cannot be extrapolated to mixed species concepts as two or more species may interact positively or negatively (Kerr et al. 1992, Burkhardt and Tham 1992, Assmann 1961, Wiedemann 1943).

(2) Yield class: One of the most important aspects of the yield tables is the distinction of yield classes. They are based on species specific height growth curves, which are relatively independent of thinning. For the main forestry species up to 6 yield classes are distinguished. the optimum growth conditions are designated yield class I (OH40 for Assmann-Franz tables), the poorest yield class VI (OH20).

The yield classes reflect the species-specific reaction to site conditions, the most important factor in general being the water availability, but also climatic factors, like the length of the growing season, play a certain role (Barnes et al. 1998, pp. 145, Kramer and Boyer 1995, Kozlowski and Pallardy 1997, Lyr et al. 1992, pp. 419). Similar yield classes of different species do not refer to similar site conditions.

(3) Thinning: the yield tables assume a regular thinning at two intensity levels: moderate and strong. Further more, the type of thinning may differ, e.g. while in spruce and pine stands, mostly growth retarded trees are thinned out (thinning from below), in beech and oak stands also strong trees are removed (thinning from above). As already said, the artificial regulation of the stem density poses a general problem to drawing conclusions on allometric mechanisms from yield tables.

(4) Structure: In general, yield tables refer to even-aged forests, managed to develop a high yield. In comparison, forests not managed for timber extraction, typically possess lower densities and/ or a more heterogeneous age- and height structure, especially natural forests. As long as an upper canopy height can be defined, the concept of height-biomass allometry from Ch. 2.4.1 can be adapted (detailed in Ch. 2.6).

(5) Growth: Today, the growth rates of the forests are often higher than in the yield tables mainly due to nitrogen fertilizing from anthropogenic exhaustion, but also due to a higher atmospheric CO_2 concentration and the elongation of the vegetation period through rising temperatures (Pretzsch 1999, Myneni et al. 1997, FAO 2001a, pp. 65). Such changing growth conditions might explain a yield-class 'hopping' of forests (Moosmayer 1970, Pretzsch 1999) although also the yield tables were certainly not set up under constant conditions either. In terms of forest allometry it is important to know, whether these environmental changes only affect the growth or also the size relations within forests. Franz and Pretzsch (1988) and Elling (1993) consternate a stronger reduction in dbh growth than height growth for Norway spruce and White fir under increasing immission of pollutants. The interrelation between growth factors and growth response is very complex, one factor might even have opposite effects under two different conditions.

As reference height and biomass measures from the yield tables were chosen: mid height and usable biomass. As discussed in Ch. 2.2.2, mid height can serve as an upper canopy height measure, if the forest consists of one narrow height layer, or if it is defined separately for the upper canopy. The reason to prefer the mid height and not the top height h_{100}, was because also in the inventory data, the mid height of the upper canopy layer is calculated. It must be paid attention to the fact that – in contrast to the h_{100} – the mid height is calculated from a changing collective as retarded trees are thinned out during the stand development. The problem of the 'usable' criterion for the biomass of low tree heights (Ch. 2.1., Ch. 2.2.2) is not serious in the yield tables, because typically only one or two of the youngest age classes are affected.

2.4.3 Reference height-biomass allometry and allometric level

The allometry between height and biomass is not new in forestry (see Assmann 1961, Pretzsch 2001, pp. 89). The close relation between (mid) height and (stem) volume was first described by Eichhorn in 1902. He discovered that the volume of White fir (*Abies alba*) forests was constant for a given height, regardless of the yield class. This rule was termed law of Eichhorn, and extended by Gehrhardt in 1909. He reasoned that not the standing stem volume should be referred to, but standing + harvested volume. This way, the height-volume allometry is not only independent of yield class, but also of the thinning practise (extended law of Eichhorn). The last change was introduced by Assmann and Franz (1963/ 1965) who discovered that the height-volume allometry (standing + harvested) was not absolutely independent of the site conditions, but varies by +/-15%. They called these differences in the height-volume allometry yield levels.

Regarding the extended rule of Eichhorn and the yield levels of Assmann and Franz, which consternate an allometry between height and total volume (standing + harvested), we need to step back to the original rule of Eichhorn which refers to the actual standing volume. Of course, special respect has to be paid to the effect of thinning.

According to the concept in Ch. 2.4.1, the first task is the selection of a sensible reference yield table. The choice fell on the Norway spruce table of Assmann and Franz (1963) for average yield level, yield class OH40-20. The reasons were:

- Norway spruce is a widely distributed temperate and boreal tree species,
- Norway spruce is one of the economically most important tree species in Middle and North Europe,
- Norway spruce reaches high stand densities, hence, is expected to represent the upper biomass boundary for a given height,
- thinning does not strongly affect the allometry, and the allometry can be well matched with the allometric formula (Eq. 2-9),
- the yield tables are based on a large data set, approved and recommended (Assmann and Franz 1965, BMELF 1979).

The height-biomass allometry of the named Norway spruce yield table is shown in Fig. 2-15. It can be seen, that it matches Huxley's allometric equation (Eq. 2-9), and is almost independent of the yield class (rule of Eichhorn). The corresponding height-biomass reference allometry was derived as a regression through all yield classes of the mentioned Norway spruce yield table (Assmann and Franz 1963, avrg.yld.lev.):

$$Biomass = 1.66 \cdot height^{1.58}$$

$$a_{ref} = 1.66 \qquad \textbf{Eq. 2-17}$$

$$c_{ref} = 1.58$$

The reference exponent c_{ref} and allometric factor a_{ref} are important for the determination of the allometric level for the following comparison to other yield tables.

Having decided upon the reference equation (Eq. 2-17), now the height-biomass allometry from yield tables shall be analysed for differences between species, yield classes and thinning practises. This is done by means of the allometric level (Ch. 2.3.1, Eq. 2-12).

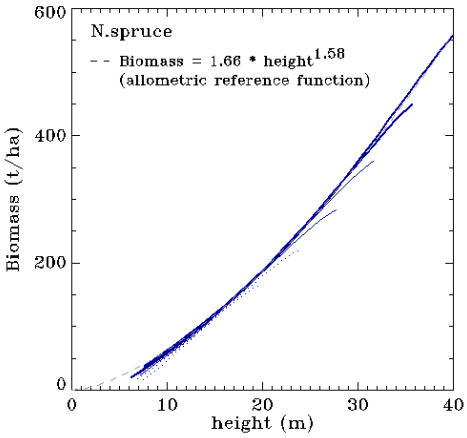

Fig. 2-15 Reference height-biomass allometry from the Norway spruce yield tables of Assmann and Franz (1963, average yield level, yield classes OH20-40)

To determine the allometric level with respect to the reference function, the exponent of c_{ref}=1.58 is enforced upon the height-biomass allometry for the other yield tables. Since this exponent was not always appropriate - as will be shown –the allometric level had to be determined carefully and was based on a 'characteristic' part of the curve. Empirically, the best fitting results were obtained when fitting the allometric function through the height-biomass coordinate at the mid age of the yield table. The allometric level l_a is then retrieved as the ratio between actual allometric factor a and the reference factor a_{ref} = 1.66 (cf. Eq. 2-12):

$$l_a = B / B_{\exp} = B / (1.66 \cdot h^{1.58}) \qquad \textbf{Eq. 2-18}$$

The allometry from Norway spruce shall now be compared with three further important tree species, Scots pine, beech, oak (Fig. 2-16):

- Scots pine (Fig. 2-16.a): Up to 15m height, Scots pine exhibits the same height-biomass relation as Norway spruce, but falls short for higher heights, resulting in an overall allometric level of 0.75. Here, the reason lies in an increased mortality in old pine stands which was characteristic for Eastern Germany at the times when the yield tables were set up. This makes the fitting of a power function difficult, and leads to the characteristic hooks in old stands.
- European beech (Fig. 2-16.b): The height-biomass allometry from the beech yield tables reaches almost the allometric level of Norway spruce (0.95). Notably, the level increases with deteriorating site conditions, and the shape of the curves appears more linear than the reference exponent of c_{ref} = 1.58. The reason for this lies in the thinning practise from above.
- Common oak (Fig. 2-16.c): The oak curves resemble the ones from beech, the site conditions have less effect, the linearity is more pronounced, and the allometric level lies at 0.87.

In Fig. 2-17, the allometric level is compared for the 21 yield tables considered in this study. For each yield table, the allometric level was determined across all yield classes. The differences between species, yield classes and thinning shall be summarized:

- Species: Comparing the moderate thinning intensity, the allometric level varies in dependence of the species from 0.7-1 with exception of birch (0.5) and poplar (0.3). As expected, Norway spruce exhibits the highest allometric level, along with White fir (Württemberg) and beech (~0.95-1), followed by oak (~0.85), White fir (NW-Germany), Douglas fir, Scots pine (~0.75), then European larch (~0.7). Interestingly, spruce, fir and beech are the climax forest species in Middle Europe, and the pioneer character increases from oak to Scots pine, larch and ash to birch and poplar (Ellenberg 1996, Annex 7.2). The fir tables reveal that also regional differences affect the allometric level.
- Yield classes: are in the first order an indicator of the site conditions. In general the differences between the, of one tables were so low that they were averaged in one common allometric level. But differences due to site conditions can be observed from yield tables for the yield levels of the Assmann-Franz Norway spruce tables (+/-10%). Deviations from the average allometric level can also become large when mortality increases in old stands as for Scots pine (Fig. 2-16.a).
- Thinning: The allometric level in the yield tables with strong thinning is reduced by approximately 10-20% compared to moderate thinning. The decrease in density is not proportional to the tree number, because trees compensate the basal area loss at least partly with increased dbh-growth. How far thinning alters the natural height-biomass allometry cannot be assessed from the yield tables, but will only show under self-thinning conditions.

The allometric level can be regarded as height-specific density measure that integrates basal area, wood density and shape

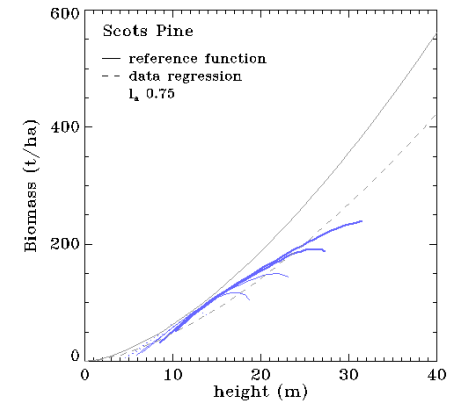

a

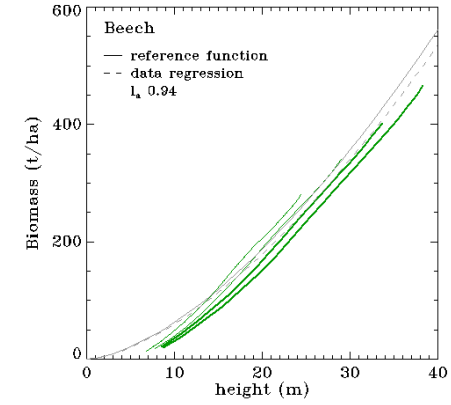

b

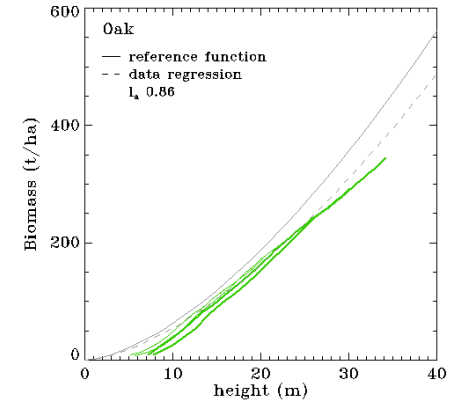

c

Fig. 2-16 Height-biomass allometry of (a) Scots pine, (b) beech, and (c) oak

(a) Scots Pine (Wiedemann 1946, moderate thinning, yld.cl. I-VI), (b) European beech (Schober 1967, moderate thinning, yld.cl. I-IV), (c) common oak (Jüttner 1955, moderate thinning, yld.cl. I-IV). In general, the differences between the yield classes within each yield table are low. Differences between the species can be seen in the shape of the curve and the allometric level (relative to the reference function Eq. 2-17)

factor (Eq. 2-3). Consequently, in the case of different thinning intensities, the allometric level corresponds to the basal area ratio of the respective tables. But also, different species can possess the same allometric level with different basal areas, if wood density has a compensating effect. Beech and oak, for instance, grow with lower basal areas (for a given height) than Norway spruce. But the higher wood density partly compensates the lower basal area. These aspects are addressed more detailed in Ch. 2.4.4.

Last but not least, a comparably small role plays also the 'usable' criterion of the biomass definition (Ch. 2.2.2). This can be seen from the low heights in Fig. 2-16. Here, the low biomass values result from the fact that the trees do almost not exceed the 'usable' dbh limit, dbh > 7 cm.

2.4.4 Related aspects to height-biomass allometry

While the previous chapter focused directly on the height-biomass allometry, now three related aspects shall be analysed more closely: (1) height-dbh allometry, (2) height-basal area allometry, and (3) the relation of dbh-N allometry to height. These three issues will provide insight into the mechanisms underlying the forest height-biomass allometry, and will be used for the allometric forest model in Ch. 2.5.2.

It must be remarked that the yield tables only allow limited conclusions about the physiological mechanisms beyond forest allometry. The main limitations for following analyses are the artificial regulation of the tree number through thinning, and changing collective behind the mid height.

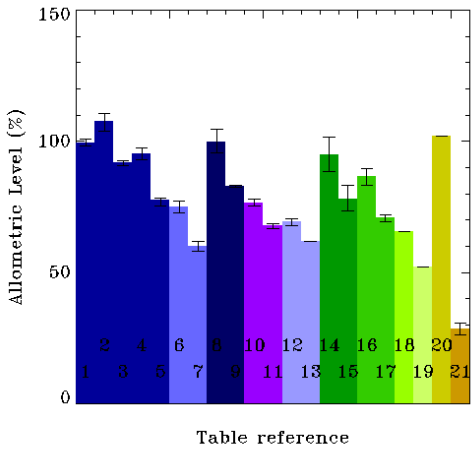

Fig. 2-17 Allometric level for the 21 considered yield tables

The allometric level was averaged over the yield classes (minimum and maximum allometric level between the yield classes indicated)

	Tree species / table	Thinning/ detail	Mean all. level
1	Norway spruce (Assmann and Franz 1963)	Average yield	1.00
2		Upper yield	1.08
3		Lower yield	0.92
4	Norway spruce (Wiedemann 1936)	Moderate	0.95
5		Strong	0.77
6	Scots pine (Wiedemann 1943)	Moderate	0.75
7		Strong	0.60
8	White fir (Hausser 1956)	Wuerttemberg	1.00
9	White fir (Schmidt1956)	NW-Germany	0.83
10	Douglas fir (Bergel 1985)	Moderate	0.77
11		Strong	0.68
12	European larch (Schober 1946)	Moderate	0.69
13		Strong	0.62
14	European beech (Schober 1967)	Moderate	0.95
15		Strong	0.78
16	Common oak (Jüttner 1955)	Moderate	0.87
17		Strong	0.71
18	Ash (Volquardts 1958)	Moderate	0.66
19	Birch (Schwappach 1903/29)		0.52
20	Black locust (Erteld 1951)		1.02
21	Poplar (Rätzel 1969)		0.29

(1) Height-dbh allometry: Fig. 2-18 shows the height and dbh growth of the 'mid' Norway spruce tree (Assmann-Franz table for average yield level, 1963), and the allometry between height-dbh and dbh-biomass. Since the 'mid' tree shifts as trees are thinned out during growth, it is a false growth curve. This shift pretends a slightly higher growth than actually occurs. Four observations can be made:

- Fig. 2-18.a/b: While height clearly approaches an asymptote during the regarded time span of 120 years, dbh keeps increasing more or less linearly. This results in a different growth rate k when fitting Richards' growth function (Eq. 2-15) The height asymptote lie at 44 m for OH40 to 24 m for OH20.
- Fig. 2-18.c: Due to the different growth rates of height and dbh, the height-dbh allometry cannot be quantified by the allometric equation (see Ch. 2.3.2). Nevertheless for an age range up to ~60 years the relationship is almost equal for all yield classes. During this growth phase, height and dbh growth have a very similar growth behaviour. Thereafter height growth ceases and approaches the yield class-dependent asymptote, while dbh does not, leading to the characteristic hooks in the dbh-height relation. In forestry, the dbh-height relation is typically quantified by the Petterson equation (Kramer and Akça 1995, p. 134).
- Fig. 2-18.d: Tree biomass, being proportional to the product of dbh^2 and height, is apparently very well related to dbh. Yet, the relation between height and dbh has two consequences for the dbh-biomass allometry: (1) dbh-biomass allometry approaches a quadratic function as height reaches its asymptote, (2) when height growth ceases, the final height scales the allometric factor. E.g. a tree of 50 cm dbh would only possess half the biomass in yield class OH20 compared to OH40. Nevertheless, over the regarded age range, the equation in Meschederu (1997) serves well (plotted in Fig. 2-18.d):

$$b_{tree} = 0.0442 \cdot dbh^{2.6597} \qquad \textbf{Eq. 2-19}$$

  This equation refers to the total aboveground biomass b_{tree}, which lies slightly higher than the usable wood biomass used here (see Ch. 2.2.4, Fig. 2-9).

Numerous studies have established allometric equations between dbh and height and dbh and biomass (Zianis and Mencuccini 2004). An interesting study in this respect is the comparative dbh-height allometry of the largest specimen of different tree species in the US (McMahon and Kronauer 1976, re-evaluated by Niklas 1994, pp. 164). The study tried to interpret the relation with two models of mechanical stability, stress similarity and elastic similarity. A regression through a large pool of data seemed to confirm the exponent for the elastic similarity model for dicot trees, but not for conifers. 'Elastic similarity' refers to the critical tree height h_{crit} and dbh at which a column undergoes elastic buckling (E = Young's modulus or elasticity, ρ = wood density):

$$h_{crit} = a \cdot \left(E / \rho \right)^{1/3} \cdot dbh^{2/3} \qquad \textbf{Eq. 2-20}$$

At the same time however, the study clearly revealed that mechanical stability is not the limiting factor for height. Niklas (1994, p. 171) speaks of a 'safety factor' of 4-5.

(2) Height-basal area allometry: As explained in Ch. 2.2.2, the height-biomass allometry is based on the allometry between height and basal area, and becomes a partial self-

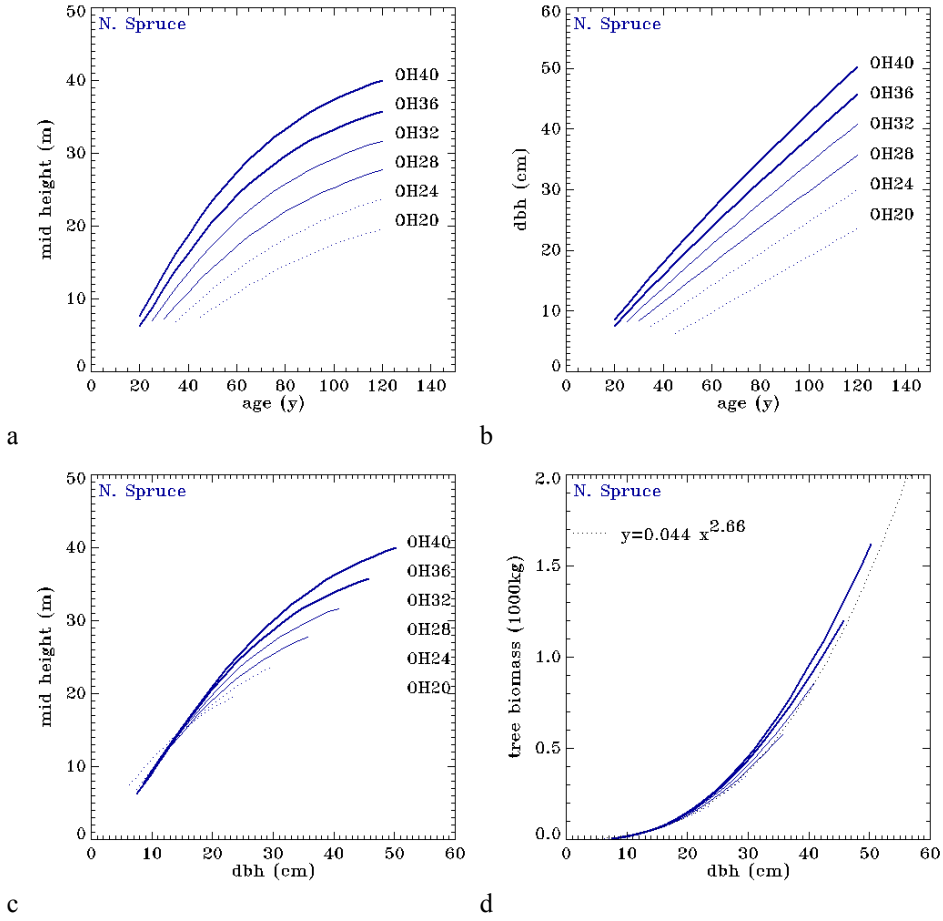

Fig. 2-18 Tree growth and allometry of Norway spruce

(a) height growth, (b) dbh growth, (c) dbh-height allometry, (d) dbh-biomass allometry. Norway spruce (Assmann and Franz (1963, average yield level, yield classes OH20-40)

correlation because height is one dimension in biomass (Eq. 2-3). Assuming a constant shape factor fz, the reference height-biomass allometry can be substituted into Eq. 2-4 in order to determine the theoretical height-basal area exponent. This exponent can be compare to the empirical one derived in Fig. 2-19.

theoretical height-basal area exponent:

$$\begin{aligned} B &\propto h^{1.58} \\ h \cdot G &\propto h^{1.58} \\ G &\propto h^{0.58} \end{aligned} \qquad \textbf{Eq. 2-21}$$

empirical height-basal area exponent:

$$G \propto h^{0.67} \qquad \textbf{Eq. 2-22}$$

Fig. 2-19 confirms the allometric relation between height and biomass. But the empirical exponent of 0.67 fits the height-basal area allometry better than the theoretical exponent 0.57. This discrepancy is due to a changing shape factor, which decreases from 0.55 for 10 m height to 0.43 for 40 m height (-20%).

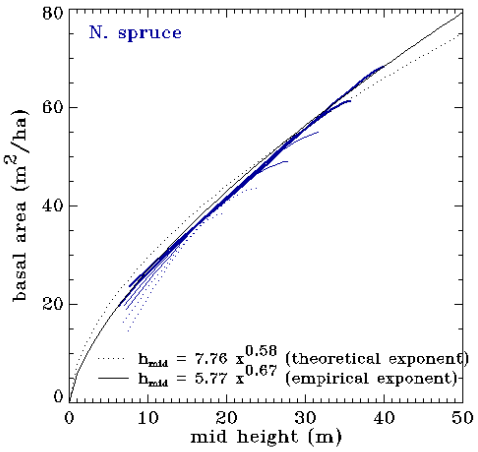

Fig. 2-19 Height-basal area allometry of Norway spruce

(Assmann and Franz 1963, average yield level, yield classes OH20-40)

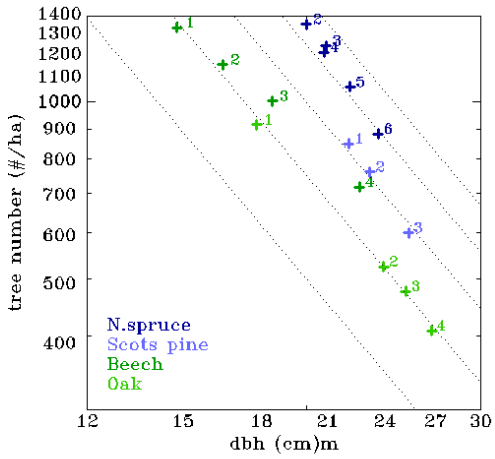

Fig. 2-20 Relation of N-dbh ratio to height for h_{mid} = 20

Dotted lines correspond to different N:dbh^2 levels, numbers to yield classes. Norway spruce (Assmann and Franz 1963, avrg yld.lev., yld.cl. OH20-40), Scots Pine (Wiedemann 1946, moderate thinning, yld.cl. I-VI), European beech (Schober 1967, moderate thinning, yld.cl. I-IV), common oak (Jüttner 1955, moderate thinning, yld.cl. I-IV).

However, the changing shape factor does not only reflect the tree shape, but also the definition of height and biomass (Ch. 2.2.1, Ch. 2.2.2). For instance, the shape factor for the h_{100} is more stable than the shape factor for h_{mid} because the tree collective, which the height refers to, does almost not change.

Such effects introduce a bias into the deduction of exponents from interrelated allometries– as in the given example. This must be avoided in physiological discussions of allometric exponents (Ch. 2.5.1).

(3) Relation of dbh-N ratio to height: It is clear, that the same biomass for a given height can be reached with different N-dbh ratios if the product of $N \cdot dbh^2$ stays constant. In Fig. 2-19, the tree number N and dbh of Norway spruce, Scots pine, beech and oak have been plotted for different yield classes in a logarithmic grid for a height of h_{mid} = 20 m.

Differences can be observed between the species and yield classes. First of all, the behaviour of the N-dbh relation on yield class is similar for all species: poor yield classes have a lower tree number, but a higher dbh than the good ones, but they do not deviate strongly from the N:dbh^2-allometry. The obvious deviations in the case of beech correspond to the yield class differences in the height-biomass allometry (Fig. 2-16.b).

The alignment of the different species indicate a decreasing basal area in the order: Norway spruce, Scots pine, beech, oak. This gradient follows – except between beech and oak – a positive gradient in wood density: Norway spruce 0.47 g cm^{-3}, Scots pine 0.52 g cm^{-3}, beech 0.72 g cm^{-3}, oak 0.69 g cm^{-3}. This shows that lower basal areas can (at least partly) compensated through higher wood densities (Ch. 2.5.1).

2.5 Interpretation of forest height-biomass allometry

In this subchapter, the results from the previous height-biomass allometry in Ch. 2.4.3 and Ch. 2.4.4 are summarized and interpreted from an eco-physiological point of view. In Ch. 2.5.1, the exponent of the reference equation is discussed including the well-known Reineke- and Yoda-rule, and the WBE-theory (Reineke 1933, Yoda et al. 1963, West et al. 1997/ 1999, Enquist et al. 1998). The allometric reference factor and the dependence of the allometric level on species, yield class and thinning are discussed. In Ch. 2.5.2, the findings are merged in a simple allometric model based on the energy balance of the tree with respect to light, water and nutrient supply.

2.5.1 Reference equation and allometric level

The reference height-biomass allometry was determined from the Norway spruce yield tables of Assmann and Franz (1963, average yield level): $Biomass = 1.66 \cdot height^{1.57}$ (Eq. 2-17) where $a_{ref} = 1.66$ is the allometric factor and $c_{ref} = 1.58$ the allometric exponent. An allometric (power) function fitted well, but it was pointed out that the height-biomass allometry is a partial self-correlation underlain by height-basal area allometry.

The allometric exponent: According to the argument of geometric similitude which postulates even growth in x-, y- and z-direction (Niklas 1994, p. 3), the basal area G would have to scale to height h with $G \propto h^2$. Almost the inverse was the case: $G \propto h^{0.66}$. Regarding the exponent as a distribution factor (Ch. 2.3.1, Eq. 2-10), this means that the forest pushes the growth in vertical direction three times more than in either horizontal direction.

Due to their physiological significance, allometric exponents have often been controversially discussed (see Ch. 2.3.1). It is not the aim of the work to enter this debate, but certain considerations related to the Reineke rule $N \propto dbh^c$ (c = -1.605, Reineke 1933), the Yoda rule $\overline{b} \propto N^c$ (c = -1.5, Yoda et al. 1963), and the $\overline{b} \propto N^c$ relation according to the WBE-theory (c = -1.33, Enquist et al. 1998, West et al. 1997/ 1999) can also be made from this work.

An important aspect from Ch. 2.4.4 was that tree height and dbh could not be related by the allometric equation. However, the dbh-height relation links the Reineke rule and the Yoda rule:

$$\left.\begin{array}{ll} \text{Reineke:} & N \propto dbh^{c(reineke)} \\ \text{Yoda:} & \overline{b} \propto h_{mid} \cdot dbh_{mid}^2 \propto N^{c(yoda)} \end{array}\right\} \quad h_{mid} \propto dbh_{mid}^{\left(\frac{c(yoda)}{c(reineke)}-2\right)} \qquad \textbf{Eq. 2-23}$$

This link between Reineke and Yoda can be criticized in many aspects: (1) the Reineke rule was established for self-thinning stands, (2) the Yoda rule was applied on herbaceous plants, and (3) limitations due to interrelating exponents have been demonstrated for the height-basal area allometry in Ch. 2.4.4.

Empirically, the Reineke relation can be matched well with the allometric equation. The exponents range between -1.33 and -1.8. The Yoda relation does not match the allometric equation well. In young stands, the exponent is generally lower than -2, in old stands about -1.5 which lies closer to the Yoda exponent of -1.5 than the WBE exponent of

-1.33. It should be noted that in contrast to growth allometry of Reineke and Yoda, the WBE-theory was based on comparative allometry. The exponent for biomass-N allometry was derived from the comparison of plants of different organization levels. It has a model-like character and essentially aims at very general mechanisms, rather than 'small scale' differences like between the growth behaviour of trees.

Pretzsch (2006) and Pretzsch and Biber (2005) determined for self-thinning spruce, pine, beech and oak stands exponents of -1.3 to -1.65 for the Reineke relation and -1.4 and -1.8 for the Yoda relation. The relevance of allometry in terms of eco-physiological strategies, e.g. the self-tolerance, will be discussed in the following Ch. 2.5.2.

The allometric factor: The allometric level was used as a tool to quantify the differences in the height-biomass allometry between species, yield classes and yield tables. Since the differences between the yield classes were low, a common allometric level was defined for all yield classes of one table based on the characteristic part of the allometric curve (Fig. 2-17). As could be expected from the reference level for Norway spruce delineated the upper biomass level that could be expected for a certain height. Only two more species, white fir and beech, reached the same level. Some results shall be discussed in more detail:

1. The species dependence of the height-biomass allometry revealed an interesting aspect in terms of forest ecology. Disregarding the influence of thinning, there seems to be a trend of a decreasing allometric level from climax of pioneer character of a tree species (Fig. 2-17). A possible interpretation is that pioneer species need more space to cover their energy demand needed for a fast growth or to contemplate with adverse site conditions. The highest level was found for spruce, fir and beech. Under moderate site conditions they are the most competitive tree species of Middle Europe (Annex 7.2).
2. The yield-class independence of the height-biomass allometry was described as the rule of Eichhorn (1902, Ch. 2.4.3). Regarding the yield class as a (species-specific) indicator of the site conditions (Ch. 2.4.2), the height-biomass allometry is to a large degree independent from site conditions. Deviations from the yield-class independence were noted especially for old stands of Scots pine, and beech in general (Fig. 2-16). The fact that, for a given height, the same basal area is reached with different dbh-tree number relations (Fig. 2-20), plays an important role in the allometric model in Ch. 2.5.2.
3. In the yield tables, strong thinning was found to reduce the allometric level by 10-20% compared to moderate thinning. In general, thinning enforces dbh growth, but has only little effect on height growth. Therefore, singular thinning actions are compensated soon, especially in the growth phase. Only regular thinning keeps the allometric level constantly low. In forestry practise, high thinning is applied in the regeneration phase. During these last 5-30 years of the management cycle the stand density is gradually reduced to enhance natural regeneration under a protecting canopy (Burschel and Huss 1997, pp. 123).

Last but not least, one of the apparently most restrictive aspects of the yield tables is the even-aged forest structure. But it was already said in Ch. 2.4.1, that the concept of allometric reference function and allometric level can be applied, too, as long as a height can be defined. This issue is addressed in more detail in Ch. 2.6.

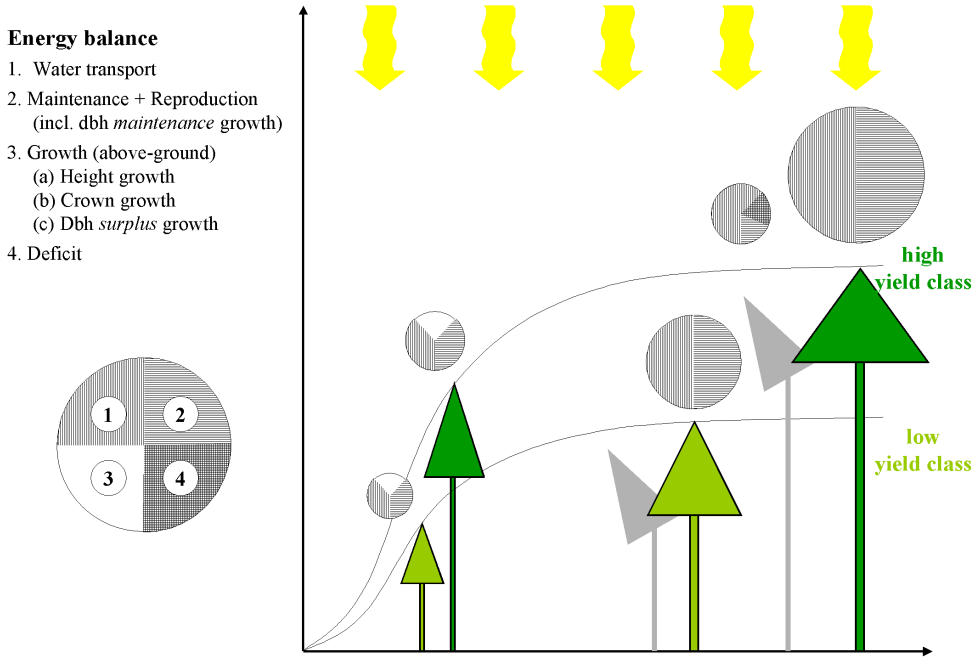

Fig. 2-21 Allometric Forest model

Forest allometry is interpreted from an energetic point of view. Higher trees demand more energy for water transport and therefore must increase their crown size – leading to thinning during growth. Restricted water availability demands bigger crowns at lower heights.

2.5.2 Allometric forest model

The collected material shall now be gathered in an eco-physiological model that interprets forest allometry from an energetic point of view. It is a strongly simplified model, which explains the growth of even-aged forests like in the yield tables. It is in the first order suitable for average growth conditions, and not for extreme events. The approach is illustrated in Fig. 2-21, and can be explained in four steps:

1. The energy input is provided from solar radiation: in Fig. 2-21, every tree gains an energy amount proportional to its horizontal crown space (circle above tree crown). The tree density is therefore a key parameter in forest allometry. As the tree grows it requires more energy and must occupy more crown space, thereby leading to a reduction of the overall tree density.
2. The height growth of a tree is necessary to gain advantage in the competition for light (Lyr et al. 1992, p. 428). Since height growth is asymptotic, we must assume a height-antagonism in accordance with Bertalanffy's 'dynamic morphology' (1942, Ch. 2.3.2). Assuming that tree statics is not the critical factor (Ch. 2.4.4, Niklas 1994, p. 171), the antagonist could be a higher energy demand for transports, probably mainly water (Strasburger 1983, p. 320, Lyr et al. 1992, pp. 155). Although the water conduction is a passive process that follows a negative pressure gradient, there are energy demanding requirements connected with the water transport to higher heights, e.g. increased cell wall stability or less 'life'-time of the conductive xylem. At a certain point, the tree cannot allow the energy demand resulting from its height

to increase, and height growth slowly ceases. Under adverse growth conditions, this equilibrium is reached at lower heights, than under good conditions. Hence, the lower height asymptote of low yield classes. This would explain that lower yield classes need lower tree number densities, i.e. more crown space, for a certain height (Fig. 2-20).

The most decisive factor for the height potential of a certain tree is in general the water availability (Barnes et al. 1998, pp. 145, Kramer and Boyer 1995, Kozlowski and Pallardy 1997), but also nutrient availability, length of growing season and other factors play a role. Pretzsch (1999) showed that a Scots pine may even reanimate its height growth. Also, internal controls like the root-shoot ratio seem to control height growth. Carmean (1970) describes how height growth of black walnut (*Juglans nigra*) in Illinois suddenly stopped as the roots reached a stagnant water table and could not further expand.

3. An increased dbh of the tree has – in contrast to height – no effect on the energy balance. Maybe undervaluing its static importance, the main reason for dbh growth is to ensure the water transport, which requires the constant replacement and expansion of inactive xylem tissue (see Ch. 2.2.3). In Fig. 2-21, the investment into the replacement was grouped under 'maintenance energy'; further dbh expansion leads to an enlargement of the conductive tissue due to the increasing crown size. This also explains the stronger reaction of dbh growth to thinning than the height growth.
4. At maturity, an investment into height growth is counter-productive for the energy balance. Dbh must at least increase to replace the aging xylem tissue (maintenance dbh), and tree number further decreases through mortality. But when height is constant, any changes in basal area, i.e. dbh or tree number, directly affects the height-biomass allometry. Therefore, in old forests, the relation between tree number and dbh plays an important role. The relation $N \propto dbh_{mid}^{-2}$ would keep the basal area constant, the relation $N \propto dbh_{mid}^{0}$ and would keep the tree number constant.

   It is hard to make predictions about the exponent. Physiologically, if the energy demand of the mature forest is at equilibrium, a constant crown area could meet the constant energy demand for maintenance (incl. dbh growth) and reproduction. Then the tree number could be kept constant while dbh still grows (exponent 0). However, natural mortality reduces the stem density, in bad years more in good years less. The exponent is therefore probably not fixed, but flexible and may also fall below -2 (= basal area decrease).

The presented forest allometric model focuses on an allometric interpretation of forest growth, and explains only very generalized mechanisms. Much more detailed growth models are described in Pretzsch (2001).

But the strong focus on height related allometry sometimes puts a new light onto forest allometry like comparison of the allometric levels between the species. One more such case shall be looked at, the relation between height and tree number being the two most important parameters in the allometric model.

The traditional allometry between tree number and dbh has found high attention, being interpreted as a species' strategy in the occupation of crown space (self-tolerance, Zeide 1985, Pretzsch and Biber 2005, Pretzsch 2006). Now, Fig. 2-22 displays the average

available crown space, i.e. the inverse tree number, as a function of tree height for different yield classes of Norway spruce and European beech. It can be seen that above 15 m, beech sequesters more crown space for a given height than Norway spruce. Although the crown space it artificially regulated through thinning, the species- and yield class-characteristics are probably not totally distorted. Then, the height-tree number allometry reveals a lower self-tolerance or higher self-competition of beech as well as the dbh-tree number allometry. The differences between the yield classes can be interpreted by the allometric model as resulting from the higher energy demand for a given height under adverse site conditions.

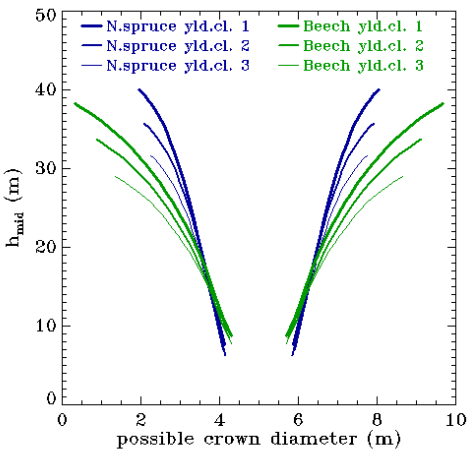

Fig. 2-22 Crown space sequestration of spruce and beech trees during growth

Norway spruce, (Assmann and Franz 1963, avrg.yld.lev., OH40-32); European beech (Schober 1967, mod.thin., yield classes I-III)

2.6 Height-biomass allometry with remote sensing height data

The aim of Ch. 2 was to establish a concept of how to estimate forest biomass from forest heights derived from remote sensing data. The concept was introduced in Ch. 2.4.1. It involved the definition of a reference height and biomass in Ch. 2.2.2, the selection of a reference forest type (Ch. 2.4.2) and the realization in Ch. 2.4.3. Now, the results and considerations shall be summarized and reviewed for practical implementation with remote sensing height data. Then, the concept of height-biomass allometry shall be refined and condensed in a 3-step conversion procedure that can be adapted to different forest types as well as sensor types.

Reference height and biomass (Ch. 2.2.2): Before the derivation of a height-biomass allometry, it was necessary to agree on a rational definition of forest height and biomass. The following aspects should be outlined in terms of forest height:

- Two demands were imposed: (1) When not resolving single trees, the reference height is not tree height, but forest height. (2) It was recommended to refer to a forestry standard, but not to stick too literally to it in order to allow flexibility in the use of different data sources.
- The upper canopy height was introduced as the most characteristic forest height. In general, the h_{100} is the typical forestry standard for the upper canopy height. In the yield tables, the mid height served as the upper canopy measure since the stands are composed of a single layer. The concept of the upper canopy height meets its limits where the height of the uppermost tree layer is variable (Fig. 2-5). Here, it might be better to distinguish an emergent layer and a true upper canopy. It was tried to avoid this case in this work, but in terms of a global concept it is an essential discussion.

Concerning forest biomass, the following aspects were considered:

- The reference biomass was required (1) to be a reasonably accurate and available measure, (2) to be representative for both tall and low forests, (3) and refer to a forestry standard, again allowing some flexibility.
- The stem biomass was recommended as a reference, because it is a 1st order parameter from dbh and height, which is more accurate than measures including branch, and leaf biomass. In order to be also representative for low forests, it was recommended to avoid dbh limits. This is especially important for the inventory of young forest stadiums.

Reference forest (Ch. 2.4.2): The selection of a reference forest was necessary to make the derivation of the height-biomass allometry transparent and comprehensible. The forestry yield tables were suited in this respect:

- The even-aged forest structure and differentiation between species, yield class and thinning reduced the complexity of the height-biomass relation, and allowed to analyse the effect of the named factors.
- They are a standard tool in forestry, provide a large and differentiated data base
- The even-aged and dense forest structure requires care when extrapolating to heterogeneous forest types; the effect of thinning impedes eco-physiological conclusions.

Reference equation and allometric level (Ch. 2.4.3): The relation between height and biomass could be matched with an allometric equation of Huxley (Eq. 2-9). This made it possible to apply the concept of an allometric reference and allometric level (Eq. 2-12). The approach and results can be summarized as follows:

- The allometric reference equation was derived from the Norway spruce tables of Assmann and Franz (1963, average yield level) as a common regression through the yield classes (Eq. 2-17). Norway spruce is a widespread, and economically important tree species, which can be kept with high stand densities.
- Comparing 11 species in the 21 considered yield tables, the reference allometry from Norway spruce forms the upper biomass limit. Most other species reach allometric levels between 0.7-1 (with the exception of birch and poplar). A tendency of a decreasing allometric level from climax to pioneer character of the species was noted, but also regional differences seem to play a role. The effect of the yield class is comparably low (~10%). For strong thinning intensities it is necessary to reduce the biomass estimation by 10%-20%.

In retrospective, the evolution of the reference equation started with a linear height-biomass function for the spruce tables of Wiedemann (1943, moderate thinning): $B = 12.2 \cdot h_{mid} - 100$ for $h_{mid} > 8$ m (Mette et al. 2002). The linearity reflects the 'usable' criterion of the reference biomass. In Mette et al. (2003), the h_{100} was defined as the reference height. The reference equation $B = 0.8 \cdot h_{100}^{1.73}$, now from the Norway spruce tables of Assmann and Franz (1963), was compared to the empirical height-biomass allometry in Fichtelgebirge: $B = 0.2 \cdot h_{100}^{2}$ which lay 33% below the reference function. In Mette et al. (2004a), the concept of growth allometry was first introduced and a

common equation was defined on the basis of Norway spruce (Assmann-Franz tables), Scots pine, beech and oak: $B = 1.52 \cdot h_{mid}^{1.52}$. Here, the mid height served as the upper canopy definition in the yield tables. Realizing the similarity between the species and the compensating effect of wood density, the equation was termed a 'common allometric height biomass allometry' (Mette et al. 2004b). The final equation, $B = 1.66 \cdot h_{mid}^{1.58}$, refrained from the averaged spruce-pine-beech-oak curve and decided to use only the spruce tables for the reference equation (Mette et al. 2006a). The definition of the allometric level and its use as a density adjustment along with the 3-step height-biomass allometry (see below) were introduced in Mette et al. (subm.).

3-step height-biomass allometry: Based on the results from the yield tables and further theoretical considerations, the concept of reference allometry and allometric level shall embedded in a 3-step height-biomass conversion corresponding to 3 levels:

1. Application of the reference height-biomass allometry: this step accounts for the height dependency of biomass. The chosen reference function (Eq. 2-17) should reflect the upper biomass limit, or the biomass potential for a given height. Forest height information can help identify site conditions and growth stadiums. It is especially important to document the regeneration after a heavy disturbance like clear-cut, heavy fires, wind throws or serious calamities.
2. Correction with the average allometric level: in a first order, the allometric level adjusts the density dependence of biomass. Of the three factors considered in the yield tables, especially species and thinning have an impact on the allometric level. When density variations are low, an average allometric level may allow smoothing over occasional heterogeneities, like single emergents or local openings. When density variations are irregular and unpredictable – e.g. partial logging to enhance regeneration, or through illegal timber extraction – a small scale density information becomes very important.

   The adjustment of the allometric level requires supplementary information. It may be possible to exploit remote sensing sources, or model the allometric level from data like topography or climate.
3. Detection of 'problem' areas: A poor performance of height-biomass allometry is expected when the upper canopy layer is open or heterogeneous. Here, the definition of a reference height fails, but it is also questionable which height is extracted from processing of the remote sensing data. For such heterogeneous forest types, biomass can only be resolved from height data with individual tree resolution or exact knowledge of the height signature of the system.

   When defining 'forest' according to the FAO down to 10% canopy cover, this issue concerns whole ecosystems, especially the forest at its climatic limits: forest tundra (northern boreal, temperature limit), and savannahs (drought limit), as well as the transitions between forest and non-forest ecozones (=ecotones, Walter and Breckle 1991).

Basically, step 1 results in a map of the potential biomass for the corresponding height map. Step 2 corrects the map to the actual biomass through the allometric level. The local accuracy depends on the resolution of the allometric level map. Step 3 identifies areas which require a special treatment. Such a concept is very common in vegetation

ecology; examples are the concept of potential natural vegetation (Strasburger 1983, p. 962), or the biomass extrapolation proposed in Brown (1994, Ch. 6). The latter produced a potential biomass density index (PBI) based on climate, soil, topography (equivalent to step 1). The biomass potential was refined with assumptions about the relation between population density and forest biomass (equivalent to step 2).

After all, a first concept of height biomass allometry for use with remote sensing height data was proposed. It shall be implemented and further discussed in Ch. 4 where the height-biomass allometry is validated from inventory data of the test site Traunstein. The final conclusion will be drawn after the practical implementation and validation in Ch. 4. The analysis and interpretation of the allometry from the yield tables has proven that allometry is also a powerful tool for the understanding of forest eco-physiology. In terms of the global change discussion, allometry can help to estimate the potential carbon sequestration of forests in present and future climate scenarios. For instance, the very simple allometric forest model in Ch. 2.5.2 for instance, would predict a higher C-sequestration potential when precipitation increases the water availability; a lower potential would be expected when drought periods extent.

3 Polarimetric SAR Interferometry

Polarimetric SAR interferometry (Pol-InSAR) is a radar remote sensing technique that acquires a radar image in different polarizations (polarimetry) and from slightly different viewing angles (interferometry). It combines the strength of being sensitive to the polarization-dependence of an object's scattering behaviour and the 3D-resolution of interferometry.

Using an appropriate system configuration, the Pol-InSAR signature of a forest depends to a large degree on forest height. This capability is used in this work to extract forest heights, which is the first step in the biomass estimation procedure (see Fig.1.1).

This chapter establishes the theoretical background for the Pol-InSAR forest height inversion based on the understanding of forest as a 'Random Volume over Ground' (RVoG). The main parameter is the interferometric coherence, i.e. the correlation between interferometric images. Phase and magnitude of the coherence are a function of the scatterer height distribution inside the forest. The height distribution, in turn, depends on three parameters: forest height, extinction and ground contribution. These parameters can be resolved from a Pol-InSAR data set. However, it is important that only the height dependent part of the coherence, i.e. the volume decorrelation, is used as input for the model-inversion. Other decorrelation processes must be minimized by the system configuration or otherwise tried to be compensated. The Pol-InSAR height inversion from the RVoG is validated in Ch. 4 from data of the test site Traunstein.

Ch. 3.1 provides an introduction to radar remote sensing, Ch. 3.2 covers some essentials about backscattering and polarimetry. In Ch. 3.3, the theory of radar signal processing leads to a SAR system model. This model is extended in Ch. 3.4, to represent the different coherence contributions in an interferometric SAR model. The Random Volume over Ground model (RVoG) in Ch. 3.5 is based one coherence contribution, the volume decorrelation. The inversion of the RVoG with Pol-InSAR data is addressed from an implementation-oriented point of view.

3.1 Introduction

This subchapter constitutes a brief introduction into the topic of radar remote sensing. Following a short paragraph on remote sensing in general, the image acquisition with a side-looking radar is explained. The last section provides a selected overview over air- and space borne SAR systems.

"Remote sensing is the science and art of obtaining information about an object, area, or phenomenon through the analysis of data acquired by a device that is not in contact with the object, area, or phenomenon under investigation..." (Lillesand and Kiefer 1999, p. 1). Remote sensing usually refers to optical or radar imagery from airborne or space borne platforms. As Fig. 3-1 illustrates, the corresponding portions of the electromagnetic spectrum – optical wavelengths 0.4-14μm and radio wavelengths 0.01-1m – are the only ones hat do not interfere with the atmosphere (= atmospheric windows) and therefore suitable for remote sensing of the earth surface.

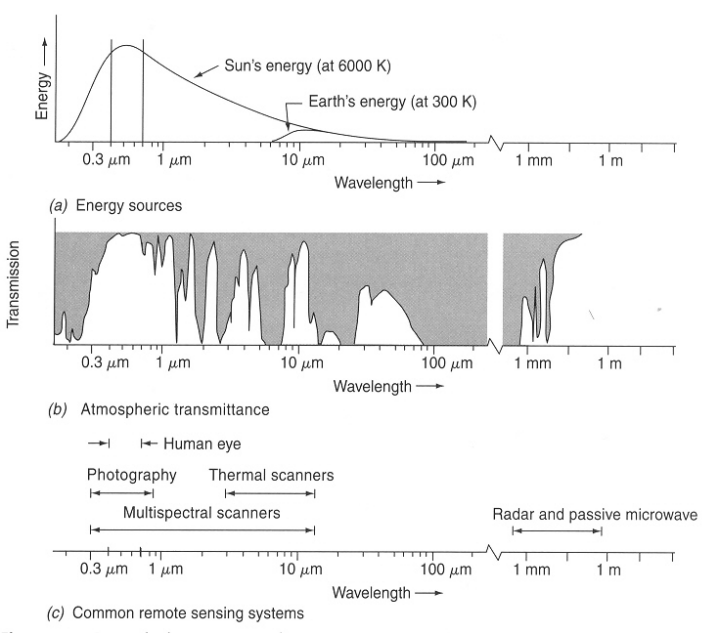

Optical Band	Wave-length [μm]
UV	0.3-0.4
Blue	0.4-0.5
Green	0.5-0.6
Red	0.6-0.7
Near IR	0.7-1.3
Mid IR	1.3-3
Far IR	3-14

Radar Band	Wave-length [cm]	Frequency [GHz]
K-band	0.8-2.4	40-12
X-band	2.4-3.8	12-8
C-band	3.8-7.5	8-4
S-band	7.5-15	4-2
L-band	15-30	2-1
P-band	30-100	1-0.3

Fig. 3-1 Electromagnetic wavelength spectrum
Source: Lillesand and Kiefer 1999, p. 11/ 637

'Radar' is an acronym for 'Radio detection and ranging'. It is only since the 1950s, that radar was employed as an imaging system, but since then airborne and satellite systems have proved valuable especially through their all-time-all-weather imaging capability and the distinct object information. The use of radar for geoscience applications took its beginning in the first Symposia of Remote Sensing in the 1960s, and the earliest work of vegetation mapping from airborne real aperture radar was introduced by Morain and Simonett (1966). A historical treatment of radar can be found in standard literature (e.g. Elachi 1987, Curlander 1991, Ulaby 1986, Henderson & Lewis 1998).

Imaging radar typically refers to side-looking radars of the type of RAR (Real Aperture Radar) and SAR (Synthetic Aperture Radar). The following two items give a basic overview over the operation mode and image formation:

(1) Operating mode: Since the sun energy emitted in the radio spectrum (0.01-1 m) is much lower than in the optical spectrum (Fig. 3-1), high resolution radar imagery is only possible when the system transmits its own pulse and receives the 'echo'. This active operation mode permits a very precise control of the illumination. Phase coherency allows high resolution SAR processing and SAR interferometry (Ch. 3.3 and Ch. 3.4). Like in optical remote sensing, the radar spectrum is divided into channels, or bands (Fig. 3-1). RGB-colour coding can be used to display image information of different wavelengths, polarizations, look angles or time series.

Furthermore, radar waves are almost not attenuated by atmospheric water and ice molecules, and penetrate the atmosphere almost undisturbed. Especially frequencies lower than X-band can 'see' through clouds. This way, radar played an important role in land surveys over continuously cloud-covered (tropical) regions, like in Panama, Venezuela or Brazil (Lillesand and Kiefer 1999, pp. 618).

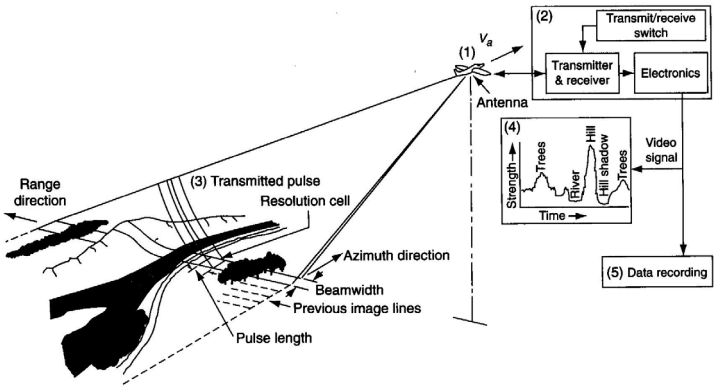

Fig. 3-2 Generation of a radar image

One range line corresponds to one pulse. The azimuth-dimension is generated through the continuous sending and receiving of pulses. Source: Lillesand and Kiefer 1999, p. 621

(2) Image formation: As the name says, radar is a 'ranging' system, which means it measures the distance to an object. This range imagery forces radar to be side-looking because a nadir, i.e. straight down looking system, would be ambiguous for object located on the right and left of the flight path. The image acquisition is illustrated in Fig. 3-2, and can be explained in four steps (number of steps does not correspond to elements in Fig. 3-2):

1. A radar pulse is transmitted by the antenna (in transmit mode) perpendicular to the flight direction (side-looking).
2. The transmitted pulse interacts with objects on the ground, and is partly backscattered towards the antenna. The time between sending and receiving corresponds to the distance (range) of the object – like an echo.
3. The antenna (in receive mode) records the backscattered pulse in time. The resulting range line is sketched in element (4) of Fig. 3-2 and shows the amplitude of the radar 'echo' on the time axis.
4. The continuous transmitting (and receiving) of pulses during the flight generates the azimuth dimension. The time between the sending of two pulses is the pulse repetition frequency PRF and determines the azimuth distance between two range lines.

The obtained data form the raw image and may require coherent pulse and synthetic aperture processing (Ch. 3.3). The particular radar geometry is termed slant range geometry. Fig. 3-3 shows an L-band backscatter image in HH-polarization of the test site Traunstein. The scene is displayed in ground geometry (Fig. 3-3.a), and radar slant range geometry (Fig. 3-3.b). Due to the left-looking E-SAR L-band antenna, the slant range image is mirrored.

In 1978, the first radar satellite, SeaSAT, was launched with a synthetic aperture system, as a counterpart to the optical LandSAT satellites (1972 LandSAT 1). Since then the qualities of radar for land- and ocean-, bio- and physiogeography were manifested in several shuttle and satellite missions like SIR-A/B 1981/ 1984 (US) and SIR-C/ X-SAR 1994 (US, Germany, Italy), ERS-1/2 1991/ 1995 (EU), JERS-1 1992 (Japan), Radar-

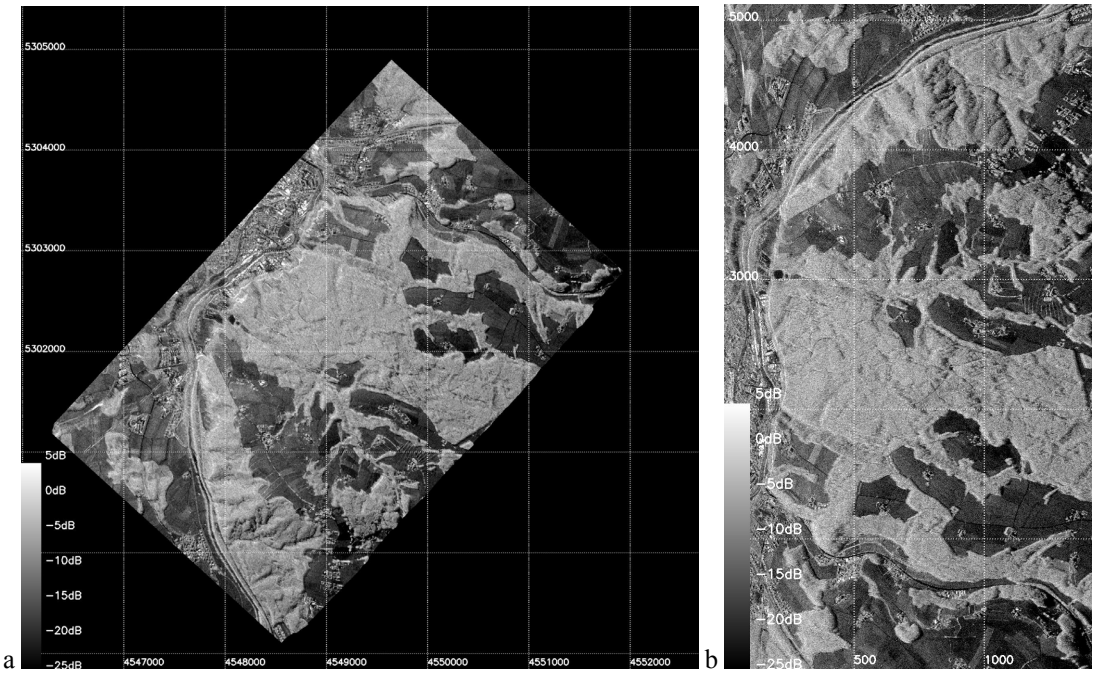

Fig. 3-3 Radar backscatter image of test site Traunstein in L-band HH-polarization

(a) in ground range geometry, (b) in slant range geometry. The image was acquired in a flight direction NE to SW. Due to the left-looking E-SAR L-band antenna, the slant range image is mirrored.

RF-Band	X-Band	C-Band	S-Band	L-Band	P-Band
RF-centre frequency	9.6 GHz	5.3 GHz	3.3 GHz	1.3 GHz	450 MHz
Transmit peak power	2500 W	750 W	2 kW	400 W	200 W
Receiver noise figure	4.0 dB	4.0 dB	5 dB	8.5 dB	4.0 dB
Antenna gain	17.5 dB	17 dB	16 dB	15 dB	12 dB
Azimuth beamwidth	17°	19°	12°	18°	30°
Elevation beamwidth	30°	33°	32°	35°	~ 60°
Antenna Polarization	H and V	H and V	H and V	H and V	H and V
IF-centre frequency	300 MHz	300 MHz	300 MHz	300 MHz	300 MHz
Max. Signalbandwidth	100 MHz	100 MHz	100 MHz	100 MHz	50 or 18 MHz
System bandwidth	120 MHz	120 MHz	120 MHz	100 MHz	60 or 25 MHz

Fig. 3-4 The airborne 'Experimental-SAR' system of DLR (E-SAR): system parameters and DO-228 carrier platform

SAT 1995 (Canada), SRTM 2000 (US, Germany), and EnviSAT 2002 (EU), and a continued flow of data is guaranteed in future missions like ALOS 2006 (Japan), TerraSAR X 2007 (Germany), or RadarSAT 2 2007 (Canada).

Also, airborne SAR systems – including AirSAR (US), GeoSAR (US), SAR 580 (Canada), EmiSAR (Denmark), CARABAS (Sweden), and E-SAR (Germany) – are constantly being refined to improve information quality in terrain mapping. They provide crucial input and preparatory work for space borne SAR missions. The German E-SAR system operates at multiple frequencies with different polarizations and interferometric modes (Horn 1994, Horn et al. 2000, Scheiber et al. 1998, Fig. 3-4). This work mainly utilizes the polarimetric interferometric capability of the E-SAR at L-Band.

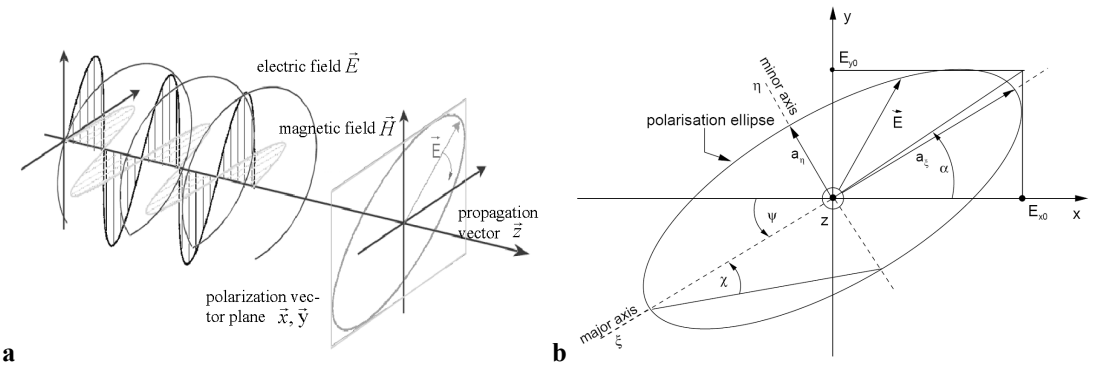

Fig. 3-5 (a) Electric and magnetic field of an electromagnetic wave, (b) polarization ellipse

3.2 Radar polarimetry

Radar backscatter images resemble optical images in some ways, because the image intensity and texture delineates the contours of objects and landscape units. However, the information content is not similar, because the interaction of radar waves with the object is different. This subchapter gives an introduction to the polarization of electromagnetic waves (Ch. 3.2.1), describes the representation of the polarimetric object signatures by the scattering matrix and scattering vectors (Ch. 3.2.2), and explains the two basic scattering mechanisms, surface and volume scattering (Ch. 3.2.3).

3.2.1 The polarized electromagnetic wave

To understand the scattering mechanisms from the basis, we need to go back to the description of the electromagnetic wave (oriented in the following at Hellmann 2001). A plane wave propagating in the direction $\vec{z}$ is made up of (a set of) coupled, time varying and mutually orthogonal electrical and magnetic vector fields (Fig. 3-5.a), and can be described by the electrical field vector $\vec{E}(z)$. The polarization of the wave is given by the vector plane perpendicular to the propagation direction, and – in the general case – describes an ellipse. Introducing an x-, y-reference coordinate system, the electrical field consists of an x-component $\vec{E}_x(z)$ and a y-component $\vec{E}_y(z)$ (with the complex amplitudes $\widetilde{E}_{x/y} = E_{x0/y0} \cdot e^{i\delta_{x/y}}$, and the wave number k = 2π/λ):

$$\vec{E}(z) = \vec{E}_x(z) + \vec{E}_y(z) \qquad \textbf{Eq. 3-1}$$

$$\vec{E}_x(z) = \vec{E}_x(z) \cdot e^{i(kz+\delta_x)} \cdot \vec{e}_x$$
$$\vec{E}_y(z) = \vec{E}_y(z) \cdot e^{i(kz+\delta_y)} \cdot \vec{e}_y \qquad \textbf{Eq. 3-2}$$

The instantaneous values for a certain time t are given by:

$$\vec{E}_x(z,t) = E_{x0}\cos(\omega t - kz + \delta_x)$$
$$\vec{E}_y(z,t) = E_{y0}\cos(\omega t - kz + \delta_y) \qquad \textbf{Eq. 3-3}$$

Tab. 3-1 Electric field vector for EM-waves of different polarizations

Polarization	elliptical at θ°	circular (right/ left)	horizontal | vertical	linear at θ°
Ampl. ratio	$a_v:a_h = \tan\theta$	$a_v:a_h = 1$	$a_h:a_v = \infty$ | $a_v:a_h = \infty$	$a_v:a_h = \tan\theta$
Phase offset		0°	- | -	0°
Orientation ψ	θ°	free	0° | 90°	θ°
Ellipticity χ	≠ 0° and ≠ 45°	45°/ -45°	0° | 0°	0°
Illustration	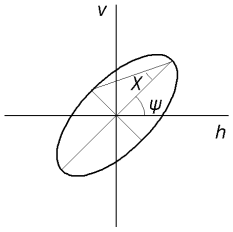	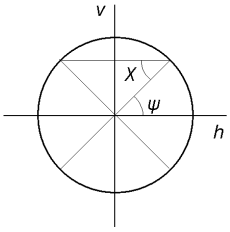	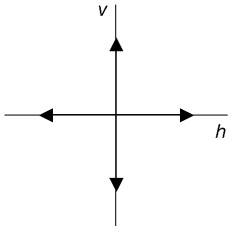	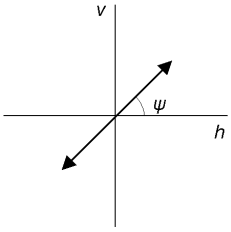

and can be resolved to the equation of an ellipse (Eq. 3-4, $\delta_0 = \delta_y - \delta_x$). ψ is the inclination angle (Eq. 3-5) and χ the ellipticity angle as the tangent between major and minor axis a_ξ and a_η respectively (Eq. 3-6). This polarization ellipse is shown in Fig. 3-5.b. Tab. 3-1 gives an overview over commonly used polarizations.

$$\left(\frac{E_x(z,t)}{E_{x0}}\right)^2 + \left(\frac{E_y(z,t)}{E_{y0}}\right)^2 - 2\left(\frac{E_x(z,t)E_y(z,t)}{E_{x0}E_{y0}}\right)\cos(\delta_0) = \sin^2(\delta_0) \qquad \textbf{Eq. 3-4}$$

$$\tan(2\psi) = \frac{2E_{x0}E_{y0}}{E_{x0}^2 - E_{x0}^2}\cos(\delta_0) \qquad \textbf{Eq. 3-5}$$

$$\tan(\chi) = \pm\frac{a_\xi}{a_\eta} \qquad \textbf{Eq. 3-6}$$

3.2.2 Polarimetric representation of objects

For the radar wave, the polarization state is usually represented by the electric field vectors in horizontal (H-) and vertical (V-) basis. Written in the Jones vector representation, the polarization in Eq. 3-1 is given by (Jones 1941, Born and Wolf 1985, Touzi 2004):

$$\vec{E} = E_h \cdot \vec{e}_h + E_v \cdot \vec{e}_v = \begin{bmatrix} E_h \\ E_v \end{bmatrix} \qquad \textbf{Eq. 3-7}$$

Upon interaction with the object on the ground the polarization state of the transmitted wave may be altered. The relation between transmitted and received wave is given by the [S]-matrix (Sinclair 1948/ 1950, Kennaugh 1951), and completely describes the polarimetric backscattering properties of the object:

$$\vec{E}^r = [S]\cdot\vec{E}^t = \frac{e^{ik_0 r}}{r}\cdot\begin{bmatrix} S_{hh} & S_{hv} \\ S_{vh} & S_{vv} \end{bmatrix}\cdot\begin{bmatrix} E_h^t \\ E_v^t \end{bmatrix} \qquad \textbf{Eq. 3-8}$$

The elements of [S] denote the complex scattering amplitudes; S_{HH} and S_{VV} are referred to as the co-polar, S_{HV} and S_{VH} as the cross-polar components. In radar, the scattering matrix is measured by transmitting and receiving successive pulses in H- and V-

polarization. The measuring of the full polarimetric scattering matrix allows characterizing an object through its polarization signature and "to identify and separate scattering mechanisms of natural media […] for the purpose of classification and parameter estimation" (Papathanassiou et al. 1999). The scattering coefficient of either matrix element is given by:

$$\sigma_{qp} \propto \frac{\left|E_q^r\right|^2}{\left|E_p^t\right|^2} = \left|S_{qp}\right|^2 \qquad \textbf{Eq. 3-9}$$

where p and q denote the transmitted and received polarization respectively.

In the backscattering case (when the transmit and receive antenna are at the same position) the cross-polarization terms are equal following the reciprocity theorem (Cloude and Pottier 2006).

A common notation instead of the 2x2 [S]-matrix is complex scattering vector $\vec{k}$ of which the lexicographic vector $\vec{k}_L$ (Bourgeaud 1989) and the Pauli vector $\vec{k}_P$ (Cloude 1986, Cloude and Pottier 1996) shall be introduced here:

$$[S] = \begin{bmatrix} S_{hh} & S_{hv} \\ S_{vh} & S_v v \end{bmatrix} \rightarrow \vec{k} = \frac{1}{2} Trace([S]\psi) = [k_0, k_1, k_2, k_3]^T \qquad \textbf{Eq. 3-10}$$

where Trace([S]) is the sum of the diagonal elements of [S] and ψ is a complete set of 2x2 complex basis matrices under a hermitian inner product (Cloude 1986). Due to reciprocity, the cross-polarized elements are similar ($S_{hv} = S_{vh}$), and the lexicographic and Pauli vectors are commonly given as the 3-element vectors $\vec{k}_{3L}$ and $\vec{k}_{3P}$:

Lexicographic:
$$\psi_L = \left\{ 2\begin{bmatrix} 1 & 0 \\ 0 & 0 \end{bmatrix}, 2\begin{bmatrix} 0 & 1 \\ 0 & 0 \end{bmatrix}, 2\begin{bmatrix} 0 & 0 \\ 1 & 0 \end{bmatrix}, 2\begin{bmatrix} 0 & 0 \\ 0 & 1 \end{bmatrix} \right\} \qquad \textbf{Eq. 3-11}$$

$$\vec{k}_L = [S_{hh}, S_{hv}, S_{vh}, S_{vv}]^T \qquad \textbf{Eq. 3-12}$$

$$\vec{k}_{3L} = [S_{hh}, 2 \cdot S_{hv}, S_{vv}]^T \qquad \textbf{Eq. 3-13}$$

Pauli:
$$\psi_P = \left\{ \sqrt{2}\begin{bmatrix} 1 & 0 \\ 0 & 1 \end{bmatrix}, \sqrt{2}\begin{bmatrix} 1 & 0 \\ 0 & -1 \end{bmatrix}, \sqrt{2}\begin{bmatrix} 0 & 1 \\ 1 & 0 \end{bmatrix}, \sqrt{2}\begin{bmatrix} 0 & -i \\ i & 0 \end{bmatrix} \right\} \qquad \textbf{Eq. 3-14}$$

$$\vec{k}_P = 1/\sqrt{2} \cdot [S_{hh} + S_{vv}, S_{hh} - S_{vv}, S_{hv} + S_{vh}, i(S_{vh} - S_{hv})]^T \qquad \textbf{Eq. 3-15}$$

$$\vec{k}_{3P} = 1/\sqrt{2} \cdot [S_{hh} + S_{vv}, S_{hh} - S_{vv}, 2 \cdot (S_{hv} + S_{vh})]^T \qquad \textbf{Eq. 3-16}$$

The Pauli vectorization is very common, because it can be physically interpreted in terms of elementary scattering mechanisms:

- Pauli 1 (S_{HH}+S_{VV}): emphasizes isotropic "odd" bounce scatterers like surfaces, through coherent addition of the copolar channels (odd phase turns in medium and BSA convention)
- Pauli 2 (S_{HH}-S_{VV}): emphasizes isotropic "even" bounce scatterers (dihedrals) – typical for the 90° angles in urban areas – by subtracting the VV- from the HH-polarization (even phase turns in medium and BSA convention)

- Pauli 3 ($S_{HV}+S_{VH}$): polarization change of the wave due to randomly oriented scatterers, especially in volumes, mostly weakest backscatter intensity.

Fig. 3-6 shows the Pauli-vectorization for the Traunstein scene (E-SAR, L-band) in RGB colour-coding. The colours indicate that the backscatter signature of media exhibits differs between the polarizations. The image is analysed with more detail in the next chapter, Ch. 3.2.2.

To analyse the polarimetric signature of natural media, where a resolution cell typically contains several scattering elements, it makes sense to perform an ensemble averaging of resolution cells (covariance and coherence matrix, Boerner and El-Arini 1981, Boerner 1992, Cloude and Pottier 1996, Touzi et al. 2004).

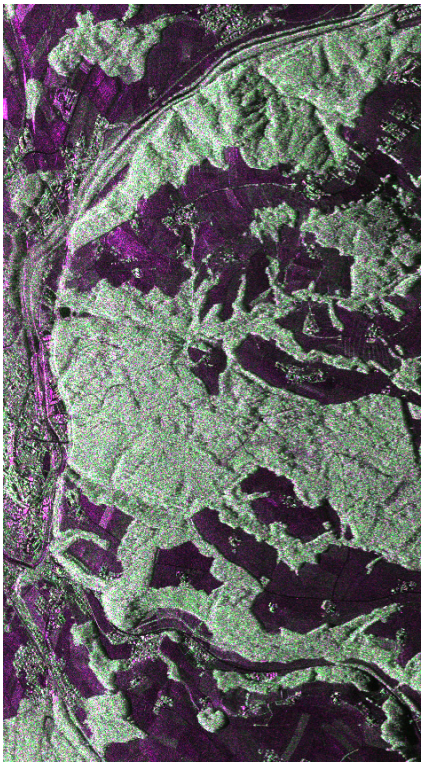

Fig. 3-6 Pauli vectorization of the Traunstein scene

Surfaces (Pauli 1, blue) and dihedrals (Pauli 2, red) can be distinguished as odd- and even-bounce scatterers. The green to white colour of the forests indicates volume scattering. Data: E-SAR, L-band, fully polarimetric, Oct.11, 2003, polarization were scaled to their respective mean.

3.2.3 Scattering of natural media

In the following the scattering behaviour in natural media is not described from a polarimetric perspective alone, but also includes the influence of wavelength. Two main mechanisms shall be distinguished, surface and volume scattering.

Surface scattering: considers the scattering processes occurring at the surface or immediate subsurface. Since the radar sensor, i.e. the antenna, measures the part of the emitted field that is backscattered in the direction of the antenna, the amount of surface backscatter increases with surface roughness (Fig. 3-7.a/b). It is obvious that 'roughness' is a question of the wavelength, and a surface that appears rough in X-band may still be smooth in P-band. Among different descriptions, the Raleigh criterion for instance states that surfaces can be considered rough for certain limits of the root-mean-square (rms) height of the surface variations (Beckmann 1963). In terms of polarimetry, flat surfaces have a low cross-polarized response.

Two special cases shall be mentioned: (1) specular scattering (Fig. 3-7a) occurs when the surface is very smooth and most of the incident field is scattered into the forward direction, and (2) dihedral scatterers (Fig. 3-7c) where the incident field is directed back towards the transmitter (90° angles). This double-bounce is the strongest natural scattering mechanism and occurs mainly for man-made, urban structures like house-walls etc., but is also characteristic for the trunk-ground interaction in forests or inundated forest areas (Smith and Ulander 2000, Alsdorf et al. 2001, Hoekmann and Quinones 2002).

Volume scattering: In contrast to the 2-dimensional surface scattering, volume scattering integrates the response from different depths of the medium (Fig. 3-7.d). The degree of volume scattering depends on the extinction of the wave in the medium, i.e. the sum of scattering and absorption[4]. It is essentially a question of the wavelength and the dielectric properties of the medium. In terms of polarization, volume scatterers are usually characterized by a significant amount of cross-polarization. Depolarisation occurs due to the orientation distribution of the scattering elements inside the medium (Fig. 3-7.d). At radar frequencies, typical volume scatterers are vegetation, esp. agricultural fields and forests, and ice. Forests are the main focus of the following treatment.

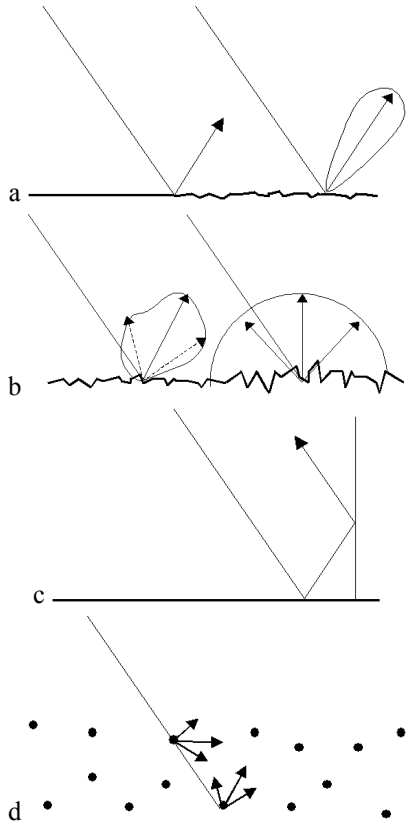

Fig. 3-7 Scattering mechanisms
(a/b) Surface backscattering increases with increasing surface roughness, (c) dihedral scattering, or double bounce, occurs at 90° angels, (d) volume scattering

Neglecting multiple scattering, the backscatter cross-section σ_{Volume} of the forest (or vegetation layer in a wider sense) can be written as the integral of all scattering elements $N \cdot \sigma_v$ over the vegetation height h; α is the extinction coefficient and θ the incidence angle (Attema and Ulaby 1978, Elachi 1987, pp. 15):

$$\sigma_{Volume} = \int_0^h N \cdot \sigma_v \cdot e^{-2\alpha \cdot z / \cos\theta} dz \qquad \textbf{Eq. 3-17}$$

Including the backscatter from the ground σ_G below the vegetation, the total backscatter of a forest σ_{VoG} (Volume over Ground) can be written as:

$$\sigma_{VoG} = \sigma_V + \sigma_G \cdot e^{-2\alpha \cdot h / \cos\theta} \qquad \textbf{Eq. 3-18}$$

Eq. 3-17 and Eq. 3-18 are used in the water cloud model (Attema and Ulaby 1978). They are also applied in the Random Volume over Ground model (RVoG, Ch. 3.5), but in this case, the emphasis lies on the coherent phase properties of the scattering elements. The RVoG can be resolved for its unknowns – h (height), α (extinction) and ground-to-volume ratio σ_G / σ_V – with polarimetric SAR interferometry.

As already mentioned, the extinction makes volume scattering wavelength dependent. According to Le Toan et al. (1992), Kasischke et al. (1995) and Castel et al. (2001), shorter wavelengths like K- and X-band interact mainly with the twigs and branches and are attenuated in the crown. C- and L-band are more sensitive to branches and the trunk and P-band, finally, seems to be scattered only from the largest branches and the tree trunk. For a certain increase in the scatterer density, the volume backscatter also in-

[4] The effect of absorption has not been differentiated from scattering loss in the following. It is generally represented by the complex dielectric constant which quantifies reflectivity and conductivity of materials.

creases, but this relation saturates due to extinction. Since the scatterer density has some relation to forest density, and hence forest biomass, the backscatter coefficient has often been proposed for forest biomass estimations. For cross-polarized L- and P-band data (HV or VH), where ground scattering is assumed negligible, the saturation limit lies at 40-100 t ha^{-1} in L-band and 120-200 t ha^{-1} in P-band (Le Toan et al. 1992, Dobson et al. 1992, Imhoff 1995, Kellndorfer et al. 2003). Only lower frequencies like the Swedish VHF sensor CARABAS (HH-polarization) can go beyond this point, but here, the backscatter-biomass model must account for the trunk-ground interaction (Fransson et al. 2000, Israelsson et al. 1997, Melon et al. 2001, Smith and Ulander 2000).

The relation between backscatter and forest biomass is essentially an indirect one. In principle it is based on the density of scattering elements, and the relationship will vary with species composition, forest structure, as well as with season and humidity conditions (Pulliainen 1999). A major uncertainty is the influence of the ground. The ground contribution depends on system parameters like wavelength, incidence angle and polarization, but also varies strongly with surface roughness, local terrain slope, and extinction. Recent results from Garestier et al. (2006) indicate that even X-band was sensible to the ground in a 20m high open pine stand. In summary, the main problems of the backscatter-biomass relations are the lack of general validity, and the saturation at comparably low biomass levels.

Pauli vectorization of the Traunstein scene (Fig. 3-6): In a final synthesis, we will reconsider the Pauli-vectorization of the Traunstein scene. It can be seen that the pure amplitude differences Fig. 3-3 are complemented by polarimetric object characteristics. After normalization of general amplitude differences, especially surfaces (fields) and forests are well distinguishable: as described, forests possess a comparably strong HV = VH response, and appear white to green. Surfaces are characterized through a relatively strong HH+VV response (Pauli-1, blue). Significant double bounce (HH-VV, Pauli-2, red) can only be noted over parts of the city of Traunstein in the extreme near range, but also here, volume scattering generally dominates.

Speckle: An important aspect of the radar signature of natural media, that has not been mentioned so far, is speckle. Speckle refers to the noise-like amplitude of distributed scatterers, i.e. scatterers with more than one scattering element per resolution cell. Here, the measured backscatter response is the coherent summation of the scattering elements, i.e. of amplitude and phase. As a result the backscatter intensity σ has a probability-density function pdf(σ) in the form of the Raleigh distribution (Oliver and Quegan 1998; p. 88, Bamler and Hartl 1998):

$$pdf(\sigma) = \frac{1}{\overline{\sigma}} \exp\left(\frac{-\sigma}{\overline{\sigma}}\right) \qquad \textbf{Eq. 3-19}$$

Amplitude accuracy can only be increased at the price of spatial uncertainty, e.g. by applying multi-look. For point scatterers, amplitude and phase of the radar signal are deterministic. Here – in contrast to distributed scatterers – one scatterer dominates the resolution cell (e.g. corner reflectors).

3.3 Radar Signal Processing

This subchapter treats the processing of a SAR image. Following the formulation of the pulse (Ch. 3.3.1), it is explained how coherent signal processing in range and azimuth can achieve high resolution (Ch. 3.3.2). In the processed SAR image, an point-like scatterer possesses a sinc-like signature (sin(x)/x) expressed by the impulse response function. The SAR system model in Ch. 3.3.3 prepares the interferometric SAR system model in Ch. 3.4, which is the basis for the inversion of forest parameters.

3.3.1 Pulse and echo

The transmitted radar pulse $A_t(t)$ can be described as a wave-package with pulse envelope a(t), carrier frequency f_0, and pulse length τ (complex signal representation):

$$A_t(t) = A_0 \cdot a(t) \cdot e^{i \cdot 2\pi \cdot f_0 \cdot t} \quad \textbf{Eq. 3-20}$$

For a linear frequency modulated pulse, i.e. the 'chirp', the envelope a(t) becomes:

chirp $$a(t) = e^{i \cdot \pi \cdot \Delta f / \tau \cdot t^2} \quad (-\tau/2 < t < \tau/2) \quad \textbf{Eq. 3-21}$$

The received (raw) signal A_r is a time delayed replica of the pulse (Eq. 3-22). Coherent (quadrature) demodulation subtracts the carrier frequency f_0 and leaves the phase term e^{-i2kR} due to the object distance (A_{rd}, Eq. 3-23). The distance $R = ½ (t_{received}-t_{transmitted})/c$ to the object is contained in the travel time of the pulse, $k = 2\pi/\lambda$ is the wave number. Omitting factors and constants for the moment:

$$A_r(t - 2R/c) = a(t - 2R/c) \cdot e^{-i\pi \cdot f_0 \cdot (t - 2R/c)} \quad \textbf{Eq. 3-22}$$

$$A_{rd}(t - 2R/c) = a(t - 2R/c) \cdot e^{-i \cdot 2kR} \quad \textbf{Eq. 3-23}$$

3.3.2 Resolution and SAR processing

Range and azimuth sampling: As described in Ch. 3.1.1, the radar image is formed in range through the sampling of the pulse, and in azimuth by the successive series of pulses. The distance between range samples is given by the range sampling frequency (RSF), the distance between the azimuth samples by the pulse repetition frequency (PRF). Note that the range sampling scales with the speed of light c while the azimuth sampling scales with the speed of the platform v (airplane or satellite):

$$range\ sample = c \cdot RSF^{-1} \quad \textbf{Eq. 3-24}$$

$$azimuth\ sample = v \cdot PRF^{-1} \quad \textbf{Eq. 3-25}$$

Resolution of un-modulated pulse and real aperture: Range and azimuth sampling are not directly related to resolution. For an un-modulated pulse in range, two objects can only be distinguished if they do not lie within the same pulse. This makes the range resolution res_{range} dependent on the pulse duration τ:

$$res_{range} = c \cdot \tau / 2 \quad \textbf{Eq. 3-26}$$

For a real aperture system (RAR) in azimuth, two objects can only be distinguished if they do not lie within the same antenna foot print, and the azimuth resolution res_{RA} de-

pends on the object distance R_0, the wavelength λ and the antenna aperture D_{RA} (subscript 'RA' for real aperture):

$$res_{RA} = R_0 \cdot \lambda / D_{RA} \qquad \textbf{Eq. 3-27}$$

Processing of linear frequency modulated pulse (chirp) and synthetic aperture: For the modulated pulse and a synthetic aperture system, the object response is spread over several range and azimuth samples respectively (raw signal in Fig. 3-8). It can be compressed through a convolution with a reference function (matched filtering). The reference function is modelled as the expected response of a point scatterer and accounts for the phase history of the signal.

In range: For a linear frequency modulated pulse a(t) (Eq. 3-21), the reference function g(t) that is set up, matches the phase of the pulse (Eq. 3-28). The processed range response after the convolution of pulse and reference function becomes a sinc-function, sin(x)/x (omitting factors and calibration constants, and the time delay –2R/c):

$$g(t) = \exp(-i \cdot \pi \cdot \Delta f / \tau \cdot t^2) \qquad \textbf{Eq. 3-28}$$

$$a(t) \otimes g(t) = \sin(\pi \cdot \Delta f \cdot t)/(\pi \cdot \Delta f \cdot t) \qquad \textbf{Eq. 3-29}$$

The frequency-modulated pulse has one strong advantage over the single pulse: for a high resolution, the un-modulated pulse requires a short pulse length of a high instantaneous power for a sufficient illumination of the scene. For a frequency modulated pulse the required instantaneous power can be distributed over a comparably long pulse.

In azimuth: For the synthetic aperture in azimuth, the object response is distributed over several azimuth samples (raw signal, Fig. 3-8). The phase changes quadratic with the distance R to the platform, and the resulting frequency $f_{SA}(t)$ can be shown to be linearly related to the illumination time t (subscript SA for Synthetic Aperture):

$$f_{SA}(t) = \frac{2 \cdot v^2 \cdot t}{\lambda \cdot R_0} \qquad \textbf{Eq. 3-30}$$

The maximum frequency range Δf_{SA} depends on the maximum possible illumination time t_{RA} which is a function of the real antenna aperture D_{RA}, the wavelength λ, the distance R_0, and the flight velocity v:

$$t_{RA} = \frac{\lambda \cdot R_0}{v \cdot D_{RA}} \qquad \textbf{Eq. 3-31}$$

$$\Delta f_{SA} = f_{SA}(t) \cdot t_{RA} = \frac{2v}{D_{RA}} \qquad \textbf{Eq. 3-32}$$

The aperture of the illumination time t_{RA} is the synthetic aperture D_{SA}. It is inversely related to the real aperture D_{RA}:

$$D_{SA} = R_0 \cdot \lambda / 2\, D_{RA} \qquad \textbf{Eq. 3-33}$$

The signal processing is similar to Eq. 3-28 and Eq. 3-29, only that the pulse duration τ corresponds to the illumination time t_{RA}. Accordingly, the azimuth reference function g(t) is given by:

$$g(t) \propto \exp(i \cdot \pi \cdot \Delta f_{SA} / t_{RA} \cdot t^2) \qquad \textbf{Eq. 3-34}$$

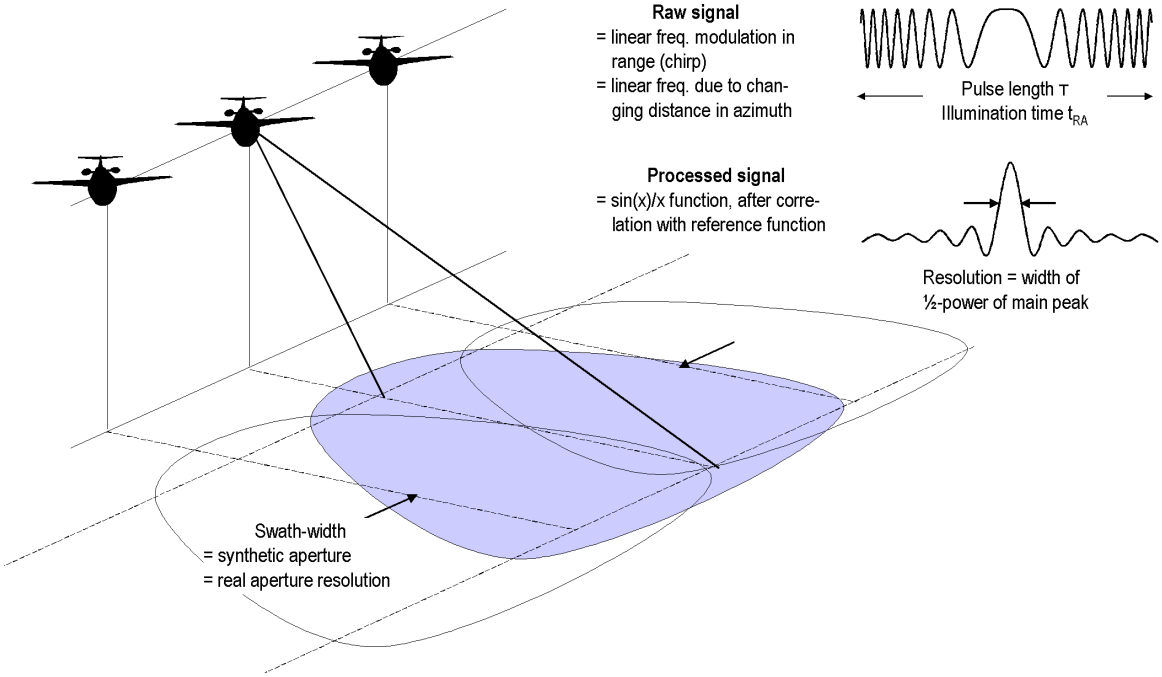

Fig. 3-8 Synthetic aperture radar (SAR)

SAR enhances the azimuth resolution by integrating the object raw signal over several pulses. The phase course has a linear frequency shift, and can be modelled with a reference function. The convolution of reference function and raw signal results in the processed signal in the form of a sinc -function. In range, the same principle is applied; here, a linear frequency modulated pulse is sent out.

Resolution and bandwidth: Resolution is defined as the width of the ½-amplitude (3 dB) of the main peak of the processed signal (Eq. 3-29, Fig. 3-8). It is dependent on Δf, i.e. the so-called bandwidth W:

$$W = \Delta f \qquad \textbf{Eq. 3-35}$$

The resolution res_{range} and res_{SA} and the bandwidth W and W_{SA} for range and azimuth respectively, are related over the speed of light c for the pulse propagation in range (Eq. 3-36), and over the speed of the carrier platform v in azimuth (Eq. 3-37):

$$res_{range} = c/2W \qquad \textbf{Eq. 3-36}$$

$$res_{SA} = v/W_{SA} = D_{RA}/2 \qquad \textbf{Eq. 3-37}$$

The term 'bandwidth' commonly refers to the pulse bandwidth (range). For the unmodulated pulse, the bandwidth is given by $W = 1/\tau$. In this sense, the convolution of the modulated pulse (Eq. 3-29) can be understood as a compression of the original pulse to a short pulse length. For the synthetic aperture, the resolution increases with decreasing antenna size (in opposite to the real aperture, compare Eq. 3-27 and Eq. 3-37), due to a larger swath width and therefore longer illumination time. High resolution of real aperture systems is enhanced through a short wavelength, small object distance, and a large antenna (Eq. 3-27).

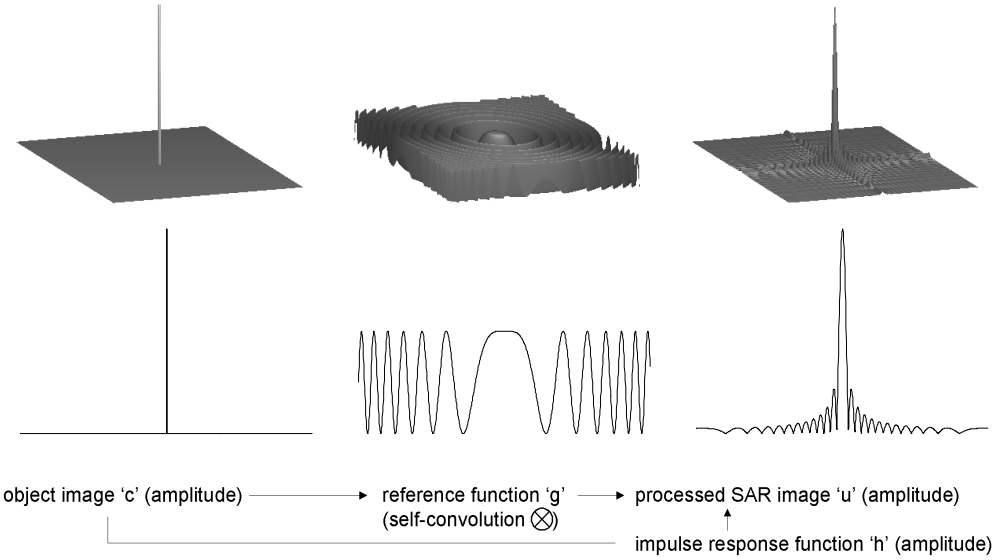

Fig. 3-9 SAR system model of a point scatterer

(left) object function of original point scatterer, (middle) reference function illustrating the phase course (real or imaginary part) of the point scatterer response SAR imagery, (right) processed SAR image (amplitude) of the point scatterer, a two-dimensional sinc-function.

3.3.3 SAR system model

Based on the signal processing now the system imaging behaviour for an object on the ground shall be modelled (Hagberg et al. 1995, Bamler and Hartl 1998).

Consider a point scatterer-type object c(x,R), where $\sqrt{\sigma}$ is the backscatter coefficient and δ(t) the delta-function, which is located at the position x', R' in a radar image of the azimuth dimension x and the range dimension R (Eq. 3-38). The convolution of the idealized SAR signal of the object is modelled through a self-convolution of the reference function g(x,R) (Eq. 3-39 to Eq. 3-41) and termed the impulse response function h(x,R) (Eq. 3-42 to Eq. 3-44). Including the phase $e^{-i\,2kR}$ due to the object distance and the additive noise component n(x,R), the modelled SAR image u(x,R) is given by Eq. 3-45. As can be seen in Fig. 3-9, it is a two-dimensional sinc-function.

Object image
$$c(x,R) = \sqrt{\sigma} \cdot \delta(x - x', R - R') \qquad \textbf{Eq. 3-38}$$

Reference function
$$g(x,R) = g(x - x') \times g(R - R') \qquad \textbf{Eq. 3-39}$$

$$g(x) \propto \exp\left(i \cdot \pi \cdot \Delta f_{SA} / t_{RA} \cdot t^2\right) \quad \text{with t = x/v} \qquad \textbf{Eq. 3-40}$$

$$g(R) \propto \exp\left(i \cdot \pi \cdot \Delta f / \tau \cdot t^2\right) \quad \text{with t = 2R/c} \qquad \textbf{Eq. 3-41}$$

Impulse response function
$$h(x,R) = g(x,R) \otimes_x \otimes_R g(x,R) \qquad \textbf{Eq. 3-42}$$

$$h(x) = \mathrm{sinc}\left(\pi \cdot \Delta f_{SA} \cdot t\right) = \mathrm{sinc}\left(\pi \cdot 2vt / D_{RA}\right) \quad \text{with t = x/v} \qquad \textbf{Eq. 3-43}$$

$$h(R) = \mathrm{sinc}\left(i \cdot \pi \cdot \Delta f \cdot t\right) \quad \text{with t = 2R/c} \qquad \textbf{Eq. 3-44}$$

Processed SAR image
$$u(x,R) = c(x,R) \cdot e^{-i \cdot 2kR} \otimes\otimes h(x,R) + n(x,R) \qquad \textbf{Eq. 3-45}$$

For distributed scatterers, it is useful to restate Eq. 3-45 in terms of a volume integral dV' = dx'dy'dz' (Eq. 3-46), where c(r) describes a 3-dimensional volume with r = (x, y, z)^T, and an expectation value of $E\{c(r)\cdot c^*(r)\} = \sigma(r)\cdot\delta(r'-r)$:

$$u(x,R) = \int_V c(r')\cdot\exp(-i\cdot 2kR')\cdot h(x-x',R-R')\,dV' + n(x,R) \qquad \textbf{Eq. 3-46}$$

Splitting R into the reference distance R_S and the distance r due to the dimension of the volume, then, under the plane wave approximation, Eq. 3-46 can be written as:

$$u(x,R) = \exp(-i\cdot 2kR_S)\cdot\int_V c(r')\cdot\exp(-i\cdot 2kr')\cdot h(x-x',R-R')\,dV' + n(x,R) \qquad \textbf{Eq. 3-47}$$

The SAR system model for one point scatterer is illustrated in Fig. 3-9, and will be extended for the interferometric case in Ch. 3.4.

3.4 SAR Interferometry

SAR interferometry mainly focuses upon the differential phase information of two SAR images, and its statistical properties, the so-called (interferometric) coherence. This subchapter begins with the interferogram formation (Ch. 3.4.1), then explains the interferometric phase (Ch. 3.4.2) and coherence (Ch. 3.4.3), and finally comes to the interferometric system model and the relation between volume decorrelation and the height of a volume scatterer like a forest (Ch. 3.4.4). The content is based on Bamler and Hartl (1998), Hagberg et al. (1995), Askne et al. (1997), and Papathanassiou (1999).

3.4.1 The SAR interferogram

Conventional SAR interferometry works with images taken from slightly different perspectives, i.e. with a so-called spatial baseline between the sensors (Fig. 3-10). If the images are acquired at the same time, i.e. single-pass interferometry, the coherence between the images is mainly affected by spatial decorrelation. If the images are acquired at different times, i.e. repeat-pass interferometry, also temporal changes deteriorate the coherence, i.e. temporal decorrelation.

An interferogram is calculated as the product of the image u_1 and the conjugate of u_2* (Eq. 3-48). The interferometric phase $\Delta\varphi$ is given by the arc tangent of the interferogram (Eq. 3-49):

$$u_1(x,R)\cdot u_2^*(x,R+\Delta R) = |u_1|\exp(i\varphi_1)\cdot|u_2^*|\exp(-i\varphi_2) = |u_1\cdot u_2^*|\cdot\exp(i\Delta\varphi) \qquad \textbf{Eq. 3-48}$$

$$\Delta\varphi = \arctan\left(\frac{\mathrm{Im}\{u_1\cdot u_2^*\}}{\mathrm{Re}\{u_1\cdot u_2^*\}}\right) \qquad \textbf{Eq. 3-49}$$

While the phase φ in a single SAR image appears equally distributed over 2π, the distribution of the interferometric phase $\Delta\varphi$ is much smaller. It is common to divide the phase of a resolution cell into a determinate component φ_{det} and a random component φ_{rd} (Eq. 3-50). φ_{det} corresponds to the distance of the sensor to the centre of the resolution cell, φ_{rd} to the phase resulting from the coherent addition of the scattering elements inside the resolution cell (see speckle in Ch. 3.2.2). Assuming the same random phase contribution in both images, φ_{rd} cancels out in the interferogram, the remaining deter-

minate phase φ_{det} only depends on the range difference ΔR and exhibits a characteristic fringe pattern (Eq. 3-51). This pattern can be seen in Fig. 3-12 and will be explained in the next section, Ch. 3.4.2.

$$\begin{aligned} \varphi_1 &= \varphi_{1\,\mathrm{det.}} + \varphi_{1rd} \\ \varphi_2 &= \varphi_{2\,\mathrm{det.}} + \varphi_{2rd} \end{aligned} \quad \text{with} \quad \begin{aligned} \varphi_{1\,\mathrm{det.}} &= \lambda/4\pi \cdot R \\ \varphi_{2\,\mathrm{det.}} &= \lambda/4\pi \cdot (R+\Delta R) \end{aligned} \qquad \textbf{Eq. 3-50}$$

from $\varphi_{1rd} = \varphi_{2rd}$ follows $\Delta\varphi = \varphi_{1\,\mathrm{det.}} - \varphi_{2\,\mathrm{det.}} = \lambda/4\pi \cdot \Delta R$ **Eq. 3-51**

For completion it must be mentioned, that before generating an interferogram, the image u_2 (slave) must be coregistrated onto image u_1 (master), so that each pixel in u_2 corresponds to the same pixel in u_1. Different algorithms have been developed that enable a coregistration on sub-pixel level (Fornaro and Franceschetti 1995, Moreira and Scheiber 2000, Scheiber 2003). Inaccuracies in the coregistration degrade the interferometric coherence, a process termed coregistration decorrelation (see Ch. 3.4.4, Scheiber 2003, Reigber 1997).

3.4.2 The interferometric phase

The importance of the interferometric phase lies in the extraction of the 3D-ground topography and the generation of digital elevation models, DEMs. As shown in Fig. 3-10, the height h of the topography can be determined if the antenna look angle θ is known:

$$h = h_0 - R \cdot \cos\theta \qquad \textbf{Eq. 3-52}$$

To determine the look angle θ, an interferometric perspective is needed. Applying the cosine law in Fig. 3-10, following equations hold:

$$\begin{aligned} &(R+\Delta R)^2 \\ &= R^2 + B^2 - 2RB\cos(\pi/2 - \theta_0 + \theta_B) \\ &= R^2 + B^2 - 2RB\sin(\theta_0 - \theta_B) \end{aligned} \qquad \textbf{Eq. 3-53}$$

$$\sin(\theta_0 - \alpha) = \frac{(R+\Delta R)^2 - R^2 - B^2}{2RB} \qquad \textbf{Eq. 3-54}$$

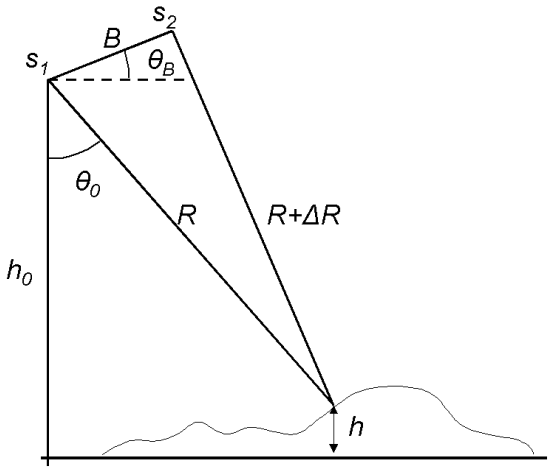

Fig. 3-10 Interferometric imaging geometry
Antenna s1 and s2, range distance R, range difference ΔR, look angle θ_0, baseline b, baseline angle α, flight altitude h_0, topographic height h

where the distance R is given by the range sampling of the master image u_1, while ΔR refers to the range difference of the coregistrated slave image u_2 (Fig. 3-10.b).

In the following, the interferometric phase Δφ shall be studied in detail. As already mentioned the phase exhibits a fringe pattern (Fig. 3-12). This fringe pattern reflects two differential phase components, the flat earth fringes $\Delta\varphi_{fe}$ and the topographic fringes $\Delta\varphi_{top}$:

$$\exp(i\,\Delta\varphi) = \exp(i\,\Delta\varphi_{fe}) + \exp(i\,\Delta\varphi_{top}) \qquad \textbf{Eq. 3-55}$$

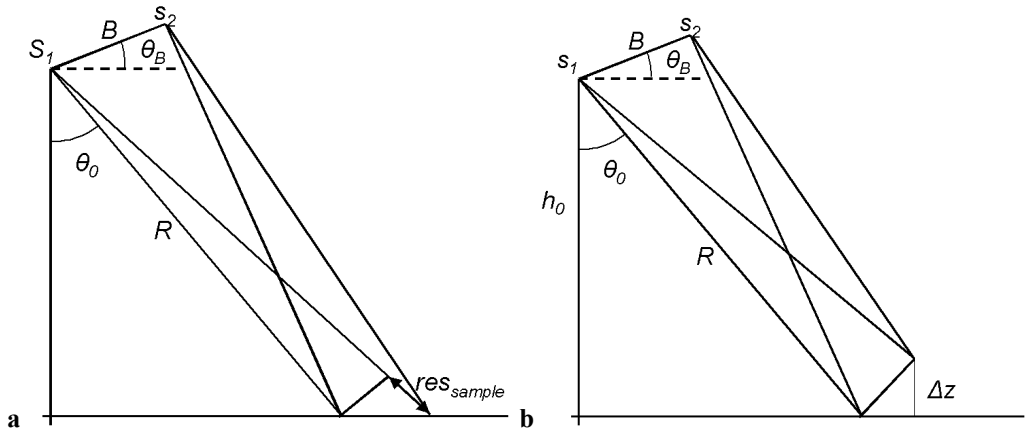

Fig. 3-11 Flat earth component (a) and topographic component (b) of the interferometric phase
Antenna s1 and s2, range distance R, range difference ΔR, look angle θ_0, baseline b, baseline angle θ_B, flight altitude h_0, topographic height h

The flat earth fringes originate from the projection of the flat ground topography onto the radar range geometry. The differential phase $\Delta\varphi_{fe}$ between two range samples located at the same height is scaled by the range sampling (Eq. 3-24) and the tangent of the look angle θ_0 (Fig. 3-11.a):

$$\Delta\varphi_{fe} = \frac{4\pi}{\lambda} \cdot \frac{B\cos(\theta_0 - \theta_B) \cdot res_{sample}}{R\tan\theta_0} \qquad \textbf{Eq. 3-56}$$

The topographic fringes originate from the differential phase $\Delta\varphi_{top}$ due to vertical topography, and are scaled by the height difference Δz and the sine of the look angle θ_0 (Fig. 3-11.b):

$$\Delta\varphi_{top} = \frac{4\pi}{\lambda} \cdot \frac{B\cos(\theta_0 - \theta_B) \cdot \Delta z}{R\sin\theta_0} \qquad \textbf{Eq. 3-57}$$

The interferometric extraction of the topography makes it possible to generate Digital Elevation Models (DEMs). From the topographic phase, the final steps towards the DEM generation are (1) to resolve the 2π ambiguity of the fringes into continuous phase, (2) to convert the phase to height, and (3) to geo-reference the obtained height. Step (1) is termed phase unwrapping, and usually involves iterative processing of a neighbourhood of pixels (Ghiglia and Pritt 1998).

Theoretically derived in 1974 (Graham), the terrain extraction with radar interferometry was first shown in 1986 from dual antenna side-looking airborne radar data (Zebker and Goldstein 1986). Today it is a key application of SAR, and missions like SRTM or Tandem X are dedicated to the generation of globally consistent high-resolution DEMs (http://srtm.usgs.gov, Photogr.Eng.Rem.Sens. 2006, Krieger et al. 2005). DEMs generated from SAR interferometry have entered many fields of earth science. Selected references are given in Ch. 3.4.5.

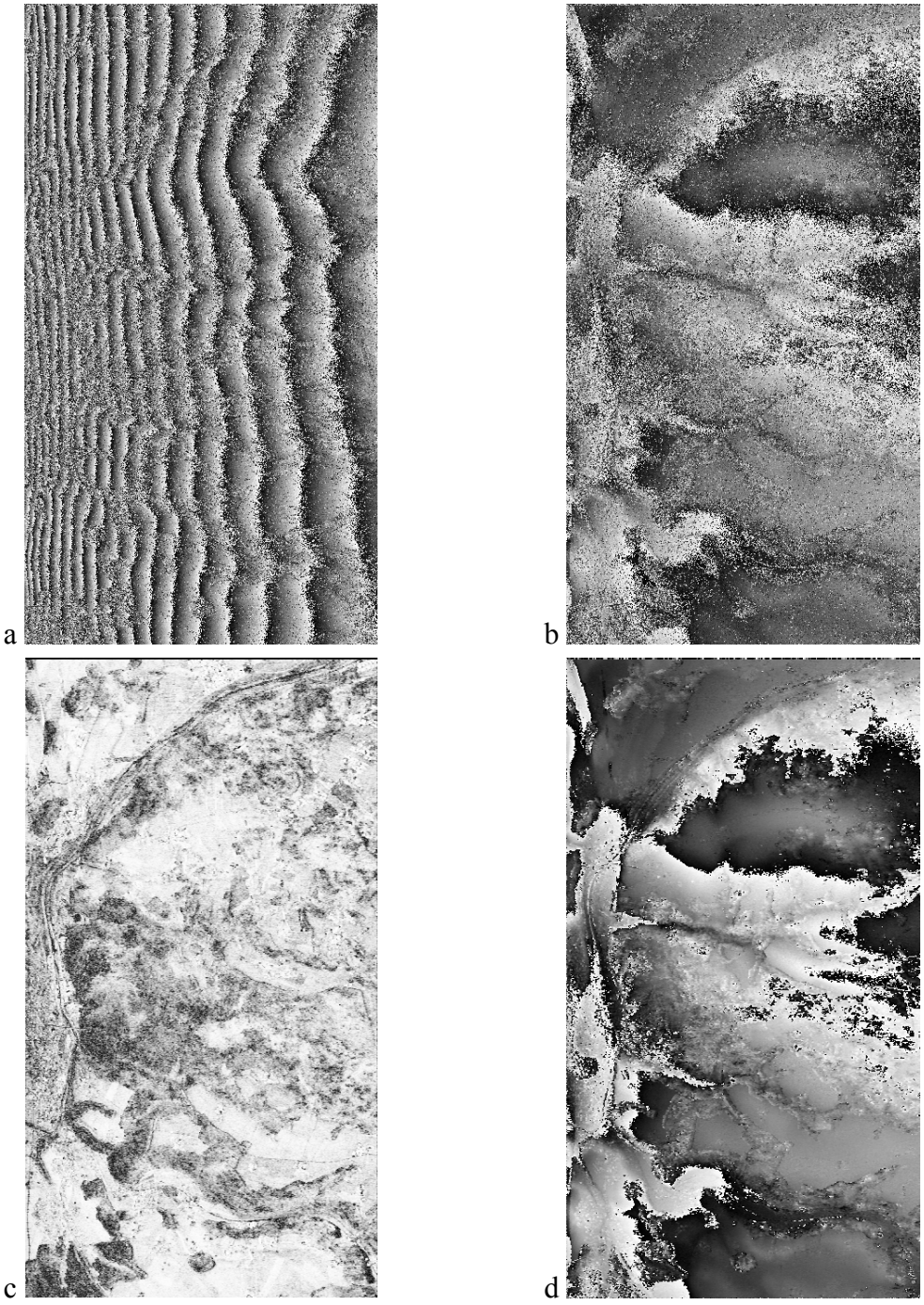

Fig. 3-12 SAR interferometric images of Traunstein (L-band HH, 5m horizontal baseline at 3000m flight level)

(a) interferometric phase before flat earth removal, (b) topographic interferometric phase after flat earth removal, (c) interferometric coherence, (d) smoothed interferometric phase of coherence.

3.4.3 Interferometric coherence and decorrelation

For the interferometric phase in Eq. 3-51, it was assumed, that the random phases of both images are equal. However, this is only partly true. Different decorrelation processes may affect the phase estimation and lead to a phase noise in the interferogram (discussed in detail in Ch. 3.4.4). This (inherent) phase decorrelation is quantified in the interferometric coherence, i.e. the normalized cross-correlation coefficient between u_1 and u_2:

$$\gamma = \frac{E(u_1 \cdot u_2^*)}{\sqrt{E(|u_1|^2) \cdot E(|u_2|^2)}} \qquad \textbf{Eq. 3-58}$$

where E denotes the expectation value. Since the coherence cannot be determined from a single interferometric observation, the expectation value is usually approximated by a spatial average over a certain window size N, assuming that mean and variance are invariant in time and space (stationarity and ergodicity, Touzi 1999):

$$\gamma = \frac{\sum_{n=1}^{N} u_1 \cdot u_2^*}{\sqrt{\sum_{n=1}^{N} |u_1|^2 \cdot \sum_{n=1}^{N} |u_2|^2}} \qquad \textbf{Eq. 3-59}$$

The absolute of the coherence γ scales between 1 and 0, i.e. total phase correlation and total phase decorrelation. The relation between phase variance and coherence is given by Eq. 3-60 and shown in Fig. 3-13.a (Bamler and Hartl 1998, Lee et al. 1994, Just and Bamler 1994):

$$pdf(\varphi) = \frac{1-|\gamma|^2}{2\pi} \frac{1}{1-|\gamma|^2 \cos(\varphi - \varphi_0)} \times \left(1 + \frac{|\gamma| \cos(\varphi - \varphi_0) \arccos(-|\gamma| \cos(\varphi - \varphi_0))}{\sqrt{1-|\gamma|^2 \cos^2(\varphi - \varphi_0)}} \right) \qquad \textbf{Eq. 3-60}$$

Eq. 3-60 describes the theoretical phase estimation from 1 sample (for a single look image). For the coherence estimation from N interferogram samples or sub-looks of lower resolution, the standard deviation of the coherence is often modelled by the Cramer-Rao bounds (Fig. 3-13.b, Bamler, Hartl 1998, Touzi et al. 1994):

$$stddev(\gamma) = \sqrt{(1-\gamma^2)^2 / 2N} \qquad \textbf{Eq. 3-61}$$

The choosing of the window size (or number of looks) therefore becomes essentially a trade-off between resolution and phase-accuracy.

It is important to realize that the deterioration of coherence, i.e. decorrelation, is not an arbitrary process. Two images taken at the same time from the same perspective should be totally correlated (Zebker 1992). Decorrelation results typically from one of the following processes (Askne et al. 1997):

- different image perspectives: baseline or spatial decorrelation $\gamma_{baseline}$
- different acquisition times: temporal decorrelation γ_{temp}
- system noise or processing uncertainties: system decorrelation γ_{system}.

Additionally, decorrelation occurs where the stationarity assumption is violated (Touzi 1999), e.g. forest edges or other discontinuities. These areas have to be masked from the coherence formation for instance with an edge preserving filter (Lee, 1980, Lopes et al. 1990). This decorrelation will be ignored in the following.

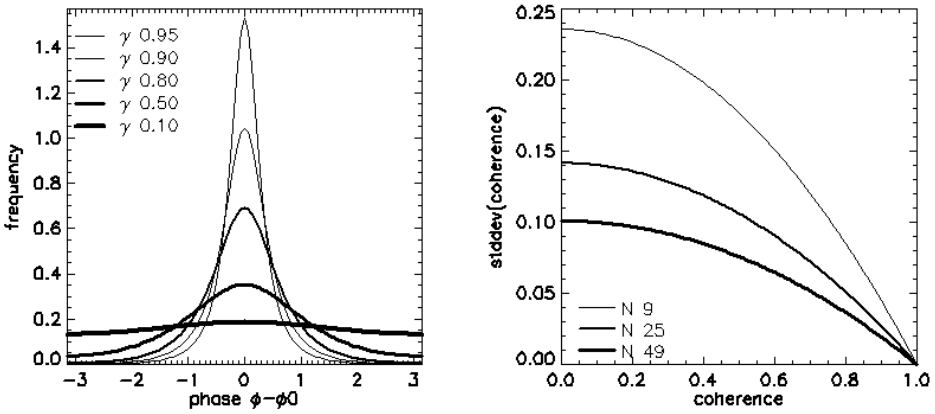

a **b**

Fig. 3-13 (a) Interferometric phase variability for different coherences, (b) Coherence standard deviation as a function of the window size N

3.4.4 Interferometric SAR system model

The SAR system model developed in Ch. 3.3.3 shall now be used to model the decorrelation processes in an interferometric SAR system model. Using Eq. 3-47 for the processed SAR image, the expectation value of the interferogram between $u_1(x,R)$ and $u_2(x,R)$ is given by Eq. 3-62 (setting x = 0, R = 0, h = h_1 = h_2, N_1=N_2):

$$E\left(u_1(x,R)\cdot u_2^*(x,R)\right) = \exp(-i\cdot 2(k_1 R_{S1} - k_2 R_{S2})) \cdot \int \sigma_{stable}(r)\cdot \exp(-i\cdot 2(k_1-k_2)\cdot r)\cdot \left|h(-x,-R)\right|^2 \, dV \qquad \textbf{Eq. 3-62}$$

In Eq. 3-62, R_1 and R_2 were split into a deterministic part R_{s1} and R_{s2} and an object part r = r_1 = r_2. Neglecting the leading phase term exp(-i·2(k_1R_{s1}-k_2R_{s2})) in Eq. 3-62, the coherence becomes:

$$\gamma = \frac{\int \sigma_{stable}(r)\cdot \exp(-i\cdot 2(k_1-k_2)\cdot r)\cdot \left|h(-x,-R)\right|^2 \, dV}{\sqrt{\int \sigma_1(r)\cdot \left|h(-x,-R)\right|^2 \, dV + N}\cdot \sqrt{\int \sigma_2(r)\cdot \left|h(-x,-R)\right|^2 \, dV + N}} \qquad \textbf{Eq. 3-63}$$

where $\sqrt{\sigma_1}$ and $\sqrt{\sigma_2}$ are the volumetric backscattering coefficients of the images individual images, and $\sqrt{\sigma_{stable}}$ the stable backscattering between the two acquisitions; unstable scatterers are averaged out (Bamler, Hartl 1998). N represents mutually uncorrelated system noise, and *dV* is the infinitesimal volume element (*dx dR*).

Eq. 3-63 describes the interferometric SAR system model. It can be broken down into the product of the three previously mentioned decorrelation processes (Ch. 3.4.3), baseline (or spatial) decorrelation, temporal decorrelation and system decorrelation:

$$\gamma = \gamma_{baseline}\cdot\gamma_{temporal}\cdot\gamma_{SNR} \qquad \textbf{Eq. 3-64}$$

The following sections will discuss each of the contributions separately. The focus lies on the baseline decorrelation, which is a function of the scatterer arrangement in the resolution cell. As will be explained, the volume contribution of the baseline decorrela-

tion is the basis for the forest height extraction in Ch. 3.5. Temporal and system decorrelation are described in less detail.

Baseline or spatial decorrelation $\gamma_{baseline}$ occurs when distributed scatterers (only the stable part) in a resolution cell are seen from different angles, i.e. with a spatial baseline. This introduces a distortion between the phases of the scattering elements:

$$\gamma_{baseline} = \frac{\int \sigma_{stable}(r) \cdot \exp(-i \cdot 2(k_1 - k_2) \cdot r) \cdot |h(-x,-R)|^2 \, dV}{\int \sigma_{stable}(r) \cdot |h(-x,-R)|^2 \, dV} \qquad \textbf{Eq. 3-65}$$

At this point it becomes important that k_1 and k_2 have actually different vector directions $\vec{k}_1$ and $\vec{k}_2$. They can be split similar to the interferometric phase into a range Δk_r and a height dependent Δk_z (compare Eq. 3-56, Eq. 3-57). Eq. 3-69 shows that Δk_r and Δk_z can be treated as first order equivalents of the effective baseline B_{eff}. Note, that in contrast to the wave number k, Δk_r and Δk_z were defined for the 2-way distance.

$$\Delta\vec{k} = \vec{k}_1 - \vec{k}_2 \qquad \textbf{Eq. 3-66}$$

$$\Delta\vec{k}_r = 4\pi / \lambda \cdot \Delta\theta / \tan\theta \qquad \textbf{Eq. 3-67}$$

$$\Delta\vec{k}_z = 4\pi / \lambda \cdot \Delta\theta / \sin\theta \qquad \textbf{Eq. 3-68}$$

where $$\Delta\theta = B_{eff} / R = B \cdot \cos(\theta - \alpha) / R \qquad \textbf{Eq. 3-69}$$

In the same manner, the r in Eq. 3-65 shall be split into η and z, i.e. the range and height extension of the volume, respectively. Assuming the scattering distribution to be only a function of height, the baseline decorrelation $\gamma_{baseline}$ can be divided into range decorrelation γ_{range} and volume decorrelation γ_{volume}:

$$\gamma_{baseline} = \frac{\int \sigma_{stable}(z) \cdot \exp(-i \cdot 2(\Delta\vec{k}_r \cdot \eta + \Delta\vec{k}_z \cdot z) \cdot |h(-x,-R)|^2 \, dV}{\int \sigma_{stable}(z) \cdot |h(-x,-R)|^2 \, dV'} \qquad \textbf{Eq. 3-70}$$

$$\gamma_{baseline} = \gamma_{range} \cdot \gamma_{volume} \quad \text{with} \quad \begin{cases} \gamma_{range} = \dfrac{\int \exp(i \cdot \Delta\vec{k}_r \cdot \eta) \cdot |h(-x,-R)|^2 \, dx d\eta}{\int |h(-x,-R)|^2 \, dx d\eta} \\ \gamma_{volume} = \dfrac{\int \sigma_{stable}(z) \cdot \exp(i \cdot \Delta\vec{k}_z \cdot z) \, dz}{\int \sigma_{stable}(z) \, dz} \end{cases} \qquad \textbf{Eq. 3-71}$$

- The range decorrelation γ_{range} in Eq. 3-71 depends on the baseline through Δk_r, and on η, i.e. the range dimension of the resolution cell. For a (hypothetical) optimal impulse response function $h(x,R) = \delta(x,R)$, the range decorrelation $\gamma_{range,opt}$ resolves to a sinc-function (Eq. 3-72, Fig. 3-14.a). The critical baseline $B_{eff,crit}$ is equal to the 2π-ambiguity of the sinc-function (Eq. 3-73). If the impulse response function is a sinc itself (Eq. 3-44), range decorrelation $\gamma_{range,sinc}$ becomes (in a first approximation) linear (Eq. 3-74, Fig. 3-14.a, compare Rosen et al. 2000):

$$\gamma_{range,opt} = \frac{\sin(½ \cdot \Delta k_r \cdot res_{range})}{½ \cdot \Delta k_r \cdot res_{range}} \qquad \textbf{Eq. 3-72}$$

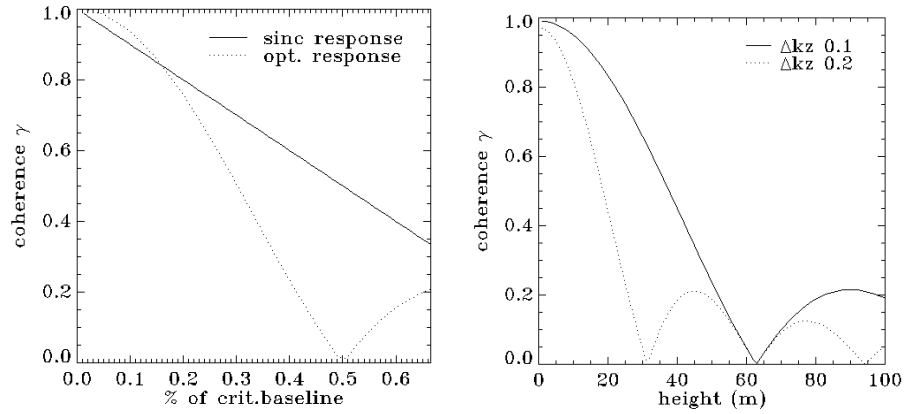

a **b**

Fig. 3-14 (a) Range decorrelation for a sinc and optimum impulse response function, (b) Volume decorrelation as a function of the volume height and Δk_z

$$2\pi = \tfrac{1}{2} \cdot \Delta k_r \cdot res_{range} = \tfrac{1}{2} \cdot \frac{4\pi}{\lambda} \cdot \frac{B_{eff,crit}}{R \tan\theta} \cdot \frac{c}{2W}$$

$$\Leftrightarrow B_{eff,crit} = \frac{\lambda \cdot R \cdot \tan\theta \cdot W}{c} \qquad \textbf{Eq. 3-73}$$

$$\gamma_{range,sinc} = 1 - \frac{B_{eff}}{B_{eff\,crit}} \quad \text{for } B_{eff} << B_{eff\,crit} \qquad \textbf{Eq. 3-74}$$

- The volume decorrelation γ_{volume} in Eq. 3-71 depends on the baseline through Δk_z, and on the height distribution of the scatterers in the volume. It is mathematically a Fourier transform of the scatterer distribution in height. For a uniform scattering profile in height, the volume decorrelation becomes a sinc-function (Eq. 3-75, discussed in detail in the next chapter, Ch. 3.5.1). The ambiguity height of the volume is given by the π-ambiguity of the sinc-function (Eq. 3-76). While in the case of range decorrelation, the range-dimension is given by the resolution and a critical baseline is defined, for volume decorrelation, the z-dimension depends on the scatterer. Hence, it is more appropriate to define a critical or ambiguity height h_{amb} than a critical baseline (Eq. 3-76, Fig. 3-14.b).

$$\gamma_{volume} = \frac{\sin(\tfrac{1}{2} \cdot \Delta k_z \cdot z)}{\tfrac{1}{2} \cdot \Delta k_z \cdot z} \qquad \textbf{Eq. 3-75}$$

$$\pi = \tfrac{1}{2} \cdot \Delta k_z \cdot h_{amb} = \tfrac{1}{2} \cdot \frac{4\pi}{\lambda} \cdot \frac{B_{eff\,crit}}{R \sin\theta} \cdot h_{amb}$$

$$\Leftrightarrow h_{amb} = \frac{\lambda \cdot R \cdot \sin\theta}{B_{eff}} \qquad \textbf{Eq. 3-76}$$

Range decorrelation can be compensated by a cut of the decorrelating parts of the spectra and a shift in the wave number domain (Gatelli et al. 1994). This wave number shift corresponds to the flat earth of the interferogram. Theoretically, also volume decorrelation can be compensated, but the scatterer distribution in height has to be known.

Temporal decorrelation γ_{temp} results from changes in the scatterer distribution between the acquisitions of u_1 and u_2. For instance, when wind shakes the tree, or rain alternates

the moisture conditions. Temporal decorrelation can be regarded as the ratio between stable vs. unstable scatterers:

$$\gamma_{temp} = \frac{\int \sigma_{stable}(r) \cdot |h(-x,-R)|^2 \, dV}{\int \sigma(r) \cdot |h(-x,-R)|^2 \, dV} \qquad \textbf{Eq. 3-77}$$

SNR decorrelation γ_{SNR}: is a system specific decorrelation and occurs in areas where due to a low backscattering coefficient a significant part of the signal is noise:

$$\gamma_{SNR} = \frac{\int \sigma(r) \cdot |h(-x,-R)|^2 \, dV}{\int \sigma(r) \cdot |h(-x,-R)|^2 \, dV + N} = \frac{1}{1 + (SNR)^{-1}} \qquad \textbf{Eq. 3-78}$$

Another system decorrelation source due to processing is the coregistration decorrelation. It is caused by slight misregistrations on the sub-pixel level and is described by (Scheiber 2003, p. 24, Reigber 1997):

$$\gamma_{coreg} = \mathrm{sinc}(\pi \cdot \Delta px) \qquad \textbf{Eq. 3-79}$$

where Δpx corresponds to the offset in % of the pixel dimension.

Volume decorrelation is fundamental in this work, because it can be used to extract the height of volume scatterers such as forests. The following items show how the data acquisition with the E-SAR system was optimised for the extraction of forest heights:

- use of L-band where vegetation attenuation is low
- the high system resolution (100 MHz) minimizes range decorrelation
- the images were acquired with a short temporal baseline

The use of a large wavelength is important in order to penetrate the forest volume down to the underlying ground. Otherwise only part of the volume is seen, and the extracted heights underestimate the actual ones. The high resolution and short temporal baseline are necessary to minimize the influence of range and temporal decorrelation, because heights can only be inverted from volume decorrelation.

3.4.5 Interferometry and forest structure

The application of interferometry in earth science is manifold. Apart from the pure DEM generation (Ch. 3.4.3), many applications involve differential interferometry (D-InSAR), which detects changes in the topography. To name few of the most known ones: glaciology, esp. glacier motion (Goldstein et al. 1993, Joughin et al. 1998), geology, esp. earthquakes (Massonet et al. 1993, Zebker et al. 1994, Bürgmann et al. 1998, Peltzer et al. 1996, Fielding et al. 1998, Massonnet et al. 1995, Massonnet and Feigl 1998, Strozzi et al. 2003, Ferretti et al. 2001, Bürgmann et al. 2000, Colesanti et al. 2003), Hydrology (Alsdorf et al. 2000, Smith and Alsdorf 1998).

For forestry applications, interferometry has been used for forest discrimination, and height and biomass estimations. Various approaches have proven a good discrimination of forests in SAR interferograms (Wegmüller and Werner 1995/ 1997). But the potential of interferometric radar lies in its sensitivity to forest structure. As already discussed in the Introduction (Ch. 1), the interferometric phase allows to estimate forest heights from

differential X-band and P-band DEMs. Also, two coherence approaches were discussed, a coherence-biomass relation (Askne et al. 2003, Pulliainen et al. 2002, Santoro et al. 2002) and the Pol-InSAR height estimation (Papathanassiou and Cloude 2001, Cloude and Papathanassiou 2003). The differences can now be discussed from the perspective of the interferometric SAR system model:

1. the coherence-biomass model regards coherence as a temporal decorrelation process, consisting of a vegetation and ground contribution. Ground and volume contribution scale to each other through the transmissivity of the forest which is related to biomass. Temporal coherence must be dominant, and volume decorrelation should be kept low – at best with a 0m-baseline. Since temporal decorrelation is influence especially by wind and weather, different scenes have to be calibrated individually from ground data.
2. the Pol-InSAR height inversion depends on the dominance of volume decorrelation; other decorrelation sources, especially temporal decorrelation must be kept low – at best with a single-baseline acquisition. The coherence-height relation is scaled by Δk_z; only the interferometric system configuration is needed for the height estimation.

Both models are similar in respect to being limited by extinction. Strong extinction leads to a saturation of the coherence-biomass or coherence height relation. Only longer wavelengths can avoid this limitation. C-band data from ERS-1/2 tandem mission (1 day and 35 day repeat pass) were found to saturate at 40-50 t ha^{-1} (Koskinen 2001, Santoro 2002) and helped to generate a 10 Mio. km^2 forest map of Siberia (Wagner et al. 2000, Gaveau et al. 2003). The Pol-InSAR height inversion was successfully applied to L-band data from SIR-C and E-SAR (Papathanassiou and Cloude 2001, Cloude and Papathanassiou 2003), and did not reach saturation up to 40 m, allometrically corresponding to biomass levels exceeding 400 t ha^{-1} (Mette et al. 2004 b/c, 2006).

Interestingly, an almost linear coherence-biomass relation also results when combining the coherence-height relation (Pol-InSAR approach) with the allometric height-biomass relation from Ch. 2. This indicates that the coherence-biomass relation in ERS 1/2 may be also explained as volume decorrelation (Ch. 4.5.2).

3.5 The Random Volume over Ground-model (RVoG)

In the previous subchapter (Ch. 3.4.4), volume decorrelation was shown to be a function of the scatterer distribution in height. This makes it principally possible to invert forest heights from coherence – as long as the other decorrelation processes can be neglected or compensated.

For a simple scatterer distribution, i.e. a uniform scattering profile in height, volume decorrelation was described to resolve to a sinc-function (Eq. 3-75). The Random Volume over Ground model (RVoG) alters the uniform scattering profile by introducing the parameters extinction α , and ground-volume ratio m. In this sense, the RVoG models the forest as a decorrelating volume of randomly distributed scatterers with a certain height h and extinction α, above a non-decorrelating ground with a certain backscatter contribution m. These parameters: height, extinction and ground cannot be inverted from a single coherence, and an extension of the observation space is required. The op-

tions are more baselines, frequencies and polarizations. This work utilizes the polarization approach with fully polarimetric interferometric SAR data (Pol-InSAR).

The RVoG model (Attema and Ulaby 1978) was implemented for height extraction from Pol-InSAR data in Papathanassiou and Cloude (2001) and Cloude and Papathanassiou (2003).

3.5.1 Modelling forest as a Random Volume over Ground (RVoG)

The volume decorrelation γ_{volume} in Eq. 3-71 describes the relation between the interferometric coherence and the scatterer height distribution $\sigma_{stable}(z)$ inside a resolution cell. In order to develop the RVoG, three simple scattering profiles have been modelled:

1. a uniform scattering profile,
2. an extincted scattering profile and
3. a uniform scattering profile with ground.

Since volume decorrelation only considers $\sigma_{stable}(z)$, the backscatter notation was shortened $\sigma(z)$ – in contrast to $\sigma(z)$ in Ch. 3.4.4 (!). Like in Ch. 3.4.4, the interferometric phase term of Eq. 3-62 was omitted, keeping the ground phase at 0.

The three cases are illustrated in Fig. 3-15 to Fig. 3-17 choosing a baseline configuration so that $\Delta k_z = 0.125$ resulting in an ambiguity height of $h_{amb} = 50$ m (Eq. 3-76). Figure (a) always shows the distribution of the volume and ground backscattering as a function of height. Figure (b) relates the coherence (absolute) to the height of the volume. In figure (c) the complex coherence (absolute and phase) are represented in polar coordinates in the unit circle. The coherence is given by the distance from the origin, the phase by the angle to the x-axis. The ground phase is located at [1,0].

1. Uniform scattering profile in height - the sinc-solution (Fig. 3-15): For a uniform backscatter height profile (Fig. 3-15.a), the solution of the volume decorrelation in Eq. 3-71 is a sinc-function. The relation between height and coherence is scaled by the vertical wave number Δk_z (Eq. 3-75):

$$\sigma(z) = const \qquad \textbf{Eq. 3-80}$$

$$\gamma_{volume} = \frac{\int \sigma \cdot \exp(-i \cdot \Delta k_z \cdot z)\ dz}{\int \sigma\ dz'} = \exp(i \cdot \tfrac{1}{2} \Delta k_z \cdot h) \cdot \frac{\sin(\tfrac{1}{2} \cdot \Delta k_z \cdot h)}{\tfrac{1}{2} \cdot \Delta k_z \cdot h} \qquad \textbf{Eq. 3-81}$$

Fig. 3-15.b shows how the absolute value of the coherence decreases as the volume height and/or Δk_z increases. In Fig. 3-15.a/c, it can be seen that also the phase, i.e. the effective scattering centre, always lies at the half-height of the volume.

2. Extincted scattering profile (Fig. 3-16): If the radar wave is extincted along its path through the volume, the backscatter from the deeper parts of the volume is damped (Fig. 3-16.a). For a constant extinction along the volume depth, the backscattering coefficient $\sigma(z)$ becomes an exponential function of the extinction α and the 2-way penetration through the height z of the volume (compare also Eq. 3-18):

$$\sigma(z) = const \cdot \int_0^h \exp(2\alpha z / \cos\theta)\ dz \quad [5] \qquad \textbf{Eq. 3-82}$$

$$\gamma_{Volume} = \exp(i\phi_0) \cdot \frac{\int \exp(2\alpha z / \cos\theta) \cdot \exp(-i \cdot \Delta k_z \cdot z)\ dz}{\int \exp(2\alpha z / \cos\theta)\ dz} \qquad \textbf{Eq. 3-83}$$

$$= \frac{\exp(-2\alpha / \cos\theta \cdot i\Delta k_z \cdot h) - 1 \,/\, -(2\alpha / \cos\theta \cdot i\Delta k_z)}{\exp(-2\alpha / \cos\theta \cdot h) - 1 \,/\, -(2\alpha / \cos\theta)}$$

In comparison to the volume without extinction, the absolute of the coherence for a given height is always higher (Fig. 3-16.b). The interferometric phase, i.e. the scattering centre, is dragged towards the volume top (Fig. 3-16.a/c). For no extinction, $\alpha = 0$, Eq. 3-83 becomes the sinc (Eq. 3-81). For infinite extinction, $\alpha = \infty$, the canopy becomes a surface with a volume coherence of 1 and a phase centre at the volume top (i.e. the outer boundary of unit circle). The strongest change in the coherence-height relation occurs for extinction between $\alpha = 0.1$ dB m^{-1} and $\alpha = 1$ dB m^{-1} (Fig. 3-16.b). For lower extinctions, the coherence of the extincted volume does not deviate strongly from the sinc-function, higher extinctions lead to an early saturation of the coherence-height relation. The effect of extinction increases for high look angles, because the effective path through the volume is longer than for steep look angles.

3. Volume over ground (Fig. 3-17): When the ground contributes to the backscattering, the total backscatter $\sigma(z)$ is the coherent sum of the effective ground σ_G and volume backscattering $\sigma_V(z)$ after extinction (Eq. 3-84). A ground-volume ratio m can be defined (Eq. 3-85), and the Volume over Ground coherence γ_{VoG} can be resolved (Eq. 3-86 and Eq. 3-87, Papathanassiou and Cloude 2001, Cloude and Papathanassiou 2003):

$$\sigma(z) = \sigma_G + \sigma_V(z) = \sigma_{G'} \cdot \exp(-2\alpha h) + \int_0^h \sigma_{V'} \exp(2\alpha z)\ dz \qquad \textbf{Eq. 3-84}$$

$$m = \sigma_G / \sigma_V(z) \qquad \textbf{Eq. 3-85}$$

$$\gamma_{VoG} = \frac{m + \gamma_{Volume}}{m + 1} \qquad \textbf{Eq. 3-86}$$

$$\gamma_{VoG} = \gamma_V + (1 - \gamma_{Volume}) \cdot \frac{m}{m + 1} \qquad \textbf{Eq. 3-87}$$

where γ_{Volume} corresponds to Eq. 3-83 (extincted scattering profile). The Volume-over-Ground coherence describes a linear function in the unit circle, which can be easily seen in Eq. 3-87. The line has its origin at the ground phase on the unit circle, where $m = \infty$, and ends where $m = 0$, i.e. pure volume decorrelation γ_{Volume} (Eq. 3-83).

As can be seen in Fig. 3-17.a/c, increasing ground contribution drags the scattering centre to the ground. The coherence-height relation is ambiguous. Compared to the sinc (m=0), the coherence decreases for a low ground contributions, and increases for high ground contributions (Fig. 3-17.b, Fig. 3-18).

[5] In Eq. 3-84, the extinction α is given as the natural logarithm [Neeper], the conversion to the decalogarithm [dB] is given by α [dB] = 8.61 α [Neeper]

It will be explained in Ch. 3.5.3 that interferometry at different polarizations introduces different ground contributions while extinction is assumed to be equal. Then, the complex coherences of the polarizations form the described line, which is the first step in the height inversion of the RVoG. For this reason the RVoG is sometimes referred to as "line" model.

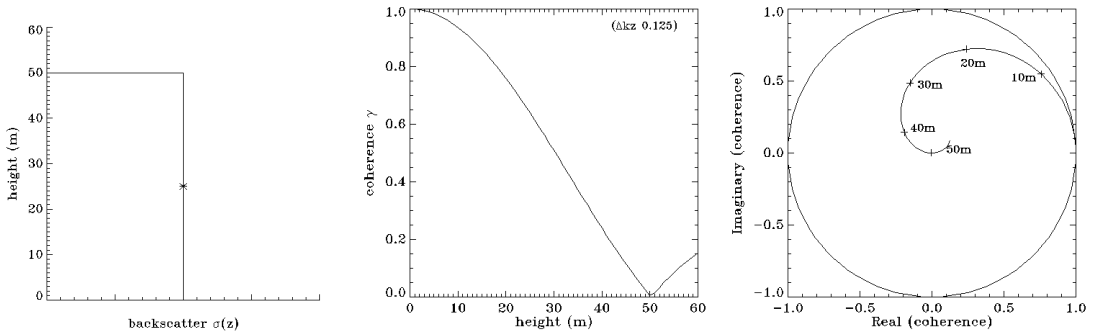

a b c

Fig. 3-15 Uniform scattering profile in height - the sinc-solution

(a) scattering amplitude; scattering centre (asterisk) lies at the ½-height, (b) coherence-height relation is a sinc-function, (c) complex coherence in unit circle. Volume heights from 10-50 m indicated.

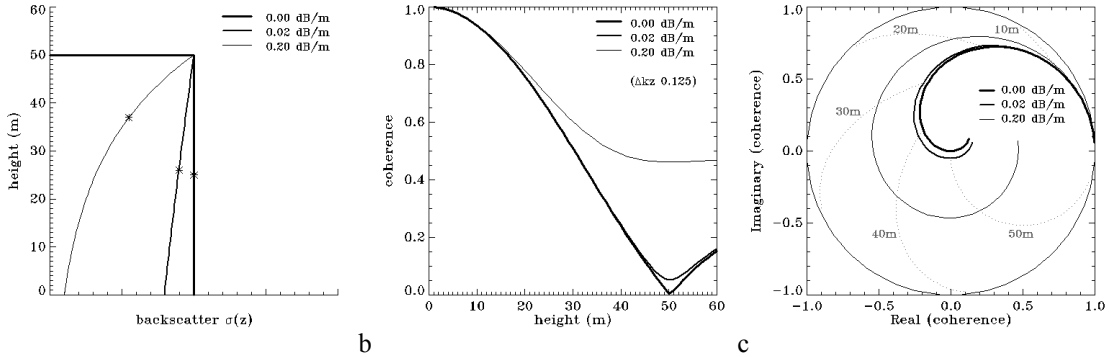

a b c

Fig. 3-16 Extincted scattering profile

(a) scattering amplitude towards the volume bottom is damped; scattering centre (asterisks) is dragged towards canopy (b) coherence-height relation saturates with extinction, (c) complex coherence is dragged towards the unit circle boundary (canopy surface). Volume heights from 10-50 m indicated.

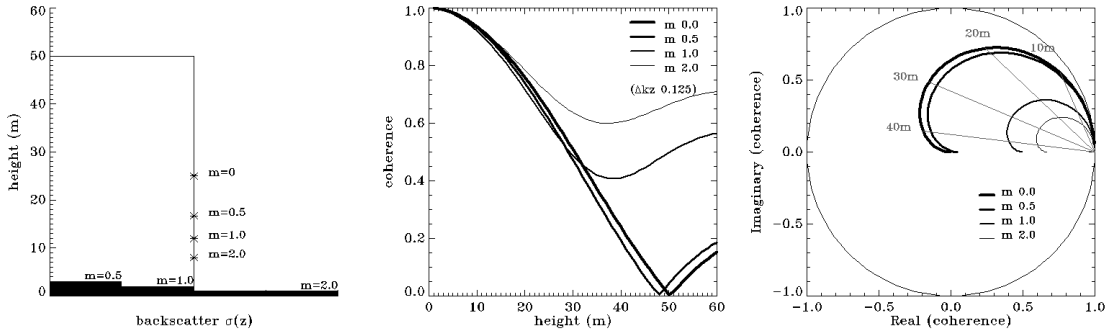

a b c

Fig. 3-17 Volume over ground

(a) scattering amplitude with ground contribution; scattering centre (asterisks) is dragged towards ground, (b) coherence-height relation decreases for low ground contribution, increases for high ground contribution, (c) complex coherence is dragged towards ground phase. Volume heights from 10-40 m indicated.

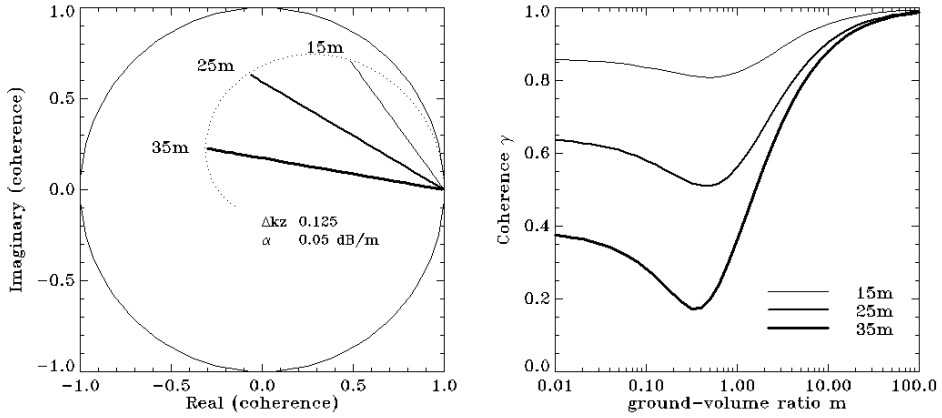

a b

Fig. 3-18 Effect of ground in the unit circle (a) and on the coherence-height relation (b)

3.5.2 Considerations on the RVoG

At this point, the two parameters extinction and ground-volume ratio, shall be discussed more closely with respect to the coherence-height relation.

- At first, the effect of extinction shall be discussed for γ_{Volume} without ground (Eq. 3-85). As described in Ch. 3.5.1, extinction leads to a saturation of the coherence-height relation at heights (e.g. in Fig. 3-16.b at $\gamma = 0.47$ for $\alpha = 0.2$ dB m^{-1}). If extinction is not accounted for, heights close to the saturation limit are underestimated. But in the unit circle (Fig. 3-16.b), it can be seen, that the phase still changes after the (absolute) coherence has reached the saturation. If it is possible to isolate the ground phase, the RVoG makes it possible to extract correct heights based on the phase information. However, the separation of the ground becomes more difficult for strong extinctions, because its contribution in the signal diminishes (Eq. 3-84).
- For a given height the ground-coherence relation is ambiguous and can be understood best from the representation in the unit circle (Fig. 3-18.a). At first coherence decreases with increasing ground contribution up to a minimum, but as the ground backscatter further increases, the coherence increases up to 1, where practically only ground is seen ($m=\infty$). The lowest possible coherence due to m depends on the location of γ_{Volume} in the unit circle, which is a function of Δk_z, height, and extinction.

Principally, ground and extinction act as antagonists: extinction drags the location of the scattering centre towards the canopy top which leads to a coherence increase; ground contribution drags the scattering centre to the ground which leads to coherence decrease (except for high ground contributions). When neither ground nor extinction is very strong, the RVoG-interpretation will not differ significantly from the sinc-solution. However, the ground can become important when double bounce occurs between ground and stem, or when extinction is little like for open forests. Extinction becomes critical if the response from lower volume parts and the ground is effectively shielded. Then, also ground and volume cannot be separated through Pol-InSAR (Ch. 3.5.4).

Important is that both extinction and ground are functions of the wavelength. Literature values summarized in Cloude et al. (2000) indicate an increasing span of the ground-

Wavelength	Ground-volume ratio m		Extinction
	Min	Max	(dB m^{-1})
C-band	1:100 (C-1)	1:10 (C-2)	0.5
L-band	1:1000 (L-1)	1:1 (L-2)	0.1
P-band	1:10000 (P-1)	30:1 (P-2)	0.05

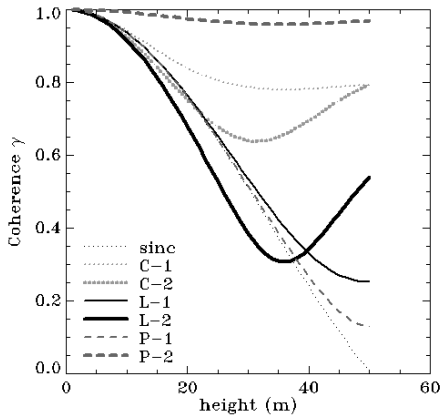

Fig. 3-19 Effect of extinction and ground on the coherence height relation for different frequencies (Cloude et al. 2000). Curve names corresponding to band and ground-volume ratio

volume ratio and a decreasing extinction from C-band to P-band (Fig. 3-19). Also, polarization and looking angle: (1) ground contribution is in general stronger in co-polarized than in cross-polarized channels, (2) an high looking angle increases the effective way of the radar wave through the medium.

3.5.3 Pol-InSAR and RVoG

As was mentioned, the parameters of the RVoG-model: height h, extinction α and ground-volume ratio m, cannot be resolved from a single interferometric observation. Hence, an increase in the observation space is required, i.e. more baselines, frequencies or polarizations. It is important, that additional observations do not increase the parameter space, e.g. additional frequencies also entail additional extinctions and ground contributions.

In this work the approach with different polarizations is chosen (Papathanassiou et al. 1999, Papathanassiou and Cloude 2001). It is assumed that the extinction is polarization-independent, and the ground-volume ratio polarization dependent (Ch. 3.2.3). This means that the coherences of the three polarizations form a line in the unit circle as described by Eq. 3-86 and Eq. 3-87 and Fig. 3-17.c. For three polarizations HH, VV and HV = VH, the RVoG-model has six variables which are matched by six observables:

$$\begin{array}{ll} \textit{System observables}: & \textit{RVoG unknowns}: \\ \textit{HH coherence} + \textit{phase} & \textit{height } h \\ \textit{VV coherence} + \textit{phase} \quad \Leftrightarrow & \textit{extinction } \alpha \quad (\alpha_{HH} = \alpha_{VV} = \alpha_{HV}) \\ \textit{HV coherence} + \textit{phase} & \textit{gr.contributions } m_{HH} \neq m_{VV} \neq m_{HV} \\ & \textit{ground phase } \phi_0 \end{array} \qquad \textbf{Eq. 3-88}$$

However, the model inversion in terms does not give a unique solution and the inversion model requires regularisation. The assumption usually made is to consider the coherence most distant from the ground phase to possess no ground contribution, m = 0

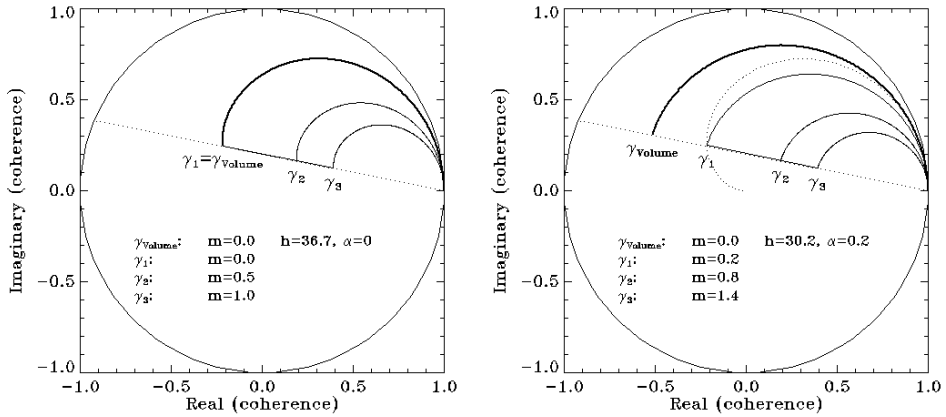

Fig. 3-20 Height inversion from Pol-InSAR and RVoG

In the RVoG, coherences at different polarizations form a line in the unit circle. (1) ground phase – intersection with unit circle, (2) volume-only coherence uncertainty, (3) canopy phase – intersection with unit circle, (4) iso-extinction line of the volume-only coherence. In the two examples, Pol. 1 was interpreted (a) as pure volume coherence γ_{Volume}, and (b) still containing residual ground contribution.

(γ_{Volume}, Eq. 3-83). Then γ_{Volume} can be solved for height and extinction. It is expected that the volume coherence is in general the cross-polarised HV channel where volume scattering generally dominates over the surface component (Cloude and Papathanassiou 2003). In some circumstances, the assumption of m = 0 is not justified, leading then to an overestimation of the forest height typically in the order of 10-20% (Cloude 2002, Mette et al. 2006b). The problem has been illustrated in Fig. 3-20, where the height solutions in with and without regularization differ by 6.5 m. Theoretically, all possible solutions lie between the assumed volume coherence and the unit circle.

3.5.4 Implementing the RVoG-model

Here, we will outline the implementation of the Random Volume over Ground-model according to the three-stage inversion described in Cloude and Papathanassiou (2003). The approach is a geometrical interpretation of the model, and strongly depends on the fit of the line. Fig. 3-21 summarizes the inversion procedure as it was applied here, alternatives are discussed in the description.

Description of the inversion steps (Fig. 3-21):

1. Least square line fitting: A line is fitted with an x-y least square minimization through the complex coherences in the unit circle. This process requires some care because the coherences may be afflicted with a certain variance and errors. These include (Cloude and Papathanassiou 2003): (i) statistical phase and coherence fluctuations (Ch. 3.4.3), (ii) coherence bias for low coherences (Ch. 3.4.3), (iii) other decorrelation sources (Ch. 3.5.5), or (iv) the presence of a more complex forest structure, e.g. with orientation effects. These effects are especially strong if the ground contribution is very similar in all polarizations, and the visible line is small (Fig. 3-20).

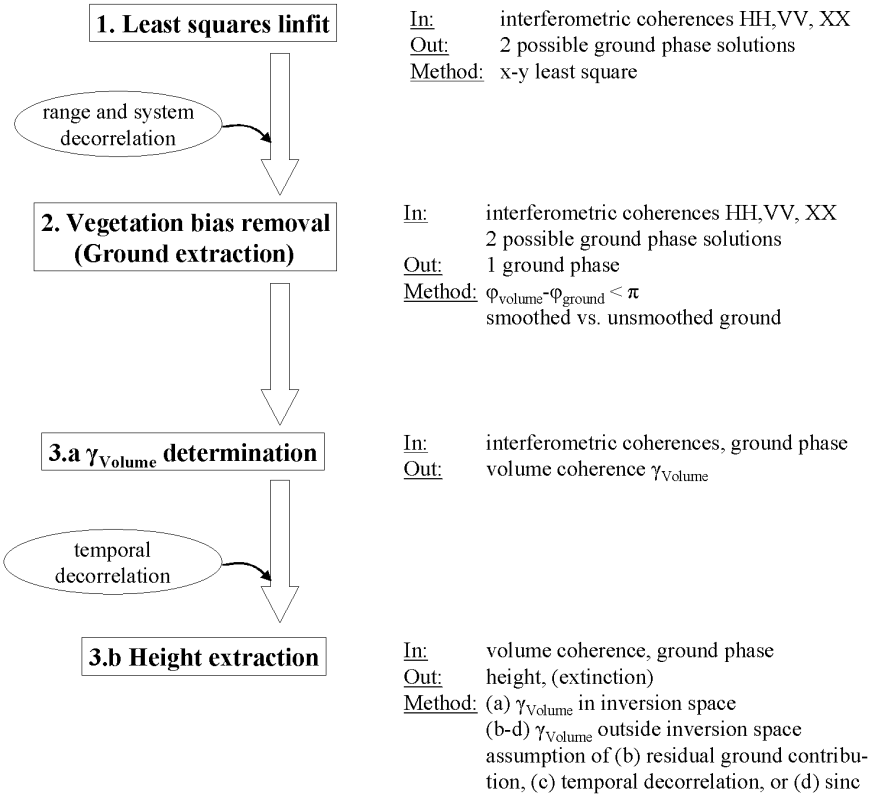

Fig. 3-21 Implementation of the 3-stage of the Random-Volume-over-Ground Model (RVoG) after Cloude and Papathanassiou (2003)

Here, only the three lexicographic coherences (HH, VV, HV = VH) were used for the fitting of the line, assuming that uncertainties are minimized by a ground phase averaging in step 2. Alternatively, coherence optimisation (Cloude and Papathanassiou 1998, Papathanassiou 1999) and rearrangement (Tabb et al. 2002, Yamada et al. 2002), or a confidence test (Isola and Cloude 2001) can support the line fitting.

System and range decorrelation need to be compensated at this point (see Ch. 3.4.5), because they affect both volume and ground, and alternate the ground phase intersection with the unit circle. Temporal decorrelation does not affect the ground and the estimated ground phase (Cloude and Papathanassiou 2003). It must therefore be compensated in step 3.

2. Vegetation bias removal (ground phase determination): One of the two intersections of the line with the unit circle is the solution for the ground phase, the other intersection has no physical solution. Here, the ground phase was chosen as the one intersection with the unit circle, which returns the lower phase $\varphi < \pi$ for the possible γ_{Volume} coherence (Fig. 3-22). This criterion generally returns the lower height solution, and can only be recommended as long as the second solution does not yield a sensible height. This is essentially a question of Δk_z as will be explained in step 3.

   Alternatively, it can be expected that the HV-polarization has the lowest ground contribution since the dihedral stem-ground interaction is stronger in the co-

polarizations HH and VV (Cloude and Papathanassiou 2003, Ch. 3.2). Then, the ground phase lies in the direction of the HH- and VV-coherence.

The extracted ground phases were expected to form a smooth topography without abrupt changes. Smoothing the ground phase can therefore compensate for uncertain line fittings and help the ground decision. An accurate ground determination is the most sensible point of the three-stage height inversion.

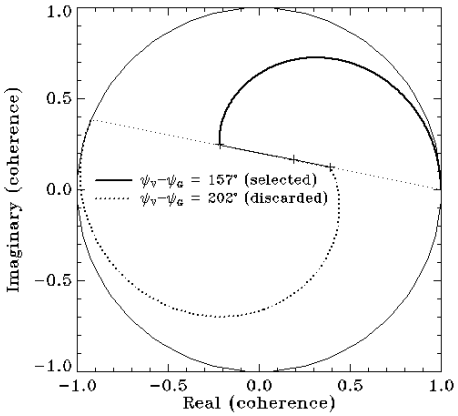

Fig. 3-22 Ground phase determination

3. Height and extinction estimation: The inversion of height and extinction is based on the volume-only coherence γ_{Volume} where m=0. It makes sense to split this step:

(a) Determination of the volume-only coherence (γ_{Volume}): The coherence with the lowest ground contribution is the assumed volume-only coherence. For a residual ground contribution, this coherence only marks the beginning of the ambiguity region (Fig. 3-20). It is the point of the minimum extinction and maximum height. The remaining solutions return a lower height and higher extinction. While the range of possible extinction solutions cover several orders of magnitude, the possible heights vary typically less than 10% (Cloude and Papathanassiou 2003, Mette et al. 2006b).

Temporal decorrelation should be compensated at this point. It is assumed that it only affects the volume-only coherence fully (Cloude and Papathanassiou 2003).

(b) Height inversion from the inversion space: For the height inversion, it is computationally useful to subtract the ground phase from γ_{Volume} and think in terms of an inversion space in the unit circle (Fig. 3-21). The inversion space is defined as the space of all possible height-extinction solutions γ_{Volume}. It is mainly scaled by Δk_z; the look angle plays a significant role only for high extinctions.

The inversion space lies between the sinc-curve (no extinction) and the unit circle boundary. Remember that the phase of the sinc corresponds to the ½–height of the forest. Therefore, the phase course on the sinc-line is only ½ the phase course on the outer circle, which corresponds to a surface like forest top.

Any γ_{Volume} in the inversion space returns a certain height-extinction pair. Volume coherences that do not lie within the inversion space (non-invertable volume coherences) cannot be inverted without certain assumptions. The assumptions and the corresponding inversion are listed in the following:

1. residual ground contribution => ‘moving up’ on the m-line until sinc-curve
2. temporal decorrelation => moving radial until sinc-curve (phase preserving)
3. RVoG does not apply => sinc-solution for absolute coherence

The inversion space for invertable γ_{Volume} is shown in Fig. 3-23.a. The three mentioned inversion options for a non-invertable γ_{Volume} are displayed in Fig. 3-23.b-d.

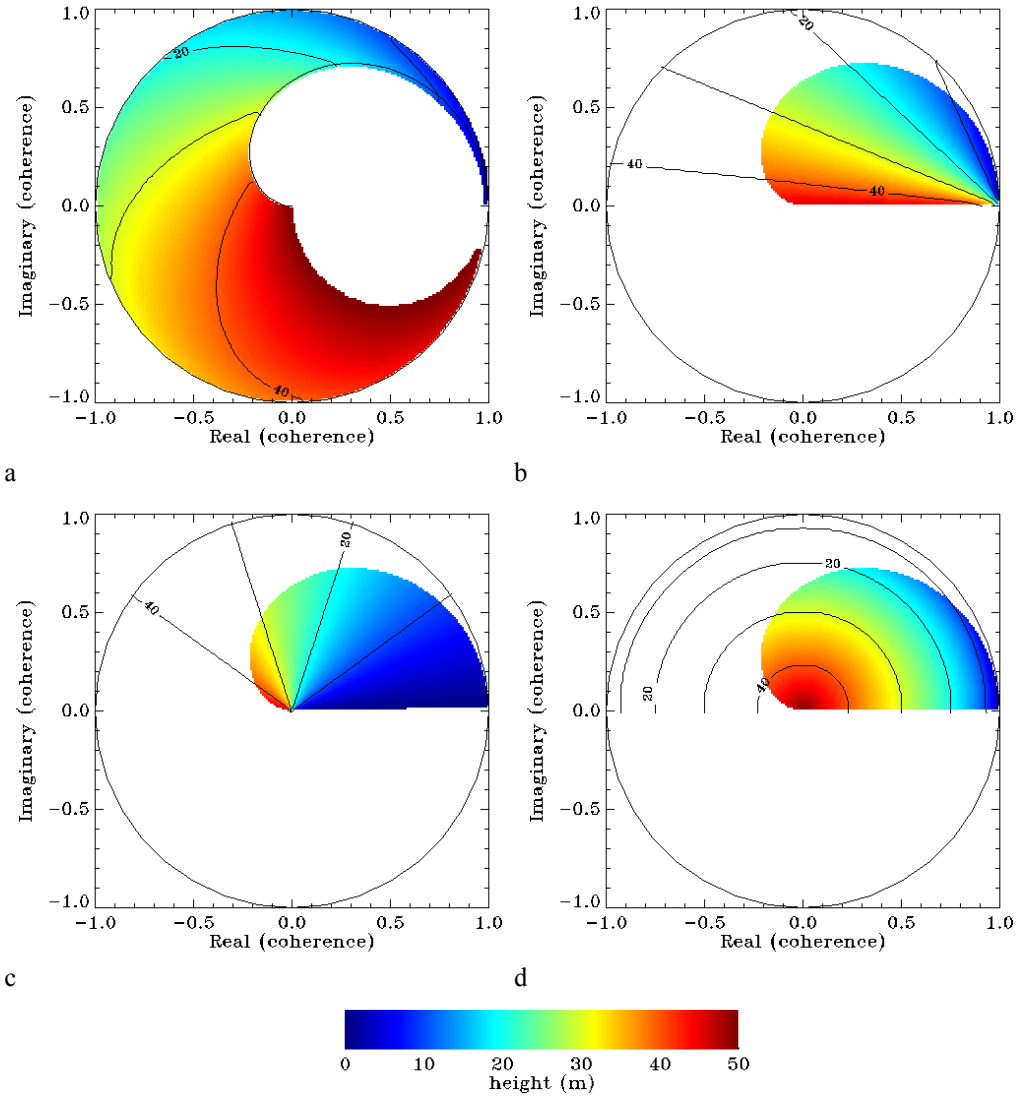

Fig. 3-23 Height inversion of the volume coherence γ_{Volume}

(a) Solutions for invertable volume coherences ($k_z = 0.1$), (b-d) height inversion of not invertable volume coherences assuming (b) residual m, (c) temporal decorrelation, and (d) RVoG model invalidity (substitution with sinc). Under these assumptions, also non-valid volume coherences can be inverted ($k_z = 0.1$).

3.5.5 k_z-sensitivity and non-volume decorrelation

The height inversion meets two important limitations: (1) High extinction can obscure lower parts of the volume as was already mentioned (Ch. 3.5.2). In this case, the coherence amplitude and phase should be equal in all polarizations. This limitation can be avoided to some degree by using steep incidence angles, thereby shortening the path through the medium. (2) The second limitation confines the inversion to a sensitive realm of k_z-values. Here, it is important to avoid Δk_z values for a low ambiguity height on the one hand and height-insensitive Δk_z values on the other hand. This aspect will be studied in more detail here.

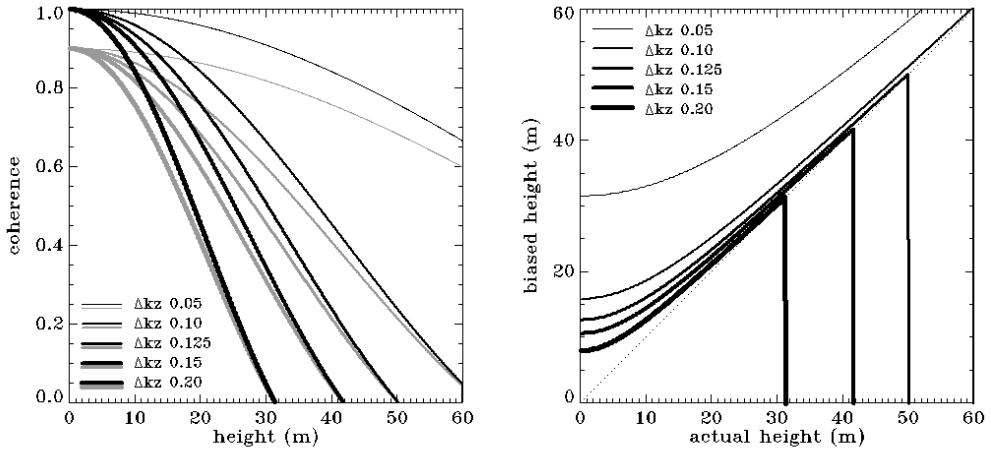

a b

Fig. 3-24 k_z-sensitivity and non-volume decorrelation

(a) Coherence-height relation for a uniform scattering profile in height (sinc-solution), considering 5 different Δk_z values. The grey curves assume a decorrelation of $\gamma_d = 0.9$. (b) The height bias resulting when the decorrelation is not accounted for (difference between grey and black curves in (a) on the x-axis), increases with decreasing Δk_z.

For simplicity, the k_z-sensitivity and relation to non-volume decorrelation shall be explained from the sinc-function (Ch. 3.5.1, Fig. 3-15). A height-sensitive Δk_z must fulfil two conditions:

- Δk_z must be small enough that the heights do not exceed the ambiguity height (or critical height, Eq. 3-76). For instance, $\Delta k_z = 0.20$ only allows height inversions up to 30 m; forest heights up to 50 m require at least a $\Delta k_z = 0.125$.
- Δk_z must be sufficiently large to allow to cover a wide coherence span for the respective height range. For instance, $\Delta k_z = 0.05$ provides only a coherence span from 0.7 to 1 for heights up to 50 m.

In this sense, for temperate forest heights that seldom exceed 40 m, the optimum Δk_z lies between 0.15 and 0.10.

The second criterion is especially important for the scaling of non-volume related decorrelation sources (range, temporal or system decorrelation) to volume decorrelation. Summarizing the prior decorrelation sources in a single 'non-volume' coherence, the decorrelation factor γ_d (Eq. 3-64, Ch. 3.4.3, Ch. 3.4.4):

$$\gamma_d = \gamma_{range} \cdot \gamma_{temporal} \cdot \gamma_{system} \qquad \textbf{Eq. 3-89}$$

the total coherence becomes the product of volume coherence and non-volume coherence, and the sinc-function must be divided by γ_d:

$$\gamma = \gamma_{vol} \cdot \gamma_d \qquad \textbf{Eq. 3-90}$$

$$\gamma_{vol} = \gamma / \gamma_d = \frac{\sin(\frac{1}{2} \cdot \Delta kz \cdot z)}{\frac{1}{2} \cdot \Delta kz \cdot z} \qquad \textbf{Eq. 3-91}$$

To illustrate the effect of uncompensated decorrelation on height for different Δk_z scenarios, Fig. 3-24.b sketches the impact of an uncompensated decorrelation of γ_d=0.9 on the height-inversion for different Δk_z-values. It can be seen, that the height error affects

Tab. 3-2 Decorrelation source and magnitude for E-SAR specifications

Decorrelation type	Calculation	Input parameters	Coherence
Range decorrelation (Hamming window approximated with sinc, Eq. 3-72)	$\gamma_{range,opt} = \frac{\sin(½ \cdot \Delta k_r \cdot res_{range})}{½ \cdot \Delta k_r \cdot res_{range}}$	Flight alt. 3000m, bandw. 100MHz B_{eff} 5m, look angle 30° B_{eff} 5m, look angle 60° B_{eff} 10m, look angle 30° B_{eff} 10m, look angle 60°	γ_{range} = 0.999 = 0.997 = 0.988 = 0.996
SNR decorrelation (Eq. 3-78)	$\gamma_{SNR} = \frac{1}{1+(SNR)^{-1}}$	SNR level –35 dB Signal –10dB Signal –20dB Signal –35dB	γ_{SNR} = 0.997 = 0.97 = 0.5
Coregistration decorrelation (Eq. 3-79)	$\gamma_{coreg} = \mathrm{sinc}(\pi \cdot \Delta px)$	Coregistration accuracy $\Delta t * B_{eff}$=0.05 pixel $\Delta t * B_{eff}$=0.1 pixel	γ_{coreg} = 0.984 = 0.935

low heights stronger than high heights, but the error increases significantly the lower Δk_z becomes. For $\Delta k_z = 0.05$, a coherence of 0.9 corresponds already to 32 m height.

Fig. 3-24 makes it also clear, how important it is to compensate any non-volume decorrelation before height inversion. For the E-SAR L-band sensor, the range, SNR- and coregistration decorrelation can be estimated from the system specifications. As Tab. 3-2 shows, from the deterministic decorrelation sources only coregistration inaccuracy can reach below $\gamma_{non\text{-}vol} < 0.95$ once low backscatter regions are excluded. Temporal decorrelation remains unknown.

In the RVoG-model, range- and system-decorrelation affect all coherences equally and should be compensated before the ground extraction (compare Eq. 3-87):

$$\gamma_{VoG} = \gamma_{range} \cdot \gamma_{system} \left(\gamma_{Volume} + (1 - \gamma_{Volume}) \cdot \frac{m}{m+1} \right) \qquad \textbf{Eq. 3-92}$$

Temporal decorrelation on the other hand, affects only the volume-coherence to the full extent; the ground remains unaffected (Cloude and Papathanassiou 2003). Therefore temporal decorrelation must only be multiplied on the volume coherence:

$$\gamma_{VoG} = \gamma_{temporal} \cdot \gamma_{Volume} + (1 - \gamma_{temporal} \cdot \gamma_{Volume}) \cdot \frac{m}{m+1} \qquad \textbf{Eq. 3-93}$$

Both decorrelation sources are considered in the RVoG scheme in Fig. 3-21. In the height inversion in Ch. 4.2 an average decorrelation factor was used and discussed.

4 Validation and Discussion

This chapter implements and validates the Pol-InSAR height inversion and the successive allometric biomass estimation with experimental data of the test site Traunstein. The goal of the validation is to determine accuracy, error sources and limitations for each step of the implementation in order to evaluate the potential of polarimetric SAR interferometry to estimate forest height and forest biomass.

The test site Traunstein is well suited for this task because the stands are comparably homogeneous, and documented by a dense grid of inventory plots. The forest heights can reach 40 m and biomass may locally amount up to more than 500 t ha^{-1}.

The forest inventory data were provided by the chair of forest yield science at the TU Munich and the Bavarian ministry of forestry. The radar data were acquired with the airborne E-SAR system of DLR. Additionally, the forest management map and an aerial photography (LVA Bayern) were available.

In Ch. 4.1, the forestry inventory data were used to choose 20 comparably homogeneous validation stands in order to avoid problems with heterogeneous forest structures. For each site, the upper canopy height and usable wood biomass was determined from the inventory data. The performance of the allometric height-biomass concept from Ch. 2.4.3 (Ch. 2.6[6]), was then checked upon the data.

In Ch. 4.2, the height inversion algorithm was implemented and validated by comparing the inverted heights with the inventory heights of the validation stands.

Finally, in Ch. 4.3, the heights from the Pol-InSAR inversion were converted to forest biomass using the height-biomass allometry from Ch. 2.4.3. Also, a direct coherence-biomass relation is introduced.

4.1 The Traunstein Forest

This subchapter will introduce the test site Traunstein, and the forest inventory data (Ch. 4.1.1). It will be explained, how the homogeneous validation stands were selected, and how the reference parameters, upper canopy height and stem biomass, were derived from the inventory data (Ch. 4.1.2 and Ch. 4.1.3). Then, the concept of the reference height-biomass allometry and allometric level from Ch. 2.4.3 is applied on the data. The allometry is validated with respect to the variance on plot and stand level, and systematic errors, which can be revealed from the growth stadium (Ch. 4.1.4).

4.1.1 Test site and selection of validation stands

The test-site Traunstein is located in the pre-alpine moraine landscape of southeastern Bavaria near the city of Traunstein. As Fig. 4-1 shows, it consists of a mosaic of agricultural fields, pasture and forests, and in the western part also the city of Traunstein.

[6] The basic concept was developed in Ch. 2.4. It was discussed and refined in Ch. 2.6.

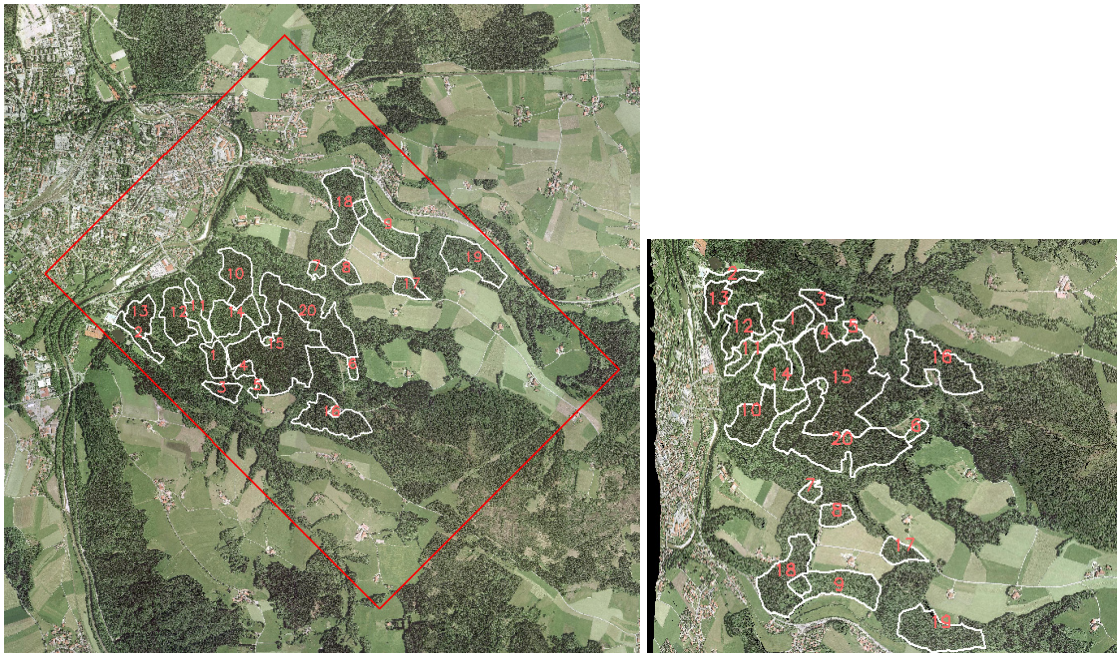

Fig. 4-1 Aerial photography of the test site Traunstein

(Left) ground range, and (right) slant range (Source: LVG Bayern). The slant range image corresponds to the red frame in the ground range image. Due to the radar acquisition geometry it is mirrored ~upside down. The selected homogeneous validation stands are numbered according to Tab. 4-1

The topography varies from 600-650 m a.s.l., with only few steep slopes. The climatic condition with a mean annual temperature of 7.8°C and precipitation of more than 1600 mm a^{-1} favour mixed mountainous forests, dominated by spruce (*Picea abies*), beech (*Fagus sylvatica*) and fir (*Abies alba*). The test-site forest includes the two forest districts "Bürgerwald" and "Heilig-Geist" and covers a total area of 218 ha.

The forest management map from 1999 divides the forest area into 165 stands, each one with a certain growth or management stadium. Quantitative information about the stands is provided by means of the forest inventory that was carried out in 1998 in a 100m x 100m grid (Ch. 2.2.5). All together, 224 inventory points were located within the test area.

Principally, the quantitative validation of the radar data is only possible in the neighbourhood of the inventory plots where height and biomass are given by the inventory data. However, in heterogeneous forests even a small misregistration between inventory coordinates and radar image may deteriorate the results. Also, the certainty of the estimated parameters increases for larger sampling areas. For these reasons it was tried to select large forest areas which were as homogeneous as possible in terms of species, height, biomass and stadium. In total, 20 validation stands covering 123 ha (average 6 ha) and including 133 inventory points were delineated on the basis of:

- the forest management map (1999) for the stadium and species
- the inventory data (1998) for species, height and biomass
- an aerial photography (LVA Bayern) to cut out local inhomogeneities

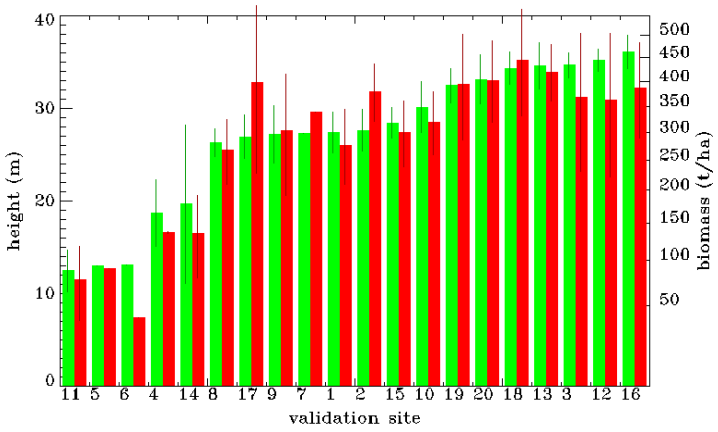

Fig. 4-2 Upper canopy height and usable wood biomass of the 20 selected validation stands

Sorted according to height. Biomass scale adapted to allometric exponent of the reference height-biomass allometry (Eq. 2-17)

Tab. 4-1 Key forest parameters of the 20 selected validation stands

Index	Area	Area SAR image	Inventory Samples	Stadium	Dom. species	All species	Upper canopy height	Usable wood biomass	Dbh_{mid}	Basal area	Tree number	All. level
#	m^2	px		(1)	(2)	(2)	m (3)	t ha^{-1} (3)	cm	m^2 ha^{-1}		(3)
1	36392	15271	4	M_{con}	Fi	Fi-Bu-Lä	27.4±2.2	277.3±67.5	31.5	40.5	520	0.89
2	27146	9233	3	G_{con}	Fi	Fi-Bu-Lä	27.6±2.2	379.0±58.1	29.6	50.0	725	1.21
3	24877	12498	3	R_{con}	Fi	Fi-Ta-Ki	34.7±1.4	367.2±135.8	51.5	50.0	240	0.82
4	13376.	6133	2	R_{con}	Fi	Fi-Bu	18.7±3.6	137.0±1.4	16.5	29.9	1400	0.81
5	10490	5242	1	G_{con}	Fi	Fi	13.0±0.0	89.3±0.0	10.7	27.9	3124	0.93
6	9433	4610	1	G_{brd}	Ah	Ah-Bu-Fi	13.1±0.0	38.7±0.0	07.1	14.3	3609	0.40
7	12148	5845	1	G_{brd}	Bu	Bu-Fi-Lä	27.3±0.0	338.2±0.0	26.1	44.2	829	1.10
8	23595	11283	2	G_{con}	Fi	Fi-Bu-Ei	26.3±1.5	267.5±57.1	27.2	40.1	690	0.92
9	75830	34583	7	G_{brd}	Bu	Bu-Ah-Es	27.2±3.1	303.3±111.2	22.5	31.6	795	0.99
10	72953	29741	7	M_{con}	Fi	Fi-Bi-Bu	30.1±2.7	319.9±59.4	35.2	45.0	463	0.89
11	39346	14559	4	G_{con}	Fi	Fi-Ta-Bu	12.5±2.3	77.0±41.1	09.5	23.1	3286	0.86
12	68178	22756	9	R_{con}	Fi	Fi-Ta-Bu	35.2±1.2	362.6±141.2	44.4	48.9	316	0.79
13	45666	13561	3	M_{con}	Fi	Fi-Bu-Ei	34.6±2.5	420.0±59.4	42.2	54.4	389	0.94
14	73268	30914	7	G_{con}	Ta	Fi-Ta-Bu	19.7±8.6	135.7±56.7	13.5	30.1	2115	0.74
15	236545	107951	24	M_{con}	Fi	Fi-Bu-Ta	28.4±1.6	299.4±60.5	34.6	43.7	465	0.91
16	92776	48046	11	R_{con}	Fi	Fi-Bu	36.1±1.8	385.8±96.7	44.6	49.7	317	0.80
17	25779	13133	4	G_{con}	Fi	Fi-Bu-Ei	26.9±2.3	397.6±169.2	29.7	53.5	770	1.32
18	108210	43466	10	R_{con}	Fi	Fi-Bu-Ah	34.3±1.8	445.2±113.4	39.3	53.3	438	1.00
19	92143	45214	11	M_{con}	Fi	Fi-Bu-Es	32.5±1.6	394.3±107.4	32.0	43.0	534	0.97
20	182350	83115	18	R_{con}	Fi	Fi-Bu-Ta	33.1±2.7	402.6±83.7	41.5	50.9	376	0.96

(1) Stadium: G=growth, M=mature, R=regenerating, subscripts 'con'=conifer, 'brd'=broadleaf

(2) Species: Fi=N.spruce (*Picea abies*), Ki=Scots pine (*Pinus silvestris*), Ta=White fir (*Abies picea*), Lä=Eur.larch (*Larix decidua*), Bu=Eur.beech (*Fagus sylvatica*), Es=ash (*Fraxinus excelsior*), Ah=maple (*Acer pseudoplatanus*), Ei=oak (*Quercus robur*), Bi=birch (*Betula pendula*)

(3) calculation Eq. 2-18

The delineation of the homogeneous stands followed the stand borders from the forest management map, and often several adjacent stands were grouped together. It should be remembered that the selection of a homogeneous areas for validation is subjective. But it was tried to combine all available sources of information along with field experience to come up with areas as large and homogeneous as possible. Fig. 4-1 shows an aerial photograph of the test with the distribution of the validation stands. In Fig. 4-2 it can be seen that the upper canopy heights range between 13-36 m, the biomass from 40-450 t ha^{-1}. Tab. 4-1 summarizes the most important parameters for the 20 selected validation stands: upper canopy height, usable wood biomass, allometric level, dominant species and stadium. The determination of the parameters from the forest inventory data is explained in the next chapter, Ch. 4.1.2.

4.1.2 Reference data from the forest inventory

The definition of the parameters was discussed in Ch. 2.2.2. Now, it shall be outlined how the parameters were derived from the inventory data. All parameter (except stadium) were derived from the layer level where the single tree information is already condensed into layers (compare Ch. 2.2.5).

The upper canopy height h was calculated for each inventory plot as the basal area (G) weighted mid height (h_{mid}) of all layers reaching 80% of the maximum mid height (Eq. 4-1, index denotes the mentioned layers). The upper canopy height of the validation stands was calculated as the average upper canopy height of the inventory plots inside the area.

$$h = \sum_{i=1}^{n} G_i \cdot h_{mid\,i} \,/\, \sum_{i=1}^{n} G_i \qquad \textbf{Eq. 4-1}$$

In this algorithm, it is possible that one single emergent tree defines the upper 'canopy' height, which is not very representative (see Fig. 2-5). Such open stands pose a general problem to the definition of a reference height, and makes the comparison to the heights extracted from remote sensing difficult. These problems were circumvented through the selection of validation stands. Fig. 4-3 shows that the upper canopy height used here (Eq. 4-1) underestimates the literal h_{100} by an average 1.8 m.

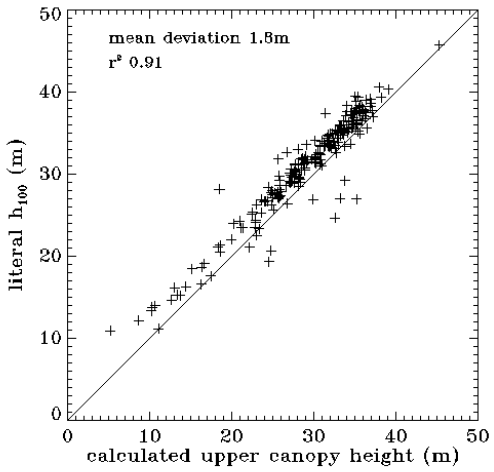

Fig. 4-3 Comparison of calculated upper canopy height and literal h_{100}-definition for the inventory plots

The usable wood biomass B of each inventory plot was calculated from the inventoried wood volume V_{inv} by multiplying with the wood raw density ρ; 10% harvest loss (HL) and 6-20% bark subtraction (BS) must be compensated (Ch. 2.2.5). Like for the upper canopy height, the biomass of the validation stands was calculated by averaging the biomass of the respective inventory plots.

$$B = V_{inv} \cdot \rho + HL + BS \qquad \textbf{Eq. 4-2}$$

Two remarks on biomass: (1) the usable wood biomass was defined and critically discussed in Ch. 2.2.2 and Ch. 2.2.4. Recall, that the attribute 'usable' restricted the biomass to the stem and branches where exceeding 7 cm diameter. According to this definition trees below 7 cm diameter (~10 m height) possess no biomass. While in well-developed stands this dbh-cap of 7 cm does usually not exclude significant biomass portions, low stands are not well represented by 'usable wood biomass'. (2) The biomass must be considered much more uncertain than height (see Ch. 2.5). The first uncertainty lies in the nature of the parameter, because the local variation in forest density are larger than in tree height. E.g. in an old stand with 100 trees per hectare (=5 trees per plot), one tree accounts for ~20% difference in biomass. Especially in heterogeneous stands, the presence or absence of one tall tree in a plot of an otherwise low trees can easily change the biomass by an order of magnitude.

Allometric level: according to Eq. 2-18, the allometric level l_a was defined as the ratio of the actual biomass to the biomass expected from the height when applying the reference height-biomass allometry (Eq. 2-17). In contrast to basal area, SDI or stocking degree (Ch. 2.2.2), the allometric level is a height-related forest density measure.

The growth stadium was taken from the forest management plan. The stadiums correspond to certain forest structural characteristics and management requirements (Fig. 4-4).

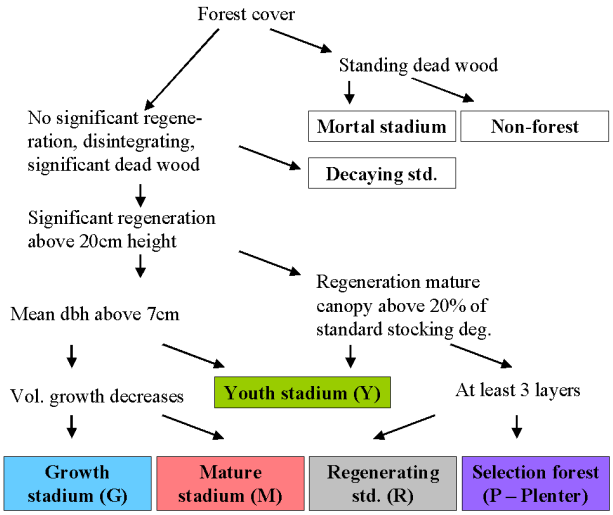

Fig. 4-4 Assignment of growth stadiums

4.1.3 Data actualisation

The inventory data for the test site Traunstein were acquired in 1998, the radar data in 2003. Since forest changes with time due to growth and management (thinning, clearing), the data must be extrapolated from 1998 to 2003. Such an actualisation of the inventory data is not possible without exact knowledge of the specific growth conditions and the forest management. In the frame of this work only height and biomass growth were modelled from the yield tables.

Theoretically, a correct growth calculation has to be carried out on a single tree basis. The simplified approach that was applied here, recalculates the upper canopy height and usable wood biomass from the layer information (Ch. 2.2.2):

Height-actualisation: The upper canopy layers of the inventory plots were separated for species, and the mid height plotted against age (Fig. 4-5.a-d). The data points were compared against sigmoid height growth in the yield tables of the corresponding species (Ch. 2.4.2). This way, each species was assigned one yield class for the whole test site. The 5-year height increase was then extrapolated from the growth curve of the determined yield class (Fig. 4-5.e). Fig. 4-5 confirms that the growth conditions in Traun-

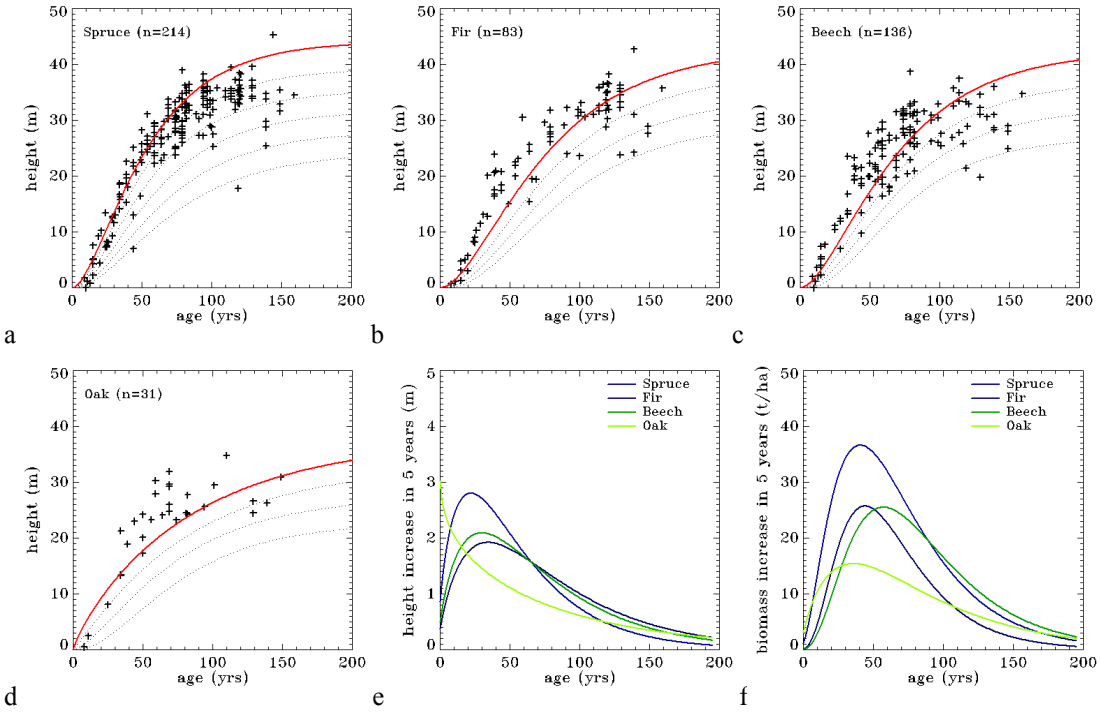

Fig. 4-5 Yield class determination and estimation of height and biomass growth for the forest data of Traunstein

(a-d) The mid height of the upper canopy layers of all inventory plots was separated for species and compared to yield tables growth curves for different yield classes (dotted curves). The red curve marks the best fitting overall yield class. (a) Spruce: Assmann and Franz 1963, average yield level, (b) Fir: Hausser 1956, (c) Beech: Schober 1967, mod. thinning, (d) Oak: Jüttner 1955, mod. thinning)

(e-f) Height and biomass increase can be extrapolated from the growth functions in (a-d) as a function of age and species. Here, the data were extrapolated from the year of the forest inventory, 1998, to the year of the radar data acquisition, 2003 (5 years).

stein are exceptionally well for all considered species and fall into the highest yield class. It is interesting to notice that growth curves are not perfectly matched by the yield table growth curves. The actual curves appear steeper than the modelled ones, which means the growth rate is higher. This might actually reflect changes in the environment like higher temperatures, atmospheric nitrogen and CO_2 fertilization (compare Kauppi et al. 1992, Spiecker et al. 2002, Pretzsch 1999).

Biomass-actualisation: The biomass actualisation is more difficult and uncertain than the actualisation of the upper canopy height, because the growth behaviour of the various layers of a forest can only be modelled with very detailed information on the social status of each tree. Here, a simplified approach was used to extrapolate biomass from 1998 to 2003: In a first step, all layers were assigned the species-specific biomass growth curve corresponding to the yield class determined from the height growth. Then, the 5-year biomass increase was derived through multiplication with the stocking degree. Fig. 4-5.f shows the 5-year biomass for 100% stocking degree.

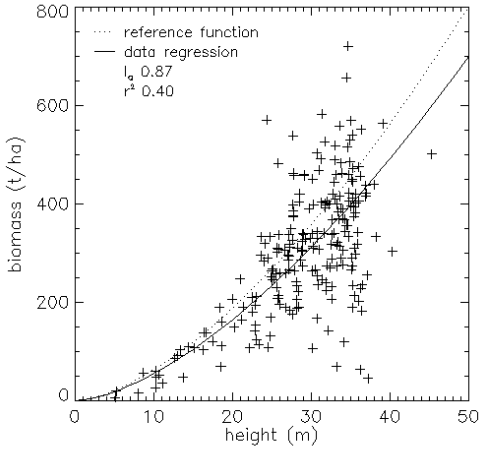

Fig. 4-6 Forest height-biomass allometry for the test site Traunstein from the inventory data

4.1.4 Height biomass allometry in Traunstein

In Ch. 2.4.3, a reference allometry was derived from the yield tables for a first estimation of forest biomass from forest height (Eq. 2-17). It was shown that in dependence of species and thinning, it might be necessary to adapt the allometric level l_a (Eq. 2-18).

Now, the performance of the reference allometry shall be validated from inventory plots of the test site Traunstein. From a species-perspective, the reference equation is expected to fit well, since spruce – on which the reference height-biomass allometry was based - is also the dominating tree species in the test site. However, the forest structure probably differs from the idealized single-layered forest in the yield tables.

Fig. 4-6 displays the height-biomass relation of all 224 inventory plots in Traunstein. The allometric relation between height and biomass is clearly visible, but with respect to the reference function we see: (1) a systematic deviation from the assumed reference equation (average allometric level $l_a = 0.87$), (2) a large variance which is quantified by the correlation coefficient $r^2 = 0.40$.

Both effects shall be examined more closely in Fig. 4-7 and Fig. 4-8.

- In Fig. 4-7, it is investigated whether the variance of the height-biomass allometry is caused by inhomogeneous inventory plots. Accordingly, the height-biomass allometry was plotted only considering the plots within the validation stands (n = 133), which were selected for their homogeneity. However, Fig. 4-7.a shows that, compared to Fig. 4-6, the variance only decreases slightly ($r^2 = 0.45$). On the other hand, when averaging the inventory data for the validation stands (n = 20), the correlation coefficient increased to $r^2 = 0.86$ (Fig. 4-7.b). This indicates that – at least for Traunstein – the variance is due to local forest density variations, which compensate on larger scales. The increase in the allometric level by 4-5% ($l_a = 0.92$) shows that, in average, the selection of homogeneous areas included stands of higher densities.
- In Fig. 4-8, the forest height-biomass allometry has been plotted separately for the growth stadiums assigned to the inventory plots (see Fig. 4-4). The main deviations from the mean allometric level (0.87) occur in the youth stadiums: $l_a(Y_{con}) = 0.36$,

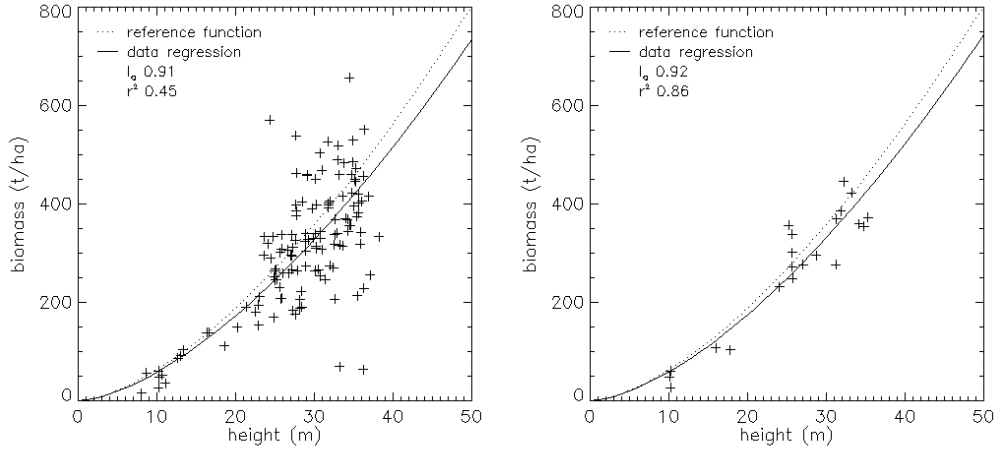

a b

Fig. 4-7 Dependency of height-biomass allometry on the area integration

(a) inventory plots inside the validation stands n=133, (b) for the averaged height- and biomass of the validation stands; l_a = allometric level (Eq. 2-18)

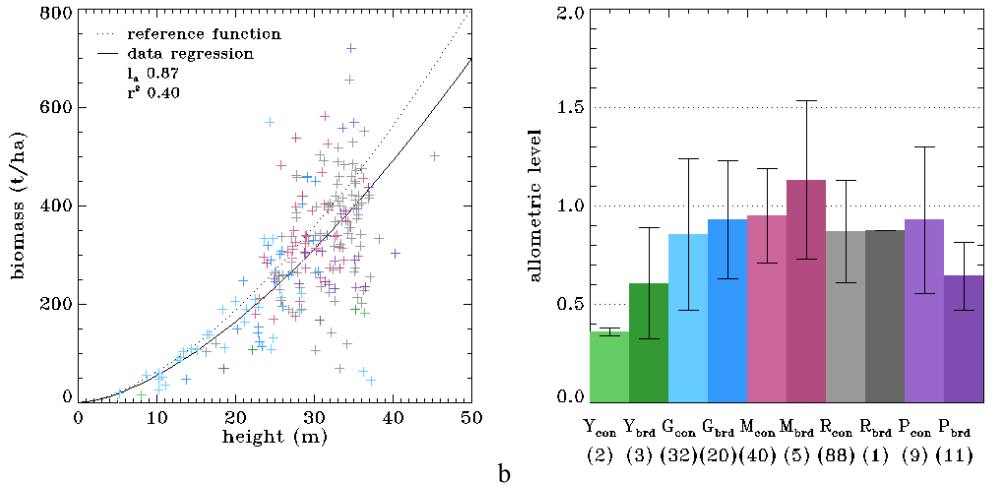

a b

Fig. 4-8 Forest height-biomass allometry for the test site Traunstein

(a) 224 plots separated according to growth stadium (colours defined in plot b), (b) average allometric level separated according to growth stadium. Growth stadiums (Fig. 4-4): Y youth stadium, G growth stadium, M mature stadium, R regenerating stadium, P selection forest ('Plenter'), subscripts 'con' and 'brd' refer to conifer and broadleaf, respectively.

$l_a(Y_{brd}) = 0.61$. Here, the presence of few leftover emergent trees defines a high upper canopy height for a plot dominated by young trees. This thinning of the upper canopy layer starts already during the regeneration stadium: $l_a(R) \sim 0.87$, although the difference to the growth stadiums: $l_a(G) \sim 0.89$, and the conifer mature stadium: $l_a(M_{con}) = 0.95$ is little. An exception is the high allometric level of the mature broadleaf stadium, $l_a(M_{brd}) = 1.13$, which is represented mainly by beech forests. This was not expected from the yield tables, and is possibly due to lower thinning intensity. The beech tables were set up for a thinning-from-above practise (compare Fig. 2-16).

The selection forests (P) are somewhat special cases due to their heterogeneous age structure, but only the broadleaf stadium: $l_a(P_{brd}) = 0.65$ deviates significantly from the average level.

Further more, the low allometric level of youth stadiums is further reinforced through the 'usable' definition of biomass, which practically assigns trees below 10 m no biomass. This effect can be well observed from the low heights in Fig. 4-8.a.

4.1.5 Summary and conclusions

The concept of height-biomass allometry, as developed and refined in Ch. 2.4 and Ch. 2.6, was implemented on the forest inventory data of the test site Traunstein. The overall height-biomass relation followed an allometric (power) function, so the reference allometry could be applied to account for the height dependency of biomass. The forest density had to be adjusted by an average allometric level of $l_a \sim 0.90$. Since the allometric level is – ex ante – not derived from height extracting remote sensing systems, it becomes the critical missing parameter for the biomass estimation. In this respect, the closer analysis between stadium and allometric level revealed four systematic effects:

1. biomass overestimation in the youth stadiums, mainly because the reference height is derived from few left-over emergent trees, but also because the 'usable' criterion under-represents the biomass of low stands
2. biomass overestimation in regenerating stadiums due to stronger thinning
3. biomass underestimation in mature broadleaf stands,
4. biomass overestimation in broadleaf selection forest (Plenter).

These effects do not necessarily translate directly into biomass estimation errors from the remote sensing height data, because also the signal height signature plays a role. As for the mentioned cases, it is likely that the heterogeneous forest structure in (1) and (4) affects also the height extraction. Here, both the remote sensing height signature and a sensible height definition must be investigated; resolution becomes an important issue for the sensitivity to canopy heterogeneities. In the cases (2) and (3), the forest height is probably more or less homogeneous. The biomass error is independent from the height extraction, and can only be avoided with additional density (-related) information. In case (2), the distinction between broadleaf and coniferous could provide such information, case (3) can only be resolved with a direct density measure, perhaps from texture parameters as proposed in Ch. 2.6.

Another important aspect is the question whether the height-biomass allometry saturates, thereby limiting biomass estimation from height. As for Traunstein, the growth conditions seemed to support spruce heights up to approximately 40 m. Up to this height, the height-biomass relation did not saturate. Locally the allometrically expected values may be exceeded, but it was shown that such local density variations compensated on large-scale averages. In general, a saturation of the height-biomass allometry would have to be addressed with the allometric level.

4.2 Radar data

This subchapter introduces the radar data set that was chosen for the height inversion. The standard parameters backscatter and interferometric coherence are compared against forest height, and discussed briefly.

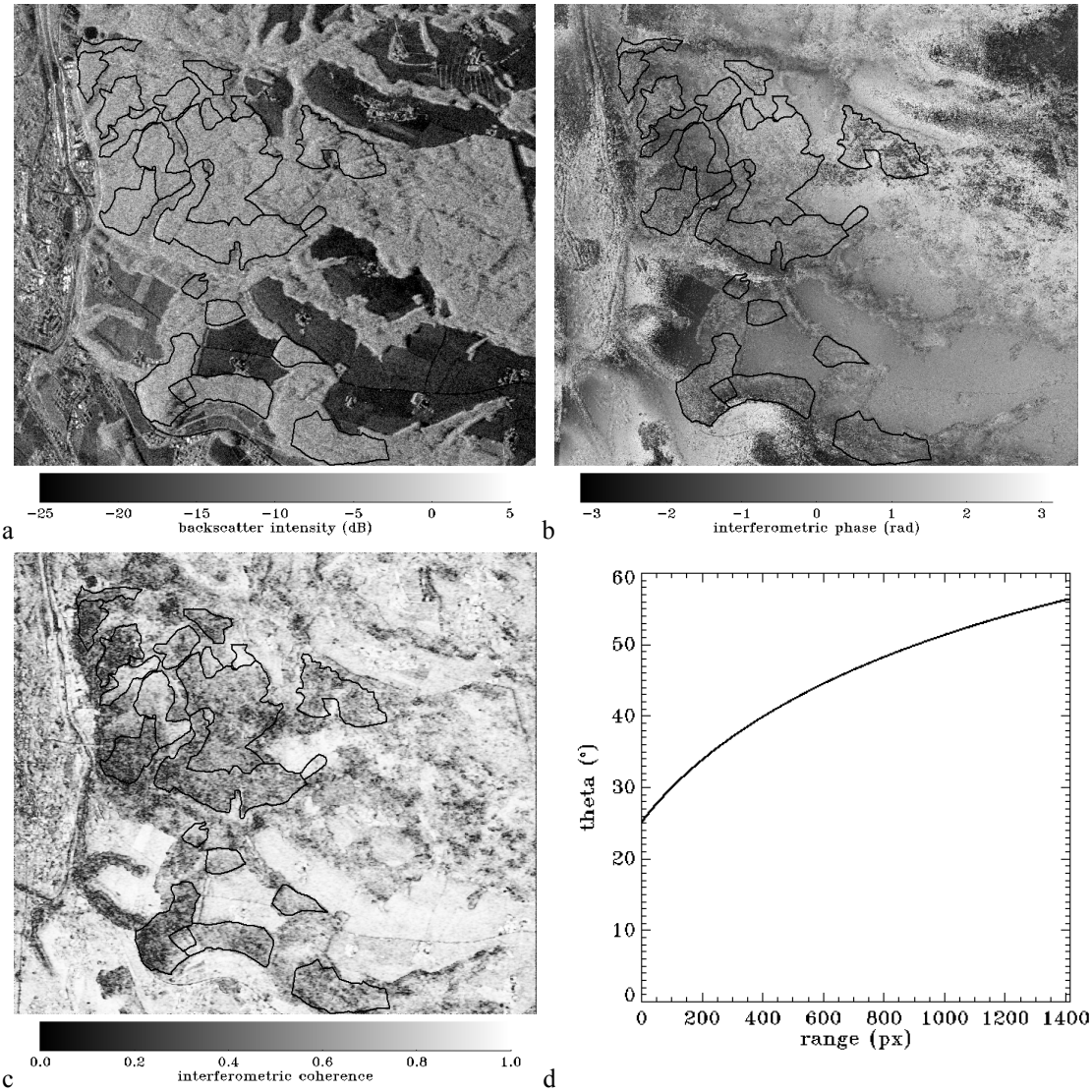

Fig. 4-9 L-band radar data of the Traunstein test site (HH-polarization)

(a) backscatter intensity, (b) interferometric phase after flat earth removal, (c) interferometric coherence, (d) incidence angle over range. Flight configuration: altitude 3000 m above ground, 5 m baseline

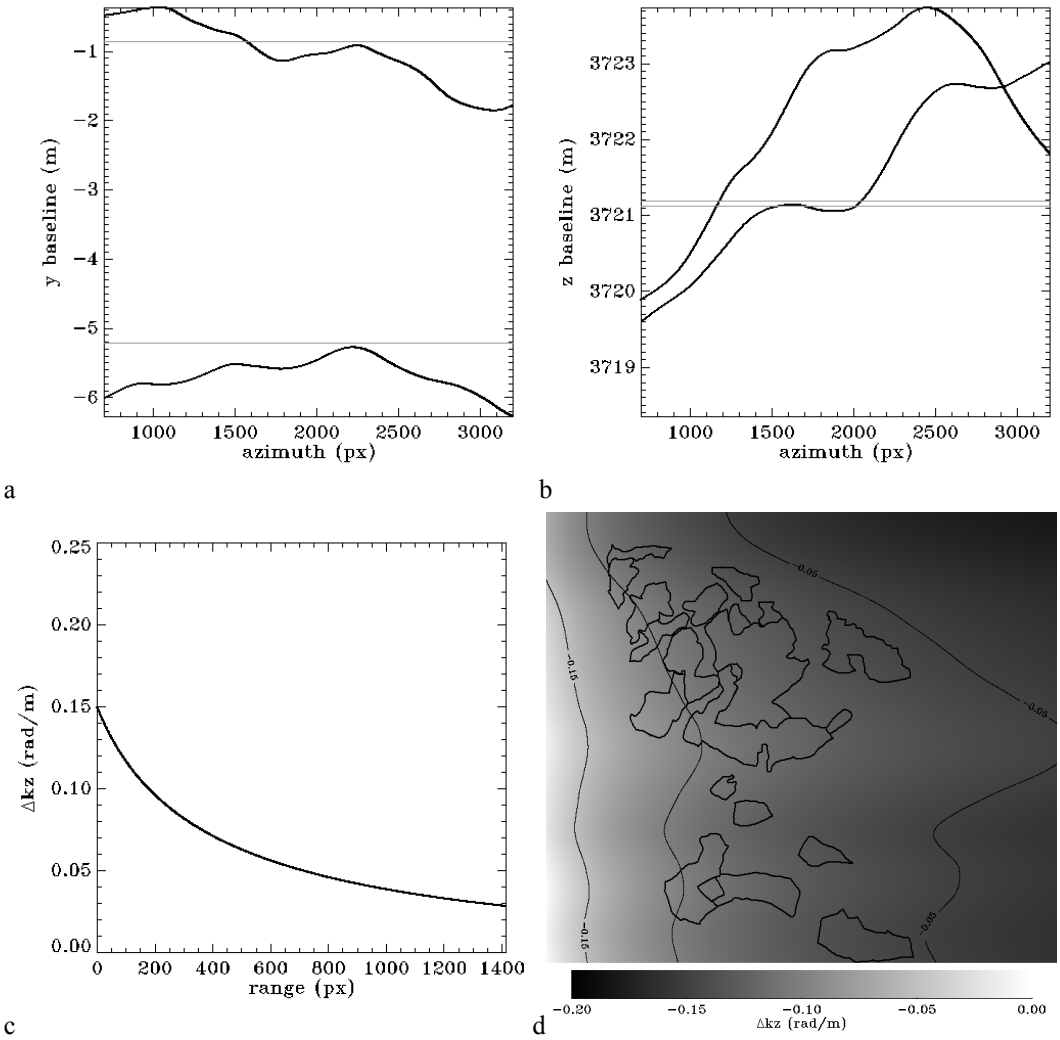

Fig. 4-10 Interferometric flight configuration for the Traunstein radar data

(a/b) flight track in y and z-plane – the azimuth values on the x-axis correspond to the cut from the whole image (pixel 700-3200), (c), reference vertical wave number Δkz, (d) 2-dimensional actual Δkz

4.2.1 Data set

The radar data of the Traunstein test site were acquired in the morning of Oct. 11, 2003 with the E-SAR system of DLR (Ch. 3.1). For the height inversion was chosen an interferometric fully polarized L-band data set with a nominal spatial baseline of 5m at a flight altitude of 3000 m above ground; the temporal baseline was 20 min. The whole strip covered an area of approximately 2.5km x 5km (Fig. 3-3), but for the validation the image was reduced to the 2.5km x 2.5km which covered the area of the validation stands. The dimension of the radar image is shown in the aerial photograph (Fig. 4-1) – note that due to antenna direction, the image is mirrored. The incidence angle increases from 25° in near range to 60° in far range.

Fig. 4-10 displays the interferometric flight parameters. Fig. 4-10.a plots the range course of the incidence angle and the average Δk_z while Fig. 4-10.b/c show the true

flight path in y- and z-coordinates. Since the straight track cannot be kept perfectly, the resulting Δk_z varies not only over range but also over azimuth (Fig. 4-10.d). The Δk_z-values of the validation stands lie between $0.05 < \Delta k_z < 0.15$, which correspond to ambiguity heights between $120\ m > h_{amb} > 40\ m$. The low Δk_z values make the height inversion very sensitive to uncompensated decorrelation (Ch. 3.5.5, Fig. 3-24).

The data were processed with a single look resolution of 1.5 m in range (100 MHz bandwidth) and 3 m in azimuth. Fig. 4-9 shows the slant range image of backscatter intensity, interferometric coherence and interferometric phase after flat earth removal.

It can be seen, that the forest area is well distinguishable in all image types:

(1) In the backscatter image the forest has a comparably strong and homogeneous radar backscatter intensity. Streets and clearings in the forest are resolved well, but the backscatter dynamic within the forest area is low

(2) The coherence over the volume scatterer 'forest' is lower than over the rough surface scatterers, like fields and meadows. It generally increases towards far range as would be expected when volume height stays equal and Δk_z increases (Ch. 3.5). Especially in near range the coherence appears to be more homogeneous and often follow the delineation of the validation stands.

(3) After the flat earth removal, the interferometric phase still contains the topographic phase component (Ch. 3.4.2). The terrain slightly rises towards far range, and in near range some ravines dissect the forest plateau. Over forests, the interferometric phase is more variable than over surfaces because the scattering centres are distributed randomly in the volume.

4.2.2 Backscatter and coherence vs. forest height

Before applying inversion algorithms, it makes sense to take a look at the relation between forest height and the standard radar parameters backscatter and coherence.

In Fig. 4-11, the average backscatter intensity and coherence is plotted against the ground measured upper canopy height of the validation stands:

- The backscatter intensity lies around -7 dB for HH, -9 dB for VV, and -12 dB for HV. No polarization shows any correlation to forest height.
- The coherence is obviously more sensitive to forest height. It drops from 0.8-0.9 for 10m height to 0.4-0.5 for 30m height and higher. The polarizations do not differ notably.

The backscatter results are not surprising. L-band backscatter is frequently described to saturate at approximately 40 t ha^{-1} (Ch. 3.2.4), which corresponds to heights roughly about 10-12 m in Traunstein. As for the coherence, the baseline-configuration, i.e. the Δk_z, theoretically allows a height extraction up to 40 m and more, if extinction does not obscure lower parts of the volume and the ground.

However, the direct coherence-height relation does not take into account Δk_z, which scales the coherence-height relation. This has no effect if Δk_z is almost constant like in satellite scenarios, but in airborne acquisitions with a large Δk_z-range (Fig. 4-10), this introduces a bias in the coherence-height relation.

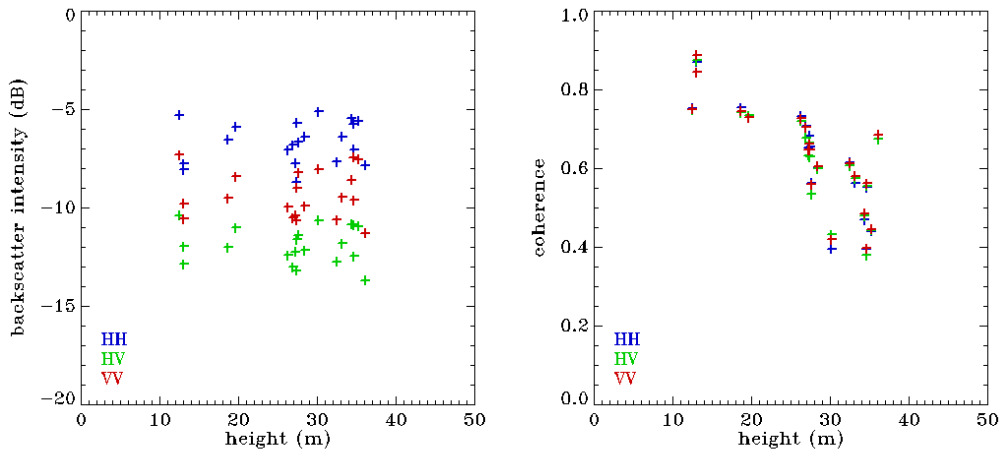

a b

Fig. 4-11 (a) Backscatter amplitude vs. forest height, (b) interferometric coherence vs. forest height for the 20 selected validation stands

4.2.3 Height inversion with the sinc

The sinc-inversion assumes a constant backscatter profile in height and does not take into account extinction and ground contribution in the signal (Ch. 3.5). The relation only depends on height and Δk_z, and can be inverted from the coherence of a single polarization (Eq. 3-81). Since there are no algebraic solutions for the inverse of the sinc, the height must be determined numerically (e.g. by using a look-up table):

$$h = 2 \cdot \mathrm{sinc}^{-1}(\gamma_{Volume}) / \Delta k_z \qquad \textbf{Eq. 4-3}$$

At first, the inversion was carried out for the coherences directly, setting:

$$\gamma_{Volume} = \gamma \qquad \textbf{Eq. 4-4}$$

The results are presented in Fig. 4-12. The extracted heights vary between 0 and > 60 m whereby heights above 50 m occur more frequently in far range (Fig. 4-12.a). Looking at the validation stands, it can be seen that height gradients often coincide with the stand delineations. The correlation with the ground-measured heights is good (r^2 = 0.71-0.75), but the extracted heights are overestimated by a constant 10-15 m (Fig. 4-12.b). This error can partly be compensated by assuming the coherences to be affected by non-volume decorrelation γ_d (Ch. 3.5.5, Eq. 3-90):

$$\gamma_{Volume} = \gamma / \gamma_d \qquad \textbf{Eq. 4-5}$$

When correcting the coherence by a decorrelation factor of γ_d = 0.90, the regression passes through the origin and the coefficient of determination increases to r^2 = 0.82-0.84 (Fig. 4-13.b). Because the decorrelation factor affects low heights stronger than tall ones (Ch. 3.5.5), only the overestimation of the low heights is compensated (increase in blue areas in Fig. 4-13.a); the tall heights remain too high. For the tall heights, either a stronger decorrelation factor has to be assumed, or a significant ground contribution (compare Fig. 3-19, curve L-2). It can be observed that the occurrence of the highest heights is not random but patch-like. This means that stronger decorrelation or ground contribution differs locally.

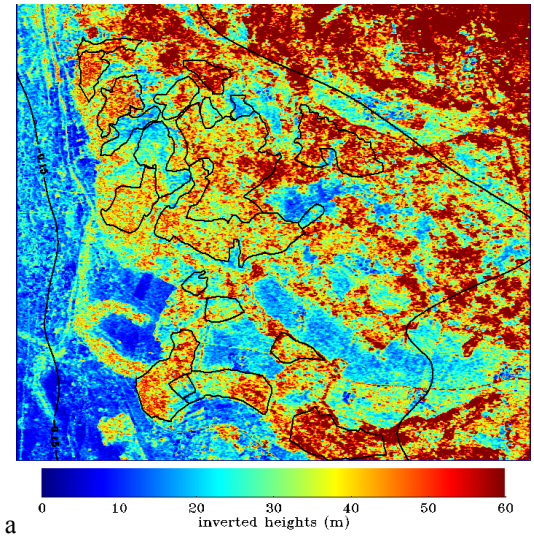

a

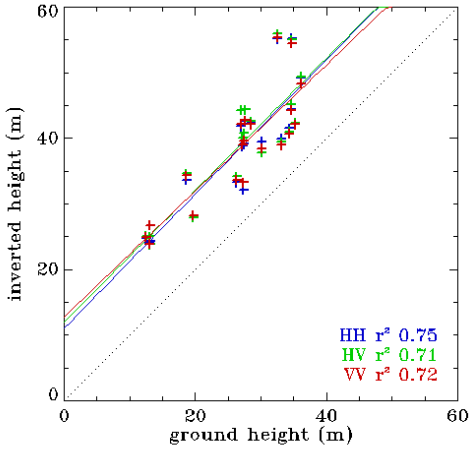

b

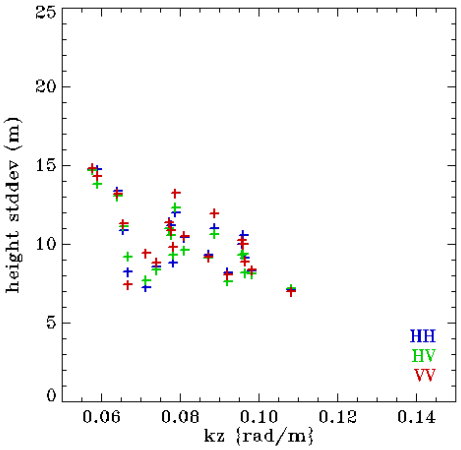

c

Fig. 4-12 Sinc-height inversion without decorrelation factor

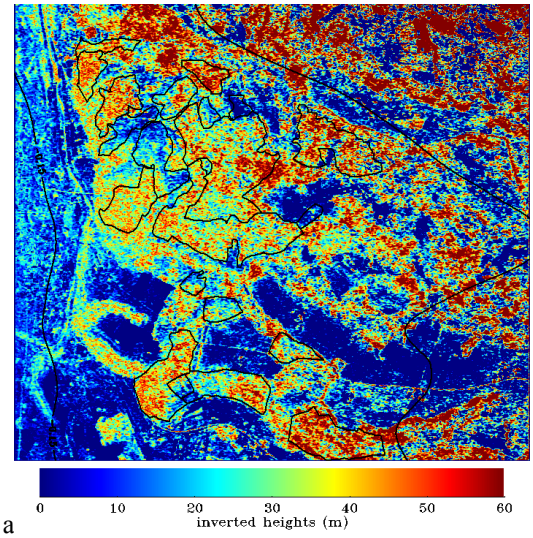

a

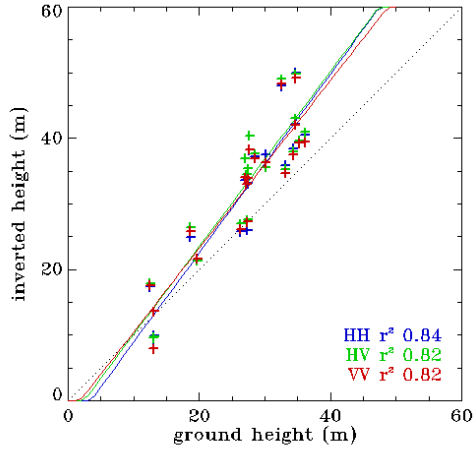

b

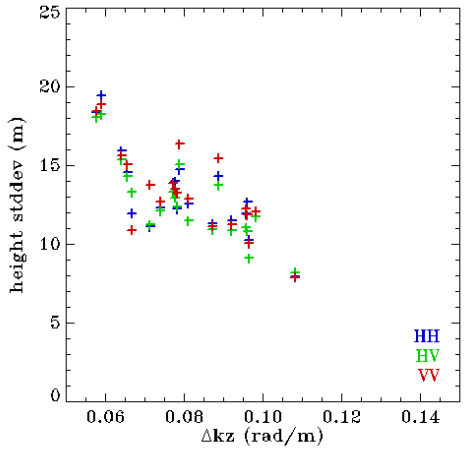

c

Fig. 4-13 Sinc-height inversion with decorrelation factor $\gamma_d = 0.9$

(a) inverted height image of the test site Traunstein, (b) inverted heights vs. ground heights, (c) standard deviation of inverted heights.

This ground-bias can (at least partly) be resolved from the full RVoG-inversion by choosing the polarization of the minimum ground contribution as γ_{Volume} (Ch. 3.5.3).

According to Tab. 3-2, a decorrelation factor of $\gamma_d = 0.90$ can be marginally reached by the range and system decorrelation. It is likely, that also temporal decorrelation is present. But in contrast to the range and system decorrelation, temporal processes are less predictable in time and space. An average decorrelation factor may therefore lead to over-compensation in some areas and still be too low for others.

The standard deviation of the extracted heights lies between 7 m and 15 m for the uncorrected heights (Fig. 4-12.c). It increases clearly with a decreasing Δkz, which is a direct consequence from the k_z-sensitivity. The standard deviation of the corrected heights lies between 7 m and 20 m, higher than for the uncorrected ones (Fig. 4-13.c). This phenomenon results from the multiplication with the decorrelation factor. Statistically, the standard deviation is important in the sense that it defines the minimum area of averaging that is needed for a certain accuracy.

Interestingly, the average coherences and hence the inverted heights do not clearly differ between the polarizations (Fig. 4-11.b, Fig. 4-12.b, Fig. 4-13.b). According to the RVoG, this indicates that the contribution of the ground is in average more or less equal in all polarizations. Then, also the average height of the scattering centre must be equal. This question is addressed in the RVoG-inversion in the next chapter, Ch. 4.2.4.

4.2.4 Height inversion with the RVoG

As explained in Ch. 3.5.1, the sinc-inversion is based on the assumption of a constant backscatter profile in height without extinction and ground (Fig. 3-16, Fig. 3-17). The good performance already indicates that both effects do not strongly alter the average coherence-height relation. But it was also noted that the overestimation of the tall heights might be due to ground contribution.

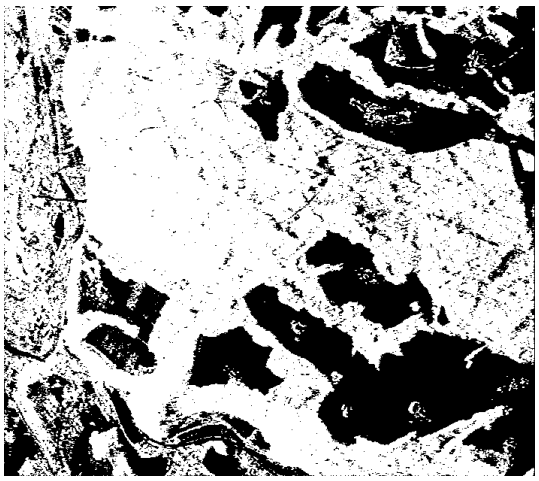

Fig. 4-14 HV-amplitude mask

Areas with low HV-response were masked choosing an intensity limit of σ > -18.5 dB (masked areas in black).

The (full) Random-Volume-over-Ground model (RVoG) separates ground and volume and can be resolved from interferometric coherences at different polarizations (Pol-InSAR) as explained in Ch. 3.5.3. The inclusion of the phase information provides a deeper understanding of the interaction of the radar wave with forest structure, and eliminates the ground-bias in the volume-decorrelation. On the other hand, the inversion methodology is more complex than the sinc-inversion, and it must be tried to minimize possible error sources.

The inversion procedure that was applied here, is outlined in Ch. 3.4.4. The steps are validated separately, and possible errors are discussed along the way. The decorrelation

factor of $\gamma_d = 0.90$ which was used for the sinc-inversion was also applied here, before the ground extraction. This means that decorrelation is assumed to equally affect ground and volume (system and range decorrelation).

In many steps, an HV-amplitude mask has been laid over the image. Typically, wave depolarisation required for the HV-response is small over surfaces, and therefore mainly surface areas are masked. The mask is shown in Fig. 4-14. The limit for the mask was set to intensity limit of $\sigma > -18.5$ dB.

The individual steps can be followed in the inversion examples in Fig. 4-15. After the correction of the coherences with the decorrelation factor (Eq. 4-5), the inner dotted circle represents the reference boundary of the unit circle where $\gamma_{Volume} = 1$.

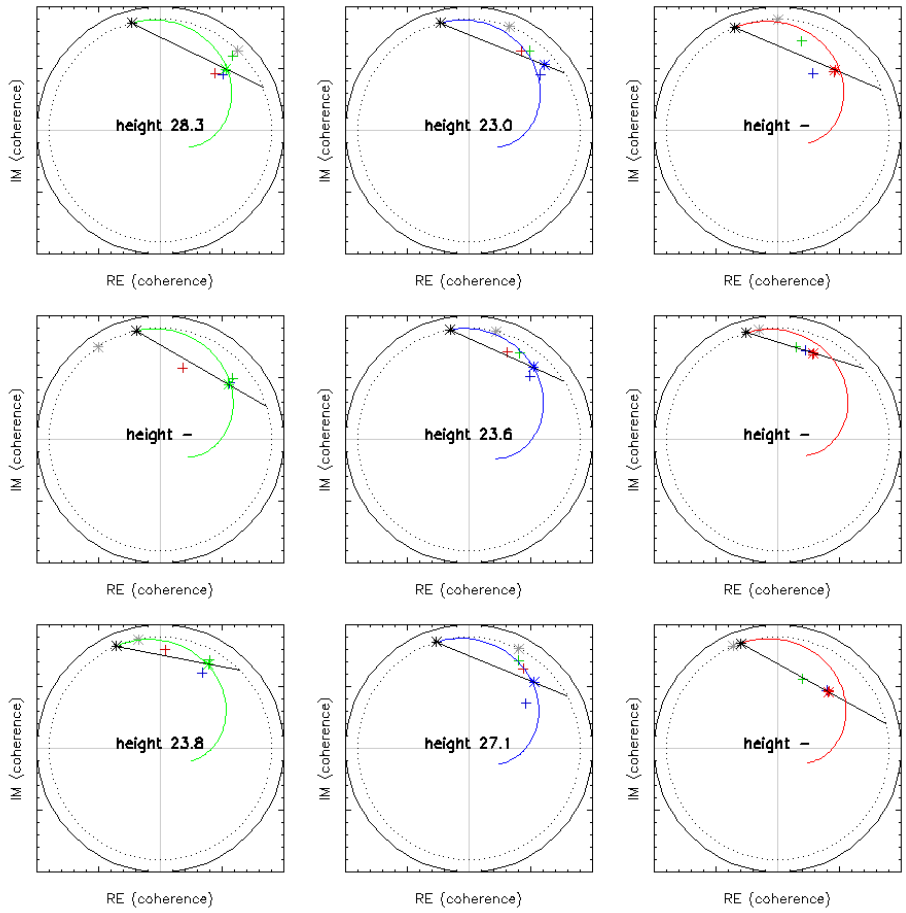

Fig. 4-15 Examples of the RVoG inversion

(black star) smoothed ground, (grey star) unsmoothed ground, (red cross) HH-coherence, (green cross) HV-coherence, (blue cross) VV-coherence, (red/ green/ blue star) volume-only coherence γ_{volume} corresponding in color of HH, HV or VV coherence, (dotted circle) assumed non-volumetric decorrelation (0.90), (black line) line fitted through the ground and volume-only coherence γ_{volume}, (red/ green/ blue curve) sinc-solution as the lower boundary for the inversion space.

The examples were taken from a neighbourhood of 11x11 pixel about the centre coordinate [552; 2440] (inside stand 15, height = 28.4 m). It can be noted that the smooth of the ground phase reduces the ground phase variance (black vs. grey stars). The RVoG only delivers heights where the volume-only coherence γ_{volume} lies between the sinc and the unit-circle boundary.

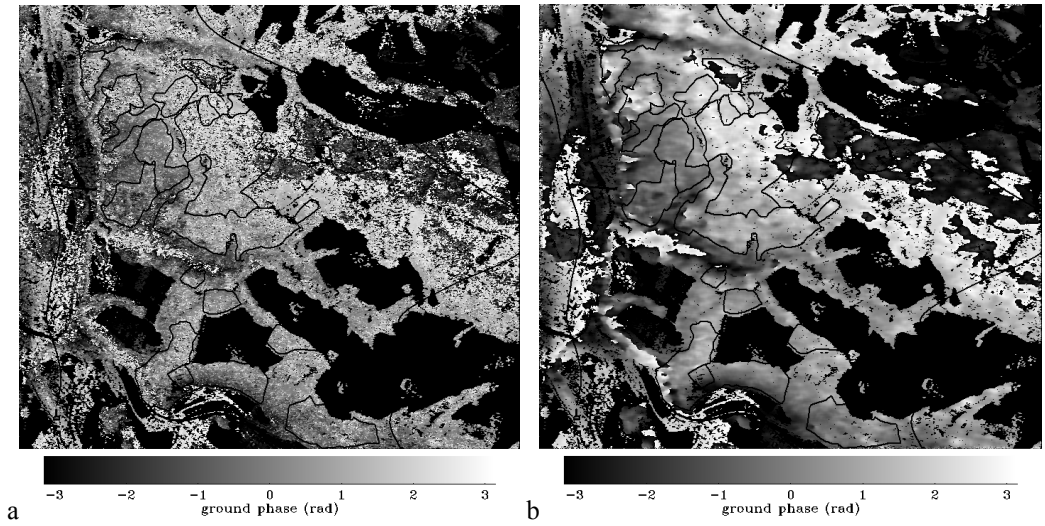

Fig. 4-16 Ground extraction: (a) unsmoothed, and (b) smoothed ground phase (box 21x21)

Step 1 – Line fitting: According to the RVoG, the interferometric coherences in different polarizations form a line in the unit circle. Consequently, the first step of the 3-stage inversion is the fitting of the line through the coherences in the unit circle. The certainty of the line fitting depends on the separation of the coherences, which in turn depends on how strong the ground contributions differ. Since only the three lexicographic coherences (HH, VV, HV = VH) were used as an input, and no coherence optimisation was carried out (Ch. 3.4.4), the reduced certainty of the line fitting was tried to be compensated by the ground smooth in Step 2.

The line fitting can only be validated from the consecutive steps and will be discussed with the ground extraction in Step 2. The examples of the line-fittings in Fig. 4-15 are already corrected with the ground smooth from Step 2. The ground of the original line fitting is indicated by the grey asterisk.

Step 2 – Ground extraction: The two intersections of the fitted line with the unit circle are the two possible ground phase solutions. The decision between the two phases was based only on the phase criterion (Fig. 3-22). As will be shown later, the polarization criterion is much more uncertain (γ_{volume} extraction).

As already mentioned above, a possible way to reduce errors in the fitted line or erroneous ground-phase decisions is to low-pass filter the ground phase ('smooth'). In the next processing steps therefore both the original phase and a smoothed phase (21 x 21 window) were considered. They are subsequently referred to as 'unsmoothed' and 'smoothed'. Both ground phases are shown in Fig. 4-16, overlaid with the HV mask.

The effect of the ground smooth can be seen in the examples in Fig. 4-15. The coherences do not always form a straight line and the ground phase of the optimum fitting line (grey asterisk) is variable even within the small neighbourhood of 11x11 pixels of the 9 plots. The application of the smooth (black asterisk) reduces the phase variance and, hence, may be a useful tool to reduce uncertainties of the individual line-fittings. The discussion of pros and cons of the smoothed ground phase will continue in the validation of the γ_{volume} extraction and the height determination.

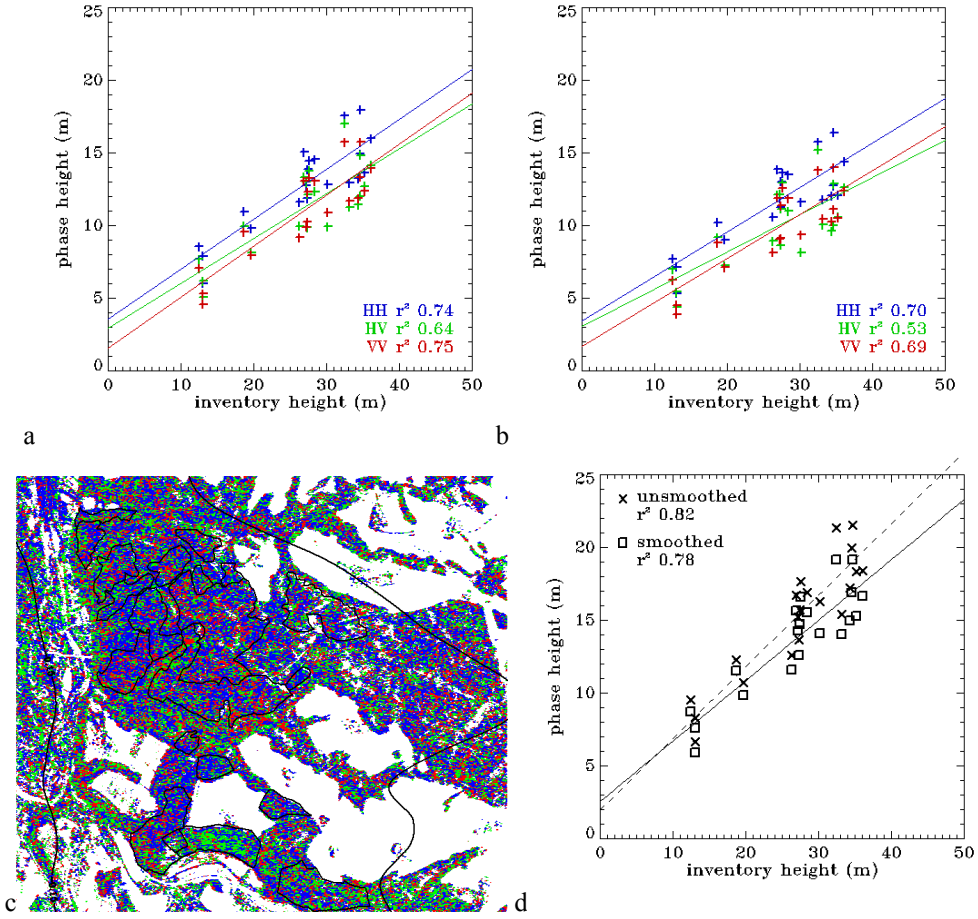

Fig. 4-17 Volume coherence γ_{Volume} –phase and polarization

(a) γ_{Volume} of the smoothed and unsmoothed inversion, (b) individual polarizations, unsmoothed inversion. (c) individual polarizations, smoothed inversion (blue) = HH, (green) = HV, (red) = VV.

Step 3.a – γ_{Volume} extraction: γ_{volume}, the volume coherence, is the coherence that is assumed to possess no ground contribution (m = 0). It is chosen as the coherence that is most distant from the ground phase (see Fig. 4-15). It is the basis for the height extraction in the next Step 3.b. This section will focus on the phase of γ_{Volume} after subtraction of the ground phase. This 'un-biased' volume phase, i.e. without ground, is related to the height of the scattering centre h_{phase} through Δk_z:

$$h_{phase} = (\varphi_{volume} - \varphi_{ground}) / \Delta k_z \qquad \textbf{Eq. 4-6}$$

Fig. 4-17.a/b illustrates the average phase centre of the HH-, HV- and VV-polarization for the 20 validation stands, Fig. 4-17.c the polarization of the chosen γ_{Volume}, and finally Fig. 4-17.d the average phase of γ_{Volume} for the stands. Three observations shall be discussed in detail:

1. The heights corresponding to the average phase centres of the polarizations (Fig. 4-17.a/b) range roughly from ~6.5-14 m (smoothed lower than unsmoothed) for inventory heights from 13-35 m. This corresponds to a relative decrease of the scattering centre from low to tall forest heights (from 50% to 40% of the height). If the phase centre is determined correctly, then two interpretations are possible: low stands

possess a higher extinction (denser) or less ground contribution (e.g. less trunk-ground interaction) than the tall stands. However, it is also possible that the ground phase is biased, e.g. underestimated for low stands (see below).

2. Both unsmoothed and smoothed ground extraction assign the HH-polarization a 2-5 m higher phase centre in the HH-polarization than in the HV- and VV-polarization (Fig. 4-17.a/b). Hence, in Fig. 4-17.c most of the forest area is dominated by the blue of the HH-coherence. The HV-coherence, which was expected to represent most of the volume coherences, becomes only important in the forest area in the lower part of the image. The VV-coherence occurs only in small patches.

   From the RVoG perspective, the volume coherence has the lowest ground contribution. This would mean that HV and VV possess more ground contribution than HH which contradicts the physical interpretation (compare Ch. 3.2). The second option is that HH is stronger extincted in the canopy, e.g. through the horizontal orientation of spruce branches. This would make the volume polarization dependent and introduce an error in the RVoG height extraction. Such OVoG cases ('Oriented' Volume over Ground) are currently applied to Pol-InSAR signatures of crops (Hajnsek and Cloude 2004).

   It shall be noted that the stand where HV dominates the volume coherence is a broadleaf stand. Taking a closer look, it appears that the broadleaf stands in the ravines and slopes are generally characterized by a higher fraction of HV-volume coherence, than the coniferous stands where HH dominates.

3. The height corresponding to the phase of γ_{Volume} should be located between the half forest height and the canopy top depending on the extinction. No ground contribution should drag the phase centre into the direction of the ground. As (Fig. 4-17.d) shows, the average heights of the scattering centres from γ_{Volume} are much higher than the individual polarizations. Again, the low heights seem to possess more extinction because the relative height of the scattering centres is higher than for the tall heights. The fact, that for some tall heights, the height of the scattering centres is less than half the forest height indicates residual ground contribution in γ_{Volume} or a bias in the estimation of the ground phase.

The difference between the inversion from an unsmoothed and smoothed ground phase becomes most obvious in Fig. 4-18. It shows the distribution of γ_{Volume} (complex) of two validation stands in the unit circle (for all stands in Annex 7.3). The following indications favour the smooth of the ground phase for the determination of the ground:

- γ_{Volume} from the unsmoothed ground is cut at 180° (Fig. 4-18.a/b) due to the phase criterion in the ground extraction (Ch. 3.4.4, Fig. 3-22).
- Some volume coherences from the unsmoothed ground extraction possess a high coherence and high phase (= height) at the same time (Fig. 4-18.a/b). This may indicate a high extinction, but may as well result from an erroneous ground extraction.
- Assuming a normal distribution of the forest height and its extinction properties, also the γ_{Volume} phase should be normal-distributed like for the smoothed ground extraction (Fig. 4-18.e/f).

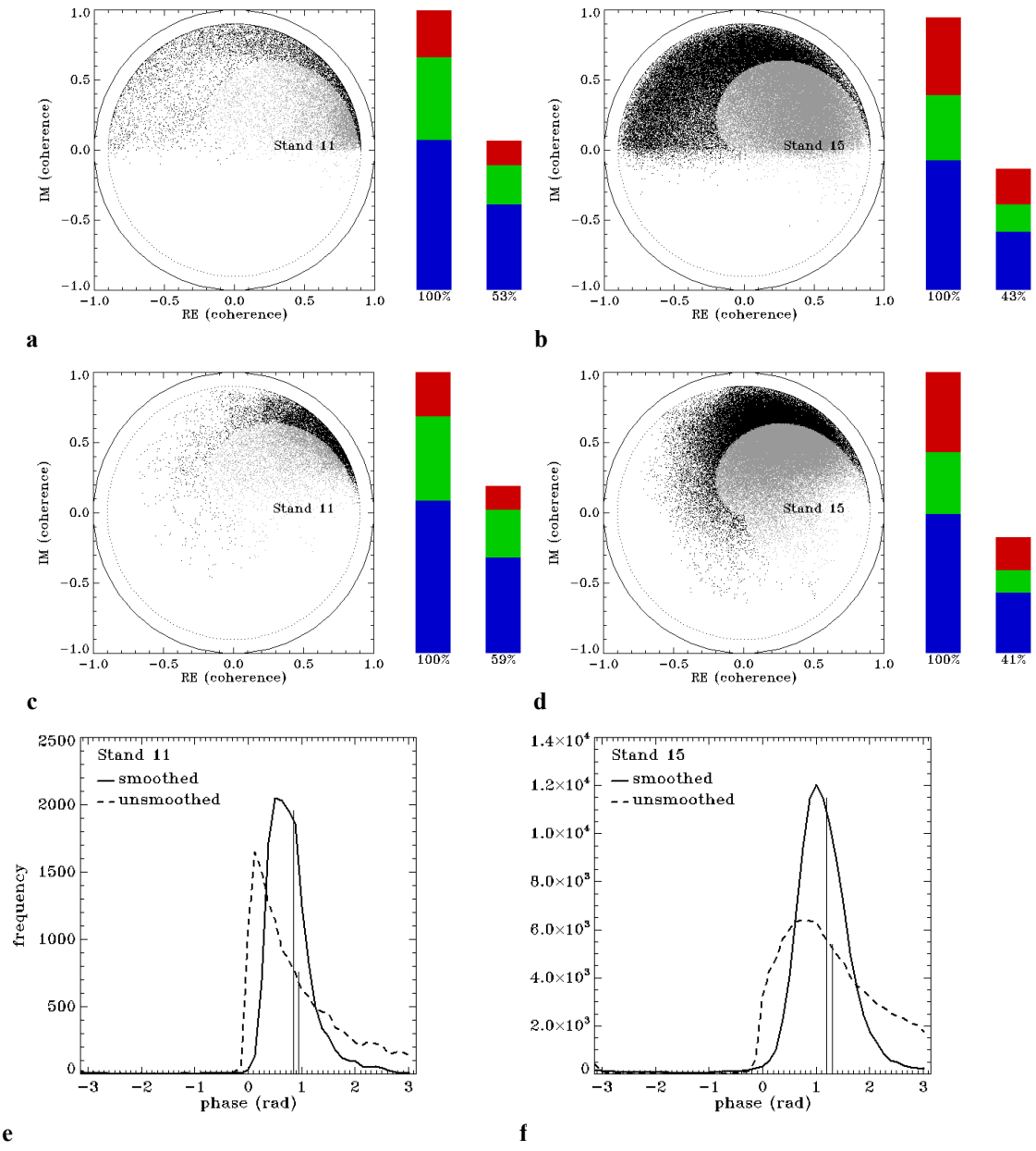

Fig. 4-18 γ_{Volume}-distribution stand 11 and stand 15

γ_{Volume}-distribution (after ground phase subtraction): (a) unsmoothed inversion, (b) smoothed inversion, (c) phase distribution. (black) invertable γ_{volume}, (grey) not-invertable γ_{volume}, (solid line) average phase, (dotted line) assumed decorrelation factor γ_d=0.9, (left bar) polarization for all γ_{volume}, (right bar) polarization for invertable γ_{volume} (HH=blue, HV=green, VV=red)

Remembering that the ground smooth was introduced to compensate a reduced certainty from a line fitting through only three coherences, it is also recommended to analyse improvements from a line-fitting through more polarizations. Also, the ground extraction should be compared to a ground phase determined from topographic information sources. This step would be extremely important in order to detect systematic biases in the ground extraction like resulting from the presence of orientation effects.

Step 3.b – Height inversion: After the subtraction of the ground phase, each determined γ_{Volume} is assigned the height and extinction corresponding to its location in the inversion space (Fig. 3-23.a). In Ch. 3.4.4, the inversion space was defined as the space between the sinc-curve (extinction $\alpha = 0$) and the unit circle (extinction $\alpha = \infty$). The non-invertable coherences were proposed to be inverted with one of three possible assumptions: (1) residual m (Fig. 3-23.b), (2) temporal decorrelation (Fig. 3-23.c), or (3) model invalidity (Fig. 3-23.d). In Fig. 4-18 where the volume-only coherences were plotted for two validation stands, the solutions that lie within the inversion space are marked black, the ones outside grey. The box-plot next to the graph shows that only about 40-60% of volume-only coherences are invertable. The remaining coherences must be inverted with one of the mentioned assumptions.

Fig. 4-19.a and Fig. 4-20.a illustrate the result from the heights only of the invertable coherences, for both the unsmoothed and smoothed ground phase. In Fig. 4-19.b/c and Fig. 4-20.b/c, the inverted heights were validated at the validation stand level. In Fig. 4-19.c/d, the height extraction from the unsmoothed inversion correlates with the inventory height with an $r^2 = 0.82$. The height extraction from the smooth ground correlates with an $r^2 = 0.83$. Both inversion heights fit the inventory heights with a tendency to overestimate the tall heights. The standard deviation of the RVoG-inverted heights lies around 5 m-15 m and decreases with increasing Δk_z (Fig. 4-19.c, Fig. 4-20.c). The height standard deviation is lower for the RVoG inversion than for the sinc-inversion which results from the exclusion of many low coherences which return high heights in the sinc-inversion. The Δk_z-trend is less obvious in the smoothed inversion procedure.

In Fig. 4-21, the non-invertable volume coherences were inverted with either of the three assumptions described above and integrated in the invertable coherences (only for smoothed ground phase). The effect is predictable from Fig. 3-23.b-d and can be summarized as follows:

- Fig. 4-21.a/b: the assumption of residual ground inversion increases especially the low heights.
- Fig. 4-21.c/d: the assumption of temporal decorrelation reduces especially the tall heights.
- Fig. 4-21.e/f: the assumption of model-invalidity (substitution with sinc) increases all heights.

Since both the residual ground-method and the sinc lead to further overestimations, it seems to be recommendable to assume temporal decorrelation and utilize the phase information of not-invertable coherences.

4.2.5 Summary and conclusions

The task of Ch. 4.2 was the implementation and validation of a forest height extraction from Pol-InSAR data of the test site Traunstein. The height inversion was employed for a uniform backscatter profile in height (sinc-function), and for the (full) RVoG, which also accounts for extinction and ground contribution. It was validated against the upper canopy height of 20 validation stands, derived from forest inventory data. A decorrela-

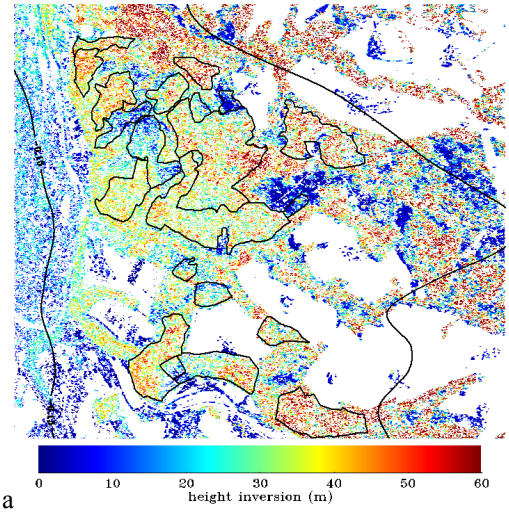

a

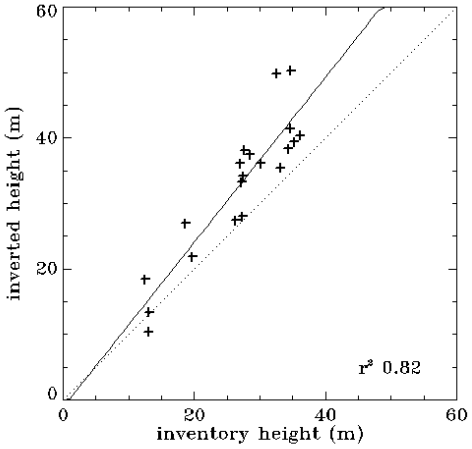

b

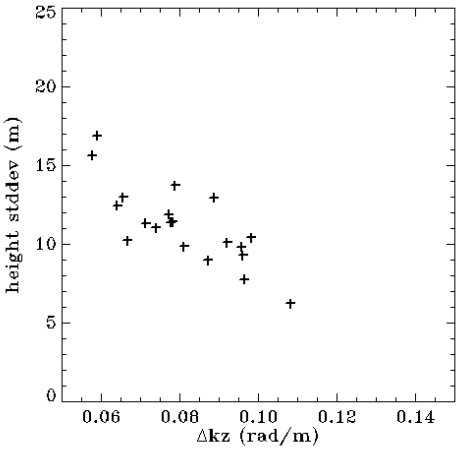

c

Fig. 4-19 Height inversion of invertable volume coherence from unsmoothed phase

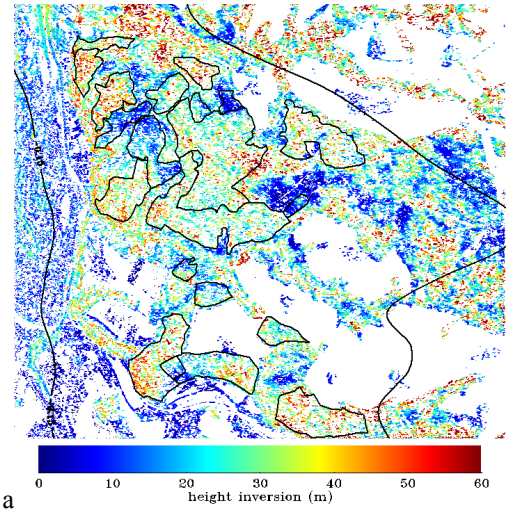

a

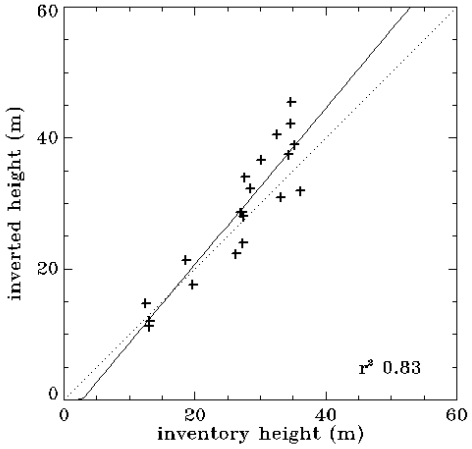

b

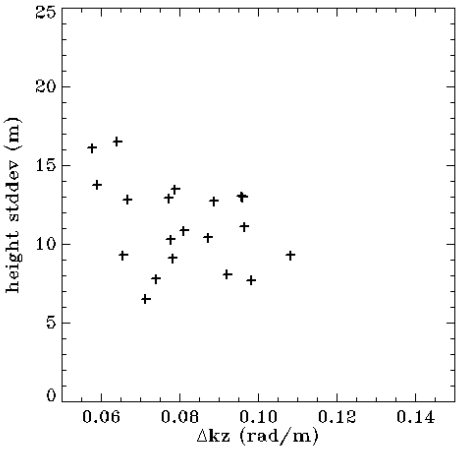

c

Fig. 4-20 Height inversion of invertable volume coherence from smoothed phase

(a) height map, (b) extracted heights vs. inventory heights, (c) height standard deviation vs. Δk_z

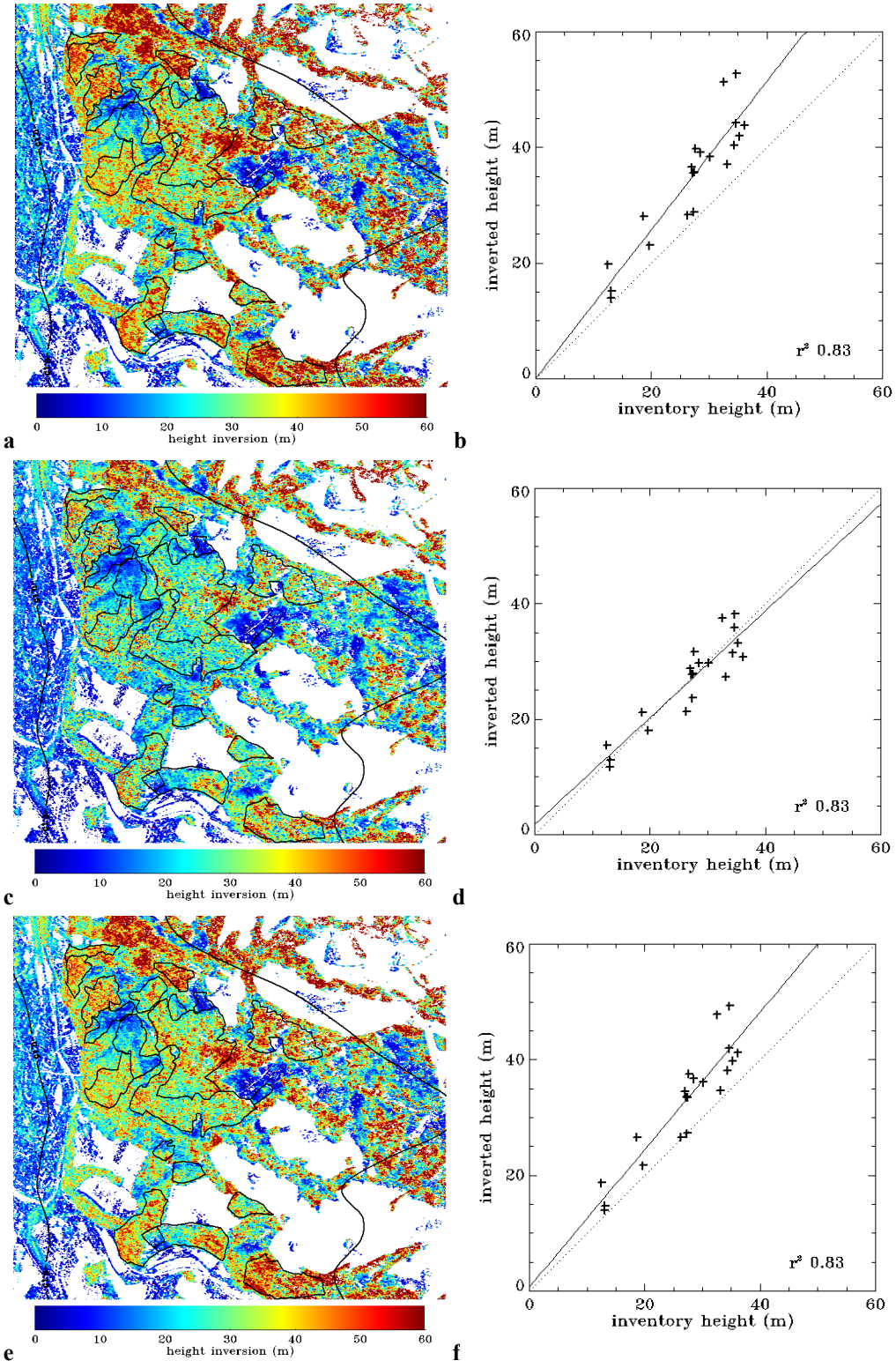

Fig. 4-21 Height determination including non-invertable volume coherences

Substitution assuming (a/b) residual m, (c/d) temporal decorrelation, and (e/f) model-invalidity (substitution with sinc).

tion factor of $\gamma_d = 0.9$ was empirically determined from the sinc-inversion, and subsequently applied also to the RVoG inversion.

The sinc-inversion proved already good results ($r^2 = 0.82$-0.84). The decorrelation factor of $\gamma_d = 0.9$ compensated mainly the overestimation of low heights, but tall heights were still overestimated. The average coherences and the inverted heights did not clearly differ between the polarizations. The results left two questions open:

- Is the overestimation of tall heights due to a higher decorrelation and/ or a ground bias in the coherence?
- Are the (average) ground contributions equal in all polarizations?

The RVoG inversion from interferometric coherences at different polarization allows addressing the two questions. The inversion separates ground and volume through different ground contributions in the polarizations, and thereby the phase provides an additional information source. Since only the three lexicographic coherences were used for the inversion, a phase smooth was implemented in order to compensate uncertainties in the fitted line and ground phase selection.

The results retrieved from the RVoG inversion proved an accuracy in the same order as the sinc-inversion ($r^2 = 0.82$-0.83). The ground smooth seemed to avoid errors in the ground decision and was recommended. The HH-polarization dominated the volume coherence, which is used for the height extraction. Approximately 40-60% of all volume coherences could be inverted. For the non-invertable coherences, residual ground contribution, temporal decorrelation or model invalidity (substitution with sinc) was assumed. The inversions with residual ground contribution and sinc-substitution resulted in an overestimation of tall heights similar to the pure sinc-inversion. Only the assumption of temporal decorrelation, which utilized the phase information, avoided the height-overestimation.

Addressing the two questions above, the RVoG inversion allows cautiously the following conclusions:

- Both ground and uncompensated decorrelation seems to be responsible for the overestimation of tall heights. The average phase centres of the individual polarizations indicate that ground is not negligible and is also present in many of the extracted volume coherences. But the results assuming temporal decorrelation suggest that also many volume coherences are not ‘pure’, being affected by a higher decorrelation than the assumed $\gamma_d = 0.9$.
- The differences between the phases of the individual polarizations deny a similar ground contribution in all polarizations. Yet, it was questioned whether the differences might partly be due to polarization sensitivity of the volume.

From the presented results, it is clear that the utilization of polarimetric interferometric data allows a deeper understanding of the interaction of the radar wave with the forest structure. Although the presented implementation of the RVoG-inversion did (of course) not fully resolve the complex scattering behaviour of the forest, some important aspects can be summarized:

- Most critical is the unknown influence of decorrelation. When interpreting coherence as pure volume decorrelation, any other decorrelation source leads to a height overestimation. Range decorrelation and system decorrelation could

only partly account for the assumed decorrelation of $\gamma_d = 0.9$. This leaves temporal decorrelation as the great unknown. The main problem of the average decorrelation factor is the spatial variation of decorrelation. It was already reasoned in Kugler (2003) that temporal decorrelation occurs rather patch-like than randomly.

- Ground has a non-negligible contribution in forest backscatter at L-band. The influence did (in average) not lead to a strong deviation from the sinc-like coherence-height relationship, but may vary under different incidence angles and topography.
- Extinction did not lead to a coherence saturation with height. This is a critical condition for an unsaturated height inversion of tall and dense forests. Ground backscatter must be present for the Pol-InSAR inversion in order to obtain the line in the unit circle.
- The fact that the phase centre of the HH-polarization was higher than the one of the VV and HV polarization was interpreted to be due to different ground contributions. Since, typically, both direct ground backscatter and dihedral ground-trunk backscatter should be stronger in HH than in HV, it was suggested that orientation effects might be present in the forest, e.g. due to the horizontal branching of Norway spruce. It is recommended to analyse other test sites and species in this respect.
- One aspect that was only marginally addressed in the validation is the standard deviation of the extracted heights. Due to the Δk_z-sensitivity of the height inversion, an interferometric configuration with a Δk_z close to the Δk_z for the needed ambiguity height is desirable (Ch. 3.5.5).

4.3 Biomass estimation from Pol-InSAR forest heights

The last step in the processing chain is the biomass estimation. This is done by applying the concept of allometric reference function and allometric level from Ch. 2.4.3 (Ch. 2.6) on the heights extracted from Pol-InSAR data from Ch. 4.2. In Ch. 4.3.1, the biomass estimation was carried out for the sinc-inversion of the HH-polarization, and the smoothed RVoG-inversions. Since the errors from the height-biomass allometry and the height inversion propagate in the biomass estimation, no separate conclusion chapter has been included in this subchapter. However, Ch. 4.3.2 presents some initial results and consideration about a direct biomass determination from a combination of sinc and height-biomass allometry.

4.3.1 Biomass estimation from height-biomass allometry

The heights from the Pol-InSAR height inversion were converted to biomass by applying the reference function (Eq. 2-17) and the allometric level (Eq. 2-18) of $l_a = 0.925$ that was determined from the Traunstein inventory data (Ch. 4.1.4), so that the final height-biomass relation results as (B = biomass, h = height):

$$B = 0.925 \cdot 1.66 \cdot h^{1.58} \qquad \textbf{Eq. 4-7}$$

The biomass conversion was carried out for the heights obtained from the sinc-inversion (Fig. 4-22, HH-polarization, $\gamma_d = 0.9$; compare Fig. 4-13), and the smoothed RVoG inversion (Fig. 4-23, Fig. 4-24; compare Fig. 4-20, Fig. 4-21). Since differences between the height inversions propagate in the biomass estimation, the results shall not be discussed for the differences between the inversions, but in terms of general observations.

The biomass-maps in Fig. 4-22 - 24 essentially follow the height maps in Fig. 4-13, Fig. 4-20 and Fig. 4-21, respectively. The relation is not linear, because due to the allometric exponent the biomass scale is stretched for lower biomass values compared to the height scale. Corresponding to the extracted heights above 50 m, frequently biomass values above 800 t ha^{-1} are determined, especially in far range. This was reasoned to result both from ground contribution and local temporal decorrelation (Ch. 4.2.5), the latter scaled by the Δk_z-sensitivity in range (Ch. 3.5.5).

The validation of the estimated biomass in Fig. 4-22, Fig. 4-23 and Fig. 4-24 against the inventory biomass shows a good correlation ($r^2 = 0.70$-0.75) without any saturation. The plotted results reflect both the height inversion and the height-biomass allometry. Three effects shall be discussed more closely:

1. Because the allometric function is not linear, the mean biomass from a height distribution is always higher than the biomass from the mean height. Similar mean heights can therefore possess different mean biomasses.
2. due to the definition of 'usable' biomass the biomass for low heights is apparently overestimated by the reference allometry (compare Fig. 4-7.b). This overestimation of low biomasses results less from an error height inversion than from the definition of biomass.

   The overestimation of tall heights is mainly due to the height overestimation (discussed in Ch. 4.2.5). Corresponding to the height inversions in Fig. 4-13, Fig. 4-20 and Fig. 4-21, the strongest overestimation is present in the RVoG-with residual ground (Fig. 4-21.f), the least in the RVoG with temporal decorrelation (Fig. 4-21.d).

A final analysis is carried out with respect to the biomass error. As demonstrated, the error sometimes lies more on the height and sometimes more on the allometric side. In a general case, the biomass under consideration of height error err_h and allometric error err_{la} resolves as:

$$Biomass = \left(1.66 + err_{la}\right) \cdot \left(height + err_h\right)^{1.58} \qquad \textbf{Eq. 4-8}$$

It is obvious that, due to the allometric exponent, the height error has a greater impact on biomass than a similar (relative) allometric error. However, the error in the height extraction and the allometric error are not necessarily independent. Locally low forest density fall below the average allometric level, but also the height extraction might underestimate an open upper canopy therefore leading to a partial compensation of height and allometric error. This is analysed in Fig. 4-25 for the sinc-results and the smoothed RVoG inversion from the invertable coherences. A regression was calculated between inventory heights and inverted heights (Fig. 4-13 and Fig. 4-19), and the deviation of the extracted heights from this regression was determined. Then, it can be seen whether height errors and allometric errors are dependent on each other. It is obvious from Fig. 4-25, that for the relatively homogeneous validation stands, height error and allometric

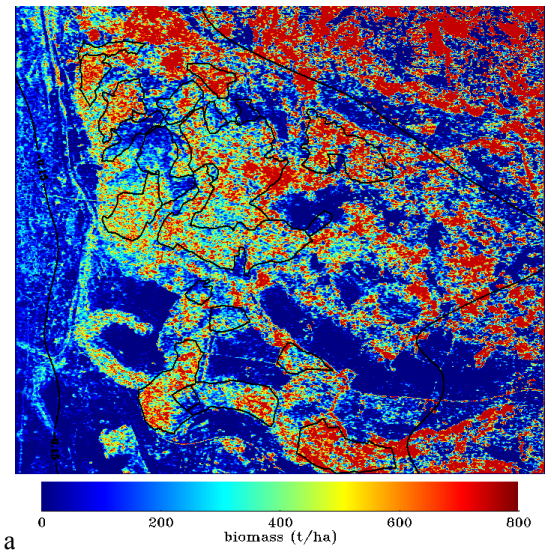

a

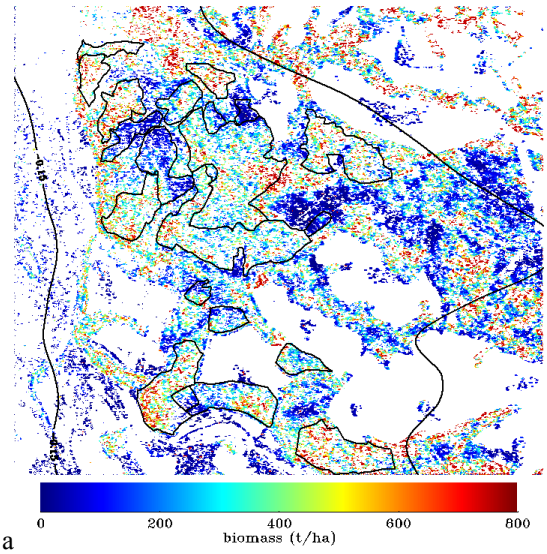

a

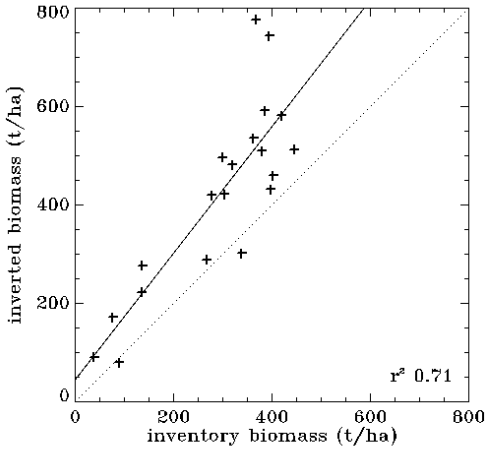

b

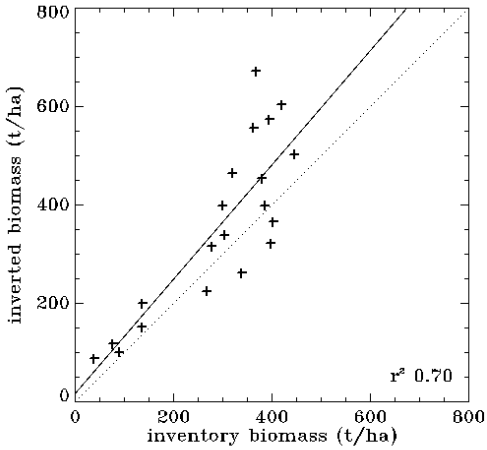

b

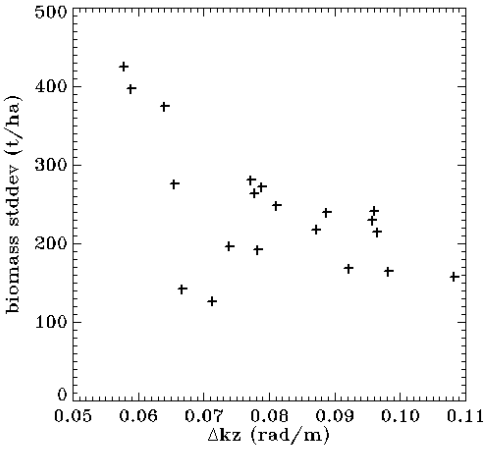

c

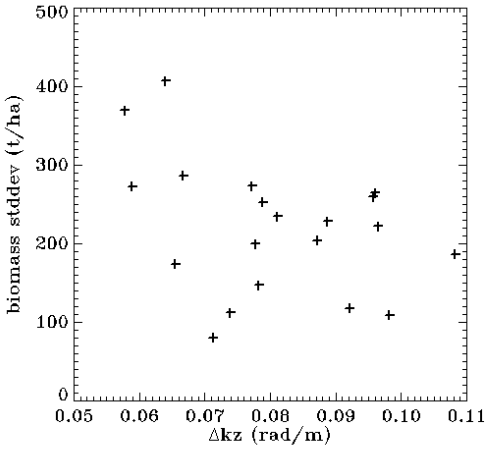

c

Fig. 4-22 Biomass estimation from heights of the sinc inversion with $\gamma_d = 0.9$ (Fig. 4-13)

Fig. 4-23 Biomass estimation from heights of the RVoG inversion of the invertable γ_{Volume} (Fig. 4-20)

(a) biomass map, (b) estimated biomass vs. inventory biomass, (c) biomass standard deviation vs. Δk_z

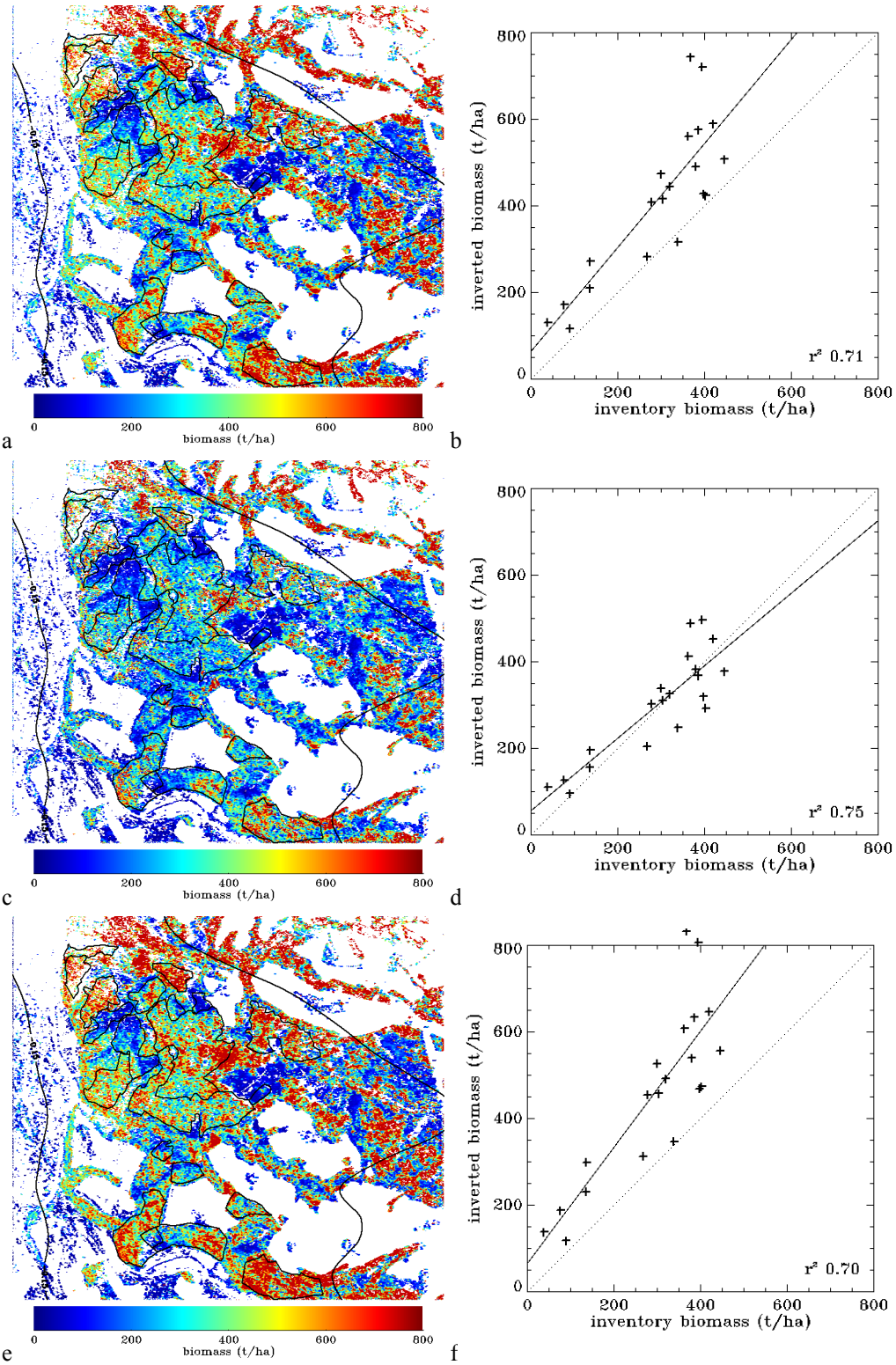

Fig. 4-24 Biomass estimation from RVoG height inversion including non-invertable γ_{Volume}

Substitution assuming (a/b) residual m, (c/d) temporal decorrelation, and (e/f) model-invalidity (substitution with sinc).

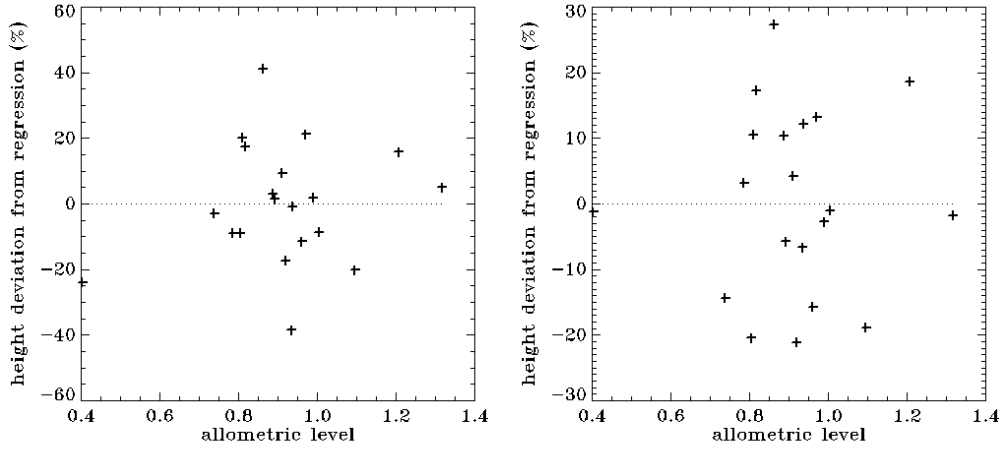

a b

Fig. 4-25 Relation of relative height error to allometric level

(a) for the sinc-inversion, (b) for the RVoG inversion assuming temporal decorrelation for the non-invertable coherences. The height error was calculated relative to a regression between inverted and inventory heights.

level are not related. It must be considered though that only one stand possessed an allometric level below 0.7, a 13 m high stand where the 'usable' biomass is not very representative (stand 6). Therefore, an error dependency cannot be excluded for densities below an allometric level of $l_a = 0.7$.

4.3.2 Direct Biomass estimation from coherence

If coherence can be related to height and height can be related to biomass, the also coherence can be related directly to biomass. This shall be applied and validated for the simplifying case of the sinc-function. Substituting the height biomass reference allometry (Eq. 2-17) into the height of the sinc-function (Eq. 3-81):

$$\begin{aligned}\gamma &= \mathrm{sinc}(½ \cdot \Delta k_z \cdot h) \\ &= \mathrm{sinc}\left(½ \cdot \Delta k_z \cdot (b/1.66)^{1/1.58}\right)\end{aligned} \qquad \textbf{Eq. 4-9}$$

An example for the coherence-biomass relation is plotted in Fig. 4-26.a for a Δk_z=0.125. As can be seen, the resulting relation between biomass and coherence is almost linear.

The ambiguity height h_{amb} (Eq. 3-76) can be substituted with the corresponding ambiguity biomass B_{amb} and returns the intercept with the x-axis (the intercept with the y-axis is at a coherence of 1):

$$\begin{aligned}h_{amb} &= 2\pi / \Delta k_z \\ B_{amb} &= 1.66 \cdot (2\pi / \Delta k_z)^{1.58}\end{aligned} \qquad \textbf{Eq. 4-10}$$

The x- and y-intercept may be altered through the allometric level l_a, and the presence of non-volume decorrelation γ_d respectively. Eq. 4-11 to 4-13 show how the linear function can be calculated with respect to γ_d and allometric level l_a. It can be seen that Δk_z is weighted by the allometric exponent and the slope is scaled by the allometric level l_a. a_0 and a_1 define the y-intercept and slope of the line:

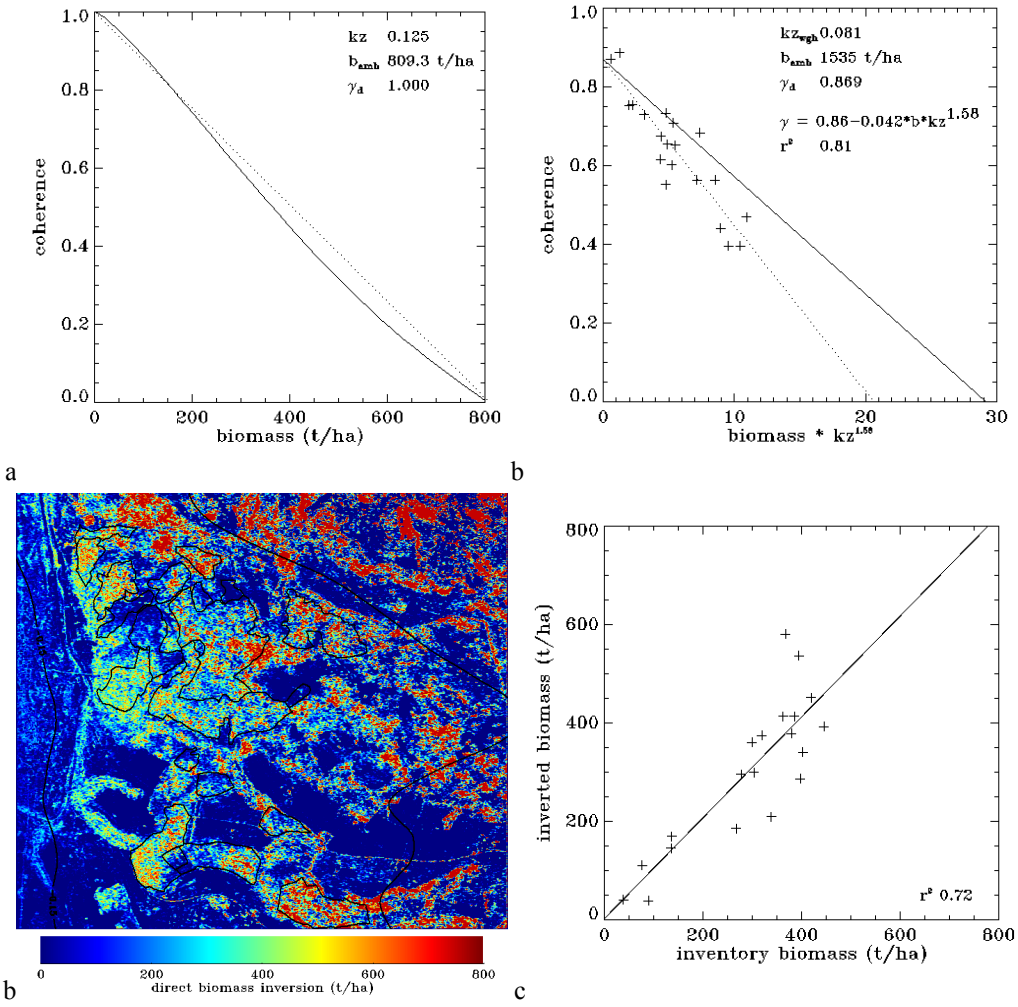

Fig. 4-26 Direct biomass inversion from the HH-coherence of the Traunstein scene

Biomass was estimated by combining the sinc-relation between coherence and height and allometric relation between height and biomass. (a) biomass-height relation for $\Delta k_z = 0.125$, (b) coherence-biomass relation; biomass multiplied by $\Delta k_z^{1.58}$ (Eq. 4-13). The linear regression reflects both the height bias in the sinc-inversion (Fig. 4-13.d) and the allometric level (Fig. 4-7.b); (c) biomass map derived from the regression in (b). (d) inverted biomass vs. inventory biomass.

$$\gamma = a_0 + a_1 \cdot B \qquad \textbf{Eq. 4-11}$$

$$\begin{aligned} a_0 &= \gamma_d \\ a_1 &= \gamma_d / B_{amb} \\ &= \gamma_d / \left(l_a \cdot 1.66 \cdot (2\pi / \Delta k_z)^{1.58} \right) \end{aligned} \qquad \textbf{Eq. 4-12}$$

$$\begin{aligned} &\gamma = \gamma_d + a_1^* \cdot \Delta kz^{1.58} \cdot B \\ &\text{with} \quad a_1^* = \gamma_d / \left(l_a \cdot 1.66 \cdot (2\pi)^{1.58} \right) \end{aligned} \qquad \textbf{Eq. 4-13}$$

The algorithm has been applied to the HH-coherences of the Traunstein data. The original coherence-height inversion with the sinc is displayed in Fig. 4-13.b. Now, Fig. 4-25.b displays the coherence-biomass multiplied by $\Delta k_z^{1.58}$ according to Eq. 4-15. The linear function that is expected from the allometric reference function and the average

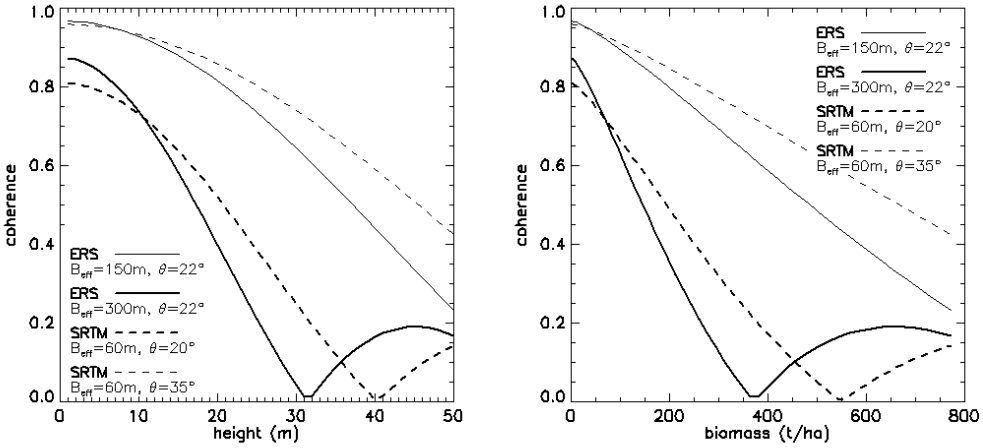

a b

Fig. 4-27 (a) Coherence-height and (b) coherence-biomass relation for interferometric satellite configurations of ERS-1/2 tandem mission and SRTM C-band

Tab. 4-2 Range decorrelation, ambiguity height and ambiguity biomass for 2 sample baselines of the ERS-1/2 tandem and 2 sample look angles of the SRTM C-band

System	Wave-length	Band-width	Flight alti-tude	Look an-gle	Base-line	Range decorrela-tion γ_{range}*	Δkz	Ambigu-ity height	Ambiguity biomass **
ERS	C-band 5.7 cm	15.6 MHz	780 km	23°	100m	0.997	0.066	94.4 m	$l_a \cdot 2092\ t\ ha^{-1}$
ERS	C-band 5.7 cm	15.6 MHz	780 km	23°	200m	0.988	0.133	47.2 m	$l_a \cdot 704\ t\ ha^{-1}$
SRTM	C-band 5.7 cm	10 MHz	233 km	15°	60m	0.970	0.212	29.7 m	$l_a \cdot 340\ t\ ha^{-1}$
SRTM	C-band 5.7 cm	10 MHz	233 km	55°	60m	0.970	0.040	158.1 m	$l_a \cdot 4702\ t\ ha^{-1}$

* Hamming weighting approximated with sinc-function (Eq. 3-72)

** l_a = allometric level

$\Delta k_z^{1.58}$ is sketched by the solid line, the actual linear regression by the dotted line. As the x-intercept shows, the actual ambiguity biomass only reaches 75% of the reference ambiguity biomass. This is not explained from the allometric level alone (92.5%, Fig. 4-7.b), but also reflects the height-overestimation of ~16% from the sinc (Fig. 4-13.d). The regression parameters can be determined from Fig. 4-25.b, the correlation coefficient is high ($r^2 = 0.81$).

Further on, a biomass inversion of the HH-coherence has been carried out with the reference equation from Fig. 4-25.b. The resulting biomass map is shown in Fig. 4-25.c, the validation against the ground measured inventory biomass in Fig. 4-25.d. In contrast to the biomass estimation from the sinc-inverted heights (Fig. 4-13.d), no systematic overestimation can be seen. This is because the regression parameters already account

for the height overestimation of the sinc. The correlation coefficient $r^2 = 0.72$ is in the same order as for the allometric biomass estimation from the sinc-inverted heights.

Basically, the linear coherence-biomass relation is not new. It has been observed empirically when correlating ERS-1/2 Tandem data (C-band 1-days repeat pass) with boreal forest biomass (Koskinen et al. 2001, Santoro et al. 2002, Wagner et al. 2000). The relation was clearest under frozen conditions probably due to a low ground contribution, and low temporal decorrelation.

This interpretation of the coherence-biomass relation makes it possible to calculate the ambiguity biomass for different system configurations. This has been done for two baselines for the ERS-1/2 tandem mission and two look angles for the SRTM C-band interferometry (Fig. 4-26, Tab. 4-2). It can be seen that the highest height sensitivity for ERS acquisitions lies between baselines of 150-300m, for SRTM between 20-35° looking angle. Range decorrelation must be accounted for due to the low bandwidth. Additionally, ERS tandem data are afflicted with a 1-day temporal decorrelation, while the SRTM-data were acquired in single pass mode. Assuming a better penetration of C-band into the forest under frozen conditions, gives the SRTM mission (Feb. 11-22, 2000) a high potential for height and biomass estimations in boreal forest. For the ERS-1/2 tandem mission (1995-1999), tandem pairs in winter already proved a better correlation with biomass (see above).

In summary, the direct biomass inversion used the simple sinc-relation between coherence and height, and the allometric height-biomass relation. It can be approximated with a linear function of which the slope reflects the allometric level and (linear) biases in the height-coherence relation. The results for the Traunstein test site are as precise as the two-step inversion. The regression was derived empirically, and compensated both for a ~16% height-overestimation of the sinc-inversion and the allometric level of ~92%. The potential of ERS-1/2 tandem data and SRTM C-band data was illustrated.

5 Conclusions and Outlook

The task of this work was to develop and validate a forest biomass estimation methodology based on polarimetric interferometric SAR and forest height-biomass allometry. The forest height biomass allometry was developed in Ch. 2, and is applicable to any remote sensing forest height source. Ch. 3 discussed the behaviour of volume decorrelation for a forest modeled as a Random-Volume-over-Ground (RVoG), and the height inversion from Pol-InSAR data. In Ch. 4, both height-biomass allometry and the height-inversion were valiated from the test site Traunstein, on the basis of forest inventory data and airborne fully polarimetric interferometric L-band data.

Now, this chapter will evaluate the observations from the validation in Ch. 4 with respect to the potential of Pol-InSAR for global biomass estimations. Since a detailed summary and discussion of the individual steps was given at the end of each subchapter (Ch. 4.1 and Ch. 4.2), only the key aspects shall be repeated here.

Forest height-biomass allometry: The concept for the use of height biomass allometry to convert remote sensing extracted forest heights to forest biomass was approached from the forest perspective. To summarize the most important aspects:

- Reference height and biomass were defined as upper canopy height and stem biomass. In order to allow flexible inclusion of different standards, it shall be emphasized again to refrain from a too literal definition. Of course, systematic biases due to different standards have to be avoided. Dbh-limits were pointed out to lead to an underestimation of (stem) biomass in regenerating forests.
- A reference height-biomass allometry was derived from even-aged, single-layered managed Norway spruce forests according to the yield tables of Assmann and Franz (1963, average yield). The allometric level was introduced as a linear factor to adjust the height-biomass to different densities. Differences in the allometric level were shown to be species- and thinning-dependent, but the site conditions had a comparably small effect (rule of Eichhorn 1902).
- The validation of the inventory data for Traunstein approved the allometric (power) relation between height and biomass, but showed how important it is to adjust the allometric level to avoid systematic biomass estimation errors.

After all, an unbiased implementation of height biomass allometry is only possible with the availability of allometric level information. As outlined in Ch. 2.6, on a regional scale, an *average* allometric level can be implemented. The relation of the allometric level to physio-environmental factors and knowledge about typical management concepts probably allows to model such allometric-level maps up to some degree. Differences on the local scale, such as selective logging or variations in the species composition, are important for local forest management, and require local density-related information sources. Both the yield tables and the inventory data showed a species-dependence of the allometric level, which might be extracted from other remote sensing sources. Also a measure for the canopy heterogeneity, e.g. from image texture, could be a feasible indicator of the forest density.

A special issue is the handling of heterogeneous forests, i.e. forests with an open or variable canopy. This problem was avoided in the validation through the selection of homogeneous validation stands, but plays an important role for many types of natural forests. The problem is two-sided, both the definition of a representative reference height, and the interpretation of the extracted heights are difficult. As a first step it might make sense to define some sort of a heterogeneity criterion to allow a distinction of different heterogeneity degrees. Of course, also the remote sensing height signature must be understood for such complex height distributions.

Pol-InSAR height inversion: The key to the height inversion is the interpretation of coherence as volume decorrelation. This makes the relation between coherence and height a function of the height distribution of the scatterers. The validation of the height extraction from the Pol-InSAR data was carried out against the upper canopy height as defined from the inventory data. This reference height makes sense since the 'Random Volume' of the RVoG refers to the scattering profile between top and bottom of the forest. The problem of forests with heterogeneous or fragmented canopies was circumvented by the selection of the validation stands. The inversion was carried out separately for the sinc-function, which assumes a uniform scattering profile in height, and the Random-Volume-over-Ground model, which includes also extinction and ground contribution in the signal. Again, the key results shall be highlighted:

- An initial sinc-inversion with the original coherences led to a constant height overestimation. This was assumed to be due to the contribution of non-volume related decorrelation. The successive inversions were carried out with coherences corrected with an average assumed decorrelation of 0.9.

  Such a decorrelation can be marginally reached with system decorrelation contributions, so that also temporal decorrelation must be assumed. It was also explained that an average decorrelation factor smoothes local differences in the decorrelation which leads to height errors.
- After coherence compensation, the regression between extracted heights and inventory heights passed through the origin, but tall heights were overestimated both in the sinc-inversion and the RVoG-inversion. The resolving of the ground phase with the RVoG –inversion helped to understand the problem, and attribute the height overestimation to a combination of residual ground and temporal decorrelation. The only inversion that avoided the height overestimation was the one assuming temporal decorrelation for the non-invertable volume coherences, an approach based on the phase information.
- The problem of temporal decorrelation was addressed as the most serious one, and strongly favors single-pass interferometric configurations where the images are acquired at the same time. Also, since the influence of decorrelation is a question of the baseline configuration (k_z-sensitivity), it must be recommended to choose the baseline with an ambiguity height close to the maximum expected height. For forests up to 60 m, a Δk_z in the order of 0.1 was recommended. Multiple baselines allow to adjust the sensitivity to different height ranges.
- Although a side result of this work, the ability of Pol-InSAR to resolve scattering processes in height, may allow to distinguish forest types through the rela-

tive location polarimetric scattering centers. It was suggested that the spruce and broadleaf forests differ in this respect.

Although the work focused on forest biomass, the product forest height itself is a highly valuable information, only to repeat its importance in determining growth stadiums, site quality, and forest classifications.

Forest Biomass estimation: Forest biomass is the final product of the Pol-InSAR height inversion and the height-biomass allometry. Consequently, the biomass estimation essentially merges both the height and allometric errors, but due to the good results from height-biomass allometry and Pol-InSAR height inversion, the biomass estimation also proved a good performance ($r^2 \sim 0.7$). It was pointed out that the errors might not be independent. Especially in open and heterogeneous forests a height-underestimation may go along with a low allometric level. However, for the selected validation stands of the test site Traunstein, the allometric level varied too little as if an error interdependence could be shown.

Due to the good performance of the sinc-inversion, also a direct relation between coherence and biomass was investigated. This was done by combining the sinc-function between coherence and height, and the height-biomass reference allometry. The resulting relation could be approximated by a linear function which is scaled by the allometric level. The performance was equal to the two step inversion procedure, but it must be pointed out, that (1) it used a regression based on ground measurements, and (2) depends on the validity of the sinc which means no strong influence of extinction and ground. This relation was discussed in the context of empirical findings from ERS1/2-tandem interferometry at C-band (Ch. 4.5.2). Here, many data sets were decorrelated with coherence < 0.4, but for a few winter scenes the coherence reached up to 0.8, and showed a linear relation to biomass. The intercept with the coherence-axis (biomass = 0 t ha^{-1}) was interpreted as ground coherence, the slope of the coherence-biomass relation as an extinction dependent parameter. Differences between scenes were explained with different extinctions under different conditions. There are many analogies with the direct biomass estimation in this work: the intercept with the coherence-axis is the temporal decorrelation, the proposed coherence-biomass slope is determined by the baseline and forest height. The baseline dependence of the slope is the distinct difference between the two interpretations, and maybe it is worth to check the effect of the baselines in the relation.

Evaluating the potential of forest biomass estimations from Pol-InSAR: In this work, polarimetric SAR interferometry at L-band was shown to be able to extract forest biomass up to levels of 450t ha^{-1}. No saturation was observed neither in the height-biomass allometry nor in the Pol-InSAR-height extraction. These results encourage to make some preliminary considerations on a space-borne Pol-InSAR mission for a global forest biomass inventory. The four most important aspects of the configuration shall be outlined; the first two of them have been mentioned before:

- single-pass acquisition to avoid temporal decorrelation;
- $\Delta k_z \sim 0.1$ to guarantee height sensitivitiy up to 60 m;
- extinction is the parameter that defines the selection of the frequency and the incidence angle. The forest scattering profile should include both crown tops

and lower volume parts, and the ground should neither be obscured nor dominant. In this work, both the coherence and the phase analysis proved that L-band did not saturate over the – even in global terms – dense forest of Traunstein;

- resolution should be chosen as high as possible. Image quality, object identifycation, segmentation and subsequent classification are directly connected to resolution. The availability of high resolution SAR sensors allows reducing the standard deviation of the obtained estimates without violating the required spatial resolution of the products. Over heterogeneous and open forests (FAO definition down to 10% canopy cover) resolution is needed to resolve the canopy heterogeneities. Additionally, a large bandwidth in range minimizes range decorrelation and provides a sufficient number of looks for reducing the variance of the observation space.

A final general comment shall be made with respect to both remote sensing and user community. This work addressed both forestry science and remote sensing techniques, and profited from both points of view. In this sense, I would like to conclude my work with a reminder from the FRA 2000 (p. 351): “Remote sensing technologies are an area where there is promising potential to improve future assessments. [However …] technology-intensive approaches generally preclude the participation of local people, thus limiting the ownership and local utilization of the information. Thus, a combination of remote sensing and ground-based assessment methodologies will continue to be needed for the foreseeable future.”

6 Literature

Aas, G., Riedmiller, A. (1987). Bäume. ISBN 3-7742-4058-2. Gräfe/Unzer. München

Alsdorf, D.E., J.M. Melack, T. Dunne, L.A.K. Mertes, L.L. Hess, and L.C. Smith, Interferometric radar measurements of water level changes on the Amazon floodplain, Nature, v. 404, p. 174-177, 2000.

Alsdorf, D.E., Smith, L.C., Melack, J.M. (2001). Amazon Floodplain Water Level Changes Measured with Interferometric SIR-C Radar. TGARS 39(2): 423-431

Andersen, H.-E., McGaughey, R., Carson, W., Reutebusch, S., Mercer, B. (2004). A comparison of forest canopy models derived from lidar and InSAR. ISPRS 20, Istanbul, Turkey, 13.-23.7.

Archard, F., Eva, H.D., Mayaux, P. (2004). Improved estimtes of net carbon emissions from land cover change in the tropics for the 1990s. Global Biogeochemical Cycles 18

Archibold, O.W. (1995). Ecology of World Vegetation. Chapman and Hall, London

Askne, J.I.H., Dammert, P.B.G., Ulander, L.M.H., Smith, G. (1997). C-band repeat-pass interferometry observation of the forest. IEEE TGARS 35(1): 25-35

Assmann, E, Franz, F. (1963). Vorläufige Fichtenertragstafel für Bayern. Inst. f. Ertragskunde der forstl. Versuchsanstalt München.

Assmann, E. (1961). Waldertragskunde. BLV Verlagsgesellschaft, Muenchen

Assmann, E. und Franz, F. (1965). Vorläufige Fichten-Ertragstafel für Bayern. Forstwissenschaftliches Centralblatt, 84(1): 13-43

Atjai, G.L., Ketner, P., Duvigneaud, P. (1979): Terrestrial Primary Production and Phytomass. In: Bolin, B., Degens, E.T., Kempe, S., Ketner, P. (eds.). The Global Carbon Cycle. SCOPE 13. Chichester, New York: Wiley, 129-182

Attema, E.P.W., Ulaby, F.T. (1978). Vegetation modeled as a water cloud. Radio Science, 13(2), 357-364.

Aulinger, T. (2005). Vergleich von Höhenmodellen aus InSAR- und Lidar-Daten über einem Naturwald im Nationalpark Bayerischer Wald. Diplomarbeit an der Fachhochschule München DLR-HR-IB-12/2005

Aulinger, T., Mette, T., Papathanassiou, K., Hajnsek, I., Heurich, M., Krzystek, P. (2005). Validation of heights from interferometric SAR and Lidar over the temperate forest test site National Park Bayerischer Wald. Proc. PolInSAR'05, Frascati, 24.-28.Jan.2005

Bailey, R. (1996). Ecosystem geography. New York, Springer.

Bamler, R., Hartl, P. (1998). Synthetic aperture radar interferometry. Inverse Problems 14

Barnes, B.V., Zak, D.R., Denton, S.R., Spurr, S.H. (1998). Forest Ecology. JohnWiley & Sons, New York

Bauer, A. (2001). Möglichkeiten zur Extensivierung der Forsteinrichtung im Hochgebirge durch Einsatz moderner Techniken der Luftbildauswertung. Forstl. ForsCh.ber. München, ISSN 0174-1810

Baulis, X., Pons, X. (1995). Approach to forest inventory and m apping by means of multi-spectral airborne data. Int.J.Rem.Sens. 16 (1): 61-80

Bazzaz, F.A. (1990). Annu.Rev.Ecol.Syst. 21, 167

Bechmann, P., Spizzichino, A. (1963). The scattering of electromagnetic waves from rough surfaces. Pergamon Press

Bertalanffy, L.v. (1942). Theoretische Biologie. Zweiter Band: Stoffwechsel und Wachstum. Borntraeger, Berlin

Biermayer, G. (1999). Ziele und Konzept der Forsteinrichtung im Staatswald Bayerns. AFZ/ Der Wald 20/1999

BMJ – Bundesministerium der Justiz (2000). Allgemeine Verwaltungsvorschrift zur Durchführung der Bundeswaldinventur II (VwV-BWI II). Bundesanzeiger 146a. www.bundeswaldinventur.de

BMVEL – Bundesministerium für Verbraucherschutz, Ernährung und Landwirtschaft (2001). Gesamtwaldbericht der Bundesregierung.

Boerner, W.-M. et al. eds. (1992). Direct and inverse methods in radar polarimetry. Kluwer Academic Publ., NL

Boerner, W.M., El-Arini, M.B. (1981). Polarization dependence in electromagnetic inverse problems. IEEE TGARS 29(2): 262-271

Born, M., Wolf, E. (1985). Principles of optics. Pergamon, N.Y.

Bourgeaud, M. et al. (1989). Theoretical models for polarimetric microwave remote sensing of earth terrain. Journal of Electromagnetic Waves and Applications, 3(1): 1-81

Brown, J.H., West, G.B. eds. (2000). Scaling in Biology. Oxford Univ.Press, Oxford

Brown, J.H., West, G.B., Enquist, B.J. (2000). Scaling in Biology: Patterns and Processes, Causes and Consequences. In Brown and West (2000): 1-25

Brown, S. (1997). Estimating Biomass and Biomass Change of Tropical Forests: a Primer. FAO forestry paper 134. Rome. ISBN 92-5-103955-0

Brown, S. (1998). Present and future role of forests in global climate change. In: Goalp, B., Pathak, P.S. and Saxena, K.G. (eds.). Ecology today: an anthology of contemporary ecological research. International Scientifi c Publications, New Delhi. p. 59–74.

Brown, S. Lugo, A.E. (1982). The storage and production of organic matter in tropical forests and their role in the global carbon cycle. Biotropica 14: 161-187

Brown, S., (1990). Volume expansion factors for tropical forests. Unpublished Paper, Prepared for the Forest resource Assessment-1990 Project (available from author) => see Brown (1997)

Brown, S., Lugo, A.E. (1992). Above ground biomass estimates for tropical moist forests of the Brazilian Amazon. Interciencia 17:8-18.

Bundeswaldgesetz. 2. Mai 1975 (BGBl. I S. 1037), last change 26. August 1998 (BGBl. I S. 2521). http://www.verbraucherministerium.de >> Bundeswaldgesetz

Bürgmann, R., Rosen, P.A., Fielding, E.J. (2000). Synthetic Aperture Radar interferometry to measure earth's surface topography and its deformation. Annual Review of Earth and Planetary Sciences, 28:169-209

Burkhart, H.E., Tham, A. (1992). Predictions from growth and yield models of the performance of mixed-species stands. In: Cannell et al. 1992: 21-34

Burschel, P., Huss, J. (1997). Grundriss des Waldbaus. Pareys Studientexte 49, Berlin

Burschel, P., Weber, M., Kürsten, E. (1992). Stellungnahme zur Anhörung der Enquete-Kommission des Dt. Bundestages zum Schutz der Erdatmosphäre am 16./17.1.1992.

Cannell, M.G.R., Malcolm, D.C., Robertson, P.A. eds. (1992). The ecology of mixed species stands of trees. Blackwell Science Publications, London

Carmean, W.H. (1970). Tree height-growth patterns in relation to soil and site. In: Youngberg and Davey (1970)

Castel, T., Beaudoin, A., Floury, N., Le Toan, T., Caraglio, Y., Barczi, J.-F. (2001). Deriving Forest Canopy Parameters for Backscatter Models Using the AMAP Architectural Plant Model. IEEE TGRS 39/3: 571-583

Cihlar, J., Heimann, M., Olson, R. eds. (2001). Terrestrial Carbon observation. Environment and Natural Resources Series No.5. Rome, FAO 2001, www.fao.org

Cloude, S.R. (1986). Polarimetry : the characterization of polarimetric effects in EM scattering. PhD. Thesis, University of Birmingham, UK

Cloude, S.R. (1992). Uniqueness of target decomposition theorems in radar polarimetry. In: Boerner (1992): 267-298

Cloude, S.R. (2002). Robust Parameter Estimation using dual baseline polarimetric SAR Interferometry. Proc. IGARSS'02 Toronto, Canada, July 2002

Cloude, S.R., Papathanassiou, K.P. (1998). Polarimetric SAR interferometry. IEEE TGRS 36(5): 1551-1565

Cloude, S.R., Papathanassiou, K.P. (2003). Three-stage inversion process for polarimetric SAR interferometry. IEE Proc. Radar Sonar Navig., 150(3), 125-134.

Cloude, S.R., Pottier, E. (1995). Concept of polarization entropy in optical scattering. Optical Engineering 34(6): 1599-1610

Cloude, S.R., Pottier, E. (1996). A review of target decomposition theorems in radar polarimetry. IEEE TGRS 34(2): 498-518

Cloude, S.R., Pottier, E. (1997). An entropy based classification scheme for land applications of polarimetric SAR. IEEE TGRS 35: 68-78

Cole, D.W., Rapp, M. (1981). Elemental cycling in forest ecosystems. In: Reichle (1981): 341-409

Colesanti, C., Ferretti, A., Novali, F., Prati, C., Rocca, F. (2003). SAR monitoring of progressive and seasonal ground deformation using the Permanent Scatterers Technique. IEEE TGARS, 41(7):1685-1701

Crandall, C. J. (1969). Radar mapping in Panama. Photogr. Eng. 35(7):641-648

Curlander, J.C., McDonough, R.N. (1991). Synthetic aperture radar: systems and signal processing. John Wiley and Sons, NY, 647 pp.

De Grandi, G., Mayaux, P., Simard, M., Saatchi, S. (2000). The global rain forest monitoring project JERS-1 radar mosaic ot tropical Africa – development and product characterization aspects. IEEE TGRS 38(5): 2218-2233

DeFries, R.S., Houghton, R.A., Hansen, M.C. (2002). Carbon emissions from tropical deforesetation and regrowth based on satellite observations for the 1980s and 90s. Proc. Nat.Acad.Sci 99: 14256-14261

Denzin (1929). Schätzung der Masse stehender Waldbäume. FA, 382-384

Dixon, R.K., Brown, S., Houghton, R.A. (1994). Carbon pools and flux of global forest ecosystems. Science 299: 185-190

Dobson M.C., Ulaby F.T., Le Toan T., Beaudoin A., Kasischke E.S., Christensen N. (1992). Dependence of Radar Backscatter on Coniferous Forest Biomass. IEEE Transactions on Geoscience and Remote Sensing, Vol. 30 (2), March, pp. 412-415.

Dong, J., Kaufmann, R.K., Myneni, R.B., Tucker, C.J., Kauppi, P.E., Liski, J., Buermann, W. , Alexeyev, V., Hughes, M.K. (2003). Remote sensing estimates of boreal and temperate forest woody biomass:carbon pools, sources, and sinks. Remote Sensing of Environment 84: 393–410

Drake, J.B., Dubayah, R.O., Clark, D.B., Knox, R.G., Blair, J.B., Hofton, M.A., Chazdon, R.L., Weishampel, J.F., Prince, S.D. (2002). Estimation of tropical forest structural characteristics using large-footprint lidar. RSEnv. 79:305-319

Dubayah R., Blair, J.B., Bufton, J., Clark, D., JaJa, J., Knox, R., Luthcke, S., Prince, S., Weishampel, J. (1997): Vegetation canopy lidar mission. In: Land Satellite Information in the Next Decade II: Sources and Applications. American Society for Photogrammetry and Remote, Sensing, Bethesda, MD: 100-112.

Dubois, P.C., Van Zyl, J.J., Engman, T. (1995). Measuring soil moisture with imaging radar. IEEE TGRS 33(4): 916-926

Eichhorn, F. (1902). Ertragstafeln für die Weißtanne. Springer, Berlin

Elachi, C. (1987). Spaceborne radar remote sensing. IEEE, New York, 255 pp.

Ellenberg, H. (1996). Vegetation Mitteleuropas mit den Alpen. (engl.: Vegetation of Middle Europe and the Alps). ISBN 3-8252-8104-3. UTB. Stuttgart.

Ellenberg, H. ed. (1986). Ökosystemforschung. Ergebnisse des Sollingprojekts 1966-86, Stuttgart

Enquist, B.J., Brown, J.H., West, G.B. (1998). Allometric scaling of plant energetics. Nature 395: 163-165

Enquist, B.J., Niklas, K.J. (2001). Invariant scaling relatioons across tree-dominated communities. Nature, 410: 655-660

Falkowski, P., Scholes, R.J., Boyle, E., Canadell, J., Canfield, D., elser, J., Gruber, N., Hibbard, K., Högberg, P., Linder, S., MacKenzie, F.T., Moore III, B., Pderson, T., Rosenthal, Y., Seitzinger, S., Smetacek, V., Steffen, W. (2000). The global carbon cycle: a test of our knowledge of the Earth as a system. Science 290, p. 291-295

FAO – Food and Agricultural Organization of the UN (2001a). State of the World's Forests. Rome. www.fao.org/forestry

FAO – Food and Agricultural Organization of the UN (2001b). Forest Resource Assessment 2000. ISSN 0258-6150, FAO forestry paper No. 140. Rome. www.fao.org/forestry

FAO (1996). Forest Resources Assessment 1990. Survey of tropical forest cover and study of change process. Forestry Paper No. 130. Rome.

FAO (2001) FRA 2000: Pan-tropical survey of forest cover changes 1980-2000. FRA Working Paper No. 49.

Ferretti, A., Prati, C., Rocca, F. (2001). Permanent scatterers in SAR interferometry. IEEE Transactions on Geoscience and Remote Sensing, 39(1):8-20

Fielding, E.J., R.G. Blom, and R.M. Goldstein, Rapid subsidence over oil fields measured by SAR interferometry, Geophysical Research Letters, v. 25, p. 3215-3218, 1998.

Fittkau, E.J., Klinge, H. (1973). On biomass and trophic structure of the central Amazonian rain forest ecosystem. Biotropica, 5:2-14

Foody, G.M., Boyd, D.S., Curran, P.J. (1996). Relations between tropical forest biophysical properties and data acquired in AVHRR channels 1-5. Int.J.Rem.Sens. 17: 1341-1355

Fornaro, G., Franceschetti, G. (1995). Image registration in interferometric SAR Processing. IEEE Radar and Sonar Navigation 142(6): 313-320

Fransson, J.E.S., Walter, F., Ulander, L.M.H. (2000). Estimation of forest parameters using CARABAS-II VHF SAR data. IEEE TGARS 38(2): 720-727

Freeman A., Durden S.L. (19989). A three-component scattering model for polarimetric SAR data. IEEE Trans. Geoscience and Remote Sensing, 36(3):963– 973, May 1998.

Fung, A.K. (1994). Microwave scattering and emission models and their applications. Artech House.

Galileo Galilei. Discorsi e dimostrazioni matematiche, intorno a due nuove scienze. 1638. (Dialogues concernine two new sciences. Trans. H. Crew, A. de Salvio. New York. 1914)

Garestier, F., Dubois-Fernandez, P., Papathanassiou, K.P. (2006). Pine forest analysis with single-pass X-band Pol-InSAR data. To be published in IEEE TGARS

Gatelli, F., Monti Guarnieri, A., Parizzi, F., Pasquali, P., Prati, C., Rocca, F. (1994). The wavenumber shift in SAR interferometry. IEEE TGARS 32(4): 855-865

Gaveau, D.L.A., Baltzer, H., Plummer, S. (2003). Forest woody biomass classification with satellite-based radar coherence over 9000000km2 in Central Siberia. ForEcoMan 174: 65-75

Gehrhardt, E. (1909). Über Bestandes-Wachstumsgesetze und ihre Anwendung zur Aufstellung von Ertragstafeln. AFJZ 85: 117-128

Ghiglia, D.C., Pritt, M.D. (1998). Two-dimensional phase unwrapping: theory, algorithms, and software. John Wiley & Sons, Inc, New York

GLCCD - Global Land Cover Characteristics Database, Version 1.2. (1998). Data available on-line at: http://edcdaac.usgs.gov/glcc/glcc.html.

Global Land Cover Characteristics Database (GLCCD), Version 1.2. 1998. Data available on-line at: http://edcdaac.usgs.gov/glcc/glcc.html.

Goldstein, R.M., H. Engelhardt, B. Kamb, and R.M. Frolich, Satellite radar interferometry for monitoring ice sheet motion: Application to an Antarctic ice stream, Science, v. 262, p. 1525-1530, 1993.

Goodale, C.L., Apps, M.J., Birdsey, R.A. (2002). Forest carbon sinks in the northern hemisphere. Ecological applications 12: 891-899

Graham, L.C. (1974). Synthetic interferometer radar for topographic mapping. Proc. IEEE 62(6): 763-768

Grayson, A.J. et Maynard, W.B. 1997. The World's Forests - Rio Plus 5: International Initiatives Towards Sustainable Management, Commonwealth Forestry Association, Oxford, R.U.

Hagberg, J.O., Ulander, L.M.H., Askne, J. (1995). Repeat-pass SAR interferometry over forested terrain. IEEE TGARS 33(2): 331-340

Hajnsek, I., Cloude, S. R. (2004): Pol-InSAR for Agricultural Vegetation. Proc. IGARSS'04, Anchorage, Alaska, Sep.2004

Hajnsek, I., Pottier, E., Cloude, S. (2003). Inversion of surface parameters from polarimetric SAR. IEEE TGRS 41(4): 727-745

Hajnsek, Irena (2001). Inversion of surface parameters using polarimetric SAR. PhD thesis Uni Jena, ISSN 1434-8454

Harding, D.J., Carabajal, C.C. (2005). ICESat waveform measurements of within-footprint topographic relief and vegetation vertical structure. Geophysical Research Letter, 32, L21S10

Harper, J.L. (1977). Population biology of plants. Academic Press, London

Hein, A. (2004). Processing of SAR data. Springer, Berlin

Hellmann, M. (2001). SAR polarimetry tutorial. 2001, http://www.sigma-nought.de

Henderson, F.L., Lewis, A.J. eds. (1998). Principles and applications of imaging radar. John Wiley & Sons, N.Y.

Hobbs, R.J., Mooney, H.A. eds. (1990). Remote sensing of biosphere functioning. Springer, N.Y.

Hoekman, D.H., Quiñones, M.J. (2002). Biophysical Forest Type Characterization in the Colombian Amazon by Airborne Polarimetric SAR. TGARS 40(6): 1288-1300

Holdridge, L.R., Grenke, W.C., Hatheway, W.H., Liang, T., Tosi, J.A. (1971). Forest environments in tropical life zones. Pergamon Press, Oxford

Horn, R. (1994). DLR airborne SAR project, objectives and status. Proc. 1st Int. Airborne Remote Sensing Conference and Exhibition, Straßburg, Sept.1994

Horn, R., Moreira, A., Buckreuß, S., Scheiber, R. (2000). Recent developments of the airborne SAR system E-SAR of DLR. EuSAR, 23.-25.5.2000, München

Houghton, R.A. (1996). Land-use change and terrestrial carbon: the temporal record. In: Apps, M.J. and Price, D.T. (eds.). Forest ecosystems, forest management and the global carbon cycle. NATO ASI Series, Vol. I 40. Springer-Verlag, Berlin, Heidelberg. p. 117–134.

Houghton, R.A. (1999). The annual net flux of carbon to the atmosphere from changes in land use, 1850-1990. Tellues Series B – Chemical and physical meteorology, 51(2): 298-313

Houghton, R.A. (2003). Revised estimates of the annual net flux of carbon to the atmosphere from changes in land use 1850-1990. Tellus, 51B: 298-313

Houghton, R.A. (2005). Aboveground forest biomass and the global carbon balance. Global Change Biology 11: 945-958

Huber, F.X. (1928). Hilfstabellen für Bedienstete des Forst- und Baufachs und auch für Ökonomen zur leichten und schnellen Bestimmung des Massengehaltes roher Holzstämme. München

Huxley, J.S. (1932). Problems of relative growth. New York: MacVeagh

Huxley, J.S., Teissier, G. (1936). Zur Terminologie des relativen Größenwachstums. Biol. Zbl. 56

Imhoff, M. L. (1995). Radar backscatter and biomass saturation ramifications for global biomass inventory. IEEE Trans. Geosci. Remote Sensing, 33/3: 511–518

IPCC (2000). Special report: Land use, land use change and forestry. http://www.ipcc.ch >> Search: special reports, active July 2005

IPCC (2001a). Third Assessment Report – Climate Change 2001: The Scientific Basis. http://www.ipcc.ch - active July 2005

IPCC (2001b). Third Assessment Report – Climate Change 2001: Impacts, Adaptions, and Vulnerability. http://www.ipcc.ch - active July 2005

Isola, M., Cloude, S.R. (2001). Forest height mapping using space-borne polarimetric SAR interferometry. Proc. IGARSS'01, Sydney, Australia

Israelsson, H., Ulander, L.M.H., Askne, J.I.H., Fransson, J.E.S., Frölind, P.-O., Gustavsson, A., Hellsten, H. (1997). Retrieval of forest stem volume using VHF SAR. IEEE TGARS 35(1): 36-40

Jarvis, P., Linder, S. (2000). Nature 405, 904

Jones, R.C. (1941). A new calculus for the treatment of optical systems II. Proof of the three general equations. Journal of the Optical Society of America 31: 493-499

Joughin, I.R., R. Kwok, and M.A. Fahnestock, Interferometric estimation of three-dimensional ice-flow using ascending and descending passes, IEEE Transactions on Geoscience and Remote Sensing, v. 36, p. 25-37, 1998.

Just, D., Bamler, R. (1994). Phase statistics of interferograms with application to synthetic aperture radar. Applied Optics 33(20): 4361-4368.

Kasischke, E. S., Christensen, N. L., Bourgeau-Chavez, L. L., Harcombe, W. P. (1995). Correlating radar backscatter with components of biomass in loblolly pine forests. IEEE Trans. Geosci. Remote Sensing, 33/5 : 643–659

Kauppi, P.E. (2003). New, low estimate fopr carbon stock in global vegetation based on inventory data. Silva fennica 37(4):

Kauppi, P.E., Mielikäinen, K., Kuusela, K. (1992). Biomass and carbon budget of European forests 1971-1990. Science 256: 70-74

Kellndorfer, J.M., Dobson, M.C., Vona, J.D., Clutter, M. (2003). Toward Precision Forestry: Plot-Level Parameter Retrieval for Slash Pine Plantations With JPL AIRSAR. IEEE TGRS 41/7: 1571-1582

Kennaugh, E.M. (1951). Effects of the type of polarization on echo characteristics. Report 389-9, Antenna Laboratory, Ohio State University, Columbus, USA

Kerr, G., Nixon, C.J., Matthews, R.W. (1992). Silviculture and yield of mixed-species stands: the UK experience. In: Cannell et al. 1992: 35-51

Klausing, H., Holpp, W. (2000). Radar mit realer und synthetischer Apertur. Oldenbourg Wissenschaftsverlag, München

Köppen. 1931. Grundrisse der Klimakunde. Berlin, Walter de Gruyter Co.

Koskinen, J.T., Pulliainen, J.T., Hyyppä, J.M, Engdahl, M. & Hallikainen, M.T. (2001). The seasonal behaviour of interferometric coherence in boreal forest. IEEE TGRS, 39(4), 820-829.

Kozlowski, T.T., Pallardy, S.G. (1997). Growth control in woody plants. Acad.Press, San Diego

Kramer, H., Akça, A. (1995). Leitfaden zur Waldmesslehre. Sauerländer. Frankfurt

Kramer, P.J., Boyer, J.S. (1995). Waster relations of plants and soils. Acad.Press, N.Y.

Krieger et al. (2005): TanDEM-X: Concept and Performance Analysis. Proc. IGARSS, Seoul, Korea, Jul. 25-29

Krogager, E. (1990). A new decomposition of the radar target scattering matrix. Electronic Letters, 26(18):1525–1526

Kugler, F. (2003). Temporäre Dekorrelation von Radarfernerkundungsdaten über einem temperaten Mischwald. Diplomarbeit an der TU München.DLR-HR-IB-551-9/2004

Smith, L.S. and Alsdorf, D.E. (1998), Control on sediment and organic carbon delivery to the Arctic Ocean revealed with space-borne synthetic aperture radar: Ob' River, Siberia, Geology, v. 26, p. 395-398.

Larcher, W. (1995) Ökophysiologie der Pflanzen. Ulmer, Stuttgart

Le Toan, T. , Beaudoin, A., Riom, J., Guyon, D. (1992). Relating forest biomass to SAR data. IEEE Trans. Geosci. Remote Sensing, vol. 30/3: 403–411

Lee, J.-S. (1980). Digital Image Enhancement and Noise Filtering by Use of Local Statistics", IEEE Transactions on Pattern. Analysis and Machine Intelligence, Vol. PAM1-2, No. 2, March, 1980

Levsky, M.A., Cohen, W.B., Acker, S.A., Parker, G.G., Spies, T.A., Harding, D. (1999a). Lidar remote sensing of the canopy structure and biophysical properties of Douglas-fir Western Hemlock forests. RSEnv. 70: 339-361

Levsky, M.A., Harding, D., Cohen, W.B., Parker, G., Shugart, H.H. (1999b). Surface lidar remote sensing of basal area and biomass in deciduous forests of Eastern Maryland, USA. RSEnv. 67:83-98

Lewis, A.J., Henderson, F.M. (eds.) (1998). Manual of Remote Sensing, Principles and Applications of Imaging Radar. Wiley & Sons, NY

Lillesand, Kiefer (1999). Remote sensing and image interpretation. John Wiley & Sons, N.Y.

Lohmann, U. (2003). Holz Lexikon Bd.1/ 2. DRW-Verlag, Leinfelden-Echterdingen

Lopes, A., Touzi, R. Nezry, E. (1990). Adaptive speckle filters and Scene heterogeneity. IEEE Transaction on Geoscience and Remote Sensing, Vol. 28, No. 6, pp. 992-1000, Nov. 1990

Loveland, T.R., B.C. Reed, J.F. Borwn, D.O. Ohlen, Z. Zhu, L. Yang, and J. Merchant. 2000. “Development of a Global Land Cover Characteristics Database and IGBP DISCover from 1-km AVHRR Data.” International Journal of Remote Sensing 21 (6-7): 1303-1330.

Lyr, H., Fiedler, H.J., Tranquillini, W. (1992). Physiologie und Ökologie der Gehölze. Gustav Fischer, Jena

Malhi, Y., Baldocchi, D.D., Jarvis, P.G. (1999). The carbon balance of tropical, temperate and boreal forests. Plant, Cell and the Environment, 22: 715-740

Massonnet, D., and K. L. Feigl, Radar interferometry and its application to changes in the Earth's surface: Rev. Geophys., v. 36, p. 441-500, 1998

Massonnet, D., M. Rossi, C. Carmona, F. Adragna, G. Peltzer, K. Feigl, and T. Rabaute, The displacement field of the Landers earthquake mapped by radar interferometry, Nature, v. 364, p. 138-142, 1993.

Massonnet, D., P. Briole, and A. Arnaud, Deflation of Mount Etna monitored by spaceborne radar interferometry, Nature, v. 375, p. 567-570, 1995.

McMahon, T.A., Kronauer, R.E. (1976). Tree structure: Deducing the principle of mechanical design. J.Theor.Biol. 59: 443-466

Means, J.E., Acker, S.A., Harding, D.J., Blair, J.B., Levsky, M.A., Cohen, W.B., Harmon, M.E., Mckee, W.A. (1999). Use of large-footprint scanning airborne lidar to estimate forest stand characteristics in the Western Cascades of Oregon. RSEnv. 67: 298-308

Melon, P., Martinez, J.-M., Le Toan, T., Ulander, L.M.H., Beaudoin, A. (2001). On the retrieving of forest stem volume from VHF SAR data : Observation and modeling. IEEE TGARS 39(11): 2364-2372

Mercer, B. (2004). DEMs created from airborne IFSAR – an update. ISPRS 20, Istanbul, Turkey, 13.-23.7.2004

Meschederu, M. (1997). Bilanzierung von Biomassen, Kohlenstoff- und Stickstoffgehalten mit dem Wuchsmodell SILVA 2.1. Ber.d. Jahrestagung d. Sektion Ertragskunde im Dt.Verb. Forstl. Forschungsanstalten, Grünberg: 35-44

Mette, T., Kugler, F., Papathanassiou, K. Hajnsek, I. (2006). Viewing forest in Pol-InSAR. Workshop on 3D Remote Sensing in Forestry, 14th-15th Feb 2006, Vienna

Mette, T., Kugler, F., Papathanassiou, K.P., Hajnsek, I. (2006). Forest and the Random Volume over Ground- nature and effect of 3 possible error types. Proc. EUSAR, Dresden (Germany), May 2006.

Mette, T., Papathanassiou, K. Hajnsek, I. (2003). Height-Biomass Allometry in Temperate Forests - Performance accuracy of height-biomass allometry. Proc. IGARSS 2003, 21.-25.Jul., Toulouse

Mette, T., Papathanassiou, K. Hajnsek, I. (2004). Estimating Forest Biomass from Polarimetric Interferometric SAR data in Combination with Forest Allometry – Results from Temperate Spruce Forest Test Site Traunstein. Proc. Retrieval of Bio- and Geophysical Parameters from SAR Data for Land Applications, 16.-19. Nov. 2004, Innsbruck

Mette, T., Papathanassiou, K. Hajnsek, I. (2004a). Potential of Forest Height Derived by Polarimetric SAR Interferometry to Estimate Forest Biomass. Proc. EUSAR 2004, 16.-18. Mai, Ulm

Mette, T., Papathanassiou, K. Hajnsek, I., Pretzsch, H., Biber, P. (2004b). Applying a Common Allometric Equation to Convert Forest Height from Pol-InSAR Data to Forest Biomass. Proc. IGARSS 2004, 20.-24. Sept., Anchorage

Mette, T., Papathanassiou, K. Hajnsek, I. (2004c). Estimating Forest Biomass from Polarimetric Interferometric SAR data in Combination with Forest Allometry – Results from Temperate Spruce Forest Test Site Traunstein. Proc. Retrieval of Bio- and Geophysical Parameters from SAR Data for Land Applications, 16.-19. Nov. 2004, Innsbruck

Mette, T., Papathanassiou, K. Hajnsek, I., Zimmermann, R. (2002). Forest Biomass Estimation Using Polarimetric SAR Interferometry. Proc. ForestSAT 2002, 5.-9. Aug., Edinburgh

Mette, T., Pretzsch, H., Papathanassiou, K., Hajnsek, I. (subm.). Forest Height-Biomass Allometry for Use with Remote Sensing Data.

Mooney, H.A., Hobbs, R.J. (1990). Introduction. In: Hobbs, R.J. and Mooney, H.A. (eds.). Remote sensing of biosphere functioning. Springer, N.Y.

Moosmayer, H.-U. (1970). Der Einfluss ertragskundlich-standortskundlicher Forschungsergebnisse auf die Bonitierung und Ertragsregelung bei der Forsteinrichtung in Baden-Wuerttemberg. AFJZ: 73-83

Morain, S.A., Simonett, D.S. (1966). Vegetation analysis with radar imagery. Proc. 4th Symp. on R.S.Env., April 12-14, Inst. of Science and Technology, University of Michigan, pp. 605-622

Moreira, A., Schreiber, R. (2000). Coregistration of interferometric SAR images using spectral diversity. IEEE Transactions on Geoscience and Remote Sensing, 38(5):2179-2191

Moreira, J., Schwäbisch, M., Wimmer, C., Rombach, M., Mura, J. (2001). Surface and ground topography determination in tropical rain forest areas using airborne interferometric SAR. Photogrammetric Week, 24.-28.Sept.2001, Stuttgart (http://www.ifp.uni-stuttgart.de/Phowo/index.htm)

Myneni, R.B., Keeling, C.D, Tucker, C.J., Asrar, G., Nemani, R.R. (1997). Increased plant growth in northern high latitudes from 1981 to 1991. Nature 386: 698-702

Nihlgard, B. (1972). Plant biomass, primary production and distribution of chemical elements in a beech and a planted spruce forest in South Sweden. Oikos 23: 59-81

Niklas, K.J. (1994). Plant allometry: the scaling of form and process. Univ. of Chicago Press, Chicago

Niklas, K.J. (2000). The Evolution of Plant Body Plans - A Biomechanical Perspective. Annals of Botany 85: 411-438

Ni-Meister, W., Jupp, D.L.B., Dubayah, R. (2001). Modeling Lidar Waveforms in Heterogeneous and Discrete Canopies. IEEE TGRS, 39(9): 1943-1958

Nultsch, W. (1996). Allgemeine Botanik. Thieme, Stuttgart

Ogilvy, J.A. (1991). Theory of wave scattering from random rough surfaces. Adam Hilger

Oh, Y., Sarabandi, K., Ulaby, F.T (1992). An empirical model and an inversion technique for radar backscattering from bare soil surfaces. IEEE TGRS 30(2): 370-381

Oldfield, S., Lusty, C., MacKiven, A. (1998). The World List of Threatened Trees. World Conservation Press

Oliver C., Quegan, S. (1998). Synthetic Aperture Radar Images. Artech House, Boston

Olson, J.S., Watts, J.A. and Allison, L.J. (1983). Carbon in live vegetation of major world ecosystems. Oak Ridge National Laboratory, ORNL-5862, Oak Ridge, Tennessee. 88 p.

Papathanassiou, K., Cloude, S.R. (2001). Single baseline polarimetric SAR interferometry. IEEE TGARS 39(11): 2352-2363

Papathanassiou, K.P. (1999). Polarimetric SAR interferometry. PhD. Thesis, University of Graz, Austria, DLR Forschungsbericht 99-07, DLR-Oberpfaffenhofen, Germany

Papathanassiou, K.P., Reigber, A., Cloude, S.R. (1999a). Vegetation and ground parameter estimation using polarimetric interferometry – Part I: the role of polarization. Proc. CEOS SAR, Toulouse, 26-29 Oct.

Papathanassiou, K.P., Reigber, A., Cloude, S.R. (1999b). Vegetation and ground parameter estimation using polarimetric interferometry – Part II: parameter inversion and optimal polarizations. Proc. CEOS SAR, Toulouse, 26-29 Oct.

Pechmann, H.v. (1974). Der Einfluss der Durchforstung auf die Holzqualität. Forstarchiv 45: 34-38

Pellinen, P. (1986). Biomasseuntersuchungen im Kalkbuchenwald. Dissertation Göttingen

Photogrammetric Engineering and Remote Sensing (2006). The Shuttle Radar Topography Mission – data validation and applications. Photogr.Eng.Rem.Sens., Special Issue.

Prentice, I.C., Farquhar, G.D., et al. (2001). The carbon cycle and atmospheric carbon dioxide. In: Houghton, J.T. et al. (eds.). Climate change 2001: the scientific basis. Cambridge Univ. Press. Cambridge. p. 183–237.

Pretzsch, H. (1999). Waldwachstum im Wandel. Forstw.Cbl. 118: 228-250

Pretzsch, H. (2001). Modellierung des Waldwachstums. Parey, Berlin

Pretzsch, H. (2002). A unified low of spatial allometry for woody and herbaceous plants. Plant Biology, 4, 159-166.

Pretzsch, H. (2005). Link between the self-thinning rules for herbaceous and woody plants. Scientia Agriculturae Bohemica, 36(3), 09-107.

Pretzsch, H. (2006). Species-specific allometric scaling under self-thinning: evidence from long-term plots in forest stands. Oecologia 146 (2006): 572-583.

Pretzsch, H., Biber, P. (2005). A re-evaluation of Reineke's rule and stand density index. Forest Science, 51(14), 304-320

Prodan, M. (1965). Holzmesslehre. Sauerländer. Frankfurt

Pulliainen, J., Engdahl, M., Hallikainen, M. (2003). Feasibility of multi-temporal interferometric SAR data for stand level estimation of boreal forest stem volume. RSEnv. 85(4): 397-409

Pulliainen, J.T., Kurvonen, L., and Hallikainen, M.T. "Multitemporal behaviour of L- and C-band SAR observations of boreal forests." IEEE TGRS 37.2 (1999): 928-9371.

Quegan, S., LeToan, T., Yu, J.J., Ribbes, F., Floury, N. (2000). Multitemporal ERS SAR analysis applied to forest mapping. IEEE TGARS 38(2): 741-753

Reichle, D.E. ed. (1981). Dynamic properties of forest ecosystems. Cambr.Univ.Press, Cambridge

Reigber, A. (1997). Multitemporale Analyse der Kohärenz von SAR Daten. Diplomarbeit an der Universität Konstanz

Reineke, L.H. (1933). Perfecting a stand density index for even-aged forests. Journal of Agricultural Research, 46:627-638

Reyes, G., Brown, S., Chapman, J., Lugo, A.E. (1992). Wood densities of tropical tree species. USDA Forest Service, General Technical Report SO-88, Southern Forest Experiment Station, New Orleans, Louisiana, USA.

Rhody, B. (1982). Ein kombiniertes Inventurverfahren mit photogrammetrischen und terrestrischen permanenten Stichproben für Intensiv- und Grossrauminventuren. Forstw.C.bl. 101

Rice, S.O. (1951). Reflection of electromagnetic waves from slightly rough surfaces. Comm. Pure Appl. Math. 4(2/3): 351-378

Richards, F.J. (1959). A flexible growth function for empirical use. J.Exp.Bot. 10:290-300

Roessel, J.W. van, Godoy, R.C. de. (1974). SLAR mosaics for Project RADAM. Photogr. Eng. 40:583-595.

Rosen, P.A., Hensley, S., Joughin, I.A., Li, F.K., Madsen, S.M., Rodriguez, E., Goldstein, R.M. (2000). Synthetic aperture radar interferometry. Proc.IEEE 88(3), 333-382

Rosenqvist, A., Shirmada, M., Chapman, B., De Grandi, G., Saatchi, S., Rauste, Y. (2000). The global rain forest monitoring project – a review. Int.J.Rem.Sens. 21(6/7): 1375-1387

Running, S.W. (1990). Estimating terrestrial primary productivity by combining remote sensing and ecosystem simulation. In: Hobbs/ Mooney 1990

Running, S.W., Peterson, D.L., Spanner, M.A., Teuber, K.B. (1986). Remote sensing of coniferous forest leaf area. Ecology, 67: 273-276

Sader, S.A., Waide, R.B., Lawrence, W.T., Joyce, A.T. (1989). Tropical forest biomass and successional age class relationships to a vegetation index derived from LandSAT TM data. RSEnv, 28: 143-156

Santoro, M. (2003). Estimation of biophysical parameters in boreal forests from ERS and JERS SAR interferometry. Dep. Geoinformatics, F.Schiller-Universität Jena, Ph.D.thesis

Santoro, M., Askne, J., Smith, G., Fransson, J.E.S. (2002). Stem volume retrieval in oboreal forests from ERS 1/2 interferometry. RSEnv. 81(1): 19-35

Santos, J.R., Neeff, T., Dutra, L.V., Araujo, L.S., Gama, F.F., Elmiro, M.A.T. (2004). Tropical forest biomass mapping from dual frequency SAR interferometry (X- and P-band). ISPRS 20, Istanbul, Turkey, 13.-23.Jul.2004

Saugier, B., Roy, J. and Mooney, H. (2001). Estimations of global terrestrial productivity: converging toward a single number? In: Roy, J., Saugier, B. and Mooney, H. (Eds).Terrestrial global productivity. Physiological Ecology: A Series of Monographs, texts and Treatises. Academic Press. San Diego San Francisco, New York, Boston, London, Sydney, Tokyo. P 543–557.

Sayn-Wittgenstein, L. (1961). Recognition of tree species on air photographs by crown characteristics. Photogrammetric engineering (27/5): 792-809

Schade, J., Hildebrandt, G. (1980). Kleinmass-staebige Luftbilder und Satellitenaufzeichnungen fuer Grossrauminventuren intensiv bewirtschafteter Waelder. AFZ 27

Scheiber, R. (2004). Hochauflösende Interferometrie für Radar mit synthetischer Apertur. Karlsruhe, Univ., Diss.

Scheiber, R., Reigber, A., Papathanassiou, K.P., Horn, R, Buckreuß, S., Moreira, A. (1999). Overview of interferometric data acquisition and processing modes of the experimental airborne SAR system of DLR. Proc. IGARSS'99, 28.6.-2.7.1999, Hamburg: 35-37

'Scheffer and Schachtschabel', Schachtschabel, P., Blume, H.-P., Brümmer, G., Hartge, K.H., Schwertmann, U. (1998). Lehrbuch der Bodenkunde. Enke, Stuttgart

Schimel, D.S., House, J.I., Hibbard, K.A:, Bousquet, P., Ciais, P., Peylin, P., Braswell, B.H. et al. (2001). Recent patterns and mechanisms of carbon exchange by terrestrial ecosystems. Nature 414: 169-172

Schober, R (1985). Ertragstafeln wichtiger Baumarten. Sauerländer's J.D. Verlag.

Schultz, J. (1995). Die Ökozonen der Erde. ISBN 3-8252-1514-8 UTB. Stuttgart.

Schütt, P., Schuck, H.J., Stimm, B. (eds.) (1992). Lexikon der Baum- und Straucharten. ISBN 3-933203-53-8. Ecomed. Landsberg/ Lech

Schweingruber, F.H. (1983). Der Jahrring. Haupt-Verlag, Bern

Simons, J.H. (1964). Some applications of side-looking airborne radar. Proc. 3rd Symp. on Rem.Sens. of Env., Oct.14-16, Univ. of Michigan, Ann Arbor

Sinclair, G. (1948). Modification of the radar range equation for arbitrary targest and arbitrary polarizations. Report 302-19, Antenna Laboratory, Ohio State University, Columbus, USA

Sinclair, G. (1950). Transmission and reception of elliptically polarized waves. Proc. IRE 38: 148-151

Siqueira, P., Hensley, S., Shaffer, S., Hess, L., McGarragh, G., Chapman, B., Freeman, A. (2000). A continental scale mosaic of the Amazon basin using JERS-1 SAR

Smith, G., Ulander, L.M.H. (2000). A model relating VHF-band backscatter to stem volume of coniferous boreal forest. IEEE TGARS 38(2): 728-740

Spiecker, H., Mielikäinen, K., Köhl, M. (2002). Growth trends in European Forests. Springer, Berlin

Sterba, H. (1981). Natürlicher Bestockungsgrad und Reinekes SDI. Cbl. ges. Forstwesen. 98 (2): 101-116.

StMELF – Bayerisches Staatsministerium für Ernährung, Landwirtschaft und Forsten (1979). Hilfstafeln für die Forsteinrichtung. Ministerialforstabteilung München.

StMELF – Bayer. Staatsministerium für Ernährung, Landwirtschaft und Forsten (1982). Richtlinien für die mittel- und langfristige Forstbetriebsplanung in der Bayerischen Staatsforstverwaltung (Forsteinrichtungsrichtlinien) FER 1982. aktualisiert 1990 u. 1991

St-Onge, B., Cavayas, F. (1995). Estimating forest stand structure from high resolution imagery using the directional variogram. Int.J.Rem.Sens. 16:1999-2021

St-Onge, B., Cavayas, F. (1997). Automated forest structure mapping from high resolution imagery based on directional semivariogram estimates. RSEnv. 61: 82-95

'Strasbuger'. Denffer, D.von, Ziegler, H., Ehrendorfer, F., Bresinsky, A. (1983). Lehrbuch der Botanik. Fischer, Stuttgart.

'Strasburger', Sitte, P., Weiler, E.W., Kadereit, A., Bresinsky, A., Körner, C. (2002). (Strasburger) Lehrbuch der Botanik. Spektrum Akademischer Verlag

Strozzi, T., Wegmuller, U., Werner, C.L., Wiesmann, A., Spreckels, V. (2003). ERS SAR interferometry for land subsidence monitoring. IEEE TGARS, 41(7):1702- 1708

Tabb, M., Flynn, T., Carande, R. (2002). Direct estimation of vegetation parameters from covariance data in PolInSAR. Proc. IGARSS'02, Toronto, Canada

Teissier, G. (1934). Dysharmonies et discontinuités dans le croissant. Act. Scient. et industry. 95

Thompson, D.A.W. (1917). On growth and form. Cambridge Univ. Press., Cambridge

Touzi, R., Boerner, W.M., Lee, J.S., Lueneburg, E. (2004). A review of polarimetry in the context of synthetic aperture radar: concepts and information extraction. Can.J.Rem.Sens. 30(3): 380-407

Touzi, R., Lopes, A., Bruniquel, J., Vachon, P.W. (1999). Coherence estimation for SAR imagery. IEEE TGARS 37(1): 135-149

Trendelenburg, R. Mayer-Wegelin, H. (1955). Das Holz als Rohstoff. Carl Hanser-Verlag, München

Treuhaft, R.N., Madsen, S.N., Moghaddam, M., van Zyl, J.J. (1996). Vegetation Characteristics and Underlying Topography from Interferometric Data. *Radio Science*, 31: 1449-1495

Treuhaft, R.N., Siqueira, P. (2000): Vertical structure of vegetated land surfaces from interferometric and polarimetric radar. Radio Science, 35(1): 141-177

Trewartha, G.T. 1968. An introduction to weather and climate. New York, McGraw-Hill.

U.S. Department of Agriculture (1978). Forester's guide to aerial photo interpretation. Agriculture Handbook 308, U.S. Government Printing Office, Washington D.C.

Ulaby, F.T., Moore, R.K., Fung, A.K. (1982). Microwave remote sensing - vol. II. Artech House, Norwood, MA., 2162 pp.

UNESCO (1973). International classification and mapping of vegetation. Ecology and Conservation No. 6. Paris.

UNFCCC (1997). Kyoto Protocol to the UNFCCC. http://unfccc.int >> Search: Kyoto Protocol, active July 2005

UNFCCC (1997). Kyoto Protocol to the UNFCCC. http://unfccc.int >> Search: Kyoto Protocol, active July 2005

UNFCCC (2004). Information on national greenhouse gas inventory data from Parties included in Annex I to the Convention for the period 1990–2002, including the status of reporting. Executive summary. http://ghg.unfccc.int/index.html, active July 2005

UNFCCC (2005). Status of ratification. Last modification on: 12 July 2005, http://unfccc.int/essential_background/kyoto_protocol, active July 2005

Wagenführ, R. (2000). Holzatlas. Fachbuchverlag Leipzig

Wagner, W., Luckmann, A., Vietmeier, J., Tansey, K., Baltzer, H., Schmullius, C., Davidson, M., Gaveau, D., Gluck, M., LeToan, T., Quegan, S., Shvidenko, A., Wiesmann, A., Yu, J.J. (2003). Large-scale mapping of boreal forest in SIBERIA using ERS tandem coherence and JERS backscatter data. RSEnv. 85: 125-144

Walter, H. & Breckle, S.-W. (2004). Ökologie der Erde. Band 3. Spezielle Ökologie der tropischen und subtropischen Zonen. Gustav Fischer, Stuttgart

Walter, H., Breckle, S.-W. (1991). Ökologie der Erde. Band 1. Ökologische Grundlagen in globaler Sicht. Gustav Fischer, Stuttgart

Walter, H., Breckle, S.-W. (1994). Ökologie der Erde. Band 4. Spezielle Ökologie der gemäßigten und arktischen Zonen Euro-Nordasiens. Gustav Fischer, Stuttgart

WBGU – Wissenschaftlicher Beirat der Bundesregierung Globale Umweltveränderungen (1998). Die Anrechnung biologischer Quellen und Senken im Kyoto Protocol: Fortschritt oder Rückschritt für den globalen Umweltschutz? – Sondergutachten. ISBN 3-9806309-0-0. Bremerhaven. www.awi-bremerhaven.de/WBGU

Wegmüller, U., Werner, C.L. (1995). SAR interferometric signatures of forest. IEEE TGARS, 33(5):1153-1161

Wegmüller,U., Werner, C. (1997). Retrieval of vegetation parameters with SAR interferometry. IEEE TGARS, 35(1):18-24

Weller, D.E. (1987). A Reevaluation Of The -3/2 Power Rule Of Plant Self-Thinning. Ecological Monographs 57: 23-43.

Weller, D.E. (1990). Will The Real Self-Thinning Rule Please Stand Up? A Reply To Osawa And Sugita. Ecology. 71: 1204-1207.

Wenk, G., Antanaitis, V., Smelko, S. (1990). Waldertragslehre. Deutscher Landwirtschaftsverlag, Berlin.

West, G.B., Brown, J.H., Enquist, B.J. (1997). A general model for the origin of allometric scaling laws in biology. Science 276: 122-126

West, G.B., Brown, J.H., Enquist, B.J. (1999). A general model for the structure and allometry of plant vascular systems. Nature 400: 664-667

Whittaker, R.H. and Likens, G. (1973). The biosphere and man. In: Lieth, H. and Whittaker, R. (eds.). Primary productivity of the biosphere. Springer-Verlag, New York. p. 305–328.

Wiedemann, E. (1943). Der Vergleich der Massenleistung des Mischbestands mit dem Reinbestand. AFJZ 119: 123-132

WRI – World Resource Institute (2001). World resources 2000-2001: People and ecosystems: The fraying web of life. ISBN: 1-56973-443-7, www.wri.org, active July 2005

Yamada, H., Sato, K., Yamaguchi, Y., Boerner, W.M. (2002). Interferometric phase and coherence of forest etsmiated by ESPRIT based PolInSAR. Proc. IGARSS'02, Toronto, Canada

Yoda, K., Kira, T., Ogawa, H., Hozumi, K. (1963). Self-thinning in overcrowded pure stands under cultivated and natural conditions (intraspecific competition among higher plants XI.). Journal of the Institute of Polytechniques, Osaka City University, Vol.14 (1), Series D: 107-129

Youngberg, C.T., Davey, C.B. eds (1970). Tree growth and forest soils. Oregon State Univ. Press, Corvallis

Zanatta, Y., Mikkola, E. (2001). Wald: Holz und Produktion. Eurostat, ISSN 1562-1359, Catalogue number KS-NN-01-009-DE-I

Zanatta, Y., Mikkola, E., Engels, M. (2000). Wald und Umwelt. Eurostat, ISSN 1562-1359, Catalogue number CA-NN-00-017-DE-I

Zebker, H.A., Goldstein, R.M. (1986). Topographic mapping from interferometric synthetic aperture radar observations. *J. Geophys. Res.* 91 : 4993–4999

Zebker, H.A., P.A. Rosen, R.M. Goldstein, A. Gabriel, and C.L. Werner, On the derivation of coseismic displacement fields using differential radar interferometry: The Landers earthquake, Journal of Geophysical Research, v. 99, p. 19617-19634, 1994.

Zebker, H.A., Villasenor, J. (1992). Decorrelation in interferometric radar echoes. IEEE TGARS 30(5): 950-959

Zeide, B. (1985). Tolerance and self-tolerance of trees. For.Ecol.Manage. 13:149-166

Zeide, B. (1987). Analysis of the 3/2 power law of self-thinning. For. Sci. 33: 517-537.

Zhu, Z., Waller, D., Davis, R. & Lorenzini, M. 1999. Global forest cover map. Interim Progress Report. FRA Working Paper No. 19. Rome, FAO.

Zianis, D., Mencuccini, M. (2004). On simplifying allometric analyses of forest biomass. For.Ecol.Man. 187: 311-332

Zöhrer, F. (1980). Forstinventur. Ein Leitfaden für Studium und Praxis. Parey, Hamburg.

7 Annex

7.1 Global tables and definitions from the FRA 2000

Source: FRA 2000 (FAO 2001b)

Continent	Ref. year	Total area	Land area						Inland water
			Forest			Other wooded land		Other land	
			Closed	Open	Planta-tion	Shrubs/ trees	Forest fallow		
	Yr	000 ha	000 ha	000 ha	000 ha	000 ha	000 ha	000 ha	000 ha
Africa	1991	3031122	352700	288906	4571	377996	52083	1902138	52728
Asia	1995	3174823	416207	58321	53791	122308	20031	2413470	90077
Oceania	1992	856388	196345	1145	2691	423519	451	224945	7292
Europe	1997	2298631	1002979		32036	29484		1195407	38674
North/ Central America	1995	2265557	508298	27367	16681	308585	26055	1215756	128591
South America	1991	1786736	858261	68846	3074	40876	28203	755481	31995
Total	1994	13413257	3334790	444585	112844	1302768	126823	7707198	349357
			(25%)	(3%)	(1%)	(10%)	(1%)	(58%)	(2%)

Forest: Land with tree crown cover (or equivalent stocking level) of more than 10 percent and area of more than 0.5 ha. The trees should be able to reach a minimum height of 5 m at maturity *in situ*. May consist either of closed forest formations where trees of various storeys and undergrowth cover a high proportion of the ground; or open forest formations with a continuous vegetation cover in which tree crown cover exceeds 10 percent. Young natural stands and all plantations established for forestry purposes which have yet to reach a crown density of 10 percent or tree height of 5 m are included under forest, as are areas normally forming part of the forest area which are temporarily unstocked as a result of human intervention or natural causes but which are expected to revert to forest. Includes: forest nurseries and seed orchards that constitute an integral part of the forest; forest roads, cleared tracts, firebreaks and other small open areas; forest in national parks, nature reserves and other protected areas such as those of specific scientific, historical, cultural or spiritual interest; windbreaks and shelterbelts of trees with an area of more than 0.5 ha and width of more than 20 m; plantations primarily used for forestry purposes, including rubberwood plantations and cork oak stands. Excludes: Land predominantly used for agricultural practices

Other wooded land: Land either with a crown cover (or equivalent stocking level) of 5-10 percent of trees able to reach a height of 5 m at maturity *in situ*; or a crown cover (or equivalent stocking level) of more than 10 percent of trees not able to reach a height of 5 m at maturity *in situ* (e.g. dwarf or stunted trees); or with shrub or bush cover of more than 10 percent.

Other land: Land not classified as forest or other wooded land as defined above. Includes agricultural land, meadows and pastures, built-on areas, barren land, etc.

Inland water: Area occupied by major rivers, lakes and reservoirs.

Natural forest: Natural forests are forests composed of indigenous trees, not planted by humans. Or in other words forests excluding plantations. Natural forests are further classified using the following criteria: forest formation (or type): closed/open, degree of human disturbance or modification, species composition.

Closed forest: Formations where trees in the various storeys and the undergrowth cover a high proportion (> 40 percent) of the ground and do not have a continuous dense grass layer (cf. the following definition). They are either managed or unmanaged forests, primary or in advanced state of reconstitution and may have been logged-over one ormore times, having kept their characteristics of forest stands, possibly with modified structure and composition. Typical examples of tropical closed forest formations include tropical rain forest and mangrove forest.

Open forest: Formations with discontinuous tree layer but with a coverage of at least 10 percent and less than 40 percent. Generally there is a continuous grass layer allowing grazing and spreading of fires. (Examples are various forms of cerrado, and chaco in Latin America, wooded savannahs and woodlands in Africa).

Plantation: Forest stands established by planting or/and seeding in the process of afforestation or reforestation. They are either: of introduced species (all planted stands), or intensively managed stands of indigenous species, which meet all the following criteria: one or two species at plantation, even age class, regular spacing. Note: Area statistics on forest plantations provided by countries should reflect the actual forest plantations resource, excluding replanting. Replanting is the reestablishment of planted trees, either because afforestation or reforestation failed, or tree crop was felled and regenerated. It is not an addition to the total plantation area.

Continent	**Total forest area 2000**	**Volume**		**Biomass**	
		by area	**Total**	**by area**	**Total**
	000 ha	m^3 ha^{-1}	Mio m^3	t ha^{-1}	Mio t
Africa	649866	72	46472	109	70917
Asia	547793	63	34506	82	45062
Oceania	197623	55	10771	64	12640
Europe	1039251	112	116448	59	61070
North and Central America	549304	123	67329	95	52357
South America	885618	125	110826	203	180210
Total	3869455	100	386352	109	422256

Growing stock: Stem volume of all living trees more than 10 cm diameter at breast height (or above buttresses if these are higher), over bark measured from stump to top of bole. Excludes: all branches

Commercial growing stock: Part of the growing stock, that consists of species considered as actually or potentially commercial under current local and international market conditions, at the reported reference diameter (DBH). Includes: species which are currently not utilized, but potentially commercial having appropriate technological properties. Note: When most species are merchantable, i.e. in the temperate and boreal zone, the commercial growing stock, in a given area or for a country, can be close to the total growing stock. In the tropics however, where only a fraction of all species are merchantable, it may be much smaller.

Woody biomass: The mass of the woody part (stem, bark, branches, twigs) of trees, alive and dead, shrubs and bushes. Includes: Above ground woody biomass, stumps and roots. Excludes: foliage, flowers and seeds.

Above-ground woody biomass: The above ground mass of the woody part (stem, bark, branches, twigs) of trees, alive or dead, shrubs and bushes. Excludes: stumps and roots, foliage, flowers and seeds.

7.2 Description of selected tree species in Middle Europe

Source: Schütt et al. 2002, Burschel and Huss 1997, Aas and Riedlmiller 1987

Species	Growth characteristics	Silvicultural significance
Norway spruce (*Picea abies*)	Climax (pioneer) species: Height growth moderate to fast (culmination at age 40), seldom >40m, high self-tolerance and basal area => high yield; age >200 yrs possible; not extremely wet/dry soils, but dry climate possible	In ME dominating forestry species (<35%), mostly monocultures, naturally codominant in (sub)montane altitudes with beech and fir, dominant in montane altitudes (Alps); important boreal and temperate species in Western Eurasia; little storm-resistance, bark beetle calamities
Scots pine (*Pinus silvestris*)	Pioneer/climax-species: Height growth fast (culmination at age 15), but seldom >30m, low self-tolerance low and basal area => low yield; age >200 yrs possible; low site demands, also wet and dry soils/ climate	In ME important forestry species (<31%), esp. in continental eastern Germany, naturally dominant under extreme site conditions (dry, wet) from planar to montane; important boreal and temperate species in Western Eurasia; relative storm, fire and calamity resistant
White fir (*Abies alba*)	Climax species: Height growth slow to moderate (culmination at age 40), exceeds 40m, self-tolerance and basal areas moderate => moderate yield; age >400yrs possible; not extremely dry and wet soils/ climate	In ME mostly in combination with Norway spruce; naturally codominant in (sub)montane altitudes with spruce and beech; important boreal and temperate species in Western Eurasia; relative storm resitant, subdue to high browsing in youth
Douglas fir (*Pseudotsuga menziesii*)	Climax species: Height growth fast (culmination at age 25), heights >50m possible, self-tolerance and basal area moderate, low tree densities => high yield; age >400yrs possible, not extremely wet soils, but wet climate	Introduced species, in ME in combination with Norway spruce, naturally often dominant species of the West coast of NA; fast growing, high yield
European larch (*Larix europea*)	Pioneer (climax) species: Height growth moderate (culmination at age 15), seldom >35m, low self-tolerance and basal areas => moderate yield; age >400yrs possible	In ME in montane to subalpine altitudes (Alps), often in combination with Norway spruce, natural areal disjunct restricted in Alps and Sudetes, very storm resistant
European beech (*Fagus sylvatica*)	Climax species: Height growth moderate (culmination at age 45), seldom >40m, low self-tolerance, but moderate basal area => moderate yield, age >200yrs possible, not extremely wet soils, humid climate	In ME most important broadleaf forestry species (<25%), mostly monocultures; naturally dominant species in ME, especially in colline altitudes, in montane altitudes often codominant with spruce and fir, storm resistant, subdue to browsing in youth
Common oak (*Quercus robur*)	Climax (pioneer) species: Height growth moderate to low (culmination at age <25), but seldom >35m, low self-tolerance and basal area => low yield (except at high age); age >400yrs possible, dry and wet soils/climate possible	In ME rare and precious forestry species (9%), mostly with hornbeam subcanopy; naturally planar and continental (dry) ME and far into continental Eurasia, mostly with shade tolerant subcanopy tree species
Ash (*Fraxinus excelsior*)	Pioneer-Climax species: height growth fast (culmination at age 20), but seldom >35m, moderate self-tolerance and low basal area => low yield; age >200yrs possible, high site demands	In ME only in combination with beech mostly colline; naturally mostly in mixed broadleaf forests in Middle and Eastern Europe, subdue to browsing in youth
Birch (*Betula pendula*)	Pioneer species: height growth fast (culmination at age <20), but seldom >25m; dbh growth moderate, self-tolerance moderate => low basal areas due to low tree-densities => low yield; age >100yrs, also dry and wet soils/climate	In ME only planted on extreme sites, planar to montane, naturally one of the most important pioneer species, especially at northern boreal forest border; fragile (storm, snow), fast rotting
Black locust (*Robinia pseudoacacia*)	Pioneer species: height growth moderate (culmination at age >20), seldom >25m, dbh growth high, moderate basal areas => moderate yield; age <100yrs, low site demands	Introduced species, in ME seldom as forests; naturally humid East coast of NA; N-fixation
Poplar (*Populus nigra var. canadensis*)	Pioneer species: height growth extremely high (culmination at age <10), up to 40 high; dbh growth extremely fast, basal area kept low => high yield at young age; age >100, high water demands, climate independent	Poplars in general are the fastest growing tree species, planted only with low densities, low wood quality; natural pioneer species of floodplains, climate independent, easy hybridising, fragile, fast rotting

7.3 Volume coherence distribution of the validation stands

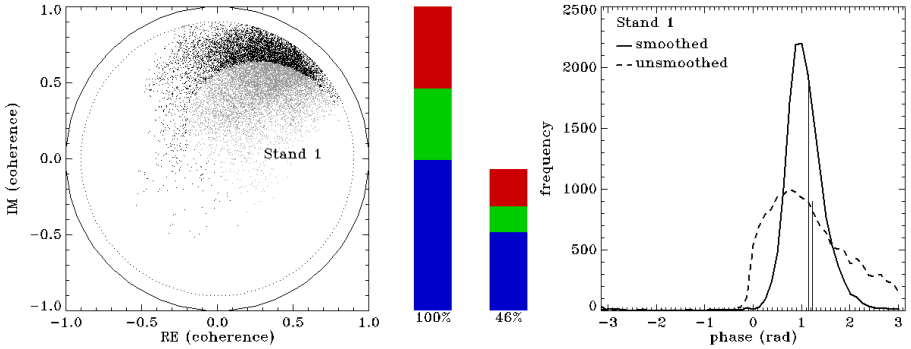

Stand 1

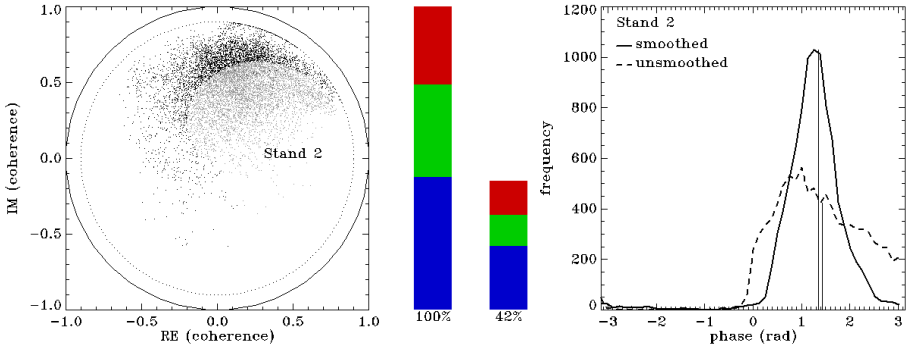

Stand 2

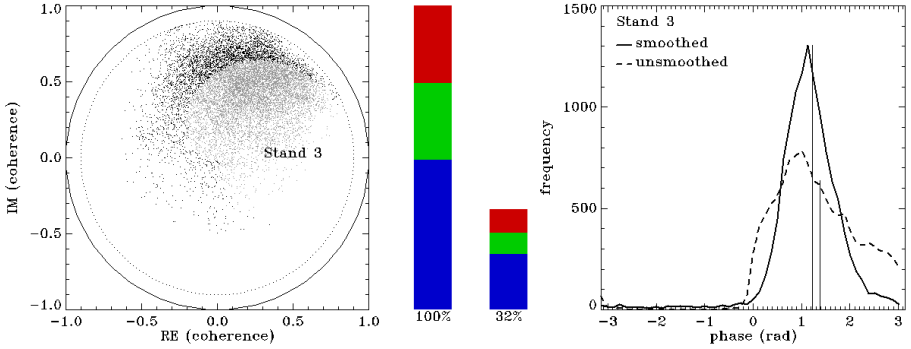

Stand 3

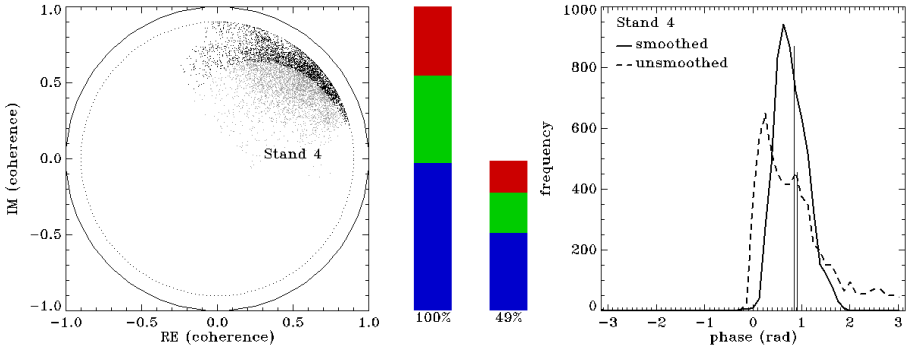

Stand 4

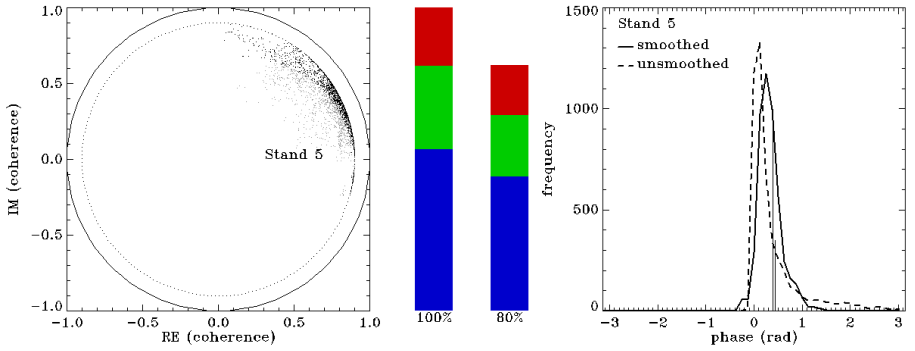

Stand 5

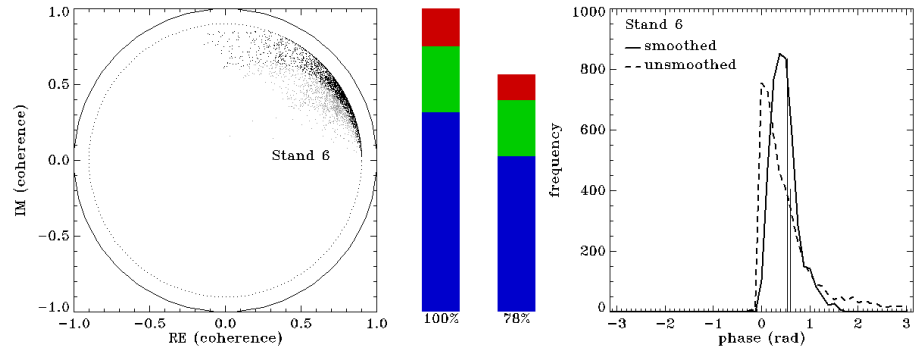

Stand 6

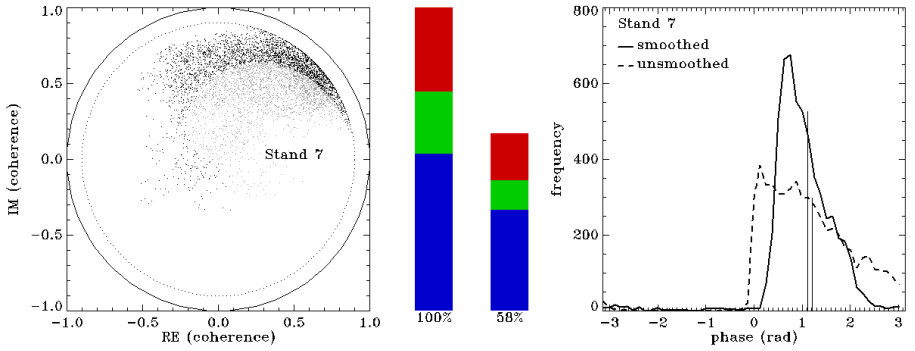

Stand 7

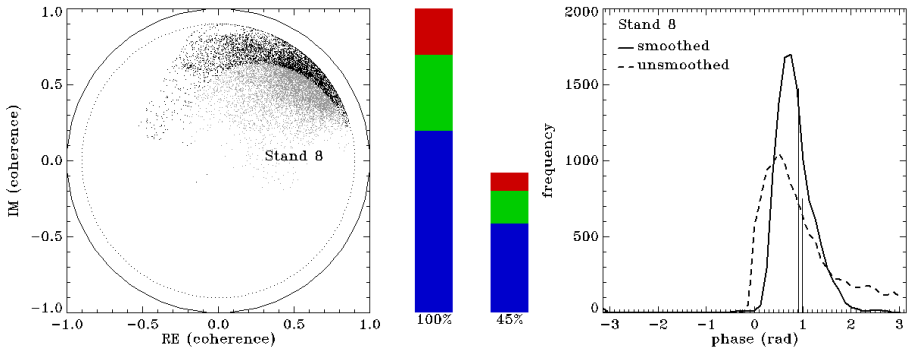

Stand 8

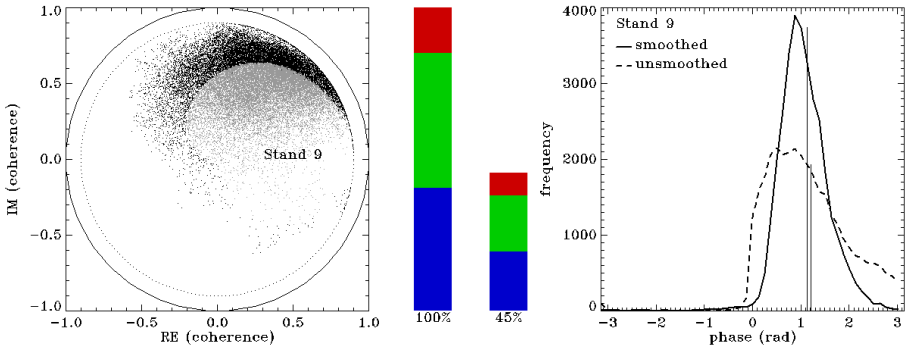

Stand 9

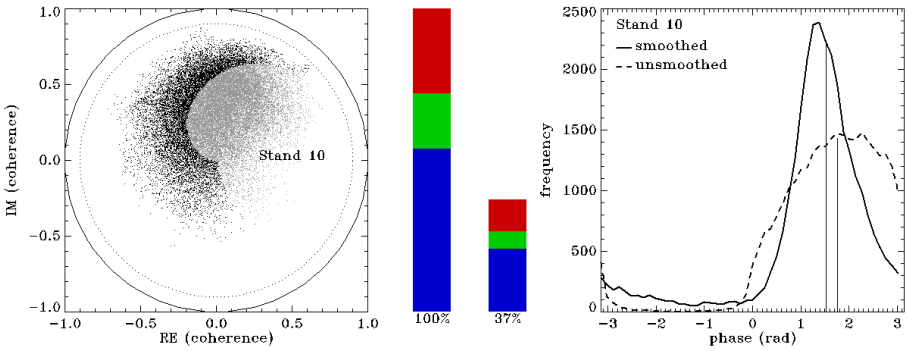

Stand 10

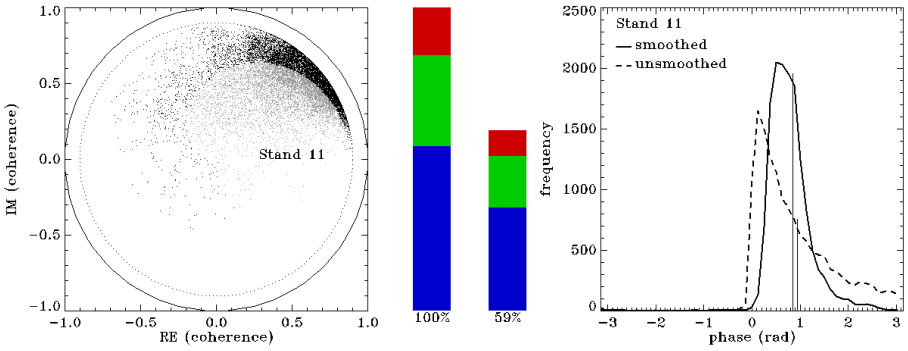

Stand 11

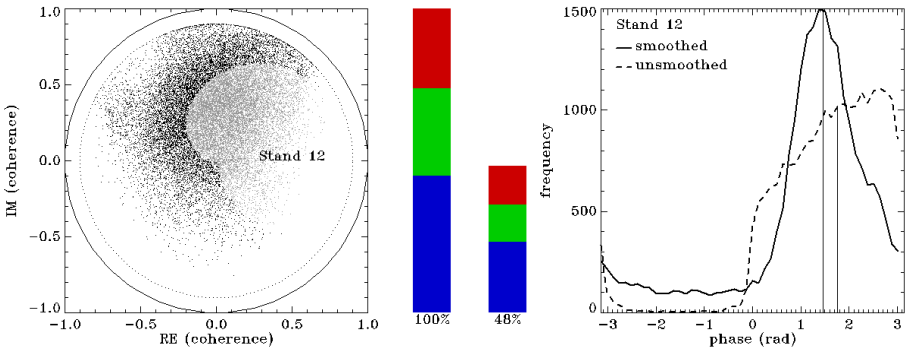

Stand 12

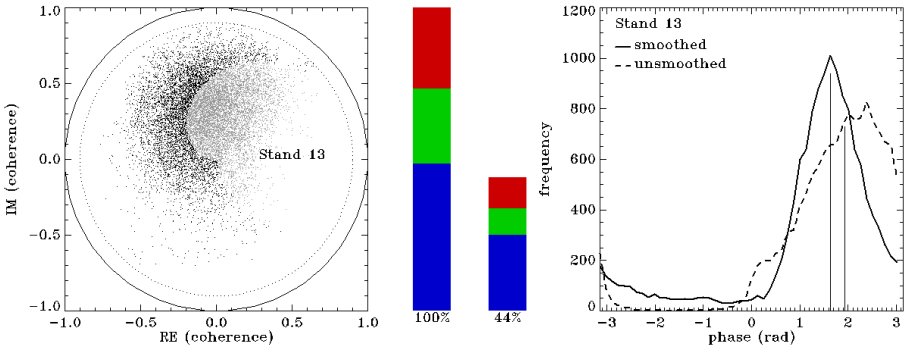

Stand 13

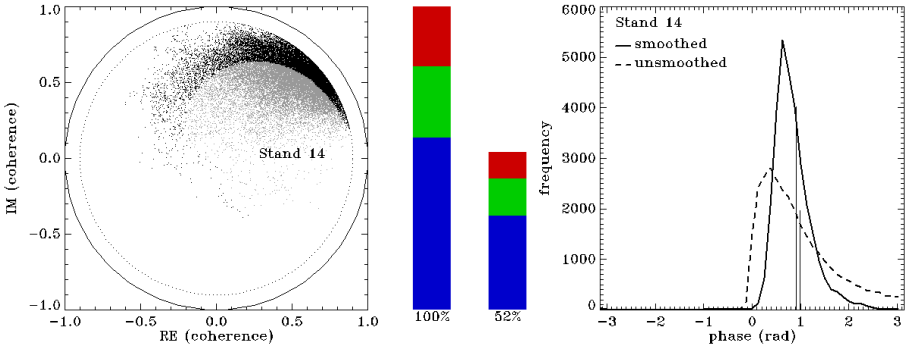

Stand 14

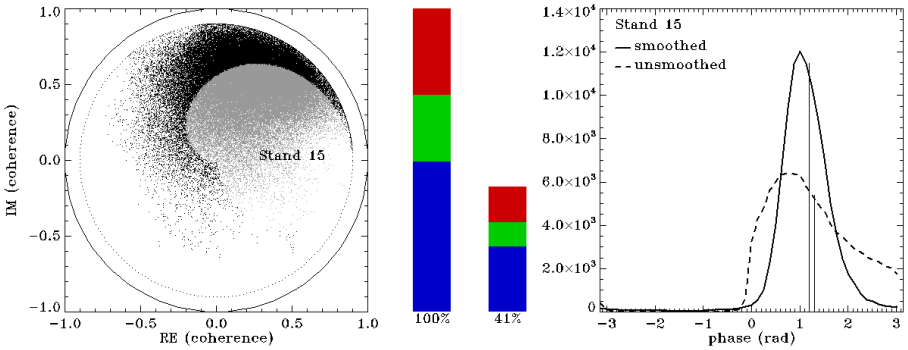

Stand 15

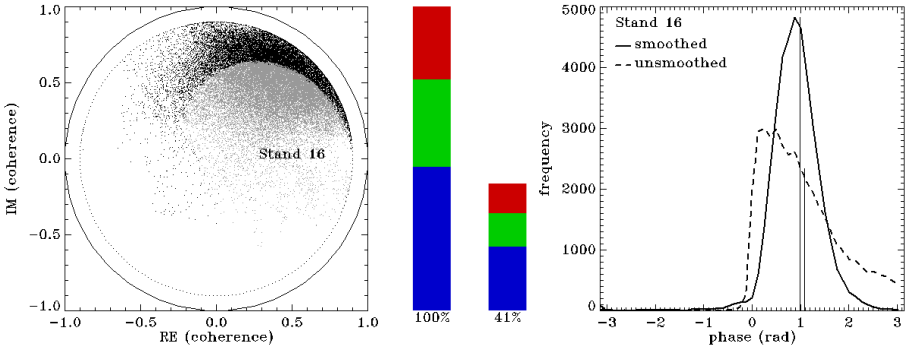

Stand 16

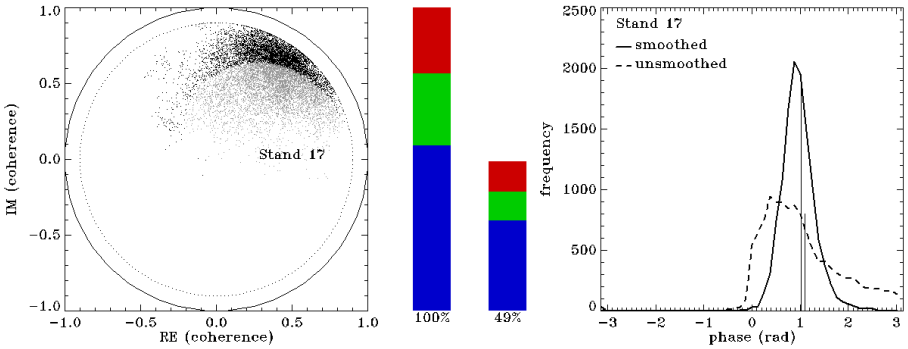

Stand 17

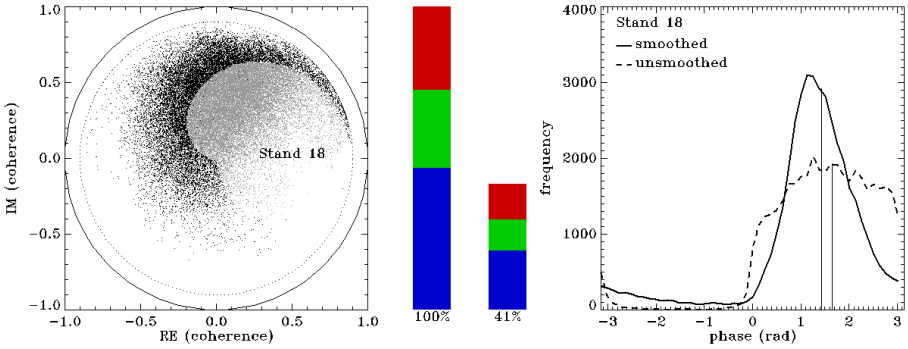

Stand 18

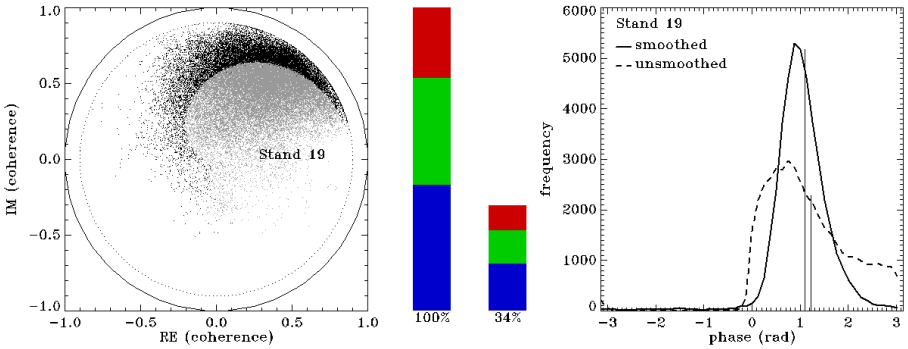

Stand 19

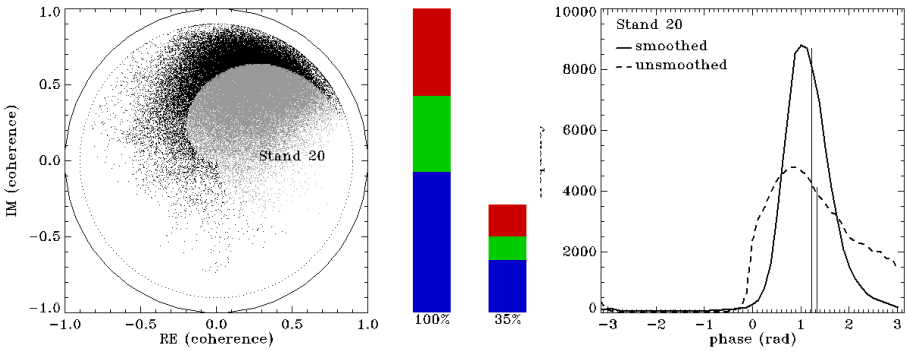

Stand 20